Integrative analysis of acquired thermotolerance in developmentally arrested Arabidopsis seedlings : Implication of energy metabolism

Élise Réthoré

UNIVERSITE ECOLOGIE
BRETAGNE GEOSCIENCES
LOIRE AGRONOMIE ALIMENTATION

université angers

THESE DE DOCTORAT DE

L'UNIVERSITE D'ANGERS
COMUE UNIVERSITE BRETAGNE LOIRE

ECOLE DOCTORALE N° 600
Ecole doctorale Ecologie, Géosciences, Agronomie et Alimentation
Spécialité : « Biologie et physiologie végétales »

Par
Elise RETHORE

Integrative analysis of acquired thermotolerance in developmentally arrested Arabidopsis seedlings

Implication of energy metabolism

Thèse présentée et soutenue à Angers, le 01/03/2018
Unité de recherche : UMR 1345 IRHS
Thèse N° : 139508

Rapporteurs avant soutenance :

Pierre Goloubinoff	Professeur, Université de Lausanne
Christian Meyer	Directeur de recherche, Institut Jean-Pierre Bourgin

Composition du Jury :

Président

Alain Bouchereau	Professeur, Université de Rennes 1
Etienne Bucher	Directeur de recherche, Agroscope, Changins (CH)
Pierre Goloubinoff	Professeur, Université de Lausanne
Christian Meyer	Directeur de recherche, Institut Jean-Pierre Bourgin

Directeur de thèse

David Macherel	Professeur, Université d'Angers

Co-encadrante de thèse

Marie-Hélène Avelange-Macherel	Maître de conférences, Agrocampus Ouest

REMERCIEMENTS

Ces trois ans et quelques mois ont été l'occasion de développer de nombreuses collaborations et échanges, et j'espère n'oublier personne dans ces quelques lignes de remerciements…

Je souhaite tout d'abord remercier les membres du jury Pierre Goloubinoff et Christian Meyer pour avoir accepté d'être rapporteurs de ma thèse, ainsi qu'Etienne Bucher et Alain Bouchereau pour être examinateurs. Un grand merci à Alain ainsi qu'à Jacques Bourguignon pour leur investissement et leurs précieux conseils lors des comités de suivi individuel.

Evidemment ce travail n'aurait pu être réalisé sans l'encadrement et la disponibilité de David et Marie-Hélène Macherel. Un énorme merci à vous deux pour m'avoir conseillée, supportée et vous être passionnés pour les résultats (parfois décevants) tout au long de cette thèse. Tant de chemin parcouru depuis la L2 et les cours de David sur la respiration et la photosynthèse ! J'ai beaucoup appris sur la mitochondrie, les HSPs, la microscopie et j'en passe, mais surtout sur moi-même. Je garderai également un très bon souvenir des quelques moments « off » tels que la fête de la science préparée avec Marie-Hélène.
Thanks a lot to David Logan for your precious advice in microscopy and your beautiful GFP mitochondria! I am still amazed by these moving organelles, since I first saw them in your courses in L3! Also a big thank for your advice and correction, even after you left the lab.

Cette thèse ne se serait pas passée de la même manière sans un environnement de travail et une équipe si accueillants ! Je remercie tout particulièrement Abdel, le roi de l'électrode et psychologue à ses heures perdues et Martine pour ton aide pour les western-blot et bien sûr nos pauses thés ! Merci également à Pascale pour ton éternelle bonne humeur et ton rire communicatif, tes petites danses et chansons, et bien sûr ton aide dans l'analyse des sucres, à Caroline pour avoir analysé les résultats de GC/MS (et ce, malgré les caprices de cette dernière) et Anis pour ton aide à l'interprétation des données de métabolomique. Dimitri, merci pour ton investissement, notamment dans la phase de correction du papier. Cette dernière manip de complémentation nous aura bien stressés ! Merci à Gaël pour m'avoir initiée à Fiji et Imaris. Daniel, merci pour le soin apporté aux plantes et tes conseils de jardinage. Merci à l'ensemble de l'ancienne équipe MitoStress et à la nouvelle équipe SMS. Bon vent à cette toute jeune équipe !

Merci également à l'ensemble du personnel du R+2 pour sa bienveillance et pour les nombreux échanges portant sur la science, l'avenir et bien souvent la nourriture, notre passion !

Je remercie chaleureusement Aurélia (vive les heures passées à regarder les crépinettes de RE et à refaire le monde !) et Fabienne du plateau IMAC, ainsi que Guillaume et Florence du SCIAM pour m'avoir fait découvrir et aimer la microscopie confocale et électronique. Merci à tous les quatre pour votre disponibilité. Florence, ta patience et ta minutie dans la réalisation des coupes m'ont épaté ! Merci à Céline Rousseau (de la plateforme PHENOTIC) pour m'avoir formée à la caméra de fluorescence de chlorophylle.

REMERCIEMENTS

Un grand merci à l'équipe Bioinfo et plus particulièrement à Sandra et Sylvain : sans vous, je n'aurais pas pu analyser mes résultats de transcriptomique ! Je tiens également à remercier Michel Zivy et Thierry Balliau de la plateforme PAPPSO pour m'avoir si bien accueillie à Gif et m'avoir fait découvrir la complexité de l'analyse protéomique. Un grand merci à Sabine pour avoir réalisé l'analyse lipidique. Merci pour ta gentillesse, ta disponibilité et ton intérêt porté à nos recherches. Merci également à Sylvain Dechaumet (IGEPP Le Rheu) pour m'avoir initiée à R/R Studio et à l'ACP lors de mon stage de Master 2. Thanks to Owen Kentish for English proofreading of the manuscript.

Je garderai également un excellent souvenir de l'expérience d'enseignement avec Françoise, Dimitri, Quentin, Marie-Anne et Kévin (quelle belle équipe de biochimistes !). Merci pour nos nombreux échanges au sein et en dehors de l'université.

Evidemment, une thèse, c'est l'occasion de rencontrer beaucoup de personnes et de partager nos réussites et nos déboires avec les autres thésards et postdocs. Tout d'abord un énorme merci à ma grande carotte Julia pour tous les bons moments passés ensemble et les heures passées dans ta voiture à refaire le monde ! Merci pour ton soutien et tes câlins, t'es la meilleure ! Merci à Souha pour ta folie (on n'oubliera pas ta soirée d'anniversaire déguisée !) et pour m'avoir rassurée à de nombreuses reprises ! Merci à Douae pour les fous rires que tu as provoqué avec tes incompréhensions (c'est culturel !), à Justine pour tes gaffes, à Alexis pour tes délicieux gâteaux et ta bonne humeur (team 1993 forever). Je fais également de gros bisous à Adrien, Eloïse, Lili, Kévin, Mathieu, Juliette, Céline et Elodie. Merci aux « anciens » Chvan, la petite Julia, Lucien et Gaël pour m'avoir rapidement intégrée à l'ARES et accueillie dans le bureau des thésards. Merci à Denise, notre rayon de soleil brésilien ! Enfin, merci à Elise (Bis), Zhijuan et Jean-Baptiste pour les bons moments passés ensemble (et les bons goûters !) depuis votre arrivée au bureau. Bonne chance pour la suite !

Je n'oublie pas les stagiaires : merci à Thomas et Romane pour votre motivation et votre travail sur les HSPs, les polyamines et la mémoire du stress. Merci également à Lydia et Martin avec qui j'ai pu passer de très bons moments au bureau.

Merci à l'équipe PAIGE et particulièrement à Sylvie et à Mathilde pour leur disponibilité lors des galères administratives !

Enfin, merci à tous mes amis pour m'avoir soutenue et divertie pendant ces trois années. Il est important de sortir la tête de la science pour mieux y revenir. Merci à mes parents de m'avoir transmis leur passion des plantes et leur curiosité, ainsi qu'à mes trois scientifiques de frère et sœurs (und mein Schwager Timo) pour m'avoir montré la voie et m'avoir encouragée ! Paul-Emile, merci pour ton indéfectible patience et ton soutien tout au long de ces cinq années ensemble.

Contents

List of figures

List of tables

Abbreviations

ABA	abscisic acid
AOX	alternative oxidase
APX	ascorbate peroxidase
CAM	Crassulacean acid metabolism
chll	chlorophyll
CNGC	cyclic nucleotide gated calcium channel
COX	cytochrome c oxidase
DR	dark respiration
DREB	dehydration responsive element binding protein
DW	dry weight
ER	endoplasmic reticulum
ETC	electron transport chain
FA	fatty acid
FW	fresh weight
GDC	glycine decarboxylase complex
GFP	green fluorescent protein
GO	gene ontology
GP	gross photosynthesis
HS	heat stress
HSF	heat shock factor
HSP	heat shock protein
HSR	heat shock response
LD	lipid droplet
MS	Murashige and Skoog
NO	nitric oxide
NP	net photosynthesis
NPQ	non-photochemical quenching
OLE	oleosin
PCD	programmed cell death
PG	plastoglobule
PPR	pentatricopeptide repeat proteins
PS I	photosystem I
PS II	photosystem II
ROS	reactive oxygen species
Rubisco	ribulose 1,5-bisphosphate carboxylase/oxygenase
SC	spectral counting
SOD	superoxide dismutase
TAGs	triacylglycerols
TCA cycle	tricarboxylic acid cycle
TF	transcription factor
UPR	unfolded protein response
XIC	extracted ion chromatogram

Foreword

One could think that plants are particularly vulnerable organisms, as they are subjected to many adverse conditions, from which they cannot escape. Despite the apparent disadvantage of being sessile, they have evolved mechanisms that have allowed them to colonize many different environments across the planet. However, even if they managed to adapt during many dramatic climate changes in the past, they are now facing a faster evolution of climate due to global warming. In this context, the increase in the frequency and intensity of abiotic stresses (heat, drought, flooding, wind) has now become evident and will likely also have an impact on biotic stresses as well. This situation constitutes a major threat for both wild and crop species, but since breeding of the latter was essentially based on yield parameters, many adaptive traits have been lost in return, making them more stress sensitive. It is thus of primary importance to understand how plants can adapt to stresses by considering the whole range of physiological and metabolic responses, instead of only selecting phenotypic traits. Moreover, breeding strategies must take into account other parameters, such as the lowering of crop inputs, which is an aim of European policy, in order to sustain a more ecological form of agriculture. The increasing world population is another constraint, which requires the maintenance or even the increase of yields, especially in unfavourable environmental conditions.

Even if genetic and genomic information has now been acquired for many crop species, model plants like *Arabidopsis thaliana* remain invaluable to study stress responses as many of their genes have been functionally characterized. This facilitates the identification of the major pathways involved in stress management when performing omics analyses. In the last decades, plant responses to several abiotic stresses, such as drought and heat, have been extensively studied, which has led to the discovery of important transcription factors, proteins and pathways. However, few studies have addressed and integrated stress responses at different scales.

The aim of this thesis was to investigate the implication of mitochondrion and chloroplast in the heat acclimation process in *Arabidopsis thaliana* seedlings. The seedling stage is an essential step in plant development, being the transition between the highly stress tolerant seeds and mature plants. Thus, successful seedling establishment is important for plant fitness.

We used an integrative approach by studying seedling responses to heat treatments at different scales, combining analyses of physiology, cell biology and molecular changes (transcriptomics, proteomics, and metabolism). The work was performed using an original system of liquid culture, which was previously set up by our team (Benamar *et al.*, 2013), in which seedlings are developmentally arrested because of nutrient limitation. This system avoids interference between stress and developmental responses. This work will be presented in five chapters, described as follows:

The first chapter will be dedicated to an introduction about the physiological and molecular responses of plants to heat stress. We will also highlight some important features about the chloroplast and mitochondrion, which are two essential organelles for energy and primary metabolism.

The second chapter, which is presented as a publication manuscript, describes the comprehensive physiological and metabolic characterization of the model system that was used for the heat acclimation study, in which Arabidopsis seedlings were grown in liquid culture, under conditions of mineral nutrient starvation.

The third chapter describes the physiological response of respiration and photosynthesis to heat shock and acclimation, together with the effects on organelle dynamics.

The fourth chapter focuses on molecular responses to heat stress, including transcriptomic, proteomic and metabolic analysis and the integration of these data.

Finally, the fifth chapter exposes preliminary experiments related to heat stress memory.

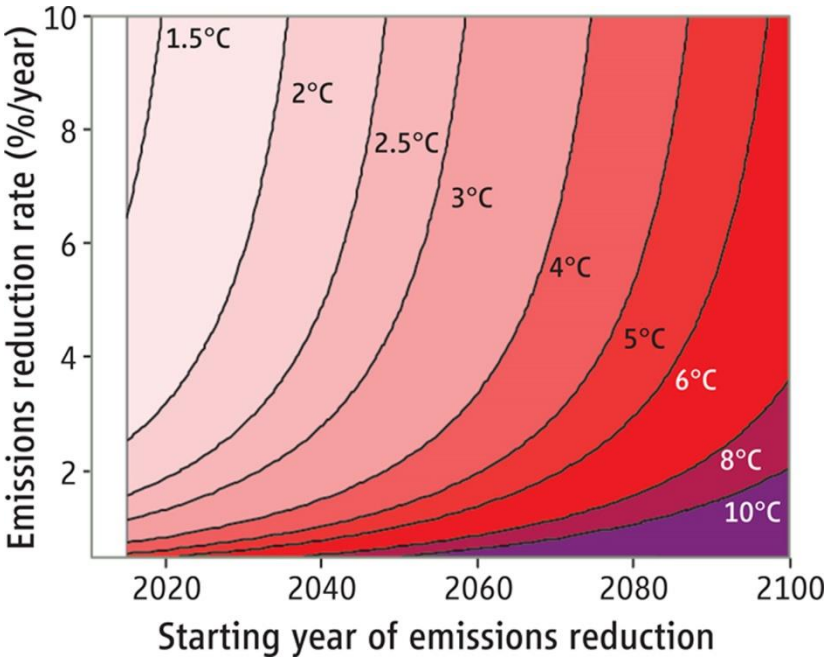

Figure 1.1: Simulation of CO_2-induced warming depending on the CO_2 emission reduction rate and the starting year of this reduction.
(Stocker, 2013).

Chapter I – Introduction

1. Impact of heat stress on plant development

1.1. Impact of climate change on crop productivity

1.1.1. Climate change and yield projections

All current predicting models agree on the fact that we are facing climate change, which is confirmed by the increased frequency and intensity of many climatic events observed nowadays (hurricanes, heat waves, floods…). In this context, abiotic stresses such as heat and drought are likely to severely disrupt the ecosystem.

Over the 1951-2010 period, surface temperature increased by around 0.7°C, and it is expected to increase by about 1-3°C by the mid-twenty-first century and by about 2-5°C by the late twenty-first century (Bokszczanin & Fragkostefanakis, 2013). Some scenarios even predict a 10°C warming at high latitudes and 3-4°C warming in the tropics by 2100 (Dusenge *et al.*, 2019). The intensity of temperature increase will greatly depend on the reduction rate of anthropogenic carbon dioxide emissions. If we consider a 5 % decrease in the CO_2 emission per year (feasible economic based model), the target of a moderate increase in the global temperature of 2°C will become unreachable from 2027, and the target of 2.5°C before 2040 (Figure 1.1, Stocker, 2013). During the 1750-2011 period, cumulative anthropogenic CO_2 emissions released into the atmosphere were around 2040 Gt CO_2, and about 40 % has remained in the atmosphere (≈ 880 Gt CO_2) (Climate Change 2014 Synthesis Report). Plant growth and development are highly dependent on their environment, and therefore, will be directly impacted by these variations in temperature and CO_2 concentration. The Fourth Assessment Report (AR4) of the Intergovernmental Panel on Climate Change (IPCC) reports a moderate increase in global crop yield for global mean temperature increase up to 3°C, mostly due to beneficial CO_2 fertilization effects on the photosynthesis rate and transpiration demand, but a general decrease above this threshold (Easterling *et al.*, 2007). Some models predicted different impacts, depending on the crop species, such as significant yield losses in maize but more positive impacts on spring wheat and soybean (Deryng *et al.*, 2014). Such predictions appear to be dependent on the regions, but also on the consideration of CO_2 fertilization effects.

The impact on yield of previous heat wave events has already been investigated in different areas and concerning different crops. For example, it was estimated that the heat wave which occurred in 2003 caused a drop of 36 % in maize yield in the Po valley in Italy, whereas in France, the maize yield was reduced by 30 % and fruit harvests declined by 25 %, compared to the previous year (Ciais *et al.*, 2005). Winter crops (wheat) had nearly achieved maturity by the time of the heat wave and therefore suffered less yield reduction (21 % decline in France) than summer crops (e.g., maize, fruit trees and vines), which were in their maximum foliar development. In another study, some researchers estimated by modelling that wheat yields could be reduced by 50 % in Australia because of an increase of only 2°C in the average growing-season temperature (Asseng *et al.*, 2011). This was correlated with earlier senescence caused by temperatures above 34°C. We can expect that such events will occur more frequently in the future, leading to a global decrease in crop yields.

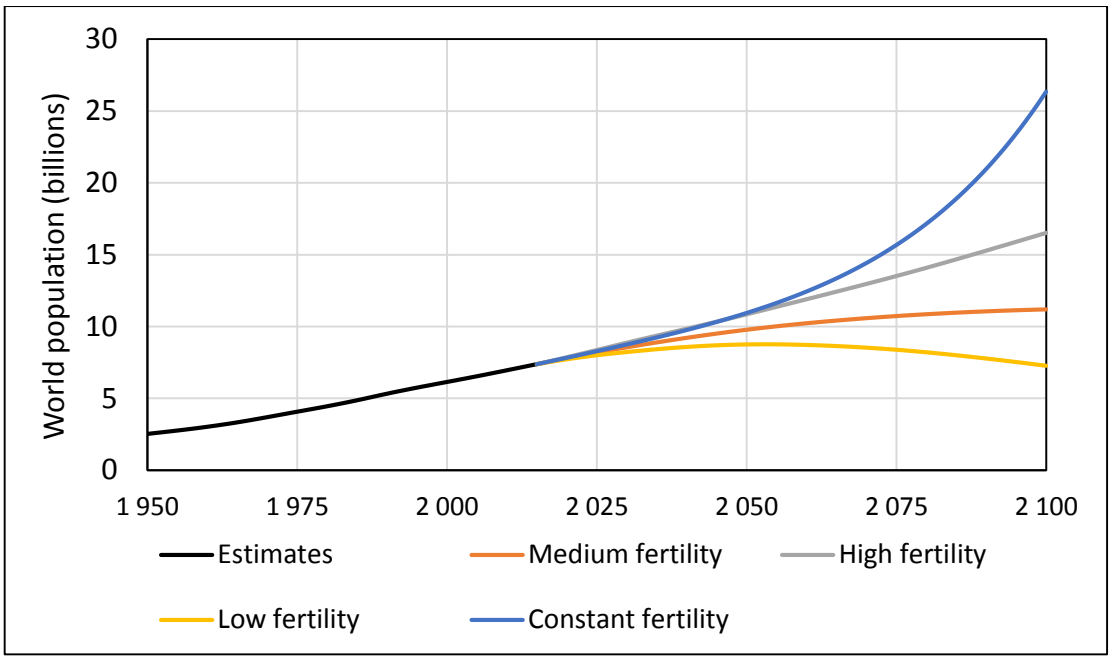

Figure 1.2: World population increase based on different projections.
(United Nations data, 2017 revision).

Moreover, climate change must be taken into account with respect to another parameter, which is the increasing world population. Over the 1974-2011 period, the global population increased by 3 billion people and projections estimate a future population of 9 billion inhabitants by 2045 (Figure 1.2., Van Bavel, 2013). The traditional breeding programs will no longer be sufficient to meet the demand for the three major cereal crops: rice (*Oryza sativa*), maize (*Zea mays*) and wheat (*Triticum aestivum*). With the increasing world population, cereal grain yields must increase by more than 70 % before 2050 (Furbank & Tester, 2011). In this context, it will be a priority to increase food production, while facing more severe and frequent stresses and decreasing the input of fertilizers and pesticides. Understanding the mechanisms that underlie crop efficiency under variables, and often unfavourable conditions, should be a priority to design more efficient cultivars or to improve crop management.

1.1.2. Heat stress impact on phenology

Heat stress (HS) can be defined as a transient change in temperature beyond the optimal growth temperatures (usually 10 to 15°C above) applied for a sufficient duration to cause a deleterious impact on plant physiology. The intensity, duration and rate of increase in temperature, must nevertheless be integrated to understand the impact of stress (Wahid *et al.*, 2007). Moreover, in the field, many parameters such as stomatal conductance, radiation and wind intensity or humidity can also affect heat response (De Boeck *et al.*, 2016).

As illustrated above concerning the impact of the 2003 heat wave in Europe, HS impact will differ depending on the species studied: for example, for a cool season vegetable like broccoli the maximal growth temperature is 25°C, however for a summer grown crop like maize, it can raise up to 38°C (Hatfield & Prueger, 2015). For *Arabidopsis thaliana*, heat conditions can usually be classified as a warm ambient temperature (about 22–27°C), a high temperature (27–37°C) and an extremely high temperature (37–42°C, also considered as HS) (Liu *et al.*, 2015). Thus, the effect of high temperature will depend on the plant's intrinsic characteristics and environmental conditions.

Overall, HS is considered to be a major factor, affecting plant productivity in many plant species. Indeed, it affects plant physiology on multiple scales and developmental stages. For most plant species, it is considered that the reproductive phase usually has a lower optimum temperature than the vegetative phase. Thus, HS effects are often higher during the reproductive stage than during vegetative growth, such as a lower rate of pollen fertility observed in many plant species. It has been suggested that high temperature stress is more deleterious during the flower bud initiation stage and then for a period of around 15 days (Bita & Gerats, 2013). In rice, it was shown that the decreased spikelet fertility was mainly due to a decrease in pollen production and reception (quantity of pollen on the stigma) (Prasad *et al.*, 2006). To counteract the effect of HS on pollen viability, some researchers have proposed to select crops for early morning flowering traits, since they showed that a rice near-isogenic line exhibiting an early morning flowering phenotype had minimized spikelet sterility compared to other cultivars (Bheemanahalli *et al.*, 2017).

Regarding other developmental stages, early seed germination is generally considered to be a heat tolerant stage, thanks to the presence of heat shock proteins (HSPs), which were accumulated during seed development. In cereals, HSPs are gradually degraded from 12 h of imbibition, and thus heat can more severely affect the later stages of germination and seedling establishment (Maestri *et al.*, 2002). If the seedling is not properly

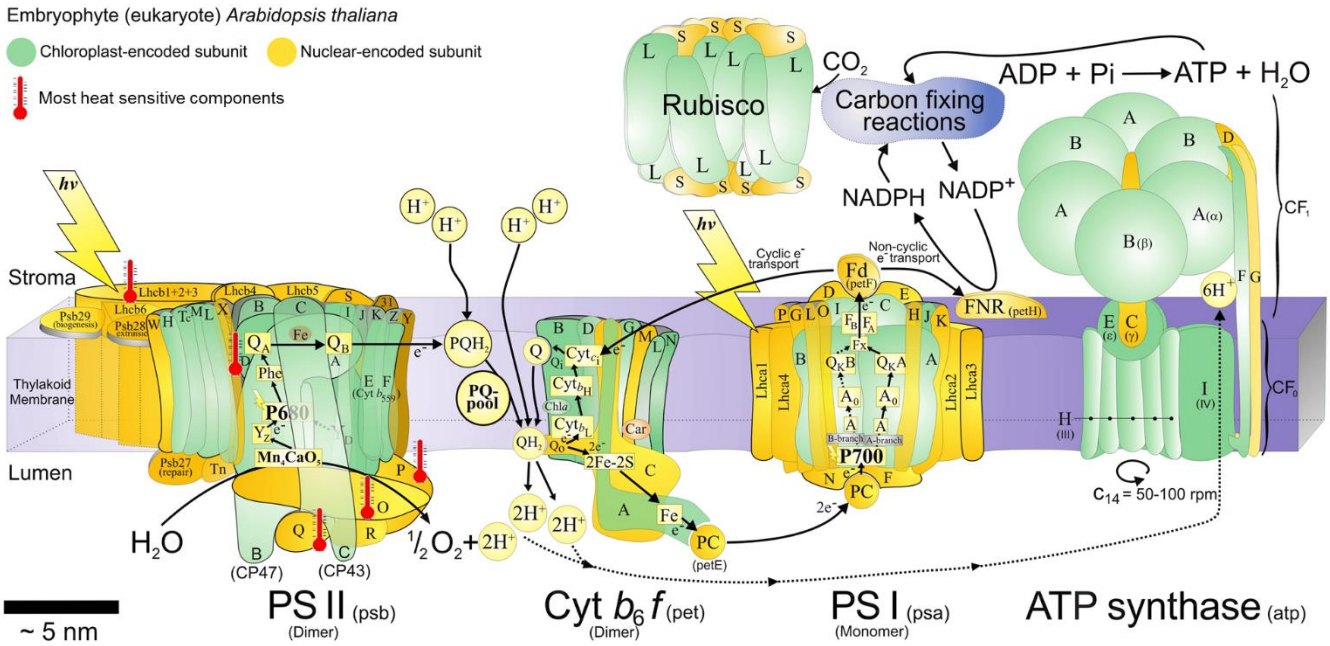

Figure 1.3: Representation of the most heat sensitive components of the photosynthetic apparatus in *Arabidopsis thaliana*.
Photosystem II (PS II); cytochrome b6f (Cyt b6f); photosystem I (PS I); Rubisco: ribulose 1,5-bisphosphate carboxylase oxygenase (adapted from Allen *et al.* (2011)).

established, this will condition future plant development and thus the final grain yield.

1.2. Heat stress impacts on plant physiology

Contrary to some stresses that only affect some parts of the plant (e.g. herbivory attacks), HS is perceived by the whole plant (leaves, flowers, fruits, roots…). Thus, it can disturb many physiological processes and cell components, with effects that depend on the intensity, duration and combination with other stresses.

1.2.1. Heat damage on photosynthesis and respiration

Photosynthesis is a mechanism that is rapidly and especially sensitive to heat stress. Extensive work on this aspect has been reviewed in Allakhverdiev *et al.* (2008) and Mathur *et al.* (2014). In *Phaseolus vulgaris*, it was found that net assimilation rate was maximal between 30°C and 35°C, and it could be reversibly impacted by moderate HS below 40°C; however, above 40°C, damage was no longer reversible (Hüve *et al.*, 2011). This disruption of photosynthetic activity was linked to a decreased photosynthetic electron transport caused by an enhanced membrane permeability and disorganization of Photosystem II (PS II), including the disruption of water splitting and the oxygen evolving complex (Figure 1.3). PS II is indeed considered to be one of the most sensitive components of the photosynthetic apparatus, compared to Photosystem I (PS I), which is much more thermostable (Berry *et al.*, 1980; Bukhov *et al.*, 1999). PS I was found to play an important role in the protection of PS II against photoinhibition, by maintaining the thylakoid proton gradient through cyclic electron transport, and thus ATP synthesis under HS (Bukhov *et al.*, 1999; Sharkey, 2005; Yamori & Shikanai, 2016). Chlorophyll degradation was also observed in many plant species, mostly due to higher activity of chlorophyllase and other chlorophyll-degrading enzymes, which might help to prevent the accumulation of phototoxic chlorophyll-species when the photosynthetic apparatus is overexcited (Wang *et al.*, 2018).

Inhibition of Rubisco (ribulose 1,5-bisphosphate carboxylase/oxygenase) activase and thus Rubisco activity can also explain the loss of photosynthetic activity under moderate HS (Salvucci & Crafts-Brandner, 2004). However, in Pima cotton (*Gossypium barbadense*), photosynthetic activity was found to be mainly limited by electron transport and the regeneration of ribulose-1,5-bisphosphate (RuBP), but not by Rubisco activity (Wise *et al.*, 2004).

Stomatal conductance is also affected by heat: it was shown to be increased in response to high temperatures in Arabidopsis and tobacco but also in some tree species, which would help to lower leaf temperature, facilitate gas exchanges, and thus carbon fixation (Rizhsky *et al.*, 2002, 2004; Urban *et al.*, 2017). However, when applying both heat and drought stress, stomatal conductance and photosynthetic activity were much lower, and the leaf reached temperatures over 45°C (Rizhsky *et al.*, 2002, 2004).

The impact of temperature on respiration has also been thoroughly studied. A coefficient known as the respiratory Q_{10}, which reflects the increase in respiration per 10°C rise in temperature, is often used to determine the effect of temperature on respiration (Atkin & Tjoelker, 2003). It is often admitted for biochemical mechanisms that Q_{10} is around 2.0, meaning that respiration doubles per 10°C increase. However, the reality is more complex: Q_{10} is

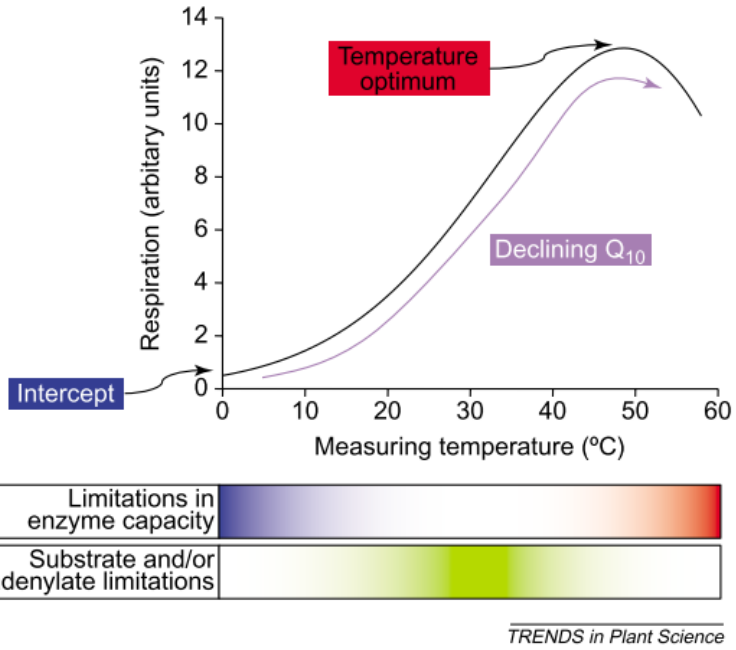

Figure 1.4: Temperature response of respiration (R).
The temperatures where respiratory flux is likely to be limited by maximum catalytic enzyme activity (i.e. Vmax) are indicated in blue (limitations in the cold) and red (limitations at supra-optimal temperatures). At moderate temperatures, respiratory flux is more likely to be regulated by the availability of substrate and/or adenylates (i.e. the absolute concentration of ADP and the ratio of ATP:ADP) (from Atkin & Tjoelker (2003)).

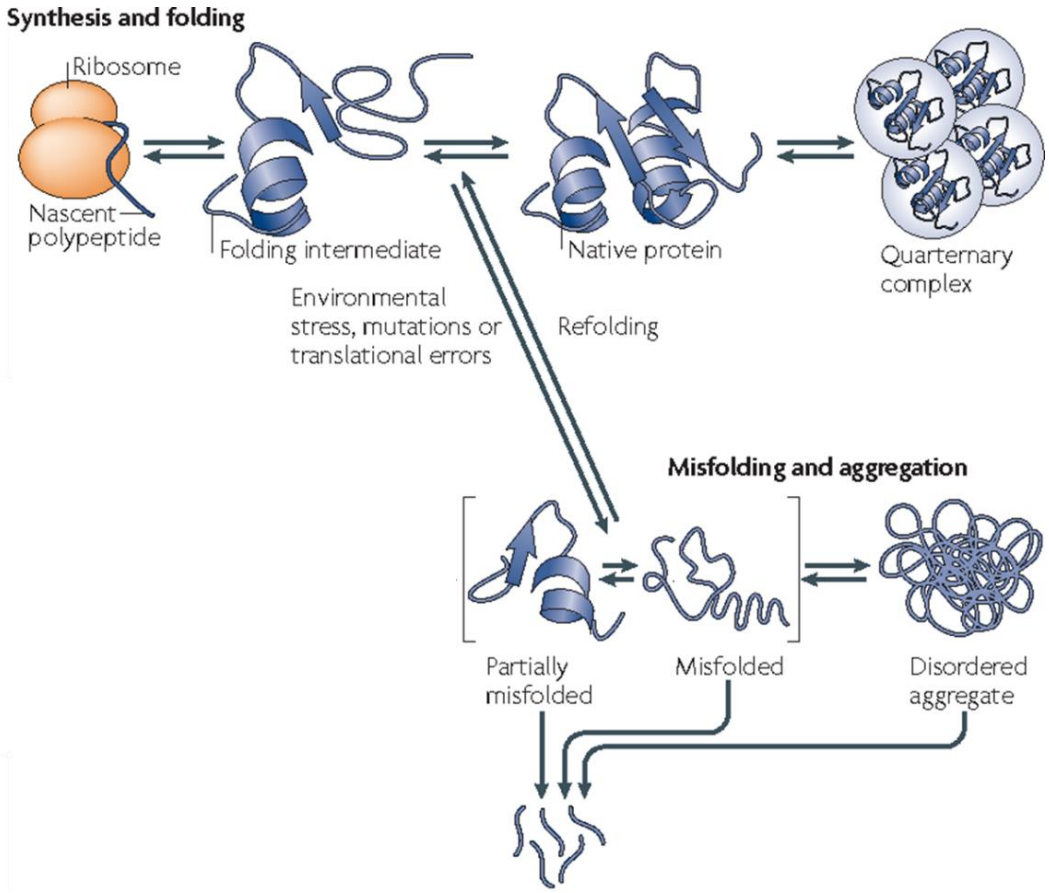

Figure 1.5: Protein states in optimal or in misfolding inducing conditions.
(adapted from Tyedmers *et al.*, 2010).

dependent on many components, such as the shape of the temperature-response curve, the range of temperatures used and the duration of temperature application. The Q_{10} varies differently in leaves and roots and can also be influenced by other factors, such as light intensity and water or nutrient supply (Atkin *et al.*, 2005). For example, in snow gum (*Eucalyptus pauciflora*), the temperature sensitivity of respiration was shown to be higher in the dark than in illuminated leaves (Atkin *et al.*, 2000). Concerning the shape of the temperature-response, it is assumed that, at low temperatures, respiration would be limited by the activity of the enzymes involved in glycolysis, the TCA cycle and mitochondrial electron transport; while, at high temperatures, increased membrane fluidity would cause the dissipation of the concentration gradients and thus lead to substrate limitations (Figure 1.4; Atkin & Tjoelker, 2003). In *Phaseolus vulgaris*, the respiration rate increased continuously with the temperature, but this increase was even faster at very high temperatures (44 to 48°C). However, this latter increase was short and respiration started to decrease after 2-3 minutes of temperature exposure. This respiratory burst was absent in experiments in which samples were exposed to the high temperature over an extended period of time. It was hypothesized that substrate and adenylate availability governed these responses (Hüve *et al.*, 2011). Differences of heat sensitivity between respiration (R) and photosynthesis (P) might affect the ratio R/P and thus, the energy balance. Even though several studies have shown that plant R/P was homeostatic when applying moderate variations in growth temperature (Atkin *et al.*, 2005; Dusenge *et al.*, 2019), severe HS may cause a major imbalance.

1.2.2. Heat perturbation on cell organization

Considering molecular aspects, temperature changes modify the global internal organization of the cell and thus homeostasis, through their impact on many different components such as proteins, membranes, cytoskeleton and nucleic acids (Richter *et al.*, 2010). Severe heat stress is well known to cause protein destabilization and even aggregation, if the folding machinery capacity is overwhelmed. Newly synthetized proteins appeared to be the most vulnerable proteins subject to misfolding when proteostasis was disrupted in human HEK293 cells (Figure 1.5; Xu *et al.*, 2016). During HS, proteins, together with RNAs, form transient stress granules, which are then disaggregated without degradation during recovery (Nover *et al.*, 1989; Wallace *et al.*, 2015; Chantarachot & Bailey-Serres, 2018). This unfolded protein response (UPR) has been highlighted in the endoplasmic reticulum (ER) and cytosol, inducing molecular responses (Mittler *et al.*, 2012). HS was also shown to inhibit translation processes: at 46°C, the inhibition of protein synthesis has been shown to occur in *Saccharomyces cerevisiae*, as translation initiation, elongation and termination factors but also aminoacyl-tRNA synthetases accumulated in stress granules and factors involved in ribosomal biogenesis, were sequestered into insoluble nuclear deposits (Cherkasov *et al.*, 2015). In *Arabidopsis thaliana,* a study showed that translation was inhibited by 50 % after 45 min at 38°C and that this decrease was greater for short mRNAs than long mRNAs (Yángüez *et al.*, 2013). Another study revealed a higher coordination between transcriptional and translational responses after 3 h at 37°C, although a group of genes was regulated at the translational level depending on the secondary structure of the mRNA (Lukoszek *et al.*, 2016). The role of stress granules in the protection of the translational apparatus during heat stress is emerging with the discoveries that translation elongation factors were sequestered together with cytosolic small HSPs (sHSPs) and ribosomal protein mRNAs in stress granules, allowing faster resumption of

translation upon recovery (McLoughlin *et al.*, 2016; Merret *et al.*, 2017).

As indicated earlier, membrane fluidization is a major effect of HS, affecting plasma and organellar membranes. The changes in properties of the lipid bilayers indirectly affect the structure and function of the proteins embedded in the membranes, including metabolite translocators, with effects on membrane functions and cellular homeostasis. This can trigger intracellular pH acidification, simultaneously with apoplastic alkalinisation (Coote *et al.*, 1991; Grams *et al.*, 2009). It was shown that plants can modify the composition of their membranes by increasing membrane fatty acid saturation in order to acclimate to high temperatures and that higher saturation levels in mutants enhance thermotolerance (Hugly *et al.*, 1989; Falcone *et al.*, 2004; Saidi *et al.*, 2010). It was demonstrated in *Physcomitrella patens* that activation of Ca^{2+} influx at the plasma membrane was one of the first signals to occur within five minutes of heat treatment, which is likely to be a consequence of membrane fluidization on the cyclic nucleotide gated Ca^{2+} channels (Saidi *et al.*, 2009; Finka *et al.*, 2012).

Reactive oxygen species (ROS) are produced during HS, as in response to many other stresses, playing dual roles in signalling towards either survival or programmed cell death, depending on their concentrations (Gechev & Hille, 2005; Suzuki & Mittler, 2006; Locato *et al.*, 2008). They can be produced at various sites in the cell, by ROS-producing enzymes or by basic cellular processes such as the energy metabolism. Disruption of the photosynthetic or respiratory apparatus occurring during HS, as discussed before, can lead to ROS overproduction at the electron transfer chains, which can be deleterious for mitochondria and chloroplasts (Belhadj Slimen *et al.*, 2014; Wang *et al.*, 2018). The membrane NADPH oxidases called respiratory burst oxidases homologs (RBOHs) were also found to be involved in ROS production (superoxide and hydrogen peroxide), acting upstream of the nitric oxide (NO) signalization to induce thermotolerance (Sagi & Fluhr, 2006; Königshofer *et al.*, 2008; Wang *et al.*, 2014a). Moreover, RBOHs were shown to be responsible for H_2O_2 accumulation in the apoplast, which then triggers a ROS wave that is involved in systemic acquired acclimation, that consists in long-distance signalling to induce acclimation of non-challenged tissues (Baxter *et al.*, 2014). H_2O_2 can be considered as a second messenger, as it has a higher half life (1 ms) than other ROS (2-4 µs) and can easily cross membranes (Gill & Tuteja, 2010). ROS can further react with many molecular cell components such as lipids, proteins and nucleic acids. If the capacity of the ROS detoxification machinery is overwhelmed, the accumulation of ROS will inevitably lead to programmed cell death (Vacca *et al.*, 2004).

Concerning DNA, HS is considered to be a damaging agent, as it can cause single- and double-stranded DNA breaks in mammalian cells and also affect the activity of the DNA repair system (Kantidze *et al.*, 2016). In tobacco, heat-induced DNA damage was observed to a greater extent in young plants than in senescent plants, but after 72 h of recovery, the percentage of damaged DNA was comparable to control in both plants, suggesting that the lesions had been repaired (Cvjetko *et al.*, 2014). Interestingly, proteins involved in DNA repair like UVH6 (UV hypersensitive 6), DDB1A and DDB2 (damaged DNA binding protein 1A and 2) appeared to contribute to thermotolerance in Arabidopsis (Larkindale *et al.*, 2005; Ly *et al.*, 2013). Heat was also found to increase organellar DNA migration towards the nucleus, which might be a source of nuclear mutation (Wang *et al.*, 2012). Additionally, prolonged high temperature causes a decrease in the number of nucleosomes and heterochromatin decondensation throughout the genome, which leads to the transcriptional activation of

repetitive elements that are normally silenced under ambient temperatures or short term HS (Pecinka *et al.*, 2010). The occupancy of H2A.Z, a histone variant, was found to decrease with rising temperatures, which facilitates the regulation of the transcription of heat-responsive genes (Kumar & Wigge, 2010).
HS also affects the RNA metabolism by inhibiting splicing in yeast or by increasing alternative splicing in *Physcomitrella patens*, *Arabidopsis thaliana* or *Boechera depauperata,* although patterns seem to be species-specific (Vogel *et al.*, 1995; Chang *et al.*, 2014; Kannan *et al.*, 2018). Because of translational inhibition, some mRNAs (such as ribosomal protein encoding RNAs) are stored in stress granules, while others target degradation (Chantarachot & Bailey-Serres, 2018). In Arabidopsis, mitochondrial RNAs were found to be upregulated by HS and a high proportion of them was polyadenylated, which is normally a signal for their degradation (Adamo *et al.*, 2008). The role of this polyadenylation under HS remains unclear.

The cytoskeleton is also affected by HS. Filamentous actin (F-actin) results from polymerization of 42 kDa proteins called globular actin subunits (G-actin), forming a helical structure (Li *et al.*, 2015). Microtubules are constituted of protofilaments, which are polymers of tubulin dimers (Nogales, 2000). As observed for other proteins, both microtubules and actin networks were shown to be destabilized by HS. In tobacco cells and in Arabidopsis roots, treatments at 42°C or 41°C, respectively, were found to disrupt microtubules (Smertenko *et al.*, 1997; Müller *et al.*, 2007). Depolymerisation of actin filaments was observed in response to a 5 minutes HS at 50°C (Malerba *et al.*, 2010). This effect was suppressed when applying Co^{2+}, an inhibitor of ethylene production, suggesting that ethylene is involved in this response.

Altogether, these deleterious effects on cell organization may lead to cell cycle and growth arrest or even cell death if the severity and/or duration of the stress is too high (Richter *et al.*, 2010). In tobacco BY-2 cells, a mild stress at 30°C could transiently block the cell cycle at the G1/S or G2/M depending on the stage at which the stress was applied (Jang *et al.*, 2005). However, a more severe HS at 55°C for 10 minutes triggered a programmed cell death (PCD) within 72 h (Vacca *et al.*, 2004). Ca^{2+} signalling might be involved in the induction of cell cycle arrest, as it was found in response to other abiotic stresses (Sano *et al.*, 2006). More recently, it was shown that changes in histone acetylation in the promoter regions of the cell cycle genes could modify their expression in response to diverse abiotic stresses in maize (Zhao *et al.*, 2014). In the next part, we will explain how the various cellular perturbations triggered by HS are integrated into a general response, to induce protection mechanisms and heat stress tolerance.

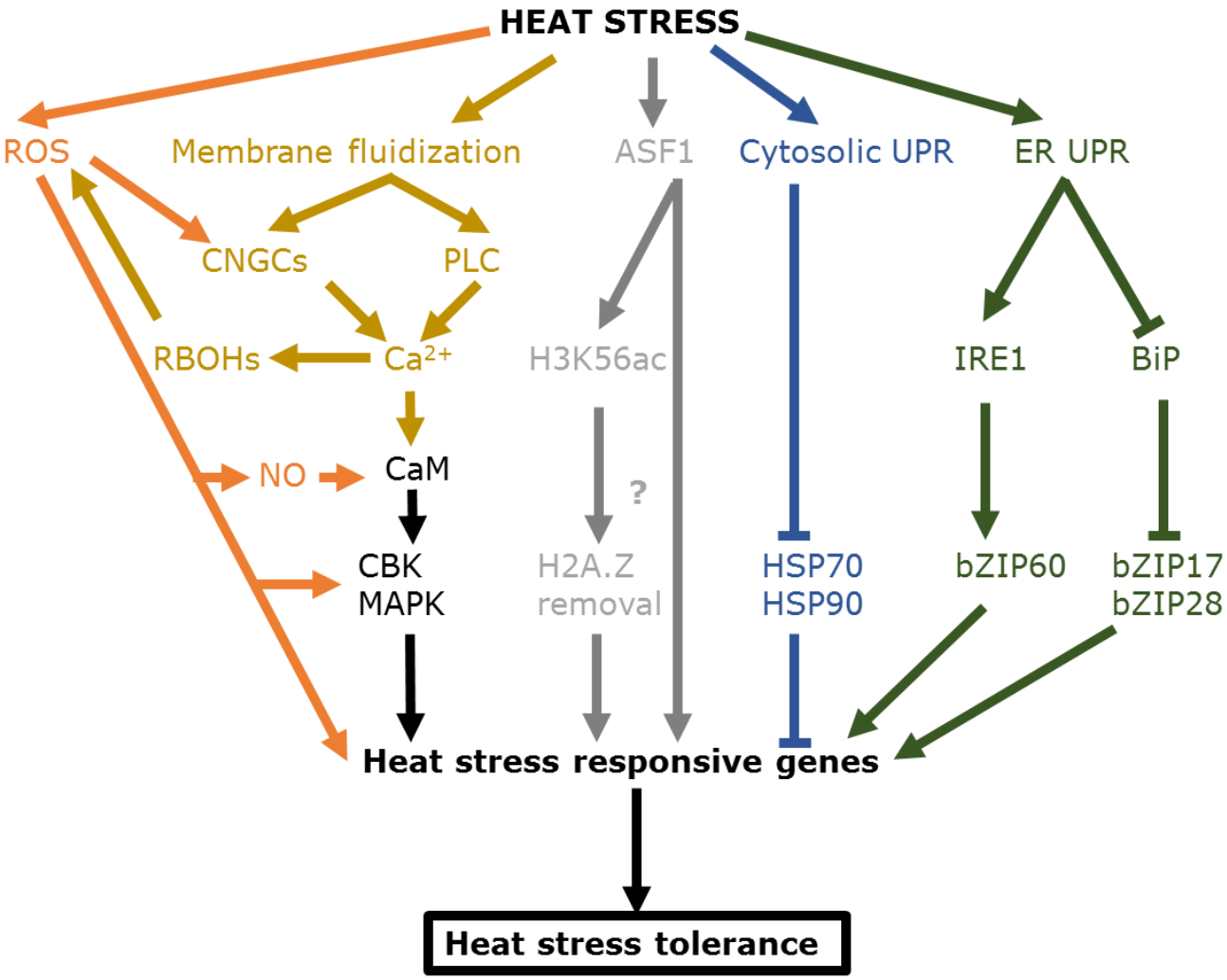

Figure 1.6: The complex early signalling cascade of heat stress response.
ASF1, anti-silencing function 1; BiP, binding immunoglobulin protein; CaM, calmodulin; CBK, calmodulin binding protein kinase, CNGCs, cyclic nucleotide gated calcium channels; ER, endoplasmic reticulum; IRE1, increased organ regeneration 1; NO, nitric oxide; PLC, phospholipase C; RBOHs, respiratory burst oxidases homologs; ROS, reactive oxygen species; UPR, unfolded protein response (adapted from Saidi *et al.* (2011)).

2. The heat stress response

As previously discussed, heat induces significant modifications at the molecular and physiological level, which can lead to programmed cell death. Plants have the ability to survive at temperatures above their optimal for growth, which is referred to as basal thermotolerance (Bokszczanin & Fragkostefanakis, 2013). They can also acclimate to otherwise lethal temperatures, when previously exposed to a sub-lethal temperature (priming), which is defined as acquired thermotolerance. Some molecular mechanisms controlling these responses are common to both basal and acquired thermotolerance, such as the expression of the heat shock transcription factors (HSFs), while others are specific (Larkindale *et al.*, 2005). In wheat, 1314 transcripts were identified as differentially expressed between acquired and basal thermotolerance (Qin *et al.*, 2008). For example, MBF1, a transcriptional regulator regulating ethylene, salicylic acid and trehalose responses during HS, is required for basal but not for acquired thermotolerance, which is also the case for catalase, an enzyme involved in reactive oxygen species (ROS) detoxification (Suzuki *et al.*, 2008). In the following part, we will present an overview of the heat shock response.

2.1. Early signalling cascade

To counteract the deleterious effects of heat on their physiology and metabolism, plants have developed a heat shock response, which is activated by a signalling pathway allowing the up-regulation of protective mechanisms. This response has been studied for years and the signalling cascade has already been well characterized, however, the identification of the primary heat sensor is still debated. As presented before, high temperatures induce major changes on different molecular components in every cell compartment: DNA/RNA and proteins unfolding, cytoskeleton disassembly, membrane fluidization, etc. (Richter *et al.*, 2010). There is therefore likely a multitude of sensors that potentially act as a network to sense temperature changes (Figure 1.6, Ruelland & Zachowski, 2010).

In plants, primary heat sensing was proposed to intervene at membrane level, which would be a conserved response with animals and micro-organisms (Vigh *et al.*, 1998; Saidi *et al.*, 2011). Membrane fluidization was shown to induce the activation of cyclic nucleotide gated calcium channels (CNGC), that are involved in the import of extracellular Ca^{2+} (Finka *et al.*, 2012; Gao *et al.*, 2012). In Arabidopsis, four CNGC (CNGC2, CNGC4, CNGC6, and CNGC16) have been identified as heat-stress responsive (Ohama *et al.*, 2017). Phosphoinositide-specific phospholipases PLC3 and PLC9 are also involved in the accumulation of intracellular Ca^{2+} in response to HS. These enzymes hydrolyse phosphatidylinositol 4,5-bisphosphate (PIP_2) into inositol-1,4,5-trisphosphate (IP_3) and diacylglycerol (DAG), and IP_3 was proposed to be an activator of Ca^{2+} release from intracellular stores (Zheng *et al.*, 2012; Gao *et al.*, 2014). They are both located at the plasma membrane, with PLC3 also located in the nucleus, and they appear to be activated within the first minutes of HS (Ren *et al.*, 2017). The increase in Ca^{2+} would then trigger a signalling cascade mediated by calmodulins (CaM) and kinases (Saidi *et al.*, 2011). Indeed, an Arabidopsis *AtCaM3* mutant displayed a lower thermotolerance than the control, and gene expression for heat shock factors (HSFs) and heat shock proteins (HSPs) was also reduced (Zhang *et al.*, 2009b). The interaction between CaM3 and a CaM-binding protein kinase 3 (AtCBK3) is proposed to activate the heat shock transcription factor 1a (HSF1a) by phosphorylation, which is involved in the transcriptional regulation of many heat responsive

genes (Liu *et al.*, 2008). In alfalfa, a mitogen-activated protein kinase (MAPK) called HAMK (heat-shock activated MAPK), is another kinase that was found to be activated by Ca^{2+} under heat (Sangwan *et al.*, 2002). Hydrogen peroxide has also been demonstrated to act together with this Ca^{2+} signalling pathway, but which one works upstream of the other is unclear, as they were both shown to act on the flux and metabolism of the other (Petrov & Van Breusegem, 2012). Ca^{2+} can activate the production of ROS via the respiratory burst oxidases homologs (RBOHs), which have regulatory domains including calcium-binding EF-hands (You & Chan, 2015), while H_2O_2 signalling is able to induce a biphasic Ca^{2+} response (Rentel *et al.*, 2004). Moreover, H_2O_2 induces the expression of calcium-dependent protein kinases (CDPKs), which might also play a role in the crosstalk between these two signalling pathways (Petrov & Van Breusegem, 2012). H_2O_2 was shown to play an important role in the activation of some HSFs that are involved in the transcriptional regulation of the heat stress response, confirming the importance of this secondary messenger (Volkov *et al.*, 2006). This would occur via "single Cys" or "two-Cys" redox sensory mechanism, which would induce a conformational change in the HSFs, leading to their trimerization and translocation to the nucleus (Driedonks *et al.*, 2015). Another secondary messenger, nitric oxide (NO), was found to act downstream of H_2O_2 in heat signalling (Wang *et al.*, 2014a). Mutants with reduced levels of endogenous NO were found to have a decreased basal thermotolerance, which was linked to a lower expression of *AtCaM3*, leading to a lower HSF-binding and a lower level of heat shock proteins accumulation (Xuan *et al.*, 2010). In this context, it is noteworthy that exogenous application of NO was shown to increase thermotolerance in many plant species (reviewed in Parankusam *et al.* (2017)).

As we described before, protein aggregation is one of the major heat effects affecting cell homeostasis, and it is logically involved in the so-called unfolded protein response (UPR), which contributes to the overall heat shock response (HSR), as it activates some HSFs, even though this response is not as quick as those of Ca^{2+} or H_2O_2 (Mittler *et al.*, 2012). UPR was mostly characterized in the cytosol and the endoplasmic reticulum (ER) but it also occurs in the organelles, such as the mitochondria and chloroplast (Pellegrino *et al.*, 2013; Rochaix & Ramundo, 2015). In the cytosol, the accumulation of misfolded proteins beyond the cytosolic chaperone capacity causes the dissociation of heat shock proteins 70 and 90 (HSP70/HSP90) complexes via a mechanism described as the "chaperone titration model" (Richter *et al.*, 2010). Dissociation of these HSP complexes allows the liberation and trimerization of HSFs that will activate the expression of heat responsive genes such as the HSPs. In Arabidopsis, the cytosolic UPR was notably found to induce the expression of *HSFA2* and *HSFA7a* (Sugio *et al.*, 2009). In the ER, the signalization of the UPR requires the activation of a serine/threonine protein kinase (IRE1b), which splices the mRNA encoding bZIP60, a basic leucine zipper domain containing transcription factor (Deng *et al.*, 2011). A second ER pathway involves two transcription factors located in the ER membrane, bZIP17 and bZIP28, which interact with a chaperone protein called BINDING IMMUNOGLOBULIN PROTEIN (BiP) under normal conditions, and which are released upon stress and then translocated to the Golgi where they are cleaved by serine proteases, allowing their activation and translocation to the nucleus, in a similar way as in mammals and yeast (Moreno & Orellana, 2011; Srivastava *et al.*, 2014; Nawkar *et al.*, 2018).

Modifications at the chromatin level, such as the H2A.Z-mediated changes in nucleosome occupancy evoked earlier, were also found to modulate the transcription of heat-responsive genes by controlling the DNA binding of

repressors and enhancers of the transcription. Indeed, H2A.Z-containing nucleosomes wrap DNA more tightly than H2A-containing nucleosomes and prevent DNA binding of regulatory components. Under high temperature, the occupancy of H2A.Z decreases, allowing the transcription of heat-responsive genes (Kumar & Wigge, 2010). Histone chaperones, which are involved in histone stabilization and nucleosome assembly, could also modulate chromatin access under heat conditions. In *Arabidopsis*, the histone chaperones ANTI-SILENCING FUNCTION 1 (ASF1A and ASF1B) were shown to be part of basal and acquired thermotolerance, by favouring RNA polymerase II accumulation at the promoter and coding regions of some heat responsive genes, such as *HSFs* and *HSPs.* They were also suggested to facilitate histone acetylation (H3K56ac), which was correlated with nucleosome removal and the transcription of *HSFA2* and *HSA32* (Weng *et al.*, 2014).
The involvement of DNA methylation in the heat response is debated (Liu *et al.*, 2015), but it was shown that it could play an important role in basal thermotolerance, as Arabidopsis mutants of the RNA-directed DNA methylation (RdDM) pathway exhibited a lower survival rate after 24-34 h of heat stress at 42°C (Popova *et al.*, 2013). In this study, the expression of several transposons was affected in a *nrpd2* mutant, which was mutated for a subunit of RNA polymerases IV and V involved in small RNA biogenesis and siRNA-dependent DNA methylation. It was proposed that activation of transposons during HS influences the transcription of the adjacent genes, but whether DNA methylation is required for this activation remains unclear.

All these molecular signals and their crosstalk are integrated by the cell to induce the HSR, involving the induction of transcription factors such as the heat shock factors (HSFs) or the dehydration responsive element binding proteins (DREB) (Ohama *et al.*, 2017).

2.2. Transcriptional factors

2.2.1. Heat shock factors

Heat shock factors (HSFs) are a family of transcription factors (TFs) involved in the heat shock response but also in other processes, such as development or ageing and responses to other stresses (Swindell *et al.*, 2007; Akerfelt *et al.*, 2010). Their activation involves their trimerization, which is necessary for DNA binding. HSFs recognize palindromic binding motifs called heat stress elements (HSE: 5' -AGAAnnTTCT- 3'), which are found in the promoter of target genes and conserved in eukaryotes (von Koskull-Döring *et al.*, 2007). In *Saccharomyces cerevisiae, Drosophila melanogaster* and *Caenorhabditis elegans*, a single *HSF* gene is involved in HSR, but also in other signalling pathways, while the mammalian genome contains four *HSFs* isoforms (*HSF1, HSF2, HSF3* and *HSF4*) with distinct biological functions (Akerfelt *et al.*, 2010). Despite a larger diversity in plants (21 different HSFs in Arabidopsis and up to 52 HSFs identified in soybean), all of these TFs harbour a DNA binding domain in their N-terminal sequence, an oligomerization domain (HR-A/B) used for both homomeric and heteromeric interactions and a nuclear localization signal in the C-terminal region of the HR-A/B (Nover *et al.*, 2001; Li *et al.*, 2010b; Scharf *et al.*, 2012). Different classes of HSFs are defined according to their structure and function. HSFA is a class of transcription activators, characterized by the presence of an activator domain (short AHA motifs containing aromatic, hydrophobic and acidic residues) and, in most of them, by an adjacent nuclear export signal in their C-terminal region (Kotak *et al.*, 2004; Scharf *et al.*, 2012). HSFs of class B have a repressor motif

(constituted of a -LFGV- tetrapeptide motif adjacent to basic clusters), and are thus negative regulators of transcription which repress the expression of other HSFs and heat shock proteins, but also of defensin genes (Czarnecka-Verner *et al.*, 2004; Ikeda & Ohme-Takagi, 2009; Kumar *et al.*, 2009; Ikeda *et al.*, 2011). Arabidopsis has only one HSF from class C, which has not been clearly characterized, no activator or repressor domains being identified so far. In monocots, there are several specific HSFC types called HSFC1a, C1b, C2a and C2b; for example, in maize, there are five HSFC members and four in rice, but again their function was not elucidated (Scharf *et al.*, 2012).

Functional characterization of HSFs has enlightened their major role in heat stress tolerance but also in salt/osmotic, anoxic or drought stress responses, especially via the induction of many components of the HSR, such as DREB2A, HSPs and ROS-scavenging enzymes (Guo *et al.*, 2016; Ohama *et al.*, 2017). Genetic evidence has shown that tomato HSFA1 was the master regulator of HSR especially by inducing HSFA2, HSFA7, HSFBs and MBF1c. In Arabidopsis, four members of the HSFA1 class (HSFA1a, HSFA1b, HSFA1d, and HSFA1e) were found as key regulators, even if the quadruple mutant still exhibited a slight acquired thermotolerance (Mishra *et al.*, 2002; Yoshida *et al.*, 2011; Liu & Charng, 2012). HSFA1a and HSFA1b appeared to interact with each other, but also with HSFA2 (Li *et al.*, 2010a,b). *HSFA2* is highly HS-inducible, like many HSFs in plants, which is a unique feature compared to other eukaryotes (Nover *et al.*, 2001). As one of the most highly overexpressed HSF under HS, HSFA2 appears to play an important role in acquired thermotolerance in Arabidopsis, but also in tolerance to anoxia (Banti *et al.*, 2010). The role of HSFA2 in the extension of thermotolerance was shown by the inability of the *hsfa2* mutant to acclimate to heat-shock from two days after a priming treatment (Schramm *et al.*, 2006; Charng *et al.*, 2007). It was also shown that a splicing variant of *HSFA2* was able to bind to a *HSFA2* promoter to positively regulate its own transcription (Liu *et al.*, 2013). *HSFA3* was found to be expressed later during HS compared to *HSFA2* and appeared to be under the control of DREB2A, another TF involved in the HSR through the regulation of dehydration responsive genes (Schramm *et al.*, 2008; Yoshida *et al.*, 2008). HSFA3 is thus a major actor in the crosstalk between heat and drought signalling. In Arabidopsis, HSFA4 was proposed to participate in H_2O_2 sensing and to activate HS-responsive genes, while HSFA5 was shown to interact with HSFA4 by inhibiting its activity in tobacco (Davletova *et al.*, 2005; Baniwal *et al.*, 2007). *HSFA6b* was found to be abscisic acid (ABA) responsive and was capable of activating the expression of DREB2A, and appeared to be the most overexpressed HSF in response to salt stress (Huang *et al.*, 2016). HSFA9 was found to be a seed specific HSF, only expressed during seed maturation under the control of ABI3 in Arabidopsis (Kotak *et al.*, 2007). In tobacco, its overexpression led to earlier cotyledon greening and unfolding during seedling establishment, by increasing the expression of genes linked to photomorphogenesis such as *PhyA* and *PhyB* (Prieto-Dapena *et al.*, 2017). In Arabidopsis, HSFB1 and HSFB2b repress HSFA2, HSFA7a and the expression of several *HSPs* during the HSR attenuation and play an important role in acquired thermotolerance, whereas HSFB1 has a synergetic effect with HSFA1a to induce the upregulation of HS responsive genes in tomato (Bhartu *et al.*, 2004; Czarnecka-Verner *et al.*, 2004; Ikeda *et al.*, 2011).

2.2.2. Other transcriptional factors involved in the HSR

Even if HSFs are the most studied TFs in heat acclimation, others actors such as MULTIPROTEIN BRIDGING FACTOR1C (MBF1C), DREB2 and bZIP28 play a part in this signalization (Ohama *et al.*, 2017). MBF1C was found

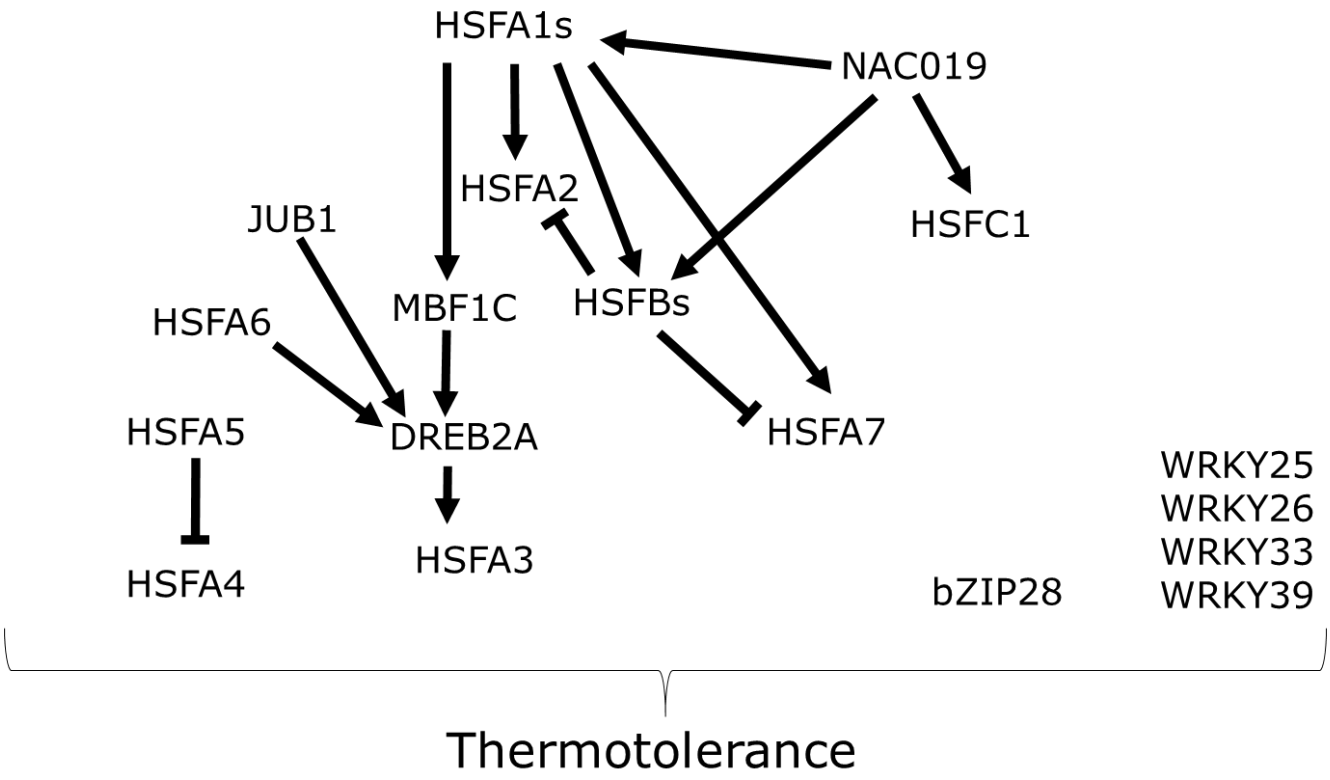

Figure 1.7: The crosstalk between transcriptional factors involved in thermotolerance in *Arabidopsis thaliana*.
bZIP, BASIC LEUCINE ZIPPER DOMAIN CONTAINING TRANSCRIPTION FACTOR; DREB2A, DEHYDRATION RESPONSIVE ELEMENT BINDING PROTEIN 2A; HSF, HEAT SHOCK FACTOR; JUB1, JUNGBRUNNEN 1; MBF1C, MULTIPROTEIN BRIDGING FACTOR 1C (adapted from Ohama *et al.* (2017)).

to play a key role in thermotolerance, upstream of salicylic acid, ethylene and trehalose signalling, but it was not required for HSP synthesis (Suzuki *et al.*, 2008). HSFA1b was demonstrated to interact with a HSE present in the promoter of MBF1c and, in tomato pollen, MBF1C appeared to act downstream of HSFA2 (Bechtold *et al.*, 2013; Fragkostefanakis *et al.*, 2016). MBF1C can activate the transcription of some TFs, including *DREB2A*, through the binding to a putative response element CTAGA (Suzuki *et al.*, 2011). Two NAC TFs, called NAC019 and JUB1, can also induce the expression of some *HSFs* or *DREB2A*, respectively (Wu *et al.*, 2012; Guan *et al.*, 2014), but how their induction is achieved remains elusive. DREBs belong to ERF (ethylene responsive elements binding factors) TF family and bind to dehydration responsive elements in the promoter of drought responsive genes. These TFs are ABA-responsive genes and thus are important integrators of different stresses (cold, drought, salinity, heat, biotic stresses…) (Khan, 2011). In Arabidopsis, *DREB2A* was identified as a drought and heat responsive gene (Sakuma *et al.*, 2006) and this TF was shown to interact with DPB3-1 to induce the transcription of target heat-stress responsive genes (Sato *et al.*, 2014). The membrane-associated basic leucine zipper bZIP28 was also identified as a heat sensor and signal transducer in the ER, as part of the unfolded protein response (Srivastava *et al.*, 2013, 2014; Kataoka *et al.*, 2017). A null mutant for this TF exhibits a heat sensitive phenotype (Gao *et al.*, 2008).

Finally, some members of the WRKY family, another major class of TFs in plants, were also found to be involved in the HSR, even if the function of these TFs was mostly studied in the context of biotic stress responses (Chen *et al.*, 2012). In Arabidopsis, 9 out of 60 analysed members of the *WRKY* family (74 members in total) were found to be affected by heat: eight were upregulated and one was downregulated (Busch *et al.*, 2004). More recently, three members of the family, WRKY25, WRKY26, WRKY33 were identified as master coordinators of the acquisition of plant thermotolerance (Li *et al.*, 2009, 2011). The same researchers also found that *WRKY39* would be involved in heat tolerance, being at the interface between salicylic acid (SA) and jasmonates (JAs) signalling pathways (Li *et al.*, 2010c).

Altogether, these data reveal the complexity of the HSR in plants and the fine regulation of HS-responsive genes expression, such as HSPs, through the crosstalk between the different HSFs and other TFs (Figure 1.7).

2.3. Implication of hormones in thermotolerance

Crosstalk between different hormonal signals are known to play an important role in growth but also in environmental responses, including high temperatures (reviewed in Wahid *et al.* (2007) and Ahammed & Yu (2016)). Abscisic acid (ABA) was found to be one of the major hormones involved in heat response, as *abi-1 (ABA-insensitive 1)*, a mutant for a protein phosphatase involved in ABA sensing, exhibited a highly reduced survival to a one hour treatment at 37°C compared to the Landsberg wild type (Larkindale & Knight, 2002). In the same study, exogenous application of ABA was also shown to slightly improve thermotolerance in seedlings. Mutants affected in ABA synthesis or sensing were found to be impacted in both basal and acquired thermotolerance, except *abi-3* which is seed specific (Larkindale *et al.*, 2005). Interestingly, HSP101 and small HSPs levels in these mutants were not lower than in WT, suggesting ABA acts independently from HSP induction.

However, a recent study in Arabidopsis and tall fescue (*Festuca arundinacea*) showed that exogenous ABA could increase the transcription of *FaHSFA2c* or *AtHSFA2* and *HSP* genes during long-term heat treatment, suggesting that ABA signalling might function upstream *HSFA2* to regulate its transcription (Wang *et al.*, 2017). In another species, *Agrostis stolonifera*, Larkindale & Huang (2005) found that ABA accumulated mostly during the recovery period. Similarly, they found that the ethylene level had increased during the cooling phase after HS. In Arabidopsis, *ein2* and *etr1* mutants, which are defective in ethylene signalling, were affected in basal thermotolerance, while exogenous application of the ethylene precursor ACC (1-aminocyclopropane-1-carboxylic acid) enhanced WT thermotolerance (Larkindale & Knight, 2002; Larkindale *et al.*, 2005). It was hypothesized that ethylene signalling would be involved in the activation of oxidative defences, which are necessary for basal thermotolerance. In tomato pollen, an ethylene-insensitive mutant was found to accumulate less sucrose than WT and exhibited a greater sensitivity to high temperature (Firon *et al.*, 2012). In pea flowers, ethylene production under HS was specifically induced in pre-pollinated ovaries to activate their senescence, but not in pollinated ovaries, which would favour the reallocation of resources towards developing fruits (Savada *et al.*, 2017). Ethylene was shown to act synergistically with jasmonates (JAs) in response to biotic stresses, but investigation of their involvement in abiotic stresses revealed a more complex crosstalk between their signalling pathways (Kazan, 2015). For instance, according to Clarke *et al.* (2009), ethylene negatively regulates HS tolerance in Arabidopsis, whereas JAs act as positive regulators. Indeed, contrary to Larkindale *et al.* (2005), they found that *ein2* mutant displayed a greater thermotolerance, but the differences were likely due to the intensity and duration of the stress and the age of the plants (45°C for 1 h on seedlings in the former and 38°C for 16 h on three-week-old plants in the latter). Levels of jasmonates were upregulated during HS and exogenous application of methyl jasmonate increased basal thermotolerance (Clarke *et al.*, 2009). Salicylic acid (SA), a hormone which is known to play an important role in the systemic acquired resistance in response to biotic stresses, was demonstrated to be essential for basal but not acquired thermotolerance (Clarke *et al.*, 2004). SA was identified as an activator of HSF-DNA binding in human and in tomato, but it is not able to directly induce the transcription of *HSFs* or *HSPs* (Jurivich *et al.*, 1991; Snyman & Cronjé, 2008).

In *Brassica napus* and tomato seedlings, brassinosteroids (BR) also appeared to enhance basal thermotolerance since, during HS, seedlings accumulated higher amounts of HSPs in the presence of 24-epibrassinolide (EBR), and the translational machinery was protected (Dhaubhadel *et al.*, 1999, 2002). Brassinosteroids interact with other hormonal signalling pathways, since exogenous EBR could induce basic thermotolerance, in mutants deficient in or insensitive to ABA, SA, JA and ethylene, in a similar manner to that observed in the wild type (Divi *et al.*, 2010).

In Arabidopsis seedlings, auxin was found to be upregulated and to induce hypocotyl elongation in response to high temperature (Gray *et al.*, 1998). During the reproductive stage, auxin appeared to be downregulated in Arabidopsis anthers or barley panicles, and exogenous application of auxin could reverse high temperature-induced male sterility (Sakata *et al.*, 2010).

Exogenous application of cytokinins could repress heat-induced senescence in grass under HS (Xu & Huang, 2009) and it also improved heat tolerance at the flowering stage, in an opposite manner to gibberellins that caused flower abortion (Sobol *et al.*, 2014). In contrast to other hormones, the exogenous application of gibberellins seems to have a negative effect on heat tolerance (Maestri *et al.*, 2002). However, gibberellins are required for

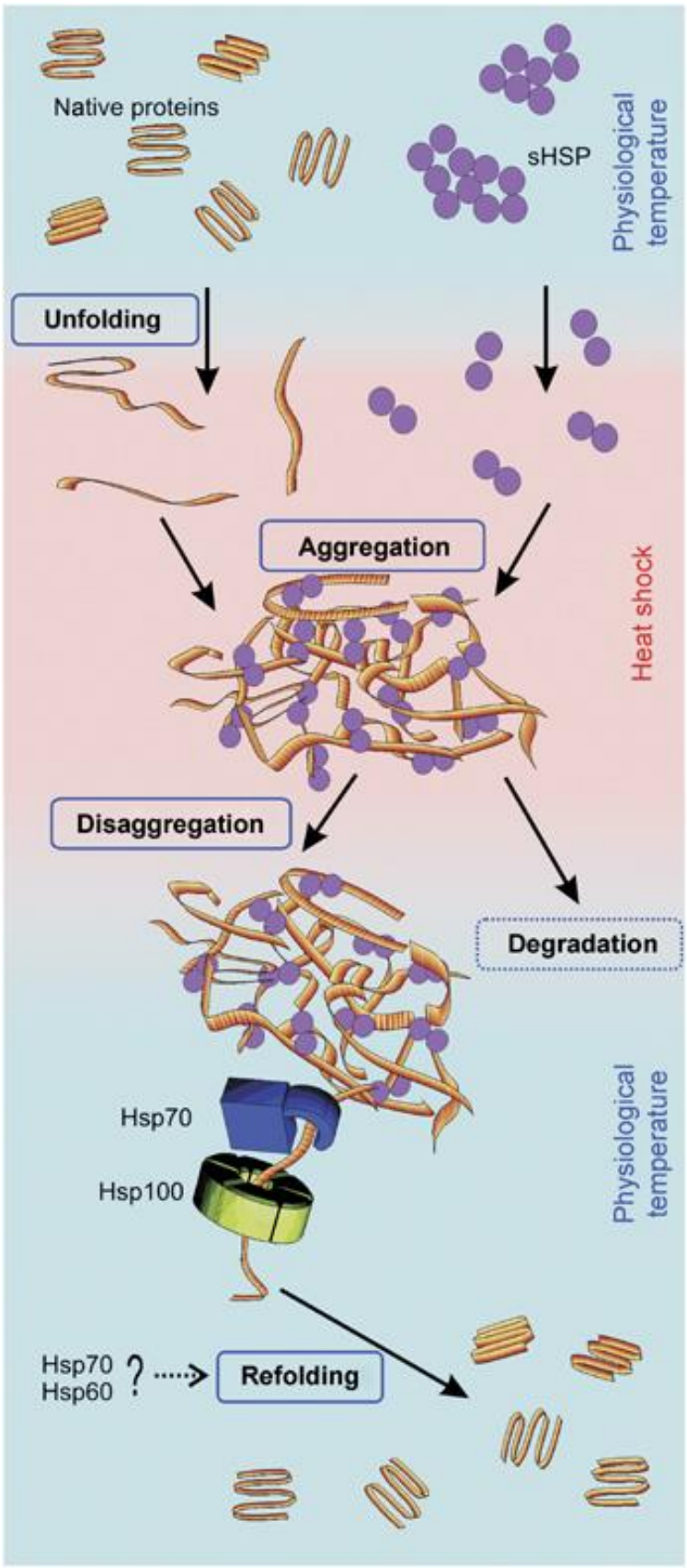

Figure 1.8: Scheme of protein disaggregation process by HSP machinery during heat stress recovery. Upon heat stress, sHSPs are activated by dimerization and bind to the unfolded proteins. They form aggregates that can be disaggregated during recovery by the HSP100/HSP70 complex, which allows protein refolding (from Liberek *et al.* (2008)).

hypocotyl elongation during seedling establishment under high temperature, together with auxin and BR (Stavang *et al.*, 2009).

Altogether, this hormonal crosstalk constitutes a complex signalization which is crucial in the HS response but also in the tolerance to combination with other stresses. However, responses might differ depending on the species, the developmental stage, the stress duration and intensity, which makes them difficult to understand and integrate.

2.4. Protective mechanisms

2.4.1. Heat shock proteins

Heat shock proteins (HSPs) are a large family of chaperone proteins found in all organisms, which were first identified as proteins that accumulate in response to heat stress, but which are also induced in response to other stresses, such as salt, drought or oxidative stress. Some of them are constitutively expressed and regulate many cellular functions such as protein folding and trafficking or signal transduction. They are present in every compartment in the eukaryotic cell and play a role in by assisting in the folding of many proteins. They are classified into different classes depending on their molecular mass: HSP100, HSP90, HSP70, HSP60, sHSP, which have different functions (Wang *et al.*, 2004; Swindell *et al.*, 2007; Richter *et al.*, 2010; Finka *et al.*, 2016; Jacob *et al.*, 2017). HSP90 are the major soluble proteins in eukaryotic cells, representing 1-2 % of total proteins in unstressed cells. They are ubiquitous and are involved in many different cellular processes such as protein folding and trafficking, signal-transduction (activation of protein kinases and hormone sensors) and cell proliferation control (Wang *et al.*, 2004; Erlejman *et al.*, 2014). Their structure comprises an N-terminal ATPase domain, a substrate binding middle domain and a C-terminal domain involved in their dimerization (Kadota & Shirasu, 2012). They are required for both normal development and stress tolerance. Arabidopsis genome encodes seven different HSP90 (four cytosolic and three targeted to either the chloroplast, mitochondria or ER) (Krishna & Gloor, 2001). Inhibition of HSP90 activity by geldanamycin or radicicol caused serious perturbations of Arabidopsis seedling development, affecting colour, shape and the growth of organs (cotyledons, root, true leaves) (Queitsch *et al.*, 2002). In an inbred line, a spectrum of different phenotypes depending on the genetic background was observed when reducing HSP90 activity, suggesting HSP90 could buffer phenotypic variability due to cryptic polymorphism. This confirmed results already observed in Drosophila (Rutherford & Lindquist, 1998). Together with HSP70s, HSP90s play a significant role in the HSR. Indeed, in normal conditions, they sequester inactive monomeric HSFA1 into complexes. Upon stress application, these HSPs will preferentially bind to the accumulating unfolded proteins, thus releasing the HSFs which can then oligomerize (active form) in the presence of ROS and translocate to the nucleus to induce transcription of their target genes (Jacob *et al.*, 2017).

HSP70/DnaK class are a family of molecular chaperones involved in the proper folding of nascent proteins and their translocation. They also prevent unfolded proteins from aggregating and participate in the refolding of aggregated proteins in cooperation with HSP100 (Figure 1.8, Liberek *et al.*, 2008; Richter *et al.*, 2010). They are assisted by the co-chaperone HSP40/DnaJ and the nucleotide releasing protein GrpE. HSP70 are constituted of a N-terminal ATPase domain and a C-terminal substrate binding domain, which are separated by a hinge region.

In many of them, a C-terminal short 5 kDa subdomain is also found and seems to be involved in the interaction with co-chaperones (Sung *et al.*, 2001a). In Arabidopsis, twelve full-length and two truncated sequences of this family were identified: five cytosolic (and potentially the two truncated), three binding proteins (BiP) in the ER, two mitochondrial and two plastidial. Even if HSP70 are constitutive, most of them were found upregulated in response to heat and/or cold but also during seed maturation, and the profiles were different depending on the organs studied (Sung *et al.*, 2001b). Overexpression of *Hsc70-1* was shown to enhance thermotolerance, although it produced a dwarf phenotype under normal conditions, while reduction of its expression appeared lethal (Sung & Guy, 2003). Mutants of the plastidial HSP70 were also produced: c*phsc70-2* had a normal phenotype, while c*phsc70-1* had an impaired development under normal conditions and exhibited a lower seed thermotolerance. No double mutant could be obtained, suggesting that these proteins are essential for survival (Su & Li, 2008).
HSP60 or chaperonins are also essential for proper development. These proteins that can be assisted by their co-chaperone HSP10/GroES are involved in the folding of newly synthetized or misfolded proteins to acquire their native structure (Wang *et al.*, 2004). They are present in the cytosol, but also in the mitochondria and chloroplast where they contribute to the folding of organellar proteins, either imported or synthesized *in organello*. In maize, mitochondrial chaperonin was indeed found to interact with newly synthetized mitochondrial proteins (Prasad *et al.*, 1990). Chloroplastic chaperonins ptCpn60α and ptCpn60β were also found to be important actors in plastid division and light-induced greening (Suzuki *et al.*, 2009).

HSP100 or Clp (caseinolytic protease) constitute an inducible class of HSPs, which functions in protein disaggregation and/or degradation in collaboration with other HSPs, in particular with the HSP70 machinery (Figure 1.8). Their role is to refold potentially harmful misfolded or denatured client proteins, thus maintaining cellular proteostasis. They possess a N-terminal domain supposed to be involved in substrate recognition and binding, and one or two nuclear binding domains involved in ATP binding and hydrolysis, and protein oligomerization. They are organized in hexameric rings (Liberek *et al.*, 2008; Mishra & Grover, 2016). In Arabidopsis, a cytosolic HSP101 mutant called *hot1* lost seed basal thermotolerance and seedling acquired thermotolerance, even though protein accumulation was similar to WT. A single mutation of Glu into Lys in the ATP binding domain, was predicted to compromise its function (Hong & Vierling, 2000; Queitsch *et al.*, 2000). It was found that a mutation in a mitochondrial transcription termination factor (*shot1*) could suppress the heat-sensitive phenotype of *hot1-4*, probably via a decrease of oxidative stress (Kim *et al.*, 2012). Recently, HSP101 was also demonstrated to be important during stress recovery by releasing ribosomal protein mRNAs from stress granules, which is essential for translation enhancement after heat shock (Merret *et al.*, 2017). Moreover, it seems that HSP101 plays an important role in acclimation memory, by promoting the production of HSA32, a 32 kDa heat-stress-associated protein important for memory, which in turn retards HSP101 degradation, thus constituting a positive feedback loop which prolongs acclimation "memory" (Wu *et al.*, 2013).
Small HSPs (sHSPs) are ATP-independent chaperones ranging from 12 to 42 kDa, which constitute the least conserved and perhaps the least understood family of molecular chaperones. These highly stress-inducible HSPs are found in all three kingdoms of life, but are especially prominent in plants with a dozen of *sHSP* genes (Waters, 2013). Their structure comprises a non-conserved N-term domain, a highly-conserved alpha-crystalline domain (ACD) and a short C-term sequence. This domain would be involved in dimerization, while NTS and CTS could

have a role in the assembly of higher-order oligomers and the interaction with unfolded polypeptides (Waters, 2013). Indeed, these proteins can co-assemble and cooperate, forming disperse hetero- or homo-oligomers (from 12 to more than 32 subunits). Their activation occurs by dissociation to a dimeric form, and their role would be to stabilize early unfolding intermediates, thus preventing irreversible protein aggregation (Figure 1.8). However, they cannot refold unfolded and aggregated proteins without the cooperation of HSP70/40 and HSP100 (Haslbeck & Vierling, 2015). Indeed, a biophysical study of *Caenorhabditis elegans* sHSP17 suggested that sHSPs form sheet-like super-molecular assemblies at high temperature, providing a platform for sequestering unfolded polypeptides to facilitate interactions with unfolding chaperones (Zhang *et al.*, 2015b). In bacteria, it seems that sHSPs interact preferentially with proteins involved in translation or metabolic enzymes and that the mass ratio instead of the molar ratio plays an important role in the interactions (Haslbeck & Vierling, 2015). In Drosophila, the endogenous overexpression of a mitochondrial sHSP could counteract oxidative stress and dramatically increase longevity (Morrow *et al.*, 2004b), while its reduction was correlated with a loss of longevity (Morrow *et al.*, 2004a,b). The Drosophila protein was also shown to increase the longevity of human fibroblast genes (Wadhwa *et al.*, 2010). Genes involved in mitochondrial energy production and protein synthesis where shown to be upregulated in flies overexpressing mitochondrial sHSP, reinforcing their role in lifespan extension and stress tolerance (Kim *et al.*, 2010; Morrow & Tanguay, 2015).

Arabidopsis genome encodes 19 different sHSPs classified into eleven classes depending on their location and structure (six cytosolic, one in the ER, one peroxisomal, one plastidial and two mitochondrial) (Siddique *et al.*, 2008). A few of them were functionally characterized, but their mode of action and their targets are still poorly understood. In the chloroplast, HSP21 was found to be involved in the protection of plastid transcription but also photosynthesis through interaction with PS II subunits (Zhong *et al.*, 2013; Chen *et al.*, 2017). In plant mitochondria sub-mitochondrial particles, sHSPs were shown to have a protective effect on the activity of complex I under heat or salt stress (Downs & Heckathorn, 1998; Hamilton & Heckathorn, 2001). In tomato cultured cells, a mitochondrial sHSP (M-sHSP) was found to accumulate in response to H_2O_2 exposure, suggesting a role in the protection against oxidative stress (Banzet *et al.*, 1998). In tobacco, the overexpression of a tomato M-sHSP considerably protected the transgenic plants from a 48°C lethal heat shock (Sanmiya *et al.*, 2004). The constitutive ectopic expression of the maize M-sHSP22 in Arabidopsis increased the expression level of several HSPs upon heat treatment, suggesting a retrograde regulation (Rhoads *et al.*, 2005). However, the thermotolerance of these overexpressing transgenic lines was only slightly improved. At a whole, sHSPs in mitochondria appear to have important roles for stress tolerance and longevity, but their molecular functions in plants still await elucidation.

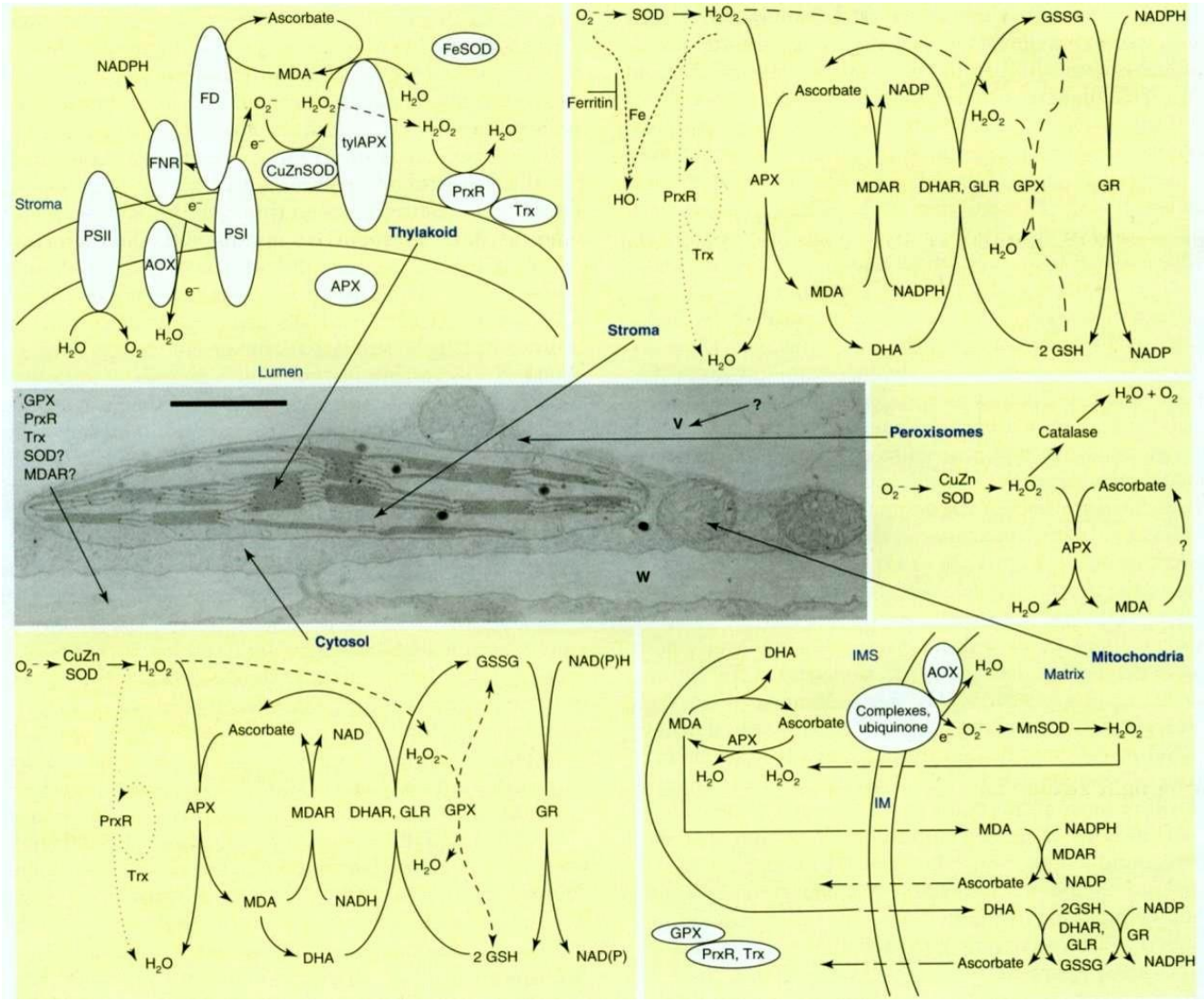

Figure 1.9: ROS scavenging pathways in plants.
AOX, alternative oxidase; APX, ascorbate peroxidase; DHA, dehydroascorbate; DHAR, DHA reductase; FD, ferredoxin; FNR, ferredoxin NADPH reductase; GLR, glutaredoxin; GPX, glutathione peroxidase; GR, glutathione reductase; GSH, reduced glutathione; GSSG, oxidized glutathione; IM, inner membrane; IMS, IM space; MDA, monodehydroascorbate; MDAR, MDA reductase; PrxR, peroxiredoxin; PSI, photosystem I; PSII, photosystem II; SOD, superoxide dismutase; Trx, thioredoxin; tyl, thylakoid (from Mittler *et al.*, 2004).

2.4.2. ROS balance

As we previously discussed, ROS play an important role in heat signalling. Contrary to Ca^{2+} which can be stored and released to control signal propagation, ROS levels essentially depend on their rate of production and detoxification because they are short-lived species (Mittler *et al.*, 2004). However, a fine regulation of cellular ROS levels is essential because their accumulation can be deleterious for cell components, and even lead to death. Indeed, oxidative stress corresponds to a situation in which imbalance of ROS production and removal by anti-oxidant systems favour the over accumulation of the potentially harmful species. Thus, the induction of ROS detoxification mechanisms during HS is expected to be essential for the acclimation process. In Arabidopsis, a network of at least 152 genes is involved in the tight control of ROS levels in the cell (Mittler *et al.*, 2004), and the compartmentation of the main ROS scavenging systems is presented in Figure 1.9. The HSR includes the upregulation of the ROS-scavenging enzymes at both transcriptional and translational levels (Rizhsky *et al.*, 2002; Vacca *et al.*, 2004). HSFA2 seems to be a major transcriptional activator of genes encoding ROS scavenging enzymes during heat stress (Driedonks *et al.*, 2015). The upregulation of ascorbate peroxidase (APX) and catalase (CAT) was observed in heat stressed tobacco cells (Locato *et al.*, 2008). Peroxisomal CAT and cytosolic APX were demonstrated to play a role in the protection against ROS-induced DNA damage. Surprisingly, the double mutant *apx1/cat2* exhibited a higher thermotolerance than the single mutants, and it was proposed that a DNA damage response was constitutively activated by ROS in this double mutant, which blocked the cell cycle but also programmed cell death (PCD). On the contrary, in the *apx1* single mutant, there was more DNA damage due to higher levels of ROS, which led to the induction of PCD. In the WT, the accumulation of detoxifying enzymes would maintain a low level of ROS and thus, would prevent DNA damage (Vanderauwera *et al.*, 2011).
H_2O_2 pre-treatment was also found to enhance thermotolerance in many plant species, by increasing the activities of APX, CAT, superoxide dismutase (SOD), glutathione reductase and the total thiol content (Hossain *et al.*, 2015). Moreover, the exogenous application of $CaCl_2$, ABA, SA and ACC were shown to enhance the activities of different ROS-scavenging enzymes upon HS (Larkindale & Huang, 2004). Another secondary messenger, NO, is tightly related to ROS metabolism. In many species, NO triggers the activity of ROS-detoxifying enzymes, such as ascorbate peroxidase or glutathione reductase and pre-treatment with sodium nitroprusside (SNP), a NO donor, increased the pool of ascorbate and glutathione (Parankusam *et al.*, 2017). HSPs have also been suggested to be involved in the enhancement of the activity of SOD, CAT and APX (Driedonks *et al.*, 2015).

2.4.3. Metabolic adaptation

Since temperature is a physical factor that has effects on the structure of cellular components, but also on the rate of biochemical reactions, high temperature stress has strong effects on metabolism. The response to high temperature includes the accumulation of molecules that could act as compatible solutes (free radical scavengers, chemical chaperone activity or maintenance of cell turgor) (Wahid *et al.*, 2007). Among them, increased levels of sugars such as raffinose, sucrose, fructose, glucose and galactinol contents were observed, while starch content decreased (Kaplan *et al.*, 2004; Rizhsky *et al.*, 2004). These changes in sugar levels might influence ROS

metabolism, membrane stability and signalization (Keunen *et al.*, 2013). The transcriptional activation of galactinol synthases and raffinose synthase by HSFA2 was shown to increase galactinol and raffinose levels, which could scavenge hydroxyl radicals and thus, decrease oxidative stress in Arabidopsis (Nishizawa *et al.*, 2008). Amino acids were also found to accumulate under abiotic stresses, which could result from increased amino acid synthesis and/or from stress-induced protein breakdown, or a decrease in protein synthesis (Krasensky & Jonak, 2012). During heat stress, the accumulation of branched chain amino acids Val, Leu and Ile and hydrophobic amino acids Phe, Trp, Tyr might participate in the stress tolerance, probably because they serve as precursors for secondary metabolites, such as glucosinolates or flavonoids (Mayer *et al.*, 1990; Kaplan *et al.*, 2004). Concerning Pro, the response appears to be variable: for example, in tomato and tobacco, Pro level is upregulated upon HS, while in Arabidopsis, it is accumulated five times less in acclimated plants than in non-acclimated plants and Pro over-accumulation in proline oxidase/dehydrogenase mutants prevented the acclimation process at 45°C (Rivero *et al.*, 2004; Larkindale & Vierling, 2007; Cvikrová *et al.*, 2012). Levels of GABA, beta-Ala and putrescine were also found to be increased in response to HS (Kaplan *et al.*, 2004). Mutants for genes encoding enzymes involved in the GABA shunt exhibited higher stress sensitivity and a higher ROS level, suggesting an important role of this pathway through ROS scavenging in relation to regulation of the carbon and nitrogen metabolism (Krasensky & Jonak, 2012). Putrescine could have a role in regulating photosynthesis under stress, as it seems to act as a buffer in thylakoids by decreasing the ΔpH, and thus maintaining electron transfer (Ioannidis *et al.*, 2012). Glycine betaine also accumulates under HS in some plant species and is suggested to protect the photosystem II and stabilize membranes; however, many plants, such as Arabidopsis, tobacco or rice do not produce glycine betaine (Wahid *et al.*, 2007; Krasensky & Jonak, 2012).

All these observations point to the occurrence of metabolic adaptations occurring under HS. However, a global overview of the regulation of these adaptations is still lacking. Indeed, the metabolic fluxes are difficult to measure and to understand, as they are highly dynamic. Rather than being constituted of independent metabolic pathways, the metabolism is a complex network, which is regulated at multiple levels: transcriptional, post-transcriptional, translational and post-translational regulations of the enzymes, biochemical properties of the enzymes and transport across or through membranes. The development of metabolome-wide fluxes (fluxomics) and its integration with expression data should lead to a better understanding of the global stress responses of plants.

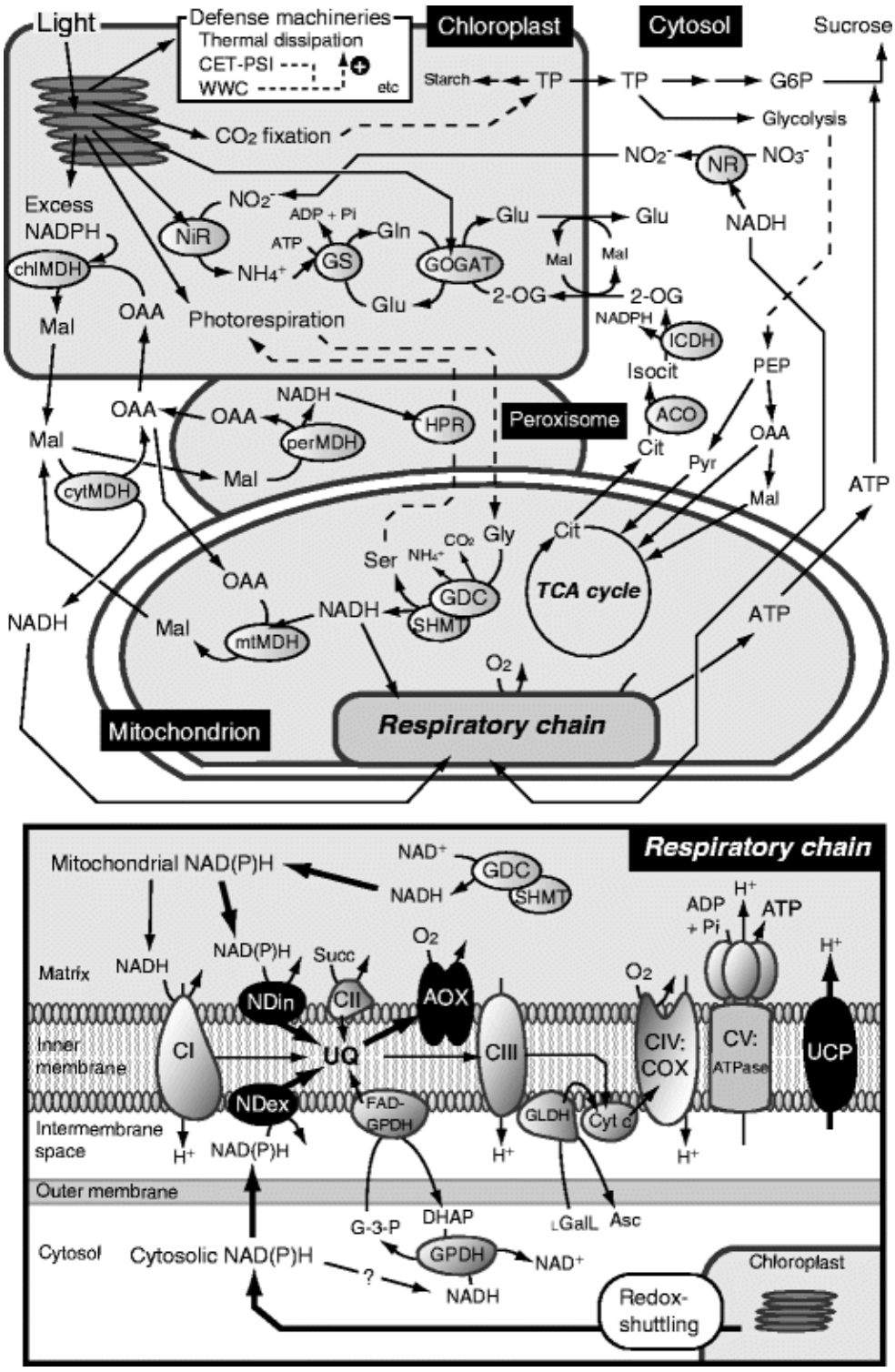

Figure 1.10: Metabolic interactions between the organelles occurring in the light.
ACO, aconitase; AOX, alternative oxidase; Asc, ascorbate; CET-PSI, cyclic electron transport around photosystem I; Cit citrate; COX, cytochrome c oxidase; DHAP, dihydroxyacetone phosphate; L Gall, L-galactono-1;4-lactone; GDC, Gly decarboxylase complex; GLDH, L GalL dehydrogenase; G-3-P, glycerol-3-phosphate; GOGAT, glutamine-2-oxoglutarate aminotransferase; GPDH, G-3-P dehydrogenase; GS, glutamine synthetase; G6P, glucose-6-phosphate; HPR, hydroxypyruvate reductase; ICDH, NADP-isocitrate dehydrogenase; IDH, NAD-isocitrate dehydrogenase; Isocit, isocitrate; Mal, malate; MDH, malate dehydrogenase; ND, NAD(P)H dehydrogenase; NiR, NO2-reductase; NR, NO3-reductase; OAA, oxaloacetate; 2-OG, 2-oxoglutarate; PEP, phosphoenolpyruvate; Pyr, pyruvate; SHMT, Ser hydroxymethyltransferase; TP, triose phosphate; UCP, uncoupling protein; UQ, ubiquinone; WWC, water–water cycle (from Yoshida & Noguchi, 2011).

3. Mitochondrion and chloroplast: two essential organelles in plant

3.1. Metabolic hubs

Mitochondria and chloroplasts are often defined as the "powerhouses" of photosynthetic cells. This definition, although simplistic, has the merit of highlighting the primordial function of these organelles in plants. Indeed, both organelles generate reducing power and ATP, which provide energy for many reactions occurring in organisms, including biosynthesis, transport and degradation pathways of RNA, proteins and metabolites. Photosynthesis and respiration are two processes that balance each other: one produces substrates that can be broken down by the other process. However, the functions of the mitochondrion and chloroplast and their interactions are much more complex, as these organelles constitute major metabolic and signalling hubs (Figure 1.10, Araújo *et al.*, 2014).

The mitochondrial energy metabolism has generally been considered to be a dedicated pathway that uses breakdown products of glycolysis to produce reductants through the TCA cycle (Fernie *et al.*, 2004). By oxidizing NADH and $FADH_2$, the electron transport chain (ETC) then builds up the proton gradient necessary for the operation of ATP synthase. However, this simple vision of the mitochondrial metabolism has evolved to a more complex one, in particular concerning the TCA cycle (Figure 1.10). The beta-oxidation of fatty acids and the degradation of amino acids (especially branched-chain amino acids) were found to be other important sources of TCA cycle metabolites (Sweetlove *et al.*, 2010). Moreover, most of the reactions of the TCA cycle can be by-passed by cytosolic enzymes and thus, the mitochondrial TCA cycle does not operate independently, but rather interacts with cytosolic and plastidial metabolites via metabolic shuttles present at the mitochondrial membrane (Sweetlove *et al.*, 2010; Millar *et al.*, 2011). Another adaptive trait of plant mitochondria is the presence of additional complexes in the ETC: an alternative oxidase (AOX), several NAD(P)H dehydrogenases and uncoupling proteins (UCPs) (reviewed in Møller, 2001; Millenaar & Lambers, 2003; Rasmusson *et al.*, 2008). They play a significant role in response to many stresses such as drought, salt and cold, by controlling the mitochondrial ROS production and maintaining photosynthetic activity throughout the operation of the malate valve (Begcy *et al.*, 2011; Dinakar *et al.*, 2016; Wanniarachchi *et al.*, 2018). AOX was also shown to contribute to the reoxidation of mitochondrial NADH during photorespiration (Vanlerberghe, 2013). These supplementary machineries increase the flexibility of energy metabolism, and thus, play an important role in the rapid adaptation to environmental changes, which is crucial for sessile organisms like plants.

Concerning photosynthesis, it has been one of the most extensively characterized physiological process in plants, as it is a major component influencing plant growth and yield. By the 1970s, a broad overview of the light reactions, the Calvin cycle and photorespiration had already been obtained (Halliwell, 1978). Besides energy transduction, plastids are involved in the biosynthesis of carbohydrates, amino acids, lipids, nucleotides, pigments, hormones and vitamins. For example, they are able to produce 17 out of the 20 proteinaceous amino acids, among which ten are exclusively synthetized in the chloroplast, which makes plastids essential components of nitrogen metabolism (Rolland *et al.*, 2018). Lipid synthesis necessitates the coordination of chloroplasts

together with the ER: C16 and C18 fatty acids are produced in the chloroplast and can then be used to produce lipids in chloroplast (said "prokaryotic pathway") or in the ER ("eukaryotic pathway") (Li-Beisson *et al.*, 2013). Metabolite exchanges between the two compartments might occur through unidentified transporters or by direct contact between their membranes (Bobik & Burch-Smith, 2015).

The chloroplast metabolism is also connected to peroxisomes because they participate in photorespiration, fatty acid degradation, ROS detoxification but also in the synthesis of hormones (JAs, auxin, SA) (Kaur *et al.*, 2009; Bobik & Burch-Smith, 2015).

The chloroplast and mitochondrion thus constitute two essential metabolic hubs connected with each other and with the rest of the cell and their various activities must be finely controlled to ensure the proper functioning of plant metabolism.

3.2. Communicating organelles: anterograde and retrograde signalling

The mitochondrion and chloroplast are organelles originating from two endosymbiotic events: the first would have derived from an alpha-proteobacterium–like ancestor entering an Archea-type host around 1.5 billion years ago, while the second would have derived from a cyanobacterium entering a mitochondriate eukaryote between 1.2 and 1.5 billion years ago (Dyall *et al.*, 2004; Martin *et al.*, 2015). After these events, the original genomes of the endosymbionts were considerably reduced, many genes being transferred to the nucleus and others lost. Thus, these previously autonomous endosymbionts changed into organelles. In *Arabidopsis thaliana*, the mitochondrial genome currently encodes around 122 protein coding genes, while the chloroplast genome encodes 88 protein coding genes as defined by the TAIR 10 database (https://www.arabidopsis.org/), while their original endosymbionts had several thousand genes. According to the subcellular localization database for Arabidopsis proteins (SUBA 4; http://suba.live/) consensus, 3060 proteins are predicted to be localized in mitochondria and 3597 proteins in plastids, which means that respectively only 4 % and 2.4 % of the mitochondrial and plastidial proteins are encoded by the organellar genomes (Hooper *et al.*, 2017). Moreover, many components of the organellar transcriptional and translational machinery are encoded by the nucleus, even if the genomes of the organelles comprise some ribosomal subunits and ribosomal RNA encoding genes (Liere *et al.*, 2011). All known organelle transcription factors including RNA polymerases are encoded by the nucleus, except one plastid-encoded RNA polymerase. Organellar post-transcriptional regulation also involves nuclear-encoded proteins for RNA splicing, processing, editing and translation, such as the pentatricopeptide-repeat (PPR) proteins, which constitute a large family of proteins conserved in eukaryotes, but with highly variable targets (Manna, 2015; Guillaumot *et al.*, 2017).

This complex partnership implies a tight coordination in the regulation of the expression of organelle and nuclear genes through anterograde (nucleus-to-organelles) and retrograde (organelles-to-nucleus) signalling pathways (Woodson & Chory, 2008). Via retrograde signalling, mitochondria and chloroplasts can transmit developmental or stress signals to the nucleus (Figure 1.11). In mitochondria, a dysfunction of the electron transfer chain affects the transcription of several genes (e.g. *AOX* in plants or genes involved in ageing control or programmed cell death in yeast or animals), via an increased concentration in ROS or Ca^{2+} which can activate kinases and protein

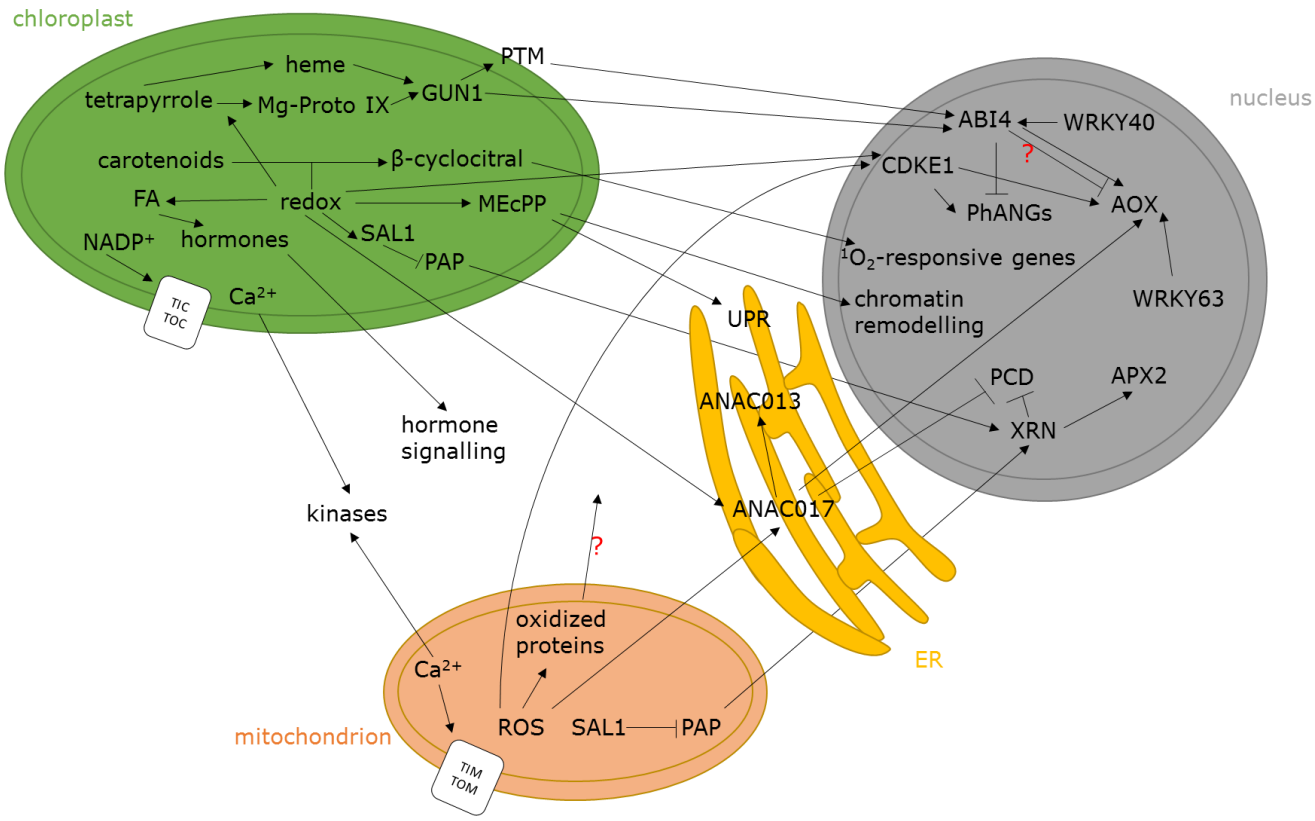

Figure 1.11: Complex crosstalk of retrograde signalling coming from chloroplast and mitochondrion. ABI4: ABA insensitive 4; AOX: alternative oxidase; APX2: ascorbate peroxidase 2; CDKE1: cyclin-dependent kinase E1; FA: fatty acids; MEcPP: methylerythritol cyclodiphosphate; $^1O_2$: singlet oxygen; PAP: 3'-Phosphoadenosine 5'-phosphate; PCD: programmed cell death; PhANGs: photosynthesis-associated nuclear genes; ROS: reactive oxygen species; TIC/TOC/TIM/TOC: translocases of the outer/inner membranes of chloroplast and mitochondrion; UPR: unfolded protein response; XRN: exoribonuclease (adapted from de Souza *et al.* (2017))

phosphatases for signal transduction (Amuthan *et al.*, 2001; Borghouts *et al.*, 2004; Lai *et al.*, 2006; Rhoads & Subbaiah, 2007). In yeast, aerobic or hypoxic conditions are perceived through the oxygenic-dependent haem synthesis, which can thereafter interact with Hap1 in the nucleus to regulate the transcription of genes involved in respiration and ergosterol synthesis (Hickman & Winston, 2007). ROS also seem to play a significant role in the oxidation of mitochondrial proteins, which would trigger their degradation. Some oxidized peptides would then be exported to the cytosol and addressed to the nucleus, where they could activate the expression of specific sets of genes (Møller & Sweetlove, 2010). However, whether such a process occurs in plants has not been clearly demonstrated.

The retrograde signalling of the chloroplast has been more extensively studied than that of the plant mitochondrion. Six Arabidopsis mutants, called *genome uncoupled* (*gun*), which exhibited deregulation of nuclear encoded plastid proteins led to the identification of key regulators of the chloroplast-nuclear communication. GUN1 encodes a PPR-containing protein that would interact with many plastidial components, such as transcriptional, translational or protein import machineries (Colombo *et al.*, 2016). GUN1 was shown to induce the transcription of *ABI4* (ABA-insensitive 4), a TF which represses several nuclear genes encoding photosynthetic proteins. The activation of *ABI4* would occur through the translocation to the nucleus of PTM, a plant homeodomain transcription factor otherwise localized at the chloroplast envelope (Chan *et al.*, 2016). GUN1 was also proposed to interact with the synthesis of tetrapyrrole derivatives such as heme or Mg-protoporphyrin IX (a precursor involved in chlorophyll biosynthesis), in which the other five *gun* mutants are involved (de Souza *et al.*, 2017). An increased level of β-cyclocitral, a byproduct of carotenoid oxidation, would also activate the transcription of the singlet oxygen responsive genes, while methylerythritol cyclodiphosphate (MEcPP), an isoprenoid precursor, would modify chromatin remodeling and thus gene expression (Chi *et al.*, 2015). As major metabolites in chloroplasts, fatty acids, and especially their oxidized derivatives, are also important actors of retrograde signaling (de Souza *et al.*, 2017).

Since mitochondria and chloroplasts are both involved in energy and primary metabolism, coordination of their activities is essential for their proper functioning, as previously discussed. However, besides the exchange of metabolites (e.g. redox shuttles, ATP, ROS …) which occurs between the organelles, the way they perceive their respective status is still misunderstood. Some studies have shown that deficiencies in one organelle can alter the transcription of components of the other, but it is unclear if this retrograde signalling goes through the nucleus and its anterograde response, or if the two organelles can directly signal to each other (Woodson & Chory, 2008). Until now, studies are rather in favour of the first hypothesis: some metabolites and TFs were found to be upregulated by both plastidial and mitochondrial signals allowing the coordination of the organelles' activities. For example, an enzyme called SAL1 is present in both the mitochondrion and chloroplast and regulates the level of phosphoadenosine phosphate (PAP) by dephosphorylating it to form AMP. PAP is supposed to be exported from the organelles and to regulate nuclear gene expression by inhibiting the activity of some exoribonucleases, resulting in an altered mRNA stability and transcriptional changes, such as the induction of ascorbate peroxidase 2 (Chi *et al.*, 2015). Some NAC domain-containing TFs localized at the ER membrane, ANAC013 and ANAC017, were also shown to migrate to the nucleus in response to oxidative stress signals coming from the mitochondrion or chloroplast (Kleine & Leister, 2016). ANAC017 and PAP pathways seem to be partly convergent and would be

involved in the suppression of programmed cell death (Van Aken & Pogson, 2017). Also, *ABI4* would integrate signals from GUN1 and from the mitochondrion to regulate the expression of *AOX1* and photosynthetic genes (Kmiecik *et al.*, 2016). It would act in synchronisation with the nuclear encoded cyclin-dependent kinase E1 (CDKE1), which integrates chloroplast and mitochondrial redox status, to regulate AOX1 but not the photosynthetic genes (Blanco *et al.*, 2014). WRKY40 and WRKY63 TFs are both responsive to plastidial and mitochondrial dysfunction, but the first would be an inhibitor of the transcription of *AOX1a*, *NDB2* (*NAD(P)H DEHYDROGENASE B2*), *UPOX* (a marker of oxidative stress), and *AtBCS1* (*CYTOCHROME BC1 SYNTHESIS*), while the other would favour their expression (Ng *et al.*, 2014; de Souza *et al.*, 2017). WRKY40 would participate in the regulation of *ABI4* (Kmiecik *et al.*, 2016). However, all these pathways are not fully elucidated and the integration of the different signals is yet to be understood. Indeed, it is suggested that mitochondria and chloroplasts might signal their functional state to the nucleus through metabolic signatures instead of unique "factors" released by the organelles (Pfannschmidt, 2010).

Organelle retrograde signalling could play an important role in the acquisition of thermotolerance, as it was recently shown that the heat induction of *HSP21*, together with *HSFA2* and other heat responsive genes, was highly reduced in the *gun5* mutant, leading to damage on the PSII and a heat-sensitive phenotype. This suggests a significant role of chloroplast retrograde signalling in the induction of plastidial thermotolerance (Chen *et al.*, 2017). ROS, tetrapyrroles and Ca^{2+} from the organelles would act together to mediate the HSR (Sun & Guo, 2016). In *Caenorhabditis elegans* and maize, mitochondrial dysfunction can also lead to the expression of mitochondrial HSPs (Kuzmin *et al.*, 2004).

Besides the regulation at the transcriptional level, the import of cytosolic proteins and their assembly into the organelles must also be finely regulated, because some important complexes such as the electron transport components comprise subunits coming from both the cytosol and the organelles. The majority of proteins are imported into the organelles via the translocases of the outer/inner membranes Toc/Tic (in chloroplast) or Tom/Tim (in mitochondrion) through the recognition of the N-terminal targeting signal of the proteins (reviewed in Paila *et al.* (2015) and Wiedemann & Pfanner (2017)). The import regulation must take into account the metabolic state of the organelles, and even though it cannot really be considered as a retrograde signalling process, it seems that the redox signals play an important role in the regulation of protein import (Stengel *et al.*, 2010). In the chloroplast outer membrane, the reduction of disulfide groups on Toc75 channel and Toc159, Toc34 and Toc64 receptors was shown to increase precursor import, while oxidation reduced import efficiency. At the inner membrane, high levels of $NADP^+$ would participate in the recruitment of Tic32, Tic55 and Tic62 close to Tic110 channel to favour the import of precursors, although some precursors were found to be imported in a $NADP^+$-independent manner (Stengel *et al.*, 2010). In mitochondrion, the regulation is quite different and only concerns some classes of proteins. Proteins which possess conserved motifs containing cysteine residues can be imported by the Tom complex in a reduced and unfolded state. They are then oxidized and thus folded by Mia40, which permits to retain these proteins in the intermembrane space. Reoxidation of Mia40 is performed by Erv1, an enzyme which uses O_2 for its own reoxidation (Stengel *et al.*, 2010). Calmodulin-mediated Ca^{2+} signalling was also proposed as a regulator of the import of inner membrane and matrix proteins, given that pharmacological inhibition of Ca^{2+} or calmodulin led to a severe impairment in mitochondrial protein import (Kuhn *et al.*, 2009).

All these redox regulations could modulate the import of proteins into the organelles and thus affect their function.

3.3. Dynamic organelles

Besides their functional metabolic and signalling interactions, organelles interact with a dynamic structural network, the cytoskeleton (microtubules and actin microfilaments), with which, or on which, they can move, and also establish physical connections (Perico & Sparkes, 2018). The cytoskeleton displays a high motility together with the ER, Golgi apparatus, peroxisomes and mitochondria. Plastid movements are rather slow and are mainly linked to external stimuli, such as light, touch or chemicals, together with endogenous regulation occurring during cell division (Suetsugu & Wada, 2007). Light-related chloroplast movement (also known as chloroplast photorelocation movement) was the most widely studied response. Exposure to high light intensity makes chloroplasts move away from the light source in order to avoid oxidative stress (avoidance response), while low light makes them move towards light to maximize photon capture (accumulation response) (Suetsugu & Wada, 2007). To induce this response, blue light is perceived by phototropins, which are located at the plasma membrane (Kong & Wada, 2014). Some major proteins, such as PLASTID MOVEMENT IMPAIRED 1 (PMI1) or PLASTID MOVEMENT IMPAIRED1-RELATED (PMIR1, PMIR2) were found to be essential for the relocation of plastids and the nucleus in response to light (Suetsugu *et al.*, 2015). CHLOROPLAST UNUSUAL POSITIONING1 (CHUP1), an actin binding protein, would also act with kinesin-like proteins (KACs) to bind actin filaments and participate in chloroplast anchoring to the plasma membrane, while other proteins, such as JAC1, PMI2 or WEB1 would be involved in the disappearance of cp-actin filaments (Oikawa *et al.*, 2008; Kong & Wada, 2014).

Mitochondria are highly dynamic organelles, which move in connection with the actin microfilaments in plants, and with the microtubule network in mammals (Logan, 2010; Li *et al.*, 2015). A plant cell can contain several hundreds of mitochondria, which are referred to as the chondriome: there are 200-300 discrete mitochondria in Arabidopsis mesophyll cells and 500-600 in tobacco mesophyll protoplasts (Logan, 2010). Mitochondria are not produced by *de novo* formation, but by growth and division (Arimura, 2018). The chondriome is highly dynamic: changes in mitochondrial shape, number, size, motility and cellular distribution are frequent and modulate many processes, including bioenergetics, autophagy or programmed cell death (PCD) (Welchen *et al.*, 2014). Mitochondrial motility is essential for mitochondria to meet and fuse, a process through which they can mix and exchange DNA, proteins or metabolites (Logan, 2010). Indeed, all mitochondria do not contain the same amount of DNA material and thus their fusion and fission are necessary for DNA replication and maintenance (Arimura, 2018). Mitochondrial movement was first reported more than a century ago (Lewis & Lewis, 1915), and since, lots of studies have tried to describe and explain their dynamics, including their fusion and fission events (Logan, 2010). Myosin proteins are likely to serve as motor proteins, allowing organellar movement along actin filaments. Mitochondrial fission and fusion events are rapid, as a green fluorescent protein (GFP) from a mitochondrion could be redistributed to the other mitochondrion of the same cultured fibroblast cell within an hour (Youle *et al.*, 2012). Components of the fission apparatus include dynamin-like proteins DRP3A and DRP3B (homologs of DNM1/DRP1 in yeast and animals, respectively) and a mitochondrial outer membrane anchored protein called BIGYIN (homologous to FIS1), because mutants affected in these genes were found to have a lower number of mitochondria but with a larger size (Logan, 2006). Another mutant called *network* (*nmt*) exhibited altered mitochondrial morphology, by the presence of long interconnected mitochondrial tubules up to 10 µm in length

(Logan *et al.*, 2003). However, the role of NETWORK was not determined to date, even if it is likely to be allelic to *elm1* (*elongate mitochondria*), a mutant defective in a mitochondrial outer membrane protein that is necessary for localization of DRP3A (Logan, 2010; Arimura, 2018). Cardiolipins, which are mitochondrial phospholipids mostly present in the mitochondrial inner membrane, were also found to stabilize DRP3 complexes (Pan *et al.*, 2014). In this study, a mutant of *cardiolipin synthase* (*cls-1*) exhibited a mitochondrial morphology similar to that of *drp3A-2 drp3B-2* double mutant, revealing the potential role of CLS in mitochondrial fission. Concerning mitochondrial fusion, little data are available, as most fusion related proteins identified in yeast and animals have no homologues in Arabidopsis (Logan, 2010). One Arabidopsis mutant called *friendly*, in which mitochondria were found to be clustered, was identified as an important factor of inter-mitochondrial association, which is required during the early steps of mitochondrial fusion (El Zawily *et al.*, 2014). A knock-out mutant in HeLa cells of CLUH, the mammalian ortholog of FRIENDLY, displayed a similar clustering phenotype, but also several metabolic alterations that strengthen the link between mitochondrial dynamics and metabolic status (Wakim *et al.*, 2017). Mitochondrial interactions with the ER also seem to play a role in their dynamics: the size of ER polygons was shown to influence the mitochondrial fusion and fission processes (Jaipargas *et al.*, 2015).

Besides its role in the maintenance of DNA and mitochondrial metabolism, mitochondrial dynamics plays an important role in the inter-organellar communication and in energy distribution within the cell. As described earlier, chloroplasts and mitochondria are essential for many cellular processes and their activities are tightly correlated. As reviewed by de Souza *et al.* (2017), morphological transition and proximity between mitochondria, chloroplasts and peroxisomes should facilitate communication and the exchange of metabolites through the tethering of their membranes in response to light and thus improve the efficiency of photorespiration. Direct interactions via stromules, matrixules and peroxules, which are thin tubules emanating from the chloroplast, mitochondrion and peroxisome, respectively, have not been clearly established, but they might also play a role in inter-organellar communication (Osteryoung & Pyke, 2014). Even though no direct physical interaction was found, mitochondria were shown to follow the pattern of chloroplasts in the avoidance response to high light, which is likely a way to favour metabolic exchanges between the two compartments (Islam *et al.*, 2009; Islam & Takagi, 2010). Although the role of organelle dynamics is still debated, it could play a significant role in stress tolerance, in particular under heat stress since dynamics and structure of the chondriome were strongly affected by a severe heat shock in Arabidopsis mesophyll protoplasts (Scott & Logan, 2008).

4. Thesis aims

This PhD research was performed at the Research Institute on Horticulture and Seeds (IRHS), in the Seedling, Metabolism & Stress team, which investigates the mechanisms that contribute to efficient seedling emergence and establishment under environmental constraints. The research was supported by the ACCLIMHOT project "*Integrative analysis of acquired thermotolerance in Arabidopsis seedlings*", within the framework of the regional programme "Objectif Végétal, Research, Education and Innovation in Pays de la Loire". The general aim was to provide a comprehensive knowledge of the mechanisms of heat stress acclimation using an integrative approach, and in particular to understand the contribution of energy metabolism.

Given the crucial role of chloroplasts and mitochondria in plant metabolism and signalling, they are already known to be important actors in plant adaptation to stresses. However, even if the HSR has already been widely explored and the impact of HS on both respiration and photosynthesis has previously been studied in many plant species, their actual contributions to HS tolerance is still poorly understood. Moreover, many data have been acquired in different species, at different developmental stages, and with different temperatures regimes, but so far, no integrative analysis has been performed in a unique system with standardized conditions for the acquisition of multiscale data. Furthermore, studies have often focused on moderate heat-stress (known as priming treatment) but not on lethal HS; it is nevertheless important to know what distinguishes the two types of cellular responses to these stresses.

The objectives of this thesis were therefore to acquire a better understanding of the acclimation of both respiration and photosynthesis in seedlings by a multiscale approach using physiology, cell biology, transcriptomics, proteomic and metabolic profiling. This study was performed in an original model system, previously developed in the team (Benamar *et al.*, 2013), which allows the analysis of HS acclimation processes in developmentally arrested seedlings, under mineral nutrient limitation. The liquid culture in mineral water provides a large and homogenous population of seedlings, making stress responses easier to study.

The different chapters aim to answer the following questions:

- How do seedlings under developmental arrest survive for weeks under nutrient limitation?
- How do respiration and photosynthesis acclimate to HS in seedlings? How are organelle dynamics and the actin network affected by HS? Are they involved in acclimation?
- What are the molecular responses involved in this acclimation to HS?
- How long do seedlings maintain acclimation memory? Are HSPs involved in the heat memory?

Chapter II- Seedlings maintained in a developmental steady state to study stress tolerance

1. Introduction

Seedling constitutes a transitive stage between the highly stress tolerant seed and the mature plant. Stress tolerance often decreases during germination and early seedling establishment and even though this stage is short, it is one of the most stress sensitive stage in plant development. Because of their ephemeral nature, it is relatively difficult to phenotype seedlings and study the responses to their environment. For example, it can be tricky to compare the behaviour of genotypes that differ in their growth rate during seedling establishment, as their expansion likely influences their response.

In our team, a system of liquid culture was previously developed in order to facilitate seedling phenotyping (Benamar *et al.*, 2013). First, some trials were done by using classical Murashige and Skoog liquid medium under shaking, but this type of culture required seed sterilization and was susceptible to fungal and bacterial contaminations. To counteract this effect, seeds were rather germinated in distilled water or in different commercial mineral waters under shaking in six-well plates or Erlenmeyer. In distilled water and several mineral waters, the elongation of radicle led to clumping of seedlings, whereas in Evian mineral water, root growth was lower and seedlings could stay dispersed in the medium (Benamar *et al.*, 2013). In this liquid culture, seedling development is rapidly arrested and they do not develop true leaves, because of nutrient limitation. In this part, we will characterize and discuss the evolution of developmentally arrested seedlings within the first four weeks of culture. This chapter is presented as a publication published in The Plant Journal.

2. Publication

Arabidopsis seedlings display a remarkable resilience under severe mineral starvation using their metabolic plasticity to remain self-sufficient for weeks

Authors:

Elise Réthoré[1], Sabine d'Andrea[2], Abdelilah Benamar[1], Caroline Cukier[1], Dimitri Tolleter[1], Anis M. Limami[1], Marie-Hélène Avelange-Macherel[1], David Macherel[1]*

Contact information :

[1]IRHS, Université d'Angers, INRA, Agrocampus-Ouest, SFR 4207 Quasav, 42 rue Georges Morel, 49071 Beaucouzé, France

[2] Institut Jean-Pierre Bourgin, INRA, AgroParisTech, CNRS, Université Paris-Saclay, RD10, 78026 Versailles, France

***Correspondence:** david.macherel@univ-angers.fr; Tel.: +33-241-225-531

Abstract

During the life cycle of plants, seedlings are considered vulnerable because they are at the interface between the highly stress tolerant seed embryos and the established plant, and must develop rapidly, often in a challenging environment, with limited access to nutrients and light. Using a simple experimental system, whereby the seedling stage of Arabidopsis is considerably prolonged by nutrient starvation, we analysed the physiology and metabolism of seedlings maintained in such conditions up to four weeks. Although development was arrested at the cotyledon stage, there was no sign of senescence and seedlings remained viable for weeks, yielding normal plants after transplantation. Photosynthetic activity compensated for respiratory carbon losses, and energy dissipation by photorespiration and alternative oxidase appeared important. Photosynthates were essentially stored as organic acids, while the pool of free amino acids remained stable. Seedlings lost the capacity to store lipids in cytosolic lipid droplets, but developed large plastoglobuli. Arabidopsis seedlings arrested in their development because of mineral starvation displayed therefore a remarkable resilience, using their metabolic and physiological plasticity to maintain a steady state for weeks, allowing resumption of development when favourable conditions ensue.

Key words: Arabidopsis, carbohydrate metabolism, energy metabolism, nutrient limitation, photorespiration, photosynthesis, plastoglobule, respiration, seedling

2.1. Introduction

Seedlings play a pivotal role in the life cycle of plants, forming the bridge between the heterotrophic embryo and the established photo-autotrophic plant. Emerging from the protective coverings of the seed coat in the soil or on the surface, the seedling is immediately exposed to a range of abiotic and biotic stressors. The success of the seedling establishment is thus critical for the development of plant populations in the natural environment and in the context of crop production (Leck *et al.*, 2008). This is reflected by the importance afforded to the concept of seed vigour, which is the combination of intrinsic seed properties that, besides storage ability, contribute to efficient germination and seedling emergence under unfavourable environmental conditions (Finch-Savage and Bassel, 2016). In spite of its essential role in plant life, there is no consensus definition of what constitutes the seedling stage, with disparities depending on species and type of study (Hanley *et al.*, 2004). While the start of the seedling stage is unequivocally marked by radicle protrusion, the timing of its end is often less clear. In the case of Arabidopsis (*Arabidopsis thaliana* (L.) Heinh.), the seminal stereologic study of (Mansfield and Briarty, 1996) described the rapid succession of developmental and physiological transitions of Arabidopsis early development. The developmental stages were later phenotypically established throughout the whole life cycle to unify the collection of phenotypic data, although a seedling stage was not clearly assigned (Boyes *et al.*, 2001). Hereafter, we will consider that the seedling stage starts with radicle emergence and terminates with the elongation of the first two leaves, lasting around six days in the conditions of Boyes *et al.* (2001). Arabidopsis, now well recognized for its central role as a genetic model, is a small ruderal weed with a rapid life cycle, which is able to thrive in poor soils and in a great variety of climates (Mitchell-Olds and Schmitt, 2006; Krämer, 2015). Its seeds are minuscule (< 0.5 mm), and the lipid reserves are sufficient only to fuel initial embryo growth, including the rapid development of photosynthetic tissues that is essential for establishment. This transition is part of photomorphogenesis, a developmental program orchestrated by photoreceptors and an array of signalling cascades that, within a few hours, transforms the germinated embryo into a phototrophic seedling (Wu, 2014; Warpeha and Montgomery, 2016). Further growth and development of the seedling appears to be largely dependent on the nutritional status, and in particular upon the C/N balance (Martin *et al.*, 2002; Zheng, 2009). This developmental regulation requires the coordinated expression of clusters of genes in response to nutrient sensing and signalling pathways, including hormones and microRNAs regulators (Liang *et al.*, 2012; Vidal *et al.*, 2014). While the mechanisms of seed storage oil mobilization have been thoroughly investigated (Graham, 2008), the physiology and metabolism of the autotrophic seedling has received less attention, though a recent study revealed a metabolic shift associated with the transition from seed to seedling, which appeared largely under transcriptional control (Silva *et al.*, 2017). Although Arabidopsis cotyledons are embryonic organs, they are partially homologous to leaves since they carry out photosynthesis, and numerous mutants show partial transformation of specific features of one organ onto the other, like for instance, the appearance of leaf trichomes on cotyledons (Chandler, 2008). The role of cotyledons as sources of photosynthesis-derived sugars to control and fuel root growth of Arabidopsis seedlings has been demonstrated, emphasizing the sequential role of light, first as a developmental trigger, then as an energy source (Kircher and Schopfer, 2012). Arabidopsis seedlings are thus pioneer individuals able to perform most of basic plant metabolism, and the importance of their early life for local adaptation was recently highlighted in a large scale field study (Postma and Ågren, 2016). In the

environment, seeds may germinate in conditions where mineral nutrients are very limited, which may compromise subsequent development and seedling establishment. To our knowledge, little is known about how seedlings adapt their metabolism to survive under nutrient starvation until conditions improve. We have previously described a liquid culture system in which the seedling stage can be extended because of nutrient limitation (Benamar *et al.*, 2013). In this system, Arabidopsis seeds are germinated in Evian natural mineral water under shaking, producing seedlings that are photosynthetically active, but unable to form leaves because of the low amount of mineral nutrients available. The initial amount of nutrients present in the mineral water avoids a rapid elongation of the radicle, preventing the clumping of seedlings that would occur in deionised water. Although seedlings are grown in liquid, the medium remains normoxic thanks to the large surface of the wells and shaking. Even though this system is artificial, and it is unlikely that seedlings would be exposed to such a severe mineral deficiency in nature, it offers a useful model to study the seedling stage, which is difficult to investigate because it is transient and accompanied by dramatic changes in development, physiology and metabolism. These "arrested-development" seedlings remain green for several weeks, but it is unclear how they manage to survive under mineral starvation. One hypothesis is that photosynthetic activity is sufficient to compensate for carbon losses via respiration and that macronutrients are recycled, as growth is completely repressed. Here, we present the results of our investigation into the physiology and metabolism of seedlings maintained for up to four weeks under conditions of "arrested-development". Besides providing a comprehensive view of the physiology of seedlings, our results uncovered the importance of energy-dissipation mechanisms to overcome the seemingly most hazardous stage in plant life.

2.2. Materials and methods

2.2.1. Plant material

Arabidopsis thaliana Col-0 dry seeds were added to the wells of six-well plates containing 6 mL of commercially available Evian natural mineral water (pH= 7.2; concentration in $mg.L^{-1}$: Ca^{2+}: 80; Mg^{2+}: 26; Na^{+}: 6.5; K^{+}: 1; SiO_2: 15; HCO_3: 360; SO_4^{-}: 12.6; Cl^{-}: 6.8; NO_3^{-}: 3.7), according to Benamar et al. (2013). Plates were incubated at 4°C in the dark for 24 h and then incubated in a growth room (16 h of light, 150 µmol $photons.m^{-2}.s^{-1}$, 21°C/19°C, 60 % humidity) under rotary shaking (135 rpm). Arabidopsis plants were grown on soil under the same growth room conditions. Some experiments were also performed using the photorespiratory mutant *glyk1-1* (Boldt *et al.*, 2005) and a line (35S:PGL35:GFP) expressing a GFP-tagged plastoglobule protein (Vidi *et al.*, 2006). For CO_2 enrichment experiments, after three days of culture the medium was changed for a solution of 10 mM $NaHCO_3$, 10 mM MOPS (pH 7.2) in 25% (v/v) Evian natural mineral water, which was then continuously renewed (around 3 mL per hour).

2.2.2. Biomass measurements

Fresh weight was measured after collecting the content of each well (seeds/seedlings) by filtration with a 0.45 µm nylon membrane (Merck KGaA, Darmstadt, Germany) using a water-driven vacuum pump aspirator. Dry weight was measured after drying the same samples for 24 h at 96°C.

2.2.3. Oxygen measurements

Measurements of O_2 exchange were performed using an Oxylab electrode system with a white light source LED1/W (Hansatech, King's Lynn, UK) at 25°C, in 1 mL Evian natural mineral water containing around 20 mg germinating seeds, 50 mg seedlings or vacuum-infiltrated fragments of mature leaves from four-week-old plants. For net photosynthesis assay, light was calibrated at 150 (growth room conditions) or 700 µmol photons.m^{-2}.s^{-1} (saturating light) using a QRT1 Quantitherm (Hansatech). For light response assay, different light intensities (from 0 to 100 µmol photons.m^{-2}.s^{-1}) were applied. Rates were standardized using dry weight or chlorophyll amount. Total chlorophyll was extracted in 1 mL dimethyl-N-formamide overnight in the dark and chlorophyll amount was determined by spectrophotometry according to the formula (Total chlorophyll (µg) = 7.04 A664 + 20.27 A647) of Moran (1982), using a microplate reader FLUOstar Omega (BMG Labtech, Ortenberg, Germany).

2.2.4. Western blot

For the immunodetection of glycine decarboxylase H protein (GDC-H), alternative oxidase (AOX1 and AOX2 isoforms) and isocitrate lyase (ICL), total proteins were extracted in 50 mM $NaPO_4$ pH 8, 10 mM Ethylenediaminetetraacetic acid (EDTA), 0.1 % (v/v) Triton-X 100, 0.1 % (m/v) Sarcosyl, 10 mM dithiothreitol (DTT), 1 mM phenylmethane sulfonyl fluoride (PMSF) and antiproteases (cOmplete EDTA-free, Roche, Basel, Switzerland). Protein concentration was determined using the Bradford protein assay (Bio-rad, Marnes-La-Coquette, France) with bovine serum albumin (BSA) as protein standard. Proteins separated on 12 % Stain Free Gels (Bio-Rad) were blotted to PVDF (Merck KGaA, Darmstadt, Germany) using tank transfer (10 mM N-cyclohexyl-3-aminopropane sulfonic acid (CAPS) pH 11, 10 % EtOH). Blots were blocked in TBST buffer (50 mM Tris–HCl, pH 7.4, 150 mM NaCl, 0.1 % (v/v) Tween 20) containing 3 % (m/v) defatted dry milk, then incubated in the same buffer containing primary antibodies for 1.5 h, at 4°C, under shaking. Anti-GDC-H (Cat# AS05074, RRID:AB_1031689), anti-AOX1/2 (Cat# AS04054, RRID:AB_1031839) and anti-ICL (Cat# AS09500, RRID:AB_1832014) rabbit polyclonal antibodies from Agrisera (Vännäs, Sweden) were respectively diluted to 1:3000, 1:1000 and 1:1000 and secondary antibody (goat anti-rabbit IgG horse radish peroxidase conjugated (Cat# AS09602, RRID:AB_1966902), Agrisera) diluted to 1:75,000. Blots were developed with Western Clarity ECL (Bio-Rad). Oleosin immunodetection was performed according to D'Andréa *et al.* (2007). Protein loading on membrane was estimated by UV detection according to Stain-free technology (Bio-Rad). For semi-quantitative analysis, pixels of chemiluminescence were quantified in every lane and were normalized based on the intensity of the RbcL band detected by UV on the membranes. For each protein, the normalized intensities were then expressed as the percentage of the signal detected in d28 sample on the same membrane.

2.2.5. Metabolic profiling

Seedlings or leaves were harvested and flash frozen using liquid N_2, lyophilized and ground with glass beads (3 mm) using a TissueLyser (Qiagen, Hilden, Germany) at 30 Hz for 1 min. Dry seed samples were ground using a mortar and pestle. Polar metabolites were extracted with 300 µL methanol/750 µL chloroform/300 µL water. Alpha-aminobutyric acid, adipate and melezitose were used as internal standards. Polar phase was dried using a miVac QUATTRO concentrator (SP Scientific, Ipswich, UK) and residue solubilized in 300 µL deionized water.

Standardized volumes of samples were dried and derivatized with 50 µL pyridine/methoxyamine hydrochloride (20 mg. mL^{-1}) for 1.5 h at 30°C and then with 50 µL N-Methyl-N-tert-butyldimethylsilyltrifluoroacetamide (MTBSTFA) for 30 min at 70°C. Analyses were carried out according to Bobille *et al.* (2016), except for the elution profile: 70°C for 5 min, linear gradient of 5°C min^{-1} to 300°C, 300°C for 5 min, resulting in a total run time of 56 min. For the detection of sugars, samples were diluted 1:80 and analysed by HPLC at 30°C with 10 % (m/v) NaOH on a Carbopac PA-1 column (Dionex Corp., Sunnyvale, CA, USA) using pulsed amperometric detection, as described by Tetteroo *et al.* (1994). Fatty acid analysis of lyophilized samples was performed according to Deruyffelaere *et al.* (2015). All metabolic data were normalized to dry weight measured after lyophilisation.

2.2.6. Optical and transmission electron microscopy

For starch detection, seedlings were depigmented with 96° ethanol overnight at 4°C and stained with Lugol's iodine solution. Observations were performed using an Axio Imager Z2 with an EC Plan-Neofluar 10x objective (Carl Zeiss Microscopy GmbH, Göttingen, Germany). For the observation of lipid droplets, seedlings were incubated for 15 min in Nile red (1 µg.mL^{-1}). Live cell confocal laser scanning microscopy was performed using a Nikon A1 microscope driven by NIS Elements software (Nikon France S.A, Champigny sur Marne, France) with a Nikon Plan Fluor 10x objective (NA 0.3) or a Nikon CFI Apo 40x WI objective (NA 1.25). Excitation/emission wavelengths (nm) were as follows: Nile red, 561/570-620; chlorophyll autofluorescence 638/662-737; GFP 488/500-550. For transmission electron microscopy, samples were fixed in 2.5 % (w/v) paraformaldehyde and 2.5 % (v/v) glutaraldehyde in 50 mM phosphate buffer (pH 7.2) overnight at 4°C under vacuum and post-fixed for 1 h in 1 % (w/v) osmium tetroxide. After dehydration with ethanol they were embedded in epon resin, and ultrathin sections (60 nm) were cut with a diamond knife using a Leica UC7 (Leica, Rueil Malmaison, France), stained with 3 % (m/v) uranyle acetate in 50° ethanol for 15 min and observed using a JEM 1400 electron microscope (JEOL, Tokyo, Japan). Plastoglobule size was measured by image analysis using Fiji software (Schindelin *et al.*, 2012).

2.2.7. Enzyme assays

Samples of dry seeds or seedlings were ground in liquid nitrogen using a mortar and pestle and proteins were extracted in 50 mM 3-(N-morpholino)propane sulfonic acid (MOPS) pH 7.2, 1 mM EDTA. After centrifugation at 15,000 g for 15 min at 4°C, the supernatant was used for enzymatic assays. Malate synthase and isocitrate lyase assays were adapted from Cooper & Beevers (1969).

Malate synthase was measured at 25°C in 50 mM tricine pH 8.0, 5 mM MgCl2, 1.5 mM DTNB (5,5'-dithio-bis-[2-nitrobenzoic acid]), 200 µM acetyl-CoA. The reaction was initiated with 20 mM glyoxylate and absorbance followed at 412 nm with a SPECTROstar Nano (BMG Labtech, Ortenberg, Germany). Isocitrate lyase assay was measured at 25°C in 50 mM MOPS pH 7.2, 5 mM MgCl2, 5 mM DTT, 10 mM phenylhydrazine. Isocitrate (5 mM) was added to start the reaction and absorbance followed at 324 nm.

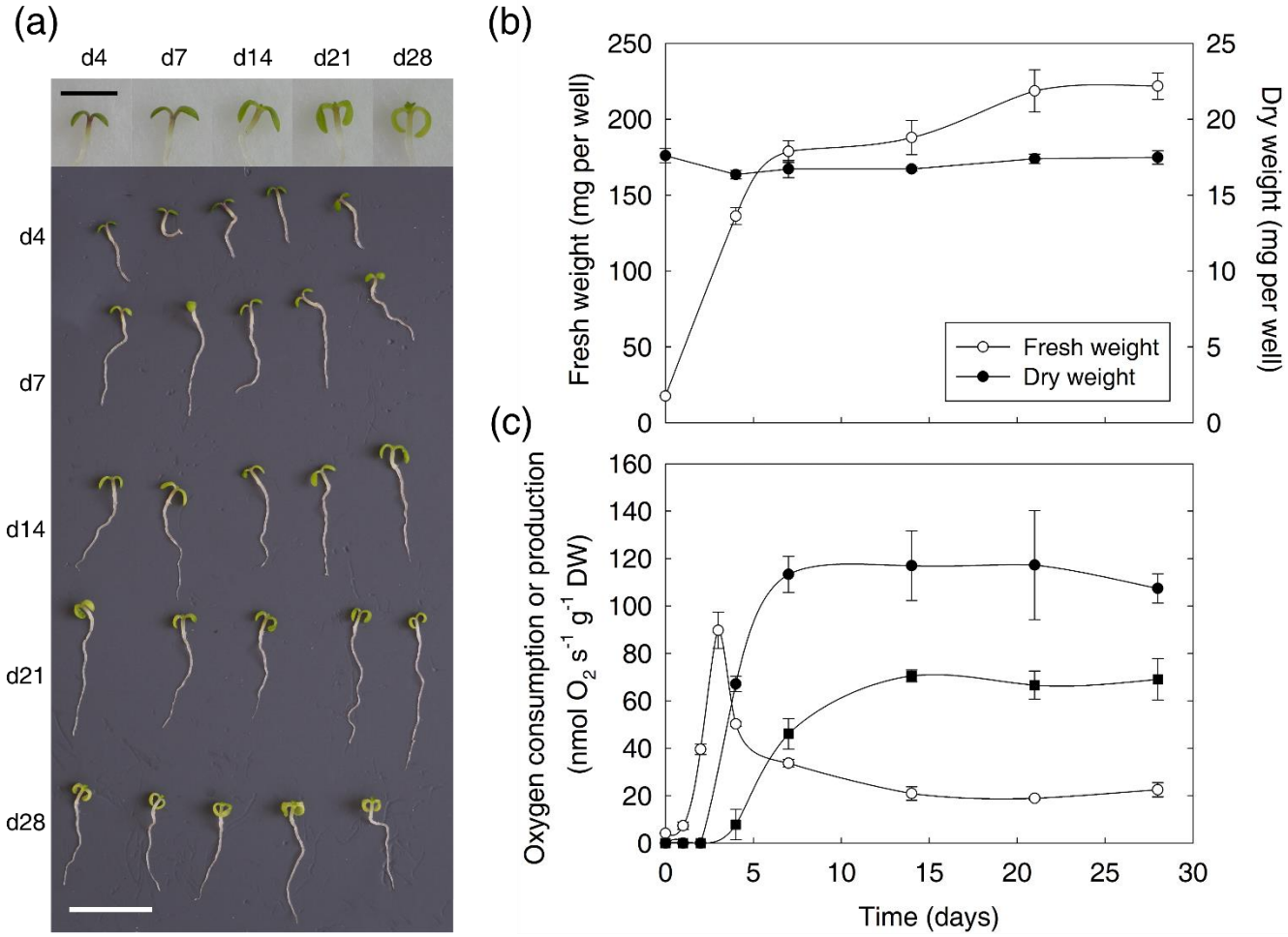

Figure 2.1: Developmental arrest and physiological responses to mineral starvation.
(a) Morphology of liquid-grown seedlings during the four weeks of culture. Five representative seedlings are shown for each time point (numbers correspond to days of culture). The upper panel shows magnification of the apex. Black scale (2 mm), white scale (5 mm). (b) Evolution of fresh and dry weight of seedlings. Fresh weight (open circles) and dry weight (closed circles) were measured for dry seeds and seedlings collected by filtration during culture. Bars indicate SD of the mean (n = 6). (c) Evolution of dark respiration and net photosynthesis. Respiratory oxygen consumption (open circle) and net photosynthesis measured at 700 (closed circle) or 150 µmol photons.m-2.s-1 (closed square) were measured by oxygraphy. Bars indicate SD of the mean (n = 3). Time 0 corresponds to the respiration measured in dry seeds imbibed for 20 minutes in the electrode.

2.2.8. Statistical analyses

After checking normality and homoscedasticity of variables, Student's test or ANOVA followed by either Tukey's or Dunnett's test were performed on data with $p<0.05$ using SigmaPlot v11.0 (Systat Software Inc., Chicago, IL, USA).

2.3. Results

2.3.1. Prolonging early seedling life

When Arabidopsis seedlings are grown in liquid culture in Evian natural mineral water, they are not able to develop true leaves, likely because of nutrient limitation (Benamar *et al.*, 2013). In order to better understand the developmental profile and long-term survival of seedlings in such conditions, we first examined their kinetics of development and growth. Hypocotyl and cotyledon emergence occurred between three and four days post-stratification, and full opening of cotyledons (Stage 1.0; Boyes *et al.*, 2001) was reached after around seven days in our system (Figure 2.1a), instead of three days post-stratification on half-strength Murashige and Skoog (MS) medium (Boyes *et al.*, 2001). Seedlings then continued to grow (radicle and cotyledon expansion) for approximately seven days, but their development was arrested since true leaves did not appear (Figure 2.1a). This arrest in development is likely due to the low amounts of nitrate (23 µg/well) and potassium (6 µg/well) and the absence of phosphate in the initial volume of Evian natural mineral water. Fresh weight increased sharply up to around 180 mg per well during the first week, then rather slowly during the three following weeks, with a maximum of around 220 mg per well, reflecting the developmental arrest of seedlings (Figure 2.1b). Dry weight remained almost constant during the four weeks of culture, which demonstrates that seedling final biomass essentially depends on initial seed mass. Interestingly, while the seedlings remained in a developmental steady state for several weeks, they remained green, without anthocyanin accumulation, and free of necrosis (Figure 2.1a). Since the medium is almost devoid of mineral nutrients after ten days of culture (Benamar *et al.*, 2013), we checked if seedlings remained fully viable, i.e. able to resume their development after transfer to soil. They were indeed able to produce normal plants on soil, even if they had spent up to four weeks in liquid medium (Supporting Information Figure S2.1). Only a slight growth retardation was observed for seedlings that stayed two to four weeks in liquid medium, compared to plants directly sown on soil. Combined, these results demonstrate that young seedlings, blocked in their development because of severe nutrient deprivation, can survive in a steady state for weeks, and resume normal development in favourable conditions.

2.3.2. Energy metabolism maintenance under developmental arrest

We hypothesized that maintenance of energy transduction would be essential to allow long term survival of seedlings under mineral nutrient starvation. During the first three days, dark respiration sharply increased up to around 90 nmol $O_2.s^{-1}.g^{-1}$ DW as there was a high energy demand for germination and early growth; then it decreased rapidly from day three until day seven, while seedlings became increasingly photosynthetically active (Figure 2.1c). Afterwards, the respiratory rate decreased more gradually to stabilize at around 20 nmol $O_2.s^{-1}.g^{-1}$ DW. The maximal net photosynthetic activity (fluence rate 700 µmol photon.$m^{-2}.s^{-1}$) increased sharply between days four and seven, and was then maintained at around 120 nmol $O_2.s^{-1}.g^{-1}$ DW (Figure 2.1c). These values of

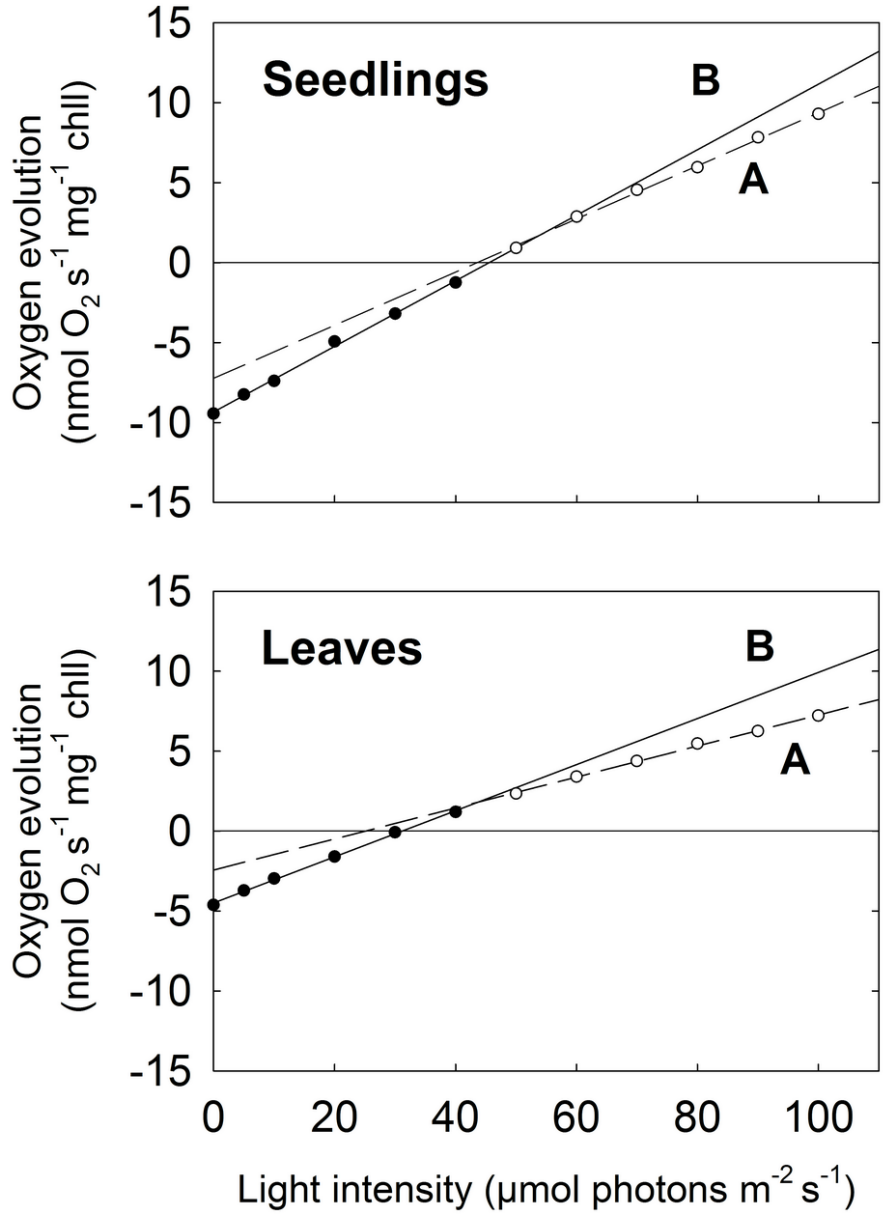

Figure 2.2: Light response of net photosynthesis of Arabidopsis seedlings and mature leaves.
The graph shows representative experiments of oxygen evolution by seven-day-old seedlings and four-week-old Arabidopsis leaves at different light regimes. Solid linear regression fits to the closed circles, below the break point (slope B), and dashed linear regression fits to the open circles above the break point (slope A). Detailed values and statistical analysis are indicated in Supporting Information Table S2.1.

net photosynthesis and dark respiration of seedlings, on a dry weight basis, were lower than those of infiltrated four-week-old leaf tissue (318 ± 35 and 38 ± 4 nmol $O_2.s^{-1}.g^{-1}$ DW, respectively). However, values based on chlorophyll amount were similar between leaf tissue and seedlings (25.4 ± 2.5 and 28.5 ± 1.6 nmol $O_2.s^{-1}.mg^{-1}$ chlorophyll, respectively) because seedlings naturally contain non-green tissues and have thus a lower content of chlorophyll, which could also decrease because of nutrient limitation. Net photosynthesis was also measured with a lower light intensity corresponding to growth room conditions (Figure 2.1c). It is noticeable that on day four, seedlings photosynthetic activity could already compensate for respiration. On day seven, the rate of net photosynthesis was twice that of dark respiration, and from day 14 to day 28 it was three times higher (Figure 2.1c). Therefore, after seven days of growth, photosynthetic activity during the day could theoretically compensate for carbon losses due to respiration both in the light and in the dark period (16h / 8h diurnal cycle). We also examined the light response of seven-day-old seedlings, in particular to determine if respiration was inhibited in the light (Figure 2.2). In many plant species, an inhibition of respiration occurs around the light compensation point, known as the Kok effect (Kok, 1949). While the underlying physiological mechanisms are still debated (Heskel *et al.*, 2013; Tcherkez *et al.*, 2017), we are not aware of any investigation of the Kok effect at the cotyledon stage. To quantify the effect, which is revealed by a typical break in the light response curve, we applied two independent linear regressions for light intensities either below (slope B), or above (slope A) the apparent breakpoint (Figure 2.2). The lower value of slope A reflects the apparent inhibition of respiration above the compensation point, and the Kok effect was thus estimated using the formula 100x[1-(A/B)]. This analysis was performed on four independent replicates (Supporting Information Table S2.1). A clear Kok effect was found in both seedlings (19.7 ± 5.8 %) and leaves (45 ± 9.6 %), but it was significantly higher in the latter. This difference could possibly be due to the activity of root respiration in seven-day-old seedlings: dissected roots contributed to 39.2 ± 4.0 % of total dark respiration. Indeed, the light inhibition in photosynthetic tissues could be partially compensated by an increase in root respiration due to increased carbohydrate supply in the light. Correlations between leaf photosynthesis and root respiration have been reported (Noguchi, 2005), but we are not aware of such data for seedlings. Whatever the mechanisms behind the Kok effect, by taking into account the overall inhibition of respiration in the light, values of gross photosynthesis could be extrapolated for seven-day-old seedlings and four-week-old leaf tissues (35.7 and 28.0 nmol $O_2.s^{-1}.mg^{-1}$ chlorophyll, respectively). Collectively, these results suggest that the photosynthetic capacity of chloroplast is comparable in leaf and cotyledon cells.

Considering the role of the alternative oxidase (AOX) pathway in energy dissipation and stress adaptation in plants (McDonald *et al.*, 2002), we sought to estimate its capacity in seedlings. The KCN-resistant oxygen consumption of seedlings was found to be sensitive to the AOX inhibitor propyl-gallate (Benamar *et al.*, 2013), but since maximal inhibition was reached only slowly, we used KCN-resistant respiration as a proxy for AOX capacity, and KCN-sensitive respiration as a proxy for the capacity of the cytochrome oxidase pathway (COX). The COX capacity showed a strong transient increase from imbibition to day three, while AOX capacity remained low, which is in agreement with the requirement for an efficient energy metabolism during germination and early seedling development (Figure 2.3a). During transition to photo-autotrophy (around day four), there was a marked change since COX capacity decreased while that of AOX increased sharply, and after day seven the AOX capacity remained around three times higher than that of the COX pathway (Figure 5a). This suggests that energy

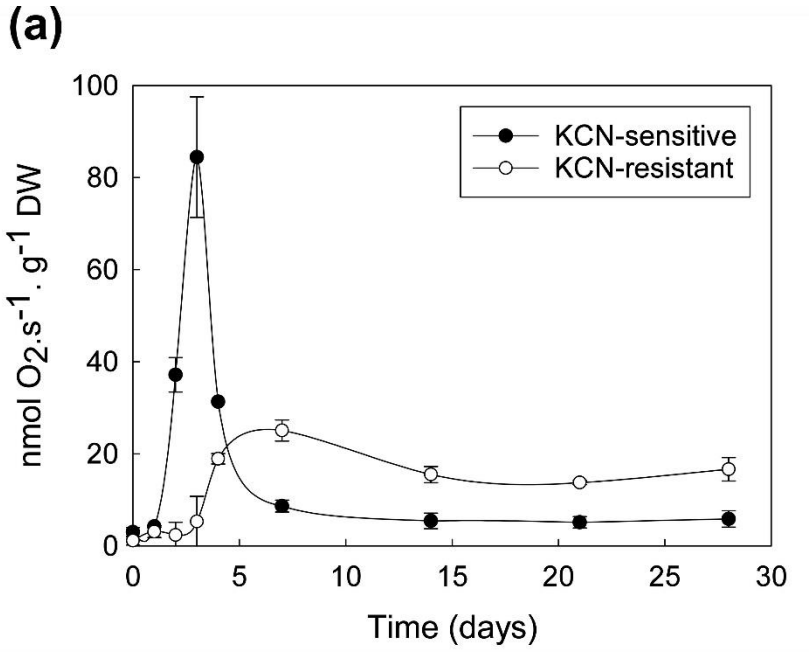

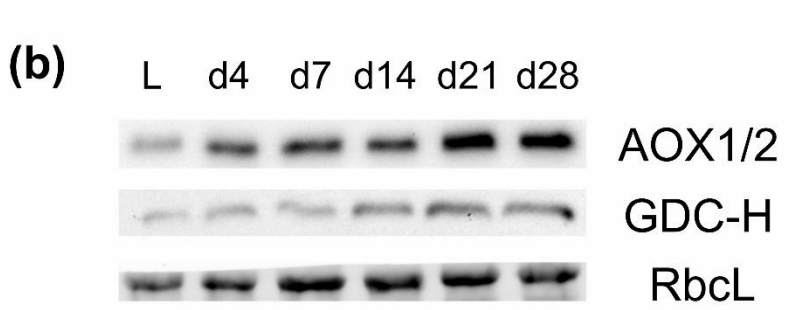

(c)

Sample	AOX	group	GDC-H	group
leaves	6.2 ± 5.5	c	27.8 ± 9.7	c
d4	40.0 ± 20.6	b	34.4 ± 14.6	c
d7	36.1 ± 16.9	b	30.1 ± 16.4	c
d14	40.2 ± 20.4	b	63.5 ± 14.3	b
d21	84.8 ± 34.8	a	107.9 ± 18.4	a
d28	100 ± 0	a	100 ± 0	a

Figure 2.3: AOX capacity and immunodetection of AOX and GDC-H in mature leaves and seedlings.
(a) Evolution of cytochrome oxidase (COX) pathway (closed circle) and AOX pathway (open circle) capacities estimated from the rates of 0.5 mM KCN sensitive or resistant oxygen consumption, respectively. Time 0 corresponds to the respiration measured in dry seeds imbibed for 20 minutes in the oxygen electrode. Bars indicate SD of the mean (n = 3). (b) Representative immunoblots of AOX and GDC-H proteins in seedlings and leaf tissue. Immunodetection was performed with anti-AOX1/2 or anti-GDC-H antibodies, and protein loading on the membrane was estimated by UV detection of Rubisco large subunit (RbcL) using Stain Free technology (Biorad). L, leaves; S, seedlings, with age in days. (c) Semi-quantitative analysis of the abundance of AOX and GDC-H proteins in each sample. On each membrane, chemiluminescence intensities in each lane were normalized to the corresponding RbcL intensity detected by UV. Data are expressed as the percentage of normalized pixels in each lane (mean ± SD) compared to d28 sample of each membrane. Letters correspond to statistically different groups according to ANOVA and Tukey's test ($p<0.05$ and $4<n<12$).

dissipation through the AOX pathway is important for seedlings maintained under mineral starvation. In comparison, in infiltrated four-week-old leaf tissue, the ratio of AOX/COX capacity was much lower (around 0.8) than in seedlings of the same age. AOX protein amounts were indeed higher in seedlings than in leaves (Figure 2.3b and 2.3c). However, the doubling of AOX abundance between day 14 and day 21 was not correlated with a corresponding increase in the seedling AOX capacity (Figure 2.3), suggesting a post-translational regulation. Another way for photosynthetic tissues to dissipate energy is through photorespiration, a pathway found in all oxygenic organisms, but which is highly active in the leaves of C3 plants exposed to stress conditions (Atkin and Macherel, 2009; Maurino and Peterhansel, 2010). We compared, in leaves and in seedlings, the level of GDC-H, a subunit of the mitochondrial glycine decarboxylase complex involved in photorespiration. The amount of GDC-H was as high in seven-day-old seedlings as in mature leaves, and increased during the following weeks of culture (Figure 2.3b and 2.3c). Although the presence of other photorespiratory proteins have not been tested, the GDC-H abundance is an indication that seedlings have the capacity to operate photorespiration. To challenge the importance of photorespiration in seedlings, we studied the behaviour of *glyk1-1,* a null mutant for D-glycerate 3-kinase, an enzyme exclusively involved in the last step of the pathway in chloroplasts (Boldt *et al.*, 2005). After one week, the *glyk1-1* mutant started to display a chlorotic phenotype that progressively led to death one week later (Supporting Information Figure S2.2). This is in fact similar to what happens when *glyk1-1* seeds are germinated on soil in normal air, since seedlings are able to reach the cotyledon stage but then rapidly die (Boldt *et al.*, 2005). We could further confirm that photorespiration was important for survival of seedlings in our system by supplementing CO_2, which was achieved by continuous perfusion of the medium with 10 mM $NaHCO_3$. In these conditions, *glyk1-1* seedlings remained green for at least two weeks (Supporting Information Figure S2.2). This strongly suggests that the photorespiratory pathway is essential for seedlings maintained under conditions of mineral nutrient starvation. Taken together, these analyses reveal that seedlings arrested at the cotyledon stage maintain a homeostatic energy balance between efficient photosynthesis, respiration and energy dissipating mechanisms.

2.3.3. Metabolic adaptation to mineral nutrient starvation

Considering the capacity of seedlings to remain alive for weeks in almost pure water, we wondered how their primary metabolism was adjusted under such steady-state conditions. Seedling metabolism was investigated by performing targeted metabolic profiling for amino acids, organic acids, and sugars during the first four weeks of their life. Dry seeds and four-week-old leaves were used for comparison. The abundances of 32 metabolites are indicated in Supporting Information Table S2.2. One striking results was that the organic/amino acids ratio was much higher in seedlings (e.g. 15x at 28 days) than in dry seeds and leaves (0.8x and 1.4x, respectively) (Figure 2.4a). Compared to leaves, seedlings had a much larger pool of organic acids and a smaller pool of amino acids. When considering the repartition within the organic acid pool, the major differences between leaves and seedlings were the large decrease in fumarate and increases in malate and oxoglutarate (Figure 2.4b). In terms of content, this corresponds to a two-fold lower amount of fumarate, and to higher amounts of malate (8x) and oxo-glutarate (30x) for 28 day-old seedlings compared to leaves of the same age (Supporting Information Table S2.2). The

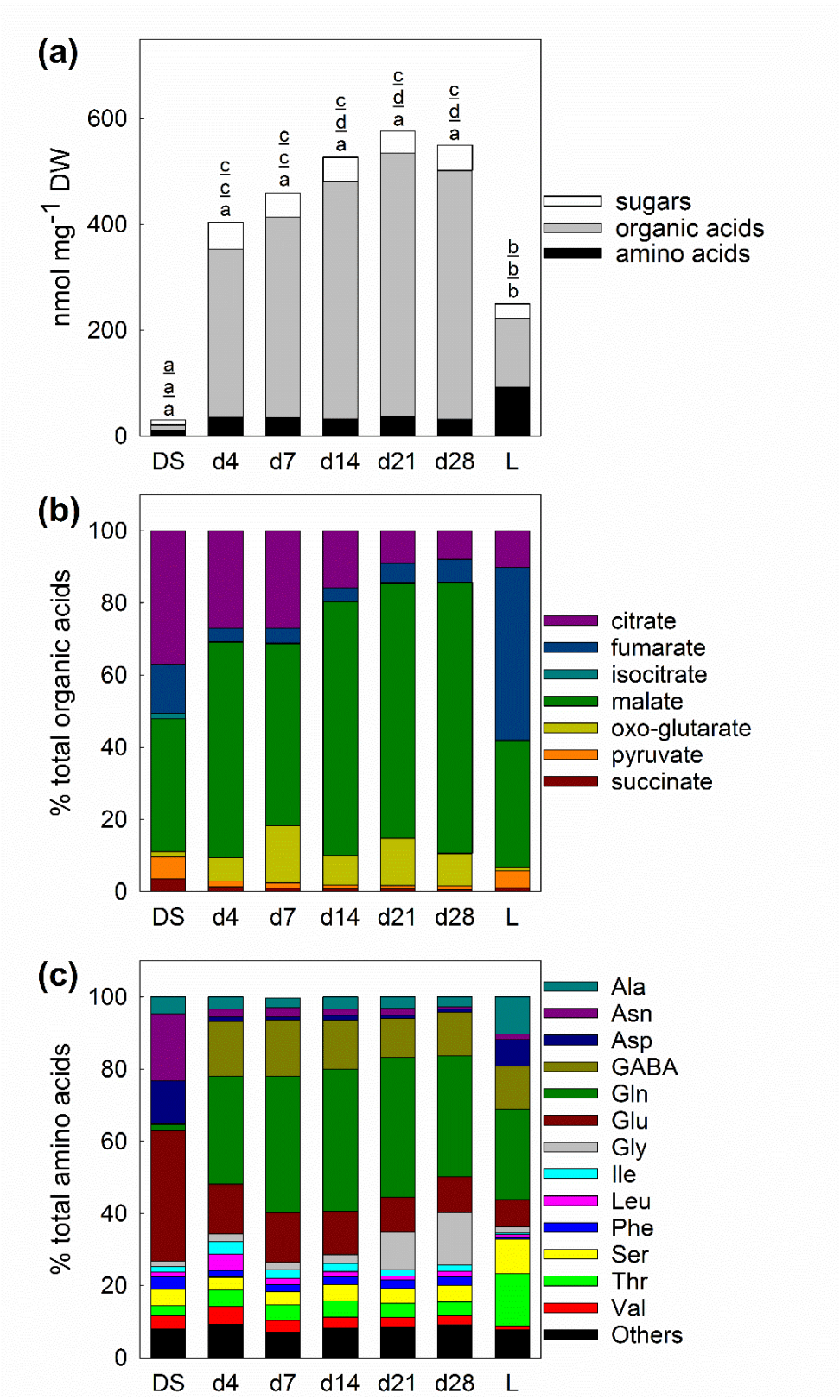

Figure 2.4: Analysis of soluble metabolites in dry seeds, seedlings and leaves.
Metabolites were extracted and quantified from dry seeds (DS), or seedlings (d4 to d28, days of culture) and leaves (L) from four-week-old plants, collected at midday. Data correspond to the mean of three biological replicates. (a) Total amounts of sugars (white), organic acids (grey) and amino acids (black). Letters above bars correspond to statistically different groups according to ANOVA and Tukey's test ($p<0.05$). (b) Proportions of organic acids. (c) Proportion of amino acids. The compounds (Met, Cys, Arg, Tyr, Trp, Pro, Lys) which represented less than 2.5 % of total amino acids in all samples are summed as "others".

malate accumulation in seedlings is impressive (up to 350 nmol.mg^{-1} DW) since it is comparable to the values found in the day for leaves of the obligate CAM species *Agave americana* (Abraham *et al.*, 2016). Concerning the repartition within the amino acid pool, the major differences between leaves and 28 day-old seedlings were the decreases in Asp, Thr, Ala, Ser and the increase in Gly (Figure 2.4c). In terms of content, this corresponds to a higher level of Gly (3x) and lower levels of Asp (27x), Thr and Ala (11x), and Ser (6x) (Supporting Information Table S2.2). Total sugar content was also higher in seedlings than in leaves, especially for glucose and fructose (Supporting Information Table S2.2). Sucrose was the major sugar in dry seeds, but very low amounts were detected in leaves or seedlings. Stachyose, an abundant oligosaccharide in seeds (approx. 20% of total sugars), was still found in seedlings at all ages, albeit at much lower levels (1-2 %), but was not detected in leaves.

As expected, metabolite content was distinctly different between dry seeds and four day-old seedlings, with the total amount of metabolites 13 times higher in seedlings (Figure 2.4a). The main modifications in the proportion of organic acids were an increase in malate and oxoglutarate and a decrease in citrate and fumarate (Figure 2.4b). The proportions of amino acids were markedly different: Glu, Asn and Asp together represented 67 % of amino acids in dry seeds, but only 17 % in four day-old seedlings, in which Gln (30 %) and GABA (15 %) were the most abundant amino acids, the latter being detected at a very low level in seeds (Figure 2.4c). Between four and 28 days of culture, there was no variation in the total amounts of sugars and amino acids, but an increase in organic acids, which was largely due to the accumulation of malate (2x), oxoglutarate (2x) and fumarate (2.5x), while citrate and succinate contents decreased approximately two-fold (Figure 2.4; Supporting Information Table S2.2). Regarding amino acid content, there was an increase in Gly (6 fold), while there was a decrease in Leu (3.5x), Ile (2.5x) and Asn (4x) over the same period. This increase in Gly content and consequently of the Gly/Ser ratio, a marker of photorespiration (Novitskaya *et al.*, 2002), in particular after day 14, supports the idea that photorespiration is taking place in seedlings. Since seedlings were grown under a diurnal light/dark cycle, we compared the metabolic data acquired for midday samples with two other time points: at the end of the light and dark periods, at day seven and day 14. There were few differences between data acquired at different times on the same day, except for a large increase in Gly and Ser at the end of the light period (Supporting Information Figure S2.3; Supporting Information Table S2.3), which further agrees with an active photorespiration. As a whole, these analyses highlight the major metabolic changes occurring after germination, and illustrate the metabolic adaptation of seedlings to survival for weeks under severe mineral starvation.

2.3.4. Carbon mobilization and storage during germination and seedling life

Since the DW was stable over the four weeks of culture, but seedlings were fully photosynthetically competent after germination, we investigated the fate of carbon mobilization and storage. Arabidopsis seeds store carbon mainly as triacylglycerols (TAGs) which are deposited in cytosolic lipid droplets (LDs) and used to sustain development of the seedling until autotrophy (Kelly *et al.*, 2011). Although, LDs are consumed rapidly after germination (Siloto *et al.*, 2006; Deruyffelaere *et al.*, 2015), it has also been shown that low nitrogen can retard the breakdown of lipid reserves in Arabidopsis seedlings (Martin *et al.*, 2002). We therefore performed microscopic observations of LDs using Nile red, a fluorescent probe which stains neutral lipids. Numerous LDs were detected in cotyledons and hypocotyls on days four and seven, but after 14 days, they were rarely observed in either tissue

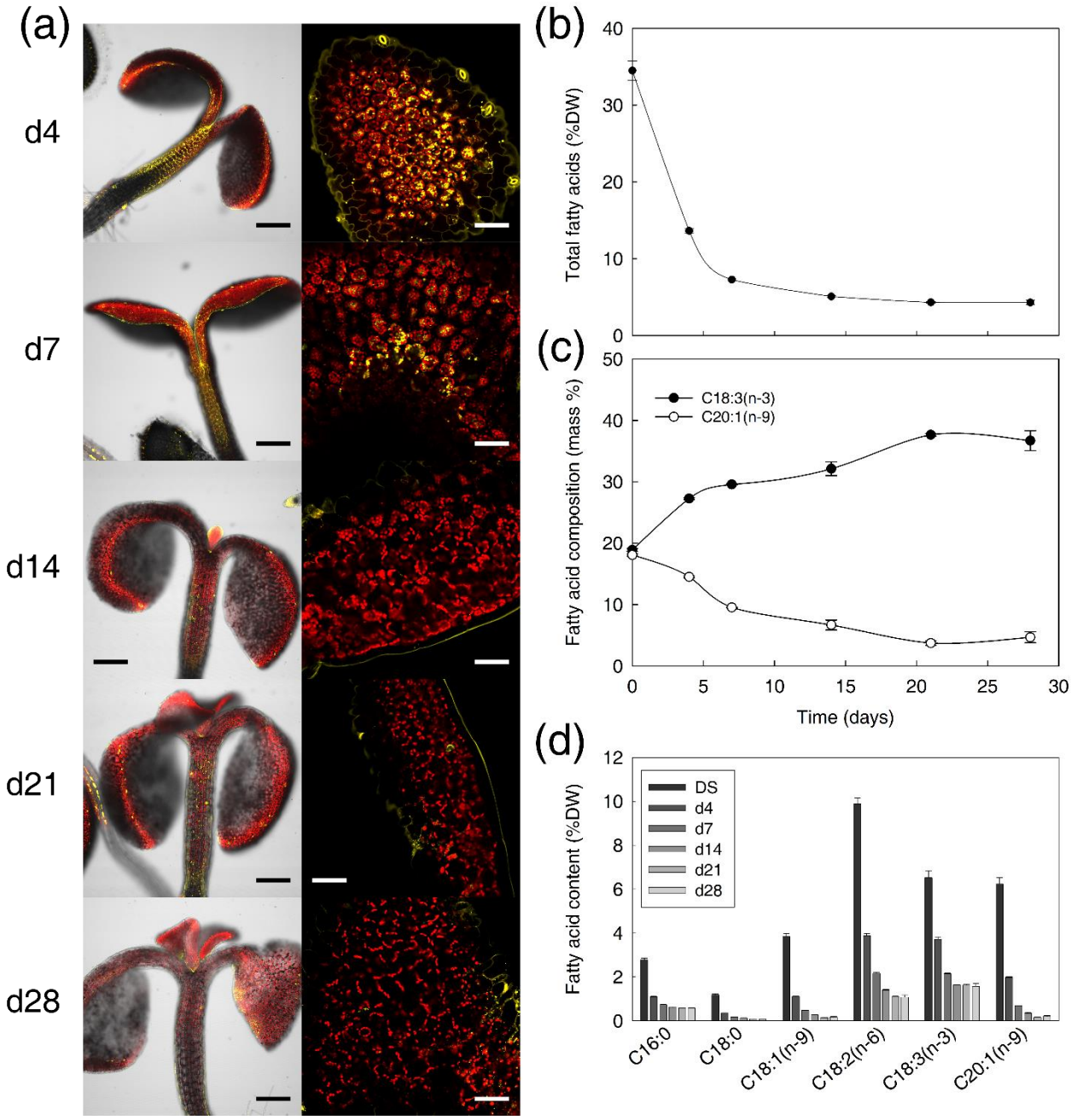

Figure 2.5: Lipid droplets and fatty acid content during seedling growth and developmental arrest. (a) Visualization of lipid droplets (LDs) in seedlings using Nile red staining. At different times of culture (days), seedlings were stained with Nile red and observed by laser scanning confocal microscopy. Representative images of the upper part of seedlings are shown on the left, with views of cotyledons at a higher magnification on the right. The fluorescence of Nile red in LDs is false coloured in yellow, and chloroplast autofluorescence is shown in red. Black scale bar, 200 µm; white scale bar, 50 µm. (b) Total fatty acid content. (c) Changes in linolenic (C18:3) and eicosanoic acid (C20:1) during seedling culture (relative to total fatty acid mass). (d) Seedling content of major fatty acids. Bars indicate SD of the mean (n = 3).

(Figure 2.5a). To link these observations with storage lipid degradation, we measured fatty acid (FA) content and composition during germination and seedling culture (Figure 2.5b, 2.5c and 2.5d). Total FA amount dropped rapidly during early seedling development, then declined with a lower rate between four and seven days, and remained stable from 14 to 28 days (Figure 2.5b). All the major FAs displayed a decrease in abundance (Figure 2.5d). Linolenic acid (C18:3) became the most abundant, representing almost 40 % of the total FA mass in 28 day-old seedlings, while eicosanoic acid (C20:1), a FA specific to seed storage lipids, was reduced to less than 5 % (Figure 2.5c). This correlated with a decrease in the abundance of several oleosin proteins (OLE1, OLE2 and OLE4), which are structural components of LDs (Supporting Information Figure S2.4). OLE2 and OLE4 proteins were detected in dry and germinating seeds but no longer after three days of germination, while OLE1 was detected up to four days, consistently with a previous observation showing that the degradation of OLE2 and OLE4 begins during germination, before the post-germinative degradation of OLE1 (Deruyffelaere *et al.*, 2015). The abundance of isocitrate lyase, as well as its activity and that of malate synthase, sharply increased during germination (maximum at day 3), then rapidly declined (Supporting Information Figure S2.4 & S2.5), indicating that glyoxylate cycle was active in the early stage of seedling growth, but not later. Taken together, these results show that in our system, seed TAG reserves are mobilized during early seedling growth, as occurs normally during Arabidopsis seedling establishment (Cornah *et al.*, 2004), and that cytosolic LDs did not reappear during long term mineral starvation. Since there was still some C20:1 remaining in the seedlings when most of the seed LDs had disappeared, we wondered whether seedlings could still store TAGs in plastoglobuli (PGs), which are small plastidial LDs which size often increase during senescence and in response to abiotic stress such as drought, high-light and nitrogen limitation (van Wijk and Kessler, 2017). We thus performed a transmission electron microscopy (TEM) analysis of cotyledons to examine chloroplast ultrastructure. Starch granules were rarely observed in chloroplasts, except in four-day-old seedlings where they were very abundant (Figure 2.6a). This was confirmed by a qualitative starch staining with Lugol (Supporting Information Figure S2.6). The transient accumulation of starch at day four could possibly buffer the flow of sugars provided by the operation of the glyoxylate cycle, or serve as a temporary store for photosynthates.

Interestingly, PGs were almost systematically detected in plastids from day seven, and their size strongly increased between day 7 and day 28 (Figure 2.6b, 2.6c). Surprisingly, when observing LDs by Nile red staining in seedlings (Figure 2.6a), we did not detect PGs, even when most chloroplasts contained large PGs according to TEM. To clarify this ambiguity, we used a line expressing a fluorescent protein localized in PGs (Vidi *et al.*, 2006). Using 14-day-old seedlings, PGs labelled with GFP were clearly detected in chloroplasts by confocal microscopy, but were not stained by Nile red (Supporting Information Figure S2.7). This suggests that the dye does not enter chloroplasts, or is not able to stain PG neutral lipids. Collectively, these results highlight the fact that seedlings maintained in nutrient limiting conditions still rely on lipid storage, but with a transition from seed-derived LDs towards PGs.

2.4. Discussion

Our results revealed the high resilience of Arabidopsis seedlings: able to survive for at least four weeks with almost no resources other than water and available carbon dioxide, while retaining the ability to develop into normal plants on soil. Under severe mineral starvation, the longevity of seedlings indicates that senescence was

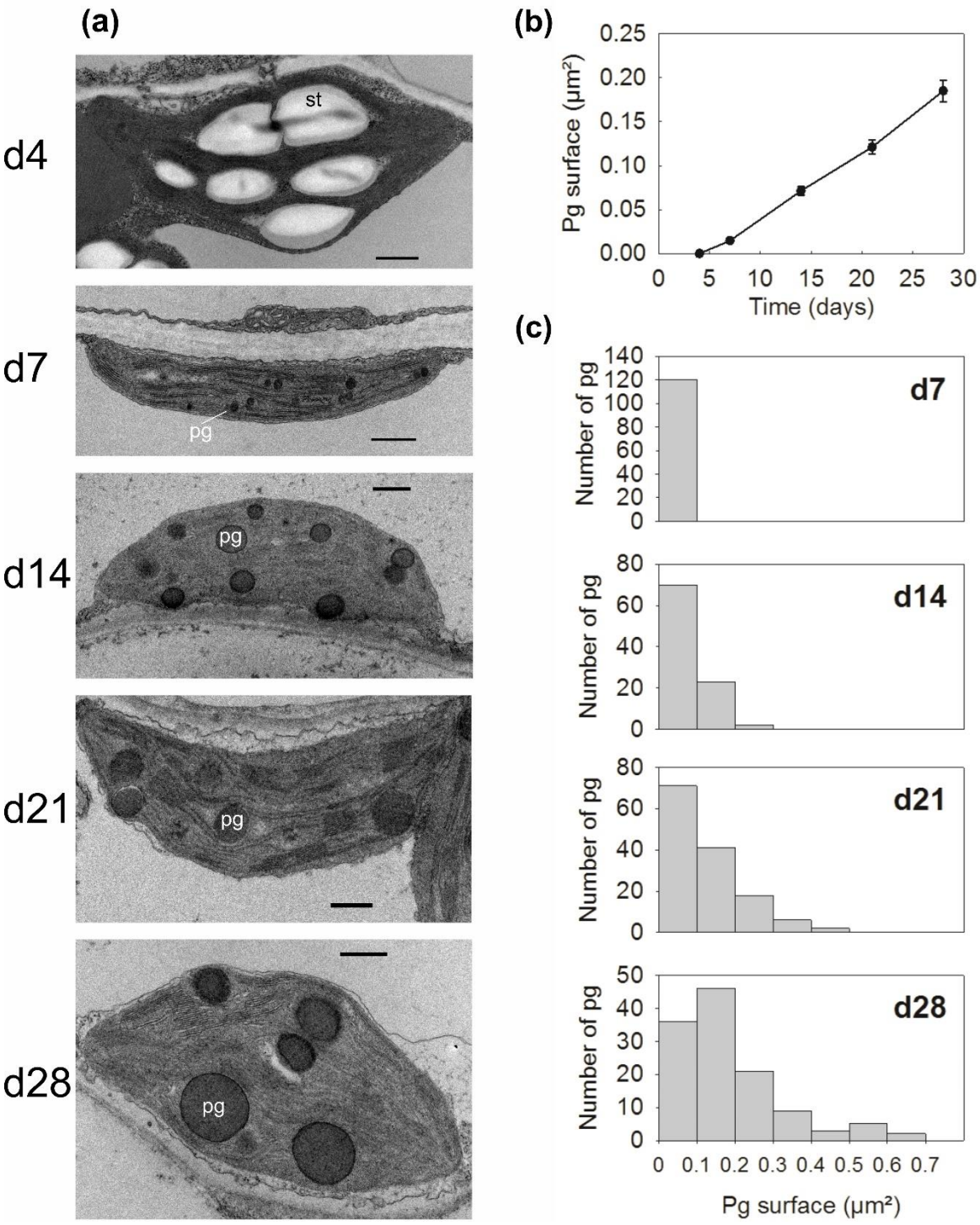

Figure 2.6: Ultrastructural analysis of chloroplast during seedling culture.
Seedlings were collected at different time points (days) and prepared for observation by transmission electron microscopy. (a) Representative micrographs of chloroplasts from cotyledon mesophyll tissue. Black scale bar, 0.5 µm; pg, plastoglobule; st, starch granule. (b) Evolution of plastoglobule surface (µm²) estimated by image analysis. Bars indicate SE of the mean ($95 < n < 138$). (c) Evolution of the frequency of plastoglobule surface values.

not induced, which is surprising because mineral deficiency promotes senescence of leaves or mature plants (Agüera *et al.*, 2010; Balazadeh *et al.*, 2014; Meng *et al.*, 2016). Organ or whole plant senescence indeed often results from a privation of nutrients since resources are allocated to other parts or organs to prioritise growth or reproduction, leading to the concept of exhaustion-death (Molisch, 1938; Thomas, 2002). Repression of senescence in our system could be due to the young developmental stage of the plants since, in young leaves, the induction of senescence is prevented by the expression of the miR164, which negatively regulates ORE1, a master regulator of senescence (Kim *et al.*, 2009; Woo *et al.*, 2013). It is not known whether such a feedback control also occurs in other organs or in whole seedling.

Since the biomass of the photosynthetically active seedlings remained constant, energy dissipation was likely important, as indicated by their high AOX capacity. While oxygen isotope fractionation would be needed to establish the actual partition of electron in the alternative pathway *in vivo*, the AOX capacity is an indicator of the potential electron flux in the pathway (Del-Saz *et al.*, 2018). AOX plays an important role in photosynthetic adaptation to high light (Yoshida *et al.*, 2007; Dinakar *et al.*, 2010) but also to macronutrients limited conditions (Sieger *et al.*, 2005; Escobar *et al.*, 2006; Vijayraghavan and Soole, 2010). The variations in AOX capacity that we observed were apparently not due to changes in protein abundance according to immunodetection, but could rather result from control by effectors such as keto-acids and the ubiquinone pool reduction state (Millenaar and Lambers, 2003; Vanlerberghe, 2013; Del-Saz *et al.*, 2018).

Leaves also dissipate energy in the light by photorespiration (Bauwe *et al.*, 2010), but whether the pathway is important in the early life of plants, especially in cotyledons of epigean seedlings, has not been thoroughly investigated. In soybean cotyledons, $^{14}CO_2$ incorporation into glycine suggested the occurrence of photorespiration (Marek and Stewart, 1992), and in Arabidopsis, leaf-type peroxisomes accumulating photorespiratory enzymes differentiated during greening of cotyledons (Fukao *et al.*, 2002; Hayashi and Nishimura, 2006). In our system, several evidences support a significant and essential photorespiratory flux in seedlings: abundance of GDC-H, increase in Gly and Ser during the day, death of the *glyk1-1* mutant without CO_2 supplementation. Since the operation of photorespiration has a major effect on cellular redox balance and energy status (Keech *et al.*, 2017), this could be linked to the high capacity of AOX, which could contribute to the reoxidation of NADH produced by GDC (Igamberdiev *et al.*, 1997). In the present study, it is conceivable that, besides other effectors, photorespiratory ammonium also contributed to an increase in AOX capacity (Escobar *et al.*, 2006).

Once seedlings reach their developmental steady-state, carbon is essentially stored as organic acids, in particular malate. Besides its role in the TCA cycle and as carbon store, malate contributes to several metabolic shuttles to control the redox balance and is a key metabolite of the CAM and C4 cycles (Zell *et al.*, 2010; Maurino and Engqvist, 2015). In Arabidopsis leaves, fumarate is expected to be a major transitory sink for photosynthates (Pracharoenwattana *et al.*, 2010), but it accumulated to a much lesser extent in seedlings. Malate storage would allow a rapid mobilization of carbon for seedlings to adapt to the availability of mineral nutrients during establishment in the soil, together with contributing to pH and osmotic regulation. The large accumulation of malate probably results from the lack of a competitive nitrogen metabolism operating as a sink for carbon skeletons used for amino acids or protein synthesis. In agreement with the study of Silva *et al.* (2017), the content of amino acids increased almost three times during germination and early seedling growth. However, it

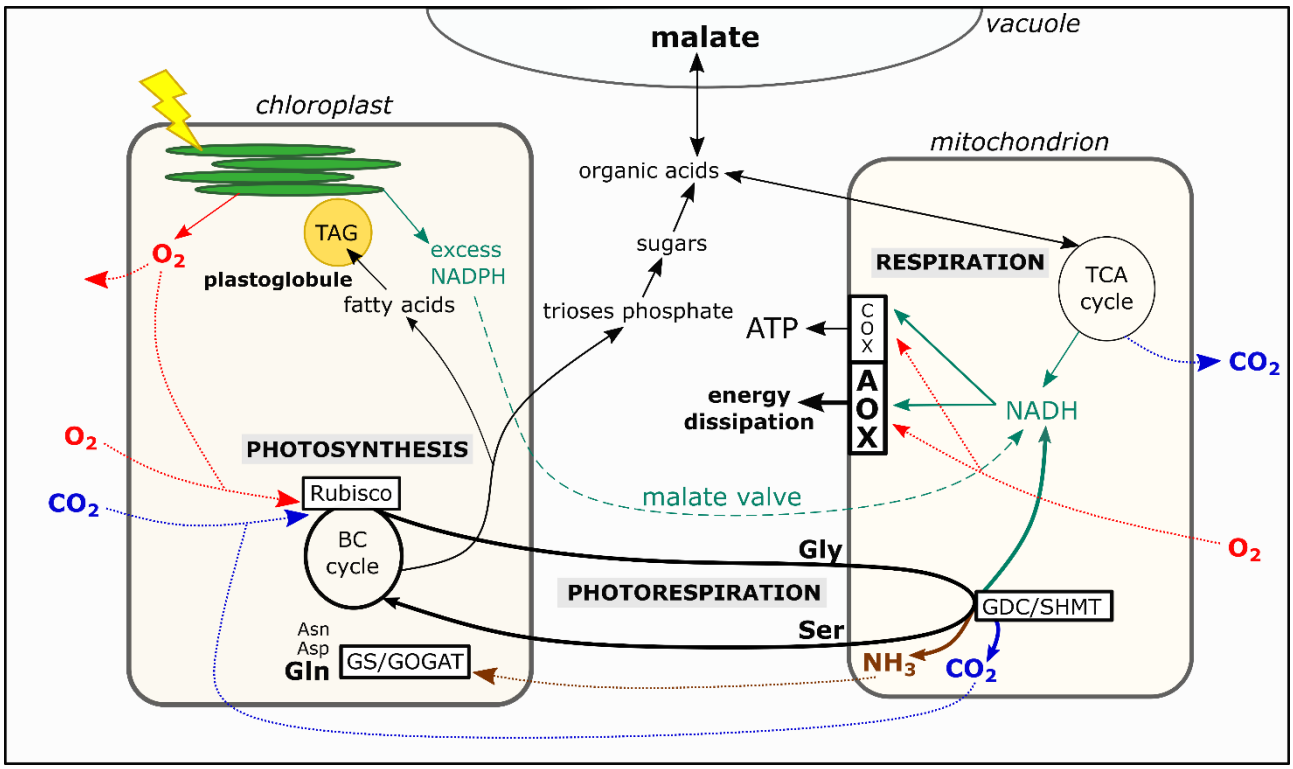

Figure 2.7: Metabolic adaptations of seedlings maintained under severe mineral starvation.
The scheme highlights the main metabolic pathways contributing to energy dissipation (AOX pathway, photorespiration) and recycling of NH_3, and possibly CO_2, that occurs in the light for seedlings arrested in their development because of nutrient limitation. It also shows that photosynthates storage occurs mainly as lipids in plastoglobules and malate in the vacuole. Dotted lines correspond to gas fluxes (CO_2, blue; O_2, red; NH_3, brown) and dashed green line to the malate valve. AOX, alternative oxidase pathway; BC cycle, Benson and Calvin cycle; COX, cytochrome oxidase pathway; GDC/SHMT, glycine decarboxylase complex-serine hydroxymethyltransferase; GS/GOGAT, glutamine synthetase/glutamine oxoglutarate aminotransferase; Rubisco, ribulose bis-phosphate carboxylase oxygenase; TAG, triacylglycerol; TCA cycle, tricarboxylic acid cycle.

remained fairly constant afterwards, which suggests that, after protein reserve mobilization, nitrogen metabolism essentially consists of the production and recycling of photorespiratory ammonium, without a net gain of nitrogen. The Gly content likely increased at the expense of other amino acids, in particular Asn. The Asp pathway which starts by the amination of oxaloacetate did not constitute a sink for C skeletons, which is consistent with the accumulation of malate. The low activity of the Asp pathway might be due to the sequestration of the amino donor Gln in the glutamine synthetase/glutamate oxoglutarate amino transferase cycle.

While the developing Arabidopsis embryo stores lipids in cytosolic LDs, seedlings in the steady state were found to display large PGs, a feature reminiscent of leaves subjected to nitrogen limitation, high light stress, or undergoing senescence (van Wijk and Kessler, 2017). To our knowledge, PG accumulation in seedlings has not been documented yet, but in our conditions, the lack of nitrogen likely explains their accumulation. Although their functions are still debated, PGs clearly contribute to the metabolic plasticity of thylakoids through lipid storage and metabolism, especially upon stress relief (van Wijk and Kessler, 2017). High C/N was earlier demonstrated to slow down lipid reserves breakdown in Arabidopsis (Martin *et al.*, 2002), while another study suggested an increase in TAG accumulation in LDs occurred in similar conditions (Yang *et al.*, 2011). In our model, seedlings slowly degraded seed storage lipids, as they still retained 11% of the initial eicosanoic acid (C20:1) content after one week of culture, and lipid storage shifted from cytosolic LDs in dry seeds to PGs in starved seedlings.

The overall results highlight the capacity of Arabidopsis seedlings arrested in their development to survive under severe mineral starvation, by entering into a stationary metabolic state (Figure 7). In some way, this is analogous to the case of microorganisms entering a stationary phase when lacking nutrients, which translate into a decrease in metabolic rates (Chubukov and Sauer, 2014). Although we did not measure CO_2 exchange, both the stability of seedling mass and the oxygraphic data support the hypothesis that photosynthetic carbon assimilation compensates for day and night carbon losses. In the illuminated seedlings, mitochondrial CO_2 production originate mostly from glycine breakdown, because the overall activity of the TCA cycle, and thus of respiratory CO_2 release, is expected to decrease because of the inactivation of pyruvate dehydrogenase, especially under photorespiratory conditions (Noguchi and Yoshida, 2008). However, the scene might be more complex because there is strong evidence for the operation of non-cyclic modes of the TCA cycle in different physiological conditions (Sweetlove *et al*., 2010). Under the prevailing low CO_2 conditions in the medium, it is tempting to postulate that CO_2 released in mitochondria could be re-assimilated in the chloroplast (Figure 7). This could likely occur by diffusion since CO_2 easily cross membranes, or through an active mitochondrial bicarbonate export system together with an organic acid shuttle from the cytosol to the plastid (Zabaleta *et al.*, 2012), since the chloroplast envelope is not permeable to bicarbonate (Tolleter *et al.*, 2017). Ammonia, which is released in large amounts during photorespiration in mitochondria, is expected to be shuttled back and re-assimilated in the plastid (Linka and Weber, 2005). In the context of the nitrogen-starved seedlings, a loss of ammonia would be unsustainable, and therefore nitrogen cycling should operate with high efficiency. Finally, since seedlings growth becomes restricted, the energy demand should be low, being essentially devoted to maintenance processes, and therefore easily supplied by mitochondrial respiration. The high capacity of AOX pathway should contribute to energy dissipation, but also to allow the maintenance of mitochondrial carbon metabolism under low energy demand.

The resilience of seedlings likely contributes to their competitiveness in the environment, and therefore to plant fitness, especially for species with small seeds like Arabidopsis. A major question arising from this study is why seedlings should finally die. Although the experiment was limited to four weeks, seedlings remained green and apparently healthy for longer. Seedlings are apparently in equilibrium, but will inevitably suffer from internal damage because of the myriads of reactions occurring in all cellular compartments, including the necessary turnover of most of cellular components. Indeed, protein quality control and cellular autophagy mechanisms play a major role to counteract cellular aging in most organisms, including plants (Lionaki and Tavernarakis, 2013; Üstün *et al.*, 2017; Broda *et al.*, 2018). There is also a strong link between oxidative stress and ageing in animals, and mitochondria have a central role in senescence (Theurey and Pizzo, 2018). Paradoxically, mitochondrial inefficiency appears as a key to longevity, in particular through mild uncoupling, that would prevent oxidative stress by decreasing the proton gradient, thus preventing formation of reactive oxygen species (ROS) (Brand, 2000). In seedlings, mitochondria, but also chloroplasts and peroxisomes are major sources of ROS, and progressive accumulation of oxidative damages could lead to oxidative imbalance, ultimately leading to death. The high capacity of AOX in seedlings should efficiently prevent mitochondrial ROS production, and possibly contribute to their prolonged life under mineral starvation.

To conclude, besides revealing the metabolic plasticity underlying the resilience of seedlings under mineral starvation, this experimental system model will be invaluable not only to study molecular mechanisms that determine lifespan, but also to examine the impact of various abiotic stressors in a stable system independent of growth and development.

2.5. Acknowledgements

We are thankful to Fabienne Simonneau and Aurélia Rolland (IMAC-QUASAV, confocal microscopy), Guillaume Mabilleau and Florence Manero (SCIAM, electron microscopy), Pascale Satour (IRHS-SMS, sugar analysis). We are grateful to Hermann Bauwe (University of Rostock) and Felix Kessler (University of Neuchâtel) for kindly providing the *glyk1-1* and 35S:PGL35:GFP lines. We thank David C. Logan for invaluable suggestions and proofreading of the manuscript. This research was conducted in the framework of the regional programme "Objectif Végétal, Research, Education and Innovation in Pays de la Loire", supported by the French Region Pays de la Loire, Angers Loire Métropole and the European Regional Development Fund.

2.6. References

Abraham, P.E., Yin, H., Borland, A.M., et al. (2016) Transcript, protein and metabolite temporal dynamics in the CAM plant Agave. *Nat. Plants*, **2**, 1–10.

Agüera, E., Cabello, P. and la Haba, P. de (2010) Induction of leaf senescence by low nitrogen nutrition in sunflower (*Helianthus annuus*) plants. *Physiol. Plant.*, **138**, 256–267.

Atkin, O.K. and Macherel, D. (2009) The crucial role of plant mitochondria in orchestrating drought tolerance. *Ann. Bot.*, **103**, 581–597.

Balazadeh, S., Schildhauer, J., Araújo, W.L., Munné-Bosch, S., Fernie, A.R., Proost, S., Humbeck, K. and Mueller-Roeber, B. (2014) Reversal of senescence by N resupply to N-starved *Arabidopsis thaliana*: Transcriptomic and metabolomic consequences. *J. Exp. Bot.*, **65**, 3975–3992.

Bauwe, H., Hagemann, M. and Fernie, A.R. (2010) Photorespiration: players, partners and origin. *Trends Plant Sci.*, **15**, 330–336.

Benamar, A., Pierart, A., Baecker, V., Avelange-Macherel, M.H., Rolland, A., Gaudichon, S., Gioia, L. di and Macherel, D. (2013) Simple system using natural mineral water for high-throughput phenotyping of *Arabidopsis thaliana* seedlings in liquid culture. *Int. J. High Throughput Screen.*, **4**, 1–15.

Bobille, H., Limami, A.M., Robins, R.J., Cukier, C., Floch, G. Le and Fustec, J. (2016) Evolution of the amino acid fingerprint in the unsterilized rhizosphere of a legume in relation to plant maturity. *Soil Biol. Biochem.*, **101**, 226–236.

Boldt, R., Edner, C., Kolukisaoglu, U., Hagemann, M., Weckwerth, W., Wienkoop, S., Morgenthal, K. and Bauwe, H. (2005) D-GLYCERATE 3-KINASE, the last unknown enzyme in the photorespiratory cycle in Arabidopsis, belongs to a novel kinase family. *Plant Cell*, **17**, 2413–20.

Boyes, D.C., Zayed, A.M., Ascenzi, R., McCaskill, A.J., Hoffman, N.E., Davis, K.R. and Gorlach, J. (2001) Growth stage-based phenotypic analysis of Arabidopsis: A model for high throughput functional genomics in plants. *Plant Cell*, **13**, 1499–1510.

Brand, M.D. (2000) Uncoupling to survive? The role of mitochondrial inefficiency in ageing. *Exp. Gerontol.*, **35**, 811–820.

Broda, M., Millar, A.H. and Aken, O. Van (2018) Mitophagy: a mechanism for plant growth and survival.

Trends Plant Sci., **23**, 434–450.

Chandler, J.W. (2008) Cotyledon organogenesis. *J. Exp. Bot.*, **59**, 2917–2931.

Chubukov, V. and Sauer, U. (2014) Environmental dependence of stationary-phase metabolism in *Bacillus subtilis* and *Escherichia coli*. *Appl. Environ. Microbiol.*, **80**, 2901–2909.

Cooper, T.G. and Beevers, H. (1969) Mitochondria and glyoxysomes from castor bean endosperm. *J. Biol. Chem.*, **244**, 3507–3513.

Cornah, J.E., Germain, V., Ward, J.L., Beale, M.H. and Smith, S.M. (2004) Lipid utilization, gluconeogenesis, and seedling growth in Arabidopsis mutants lacking the glyoxylate cycle enzyme malate synthase. *J. Biol. Chem.*, **279**, 42916–42923.

D'Andréa, S., Jolivet, P., Boulard, C., Larré, C., Froissard, M. and Chardot, T. (2007) Selective one-step extraction of *Arabidopsis thaliana* seed oleosins using organic solvents. *J. Agric. Food Chem.*, **55**, 10008–10015.

Del-Saz, N.F., Ribas-Carbo, M., McDonald, A.E., Lambers, H., Fernie, A.R. and Florez-Sarasa, I. (2018) An *in vivo* perspective of the role(s) of the alternative oxidase pathway. *Trends Plant Sci.*, **23**, 206–219.

Deruyffelaere, C., Bouchez, I., Morin, H., Guillot, A., Miquel, M., Froissard, M., Chardot, T. and D'Andrea, S. (2015) Ubiquitin-mediated proteasomal degradation of oleosins is involved in oil body mobilization during post-germinative seedling growth in Arabidopsis. *Plant Cell Physiol.*, **56**, 1374–1387.

Dinakar, C., Raghavendra, A.S. and Padmasree, K. (2010) Importance of AOX pathway in optimizing photosynthesis under high light stress: Role of pyruvate and malate in activating AOX. *Physiol. Plant.*, **139**, 13–26.

Escobar, M.A., Geisler, D.A. and Rasmusson, A.G. (2006) Reorganization of the alternative pathways of the Arabidopsis respiratory chain by nitrogen supply: opposing effects of ammonium and nitrate. *Plant J.*, **45**, 775–788.

Finch-Savage, W.E. and Bassel, G.W. (2016) Seed vigour and crop establishment: Extending performance beyond adaptation. *J. Exp. Bot.*, **67**, 567–591.

Fukao, Y., Hayashi, M. and Nishimura, M. (2002) Proteomic analysis of leaf peroxisomal proteins in greening cotyledons of *Arabidopsis thaliana*. *Plant Cell Physiol.*, **43**, 689–696.

Graham, I.A. (2008) Seed storage oil mobilization. *Annu. Rev. Plant Biol.*, **59**, 115–142.

Hanley, M.E., Fenner, M., Whibley, H. and Darvill, B. (2004) Early plant growth: Identifying the end point of the seedling phase. *New Phytol.*, **163**, 61–66.

Hayashi, M. and Nishimura, M. (2006) *Arabidopsis thaliana* - A model organism to study plant peroxisomes. *Biochim. Biophys. Acta - Mol. Cell Res.*, **1763**, 1382–1391.

Heskel, M.A., Atkin, O.K., Turnbull, M.H. and Griffin, K.L. (2013) Bringing the Kok effect to light: A review on the integration of daytime respiration and net ecosystem exchange. *Ecosphere*, **4**, 1–14.

Igamberdiev, A.U., Bykova, N. V. and Gardeström, P. (1997) Involvement of cyanide-resistant and rotenone-insensitive pathways of mitochondrial electron transport during oxidation of glycine in higher plants. *FEBS Lett.*, **412**, 265–269.

Keech, O., Gardeström, P., Kleczkowski, L.A. and Rouhier, N. (2017) The redox control of photorespiration : from biochemical and physiological aspects to biotechnological considerations. *Plant. Cell Environ.*, **40**, 553–

569.

Kelly, A.A., Quettier, A.-L., Shaw, E. and Eastmond, P.J. (2011) Seed storage oil mobilization is important but not essential for germination or seedling establishment in Arabidopsis. *Plant Physiol.*, **157**, 866–875.

Kim, J.H., Woo, H.R., Kim, J., Lim, P.O., Lee, I.C., Choi, S.H., Hwang, D. and Nam, H.G. (2009) Trifurcate feed-forward regulation of age-dependent cell death involving miR164 in Arabidopsis. *Science*, **323**, 1053–1058.

Kircher, S. and Schopfer, P. (2012) Photosynthetic sucrose acts as cotyledon-derived long-distance signal to control root growth during early seedling development in Arabidopsis. *Proc. Natl. Acad. Sci.*, **109**, 11217–11221.

Kok, B. (1949) On the interrelation of respiration and photosynthesis in green plants. *Biochim. Biophys. Acta*, **3**, 625–631.

Krämer, U. (2015) Planting molecular functions in an ecological context with *Arabidopsis thaliana*. *Elife*, **4**, 1–13.

Leck, M.A.., Simpson, R.L.. and Thomas, V. (2008) Why seedlings? In M. Parker, V. Thomas; Simpson, Robert L.; Alessio Leck, ed. *Seedling Ecology and Evolution*. Cambridge: Cambridge University Press, pp. 3–13.

Liang, G., He, H. and Yu, D. (2012) Identification of nitrogen starvation-responsive microRNAs in *Arabidopsis thaliana*. *PLoS One*, **7**, e48951.

Linka, M. and Weber, A.P.M. (2005) Shuffling ammonia between mitochondria and plastids during photorespiration. *Trends Plant Sci.*, **10**, 461–465.

Lionaki, E. and Tavernarakis, N. (2013) Oxidative stress and mitochondrial protein quality control in aging. *J. Proteomics*, **92**, 181–194.

Mansfield, S.G. and Briarty, L.G. (1996) The dynamics of seedling and cotyledon cell development in *Arabidopsis thaliana* during reserve mobilization. *Int. J. Plant Sci.*, **157**, 280–294.

Marek, L.F. and Stewart, C.R. (1992) Photosynthesis and photorespiration in presenescent, senescent, and rejuvenated soybean cotyledons. *Plant Physiol.*, **98**, 694–699.

Martin, T., Oswald, O. and Graham, I.A. (2002) Arabidopsis seedling growth, storage lipid mobilization, and photosynthetic gene expression are regulated by carbon: nitrogen availability. *Plant Physiol.*, **128**, 472–481.

Maurino, V.G. and Engqvist, M.K.M. (2015) 2-hydroxy acids in plant metabolism. *Arab. B.*, **13**, e0182.

Maurino, V.G. and Peterhansel, C. (2010) Photorespiration: current status and approaches for metabolic engineering. *Curr. Opin. Plant Biol.*, **13**, 248–255.

McDonald, A.E., Sieger, S.M. and Vanlerberghe, G.C. (2002) Methods and approaches to study plant mitochondrial alternative oxidase. *Physiol. Plant.*, **116**, 135–143.

Meng, S., Peng, J.S., He, Y.N., Zhang, G. Bin, Yi, H.Y., Fu, Y.L. and Gong, J.M. (2016) Arabidopsis NRT1.5 mediates the suppression of nitrate starvation-induced leaf senescence by modulating foliar potassium level. *Mol. Plant*, **9**, 461–470.

Millenaar, F.F. and Lambers, H. (2003) The alternative oxidase: in vivo regulation and function. *Plant Biol.*, **5**, 2–15.

Mitchell-Olds, T. and Schmitt, J. (2006) Genetic mechanisms and evolutionary significance of natural variation

in Arabidopsis. *Nature*, **441**, 947–952.

Molisch, H. (1938) *The longevity of plants*, Science Press, Lancaster, pp.124-143.

Moran, R. (1982) Formulae for determination of chlorophyllous pigments extracted with N,N-dimethylformamide. *Plant Physiol.*, **69**, 1376–1381.

Noguchi, K. (2005) Effects of light intensity and carbohydrate status on leaf and root respiration. In H. Lambers and M. Ribas-Carbo, eds. *Plant Respiration: From Cell to Ecosystem*. Dordrecht: Springer Netherlands, pp. 63–83.

Noguchi, K. and Yoshida, K. (2008) Interaction between photosynthesis and respiration in illuminated leaves. *Mitochondrion*, **8**, 87–99.

Novitskaya, L., Trevanion, S.J., Driscoll, S., Foyer, C.H. and Noctor, G. (2002) How does photorespiration modulate leaf amino acid contents? A dual approach through modelling and metabolite analysis. *Plant, Cell Environ.*, **25**, 821–835.

Postma, F.M. and Ågren, J. (2016) Early life stages contribute strongly to local adaptation in *Arabidopsis thaliana*. *Proc. Natl. Acad. Sci.*, **113**, 7590–7595.

Pracharoenwattana, I., Zhou, W., Keech, O., Francisco, P.B., Udomchalothorn, T., Tschoep, H., Stitt, M., Gibon, Y. and Smith, S.M. (2010) Arabidopsis has a cytosolic fumarase required for the massive allocation of photosynthate into fumaric acid and for rapid plant growth on high nitrogen. *Plant J.*, **62**, 785–795.

Schindelin, J., Arganda-Carreras, I., Frise, E., et al. (2012) Fiji: an open-source platform for biological-image analysis. *Nat. Methods*, **9**, 676–682.

Sieger, S.M., Kristensen, B.K., Robson, C.A., Amirsadeghi, S., Eng, E.W.Y., Abdel-Mesih, A., Møller, I.M. and Vanlerberghe, G.C. (2005) The role of alternative oxidase in modulating carbon use efficiency and growth during macronutrient stress in tobacco cells. *J. Exp. Bot.*, **56**, 1499–1515.

Siloto, R.M.P., Findlay, K., Lopez-villalobos, A., Yeung, E.C., Nykiforuk, C.L. and Moloney, M.M. (2006) The accumulation of oleosins determines the size of seed oilbodies in Arabidopsis. *Plant Cell*, **18**, 1961–1974.

Silva, A.T., Ligterink, W. and Hilhorst, H.W.M. (2017) Metabolite profiling and associated gene expression reveal two metabolic shifts during the seed-to-seedling transition in *Arabidopsis thaliana*. *Plant Mol. Biol.*, **95**, 481–496.

Sweetlove, L.J., Beard, K.F.M., Nunes-Nesi, A., Fernie, A.R. and Ratcliffe, R.G. (2010) Not just a circle: flux modes in the plant TCA cycle. *Trends Plant Sci.*, **15**, 462–470.

Tcherkez, G., Gauthier, P., Buckley, T.N., et al. (2017) Tracking the origins of the Kok effect, 70 years after its discovery. *New Phytol.*, **214**, 506–510.

Tetteroo, F.A.A., Hoekstra, F.A. and Karssen, C.M. (1994) Effect of abscisic acid and slow drying on soluble carbohydrate content in developing embryoids of carrot (*Daucus carota* L.) and alfalfa (*Medicago sativa* L.). *Seed Sci. Res.*, **4**, 203–210.

Theurey, P. and Pizzo, P. (2018) The aging mitochondria. *Genes (Basel).*, **9**, 22.

Thomas, H. (2002) Ageing in plants. *Mech. Ageing Dev.*, **123**, 747–753.

Tolleter, D., Chochois, V., Poiré, R., Dean Price, G. and Badger, M.R. (2017) Measuring CO_2 and HCO_3^-

permeabilities of isolated chloroplasts using a MIMS-^{18}O approach. *J. Exp. Bot.*, **68**, 3915–3924.

Üstün, S., Hafrén, A. and Hofius, D. (2017) Autophagy as a mediator of life and death in plants. *Curr. Opin. Plant Biol.*, **40**, 122–130.

Vanlerberghe, G. (2013) Alternative oxidase: a mitochondrial respiratory pathway to maintain metabolic and signaling homeostasis during abiotic and biotic stress in plants. *Int. J. Mol. Sci.*, **14**, 6805–6847.

Vidal, E.A., Moyano, T.C., Canales, J. and Gutiérrez, R.A. (2014) Nitrogen control of developmental phase transitions in *Arabidopsis thaliana*. *J. Exp. Bot.*, **65**, 5611–5618.

Vidi, P.A., Kanwischer, M., Baginsky, S., Austin, J.R., Csucs, G., Dörmann, P., Kessler, F. and Bréhélin, C. (2006) Tocopherol cyclase (VTE1) localization and vitamin E accumulation in chloroplast plastoglobule lipoprotein particles. *J. Biol. Chem.*, **281**, 11225–11234.

Vijayraghavan, V. and Soole, K. (2010) Effect of short-and long-term phosphate stress on the non-phosphorylating pathway of mitochondrial electron transport in *Arabidopsis thaliana*. *Funct. Plant Biol.*, **37**, 455–466.

Warpeha, K.M. and Montgomery, B.L. (2016) Light and hormone interactions in the seed-to-seedling transition. *Environ. Exp. Bot.*, **121**, 56–65.

Wijk, K.J. van and Kessler, F. (2017) Plastoglobuli: plastid microcompartments with integrated functions in metabolism, plastid developmental transitions, and environmental adaptation. *Annu. Rev. Plant Biol.*, **68**, 253–289.

Woo, H.R., Kim, H.J., Nam, H.G. and Lim, P.O. (2013) Plant leaf senescence and death - regulation by multiple layers of control and implications for aging in general. *J. Cell Sci.*, **126**, 4823–4833.

Wu, S.-H. (2014) Gene expression regulation in photomorphogenesis from the perspective of the central dogma. *Annu. Rev. Plant Biol.*, **65**, 311–333.

Yang, Y., Yu, X., Song, L. and An, C. (2011) ABI4 activates DGAT1 expression in Arabidopsis seedlings during nitrogen deficiency. *Plant Physiol.*, **156**, 873–883.

Yoshida, K., Terashima, I. and Noguchi, K. (2007) Up-regulation of mitochondrial alternative oxidase concomitant with chloroplast over-reduction by excess light. *Plant Cell Physiol.*, **48**, 606–614.

Zabaleta, E., Martin, M.V. and Braun, H.P. (2012) A basal carbon concentrating mechanism in plants? *Plant Sci.*, **187**, 97–104.

Zell, M.B., Fahnenstich, H., Maier, A., et al. (2010) Analysis of Arabidopsis with highly reduced levels of malate and fumarate sheds light on the role of these organic acids as storage carbon molecules. *Plant Physiol.*, **152**, 1251–1262.

Zheng, Z.-L. (2009) Carbon and nitrogen nutrient balance signaling in plants. *Plant Signal. Behav.*, **4**, 584–591.

2.7. Supporting Information

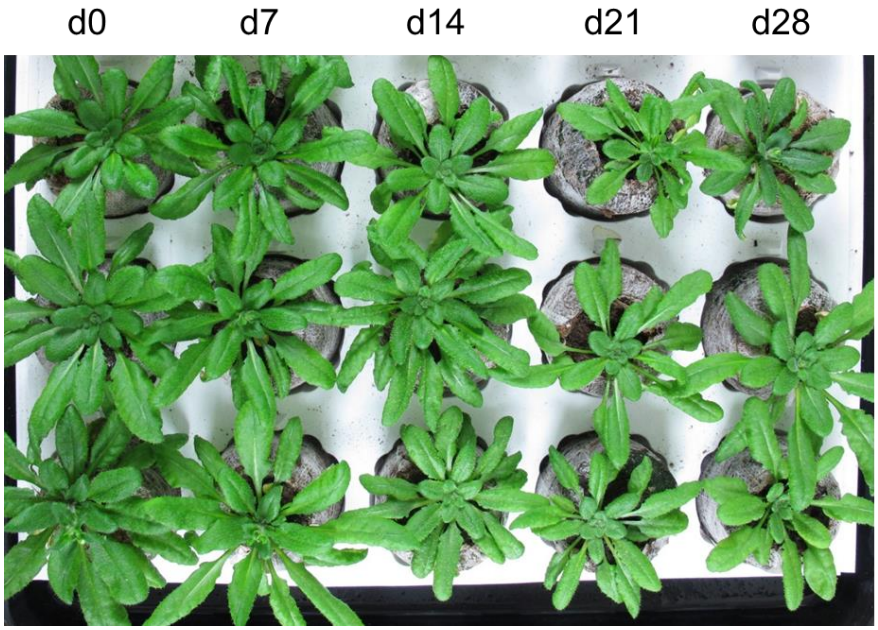

Figure S2.1: Development of plants after initial culture of seedlings under mineral starvation.
Seedlings grown in liquid culture medium for 7, 14, 21 or 28 days where transferred to compost and the photograph was taken five weeks later. d0 labelled plants are issued from seeds directly sown on compost.

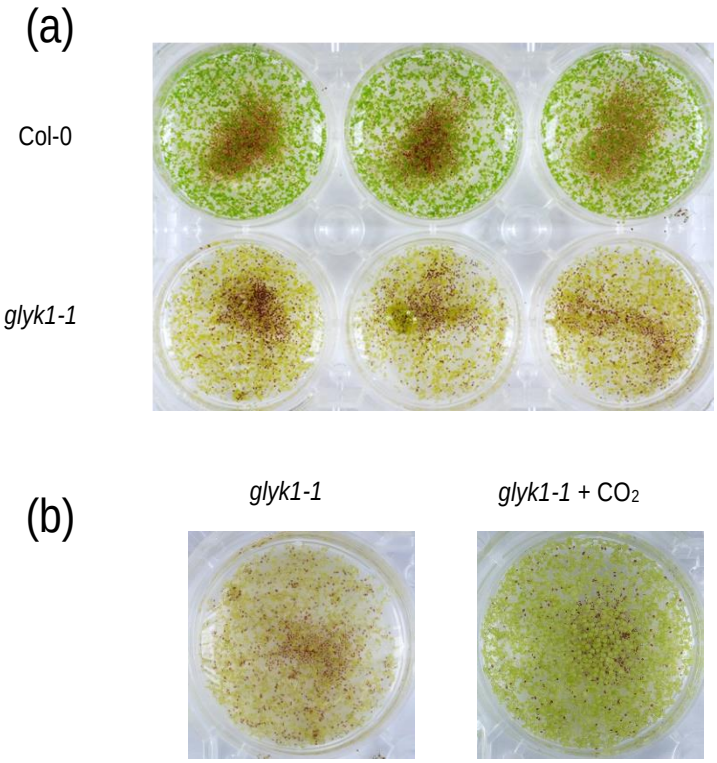

Figure S2.2: Importance of photorespiration for survival under mineral starvation.
(a) The photorespiratory mutant glyk1-1 (D-glycerate 3-kinase mutant), which was grown in the same conditions as Col-0 for two weeks, developed a chlorotic phenotype and died later. (b) Continuous supplementation of the medium with 10 mM NaHCO3 could revert this phenotype.

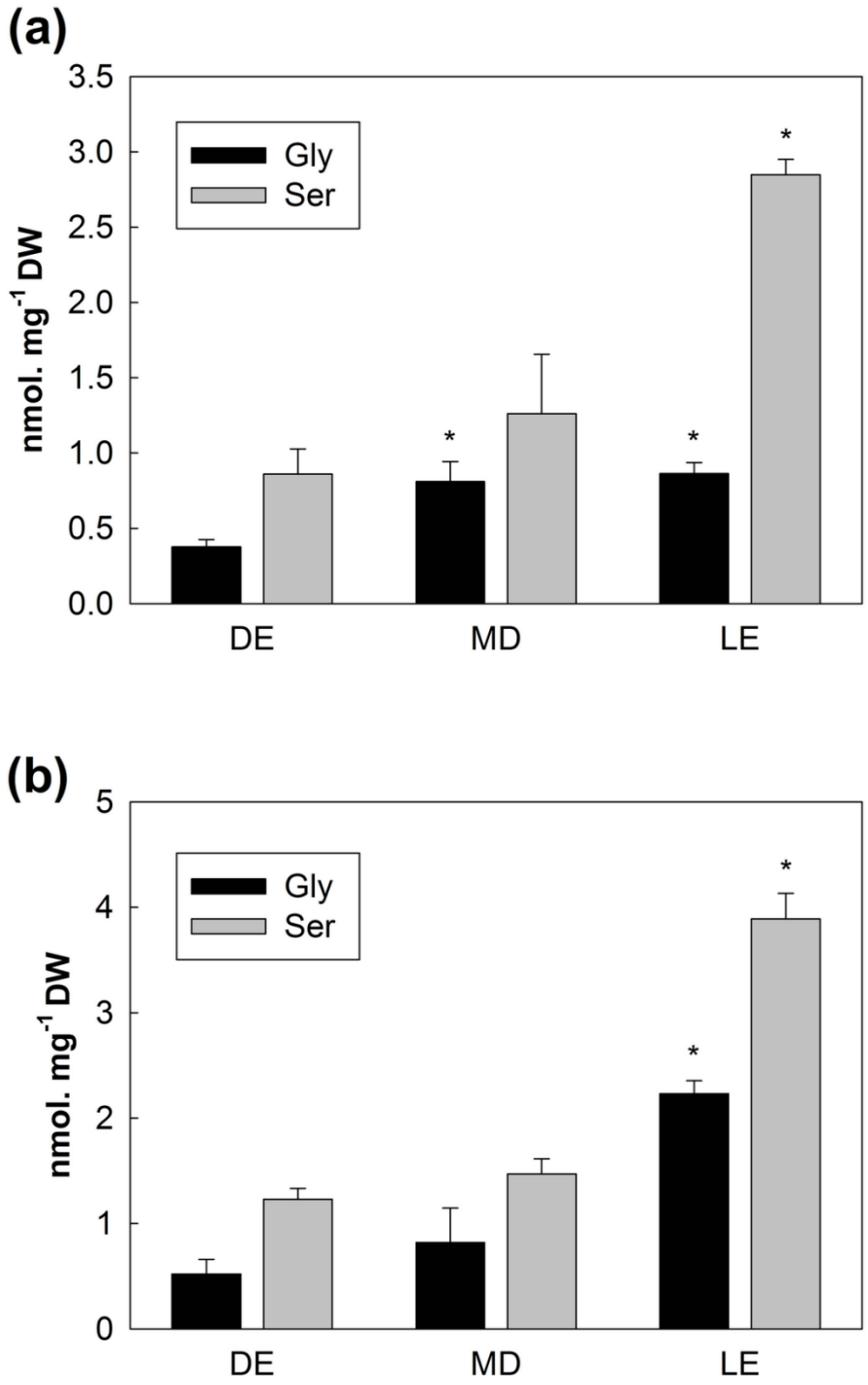

Figure S2.3: Daily evolution of glycine and serine content in seedlings.
Gly and Ser contents were measured in seven-day-old (a) and 14-day-old (b) seedlings at the end of the dark period (DE), at midday (MD) or at the end of the light period (LE). Bars indicate SD of the mean (n = 3), and asterisks indicate statistically different values using DE as reference, according to ANOVA and Dunnett's tests ($p<0.05$).

(a)

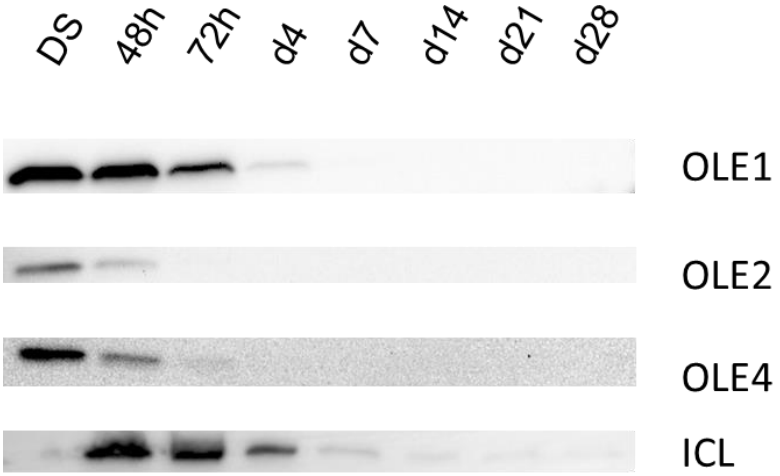

(b)

Sample	OLE1	OLE2	OLE4	ICL
DS	100 ± 0	100 ± 0	100 ± 0	11.8 ± 10.1
48 h	96.9 ± 14.9	35.5 ± 10.9	41.3 ± 15.0	100 ± 0
72 h	36.0 ± 15.4	7.60 ± 5.9	6.8 ± 3.2	93.4 ± 6.9
d4	6.8 ± 8.8	6.17 ± 6.0	4.0 ± 2.7	12.1 ± 20.7
d7	0.2 ± 0.1	8.41 ± 9.9	3.9 ± 3.2	3.0 ± 5.0
d14	0.4 ± 0.5	7.03 ± 6.8	2.9 ± 2.8	1.3 ± 2.0
d21	0.2 ± 0.1	5.74 ± 5.5	3.0 ± 2.6	1.2 ± 1.8
d28	0.3 ± 0.2	5.75 ± 4.7	2.8 ± 0.6	1.3 ± 1.9

Figure S2.4: Immunoblot analyses of oleosins (OLE1, OLE2 and OLE4) and isocitrate lyase content in dry seeds (DS) and during germination and seedling culture (up to 28 days).
Proteins extracted from an equivalent number of seeds/seedlings were loaded in each lane (0.01, 1, 0.1 for OLE1, OLE2, OLE4, respectively). For isocitrate lyase, 20 µg of total protein were loaded in each lane. (a) Representative blots for each antibody; (b) Semi-quantitative analysis of the abundance of the proteins in each sample. Data are expressed as the percentage of detected pixels in each lane (mean ± SD) compared to the highest intensity detected (which is DS for OLE1, OLE2 and OLE4 and 48 h for ICL). The different colors correspond to statistically different groups for each protein according to ANOVA and Tukey's test ($p<0.05$ and $n=3$).

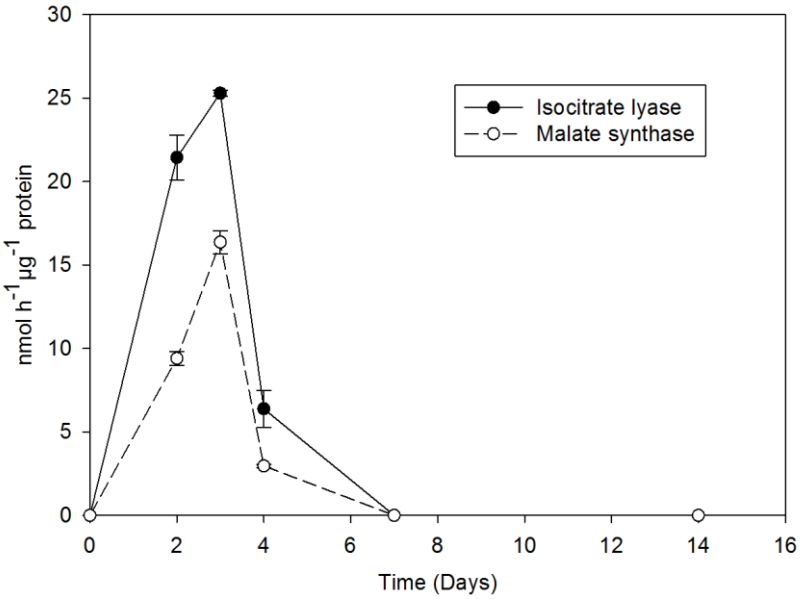

Figure S2.5: Activities of glyoxylic cycle enzymes in seedlings at different times of culture.
Malate synthase (open circles) and isocitrate lyase (closed circles) activities were measured during the two first weeks of seedlings culture. Bars indicate SD of the mean (n = 3).

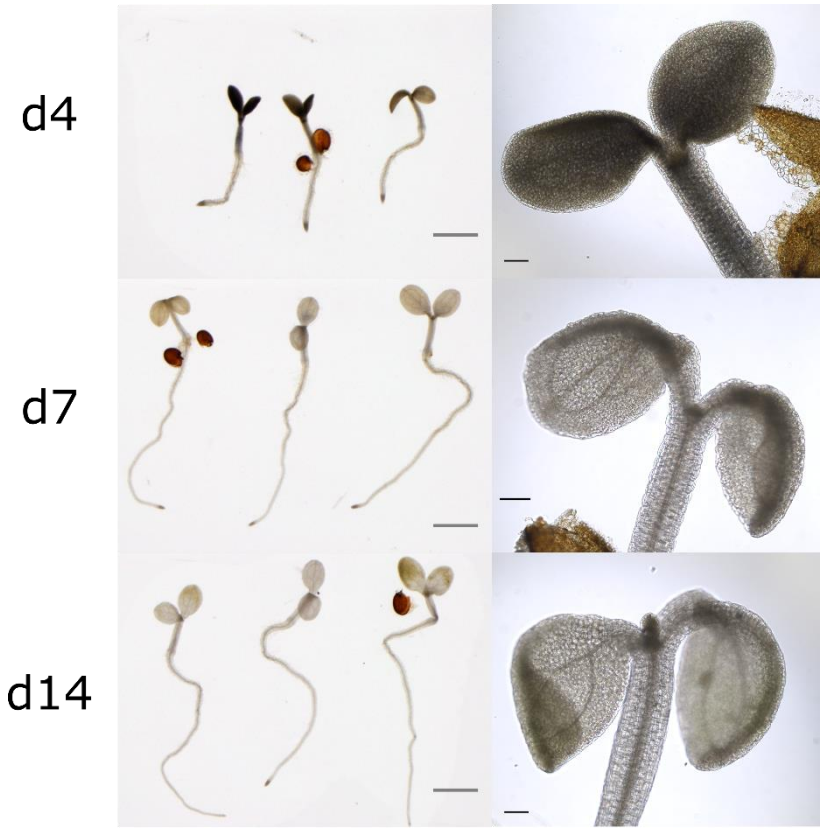

Figure S2.6: Lugol staining reveals the presence of starch on day four but not afterwards.
Grey scale bar, 1 mm; black scale, 100 µm.

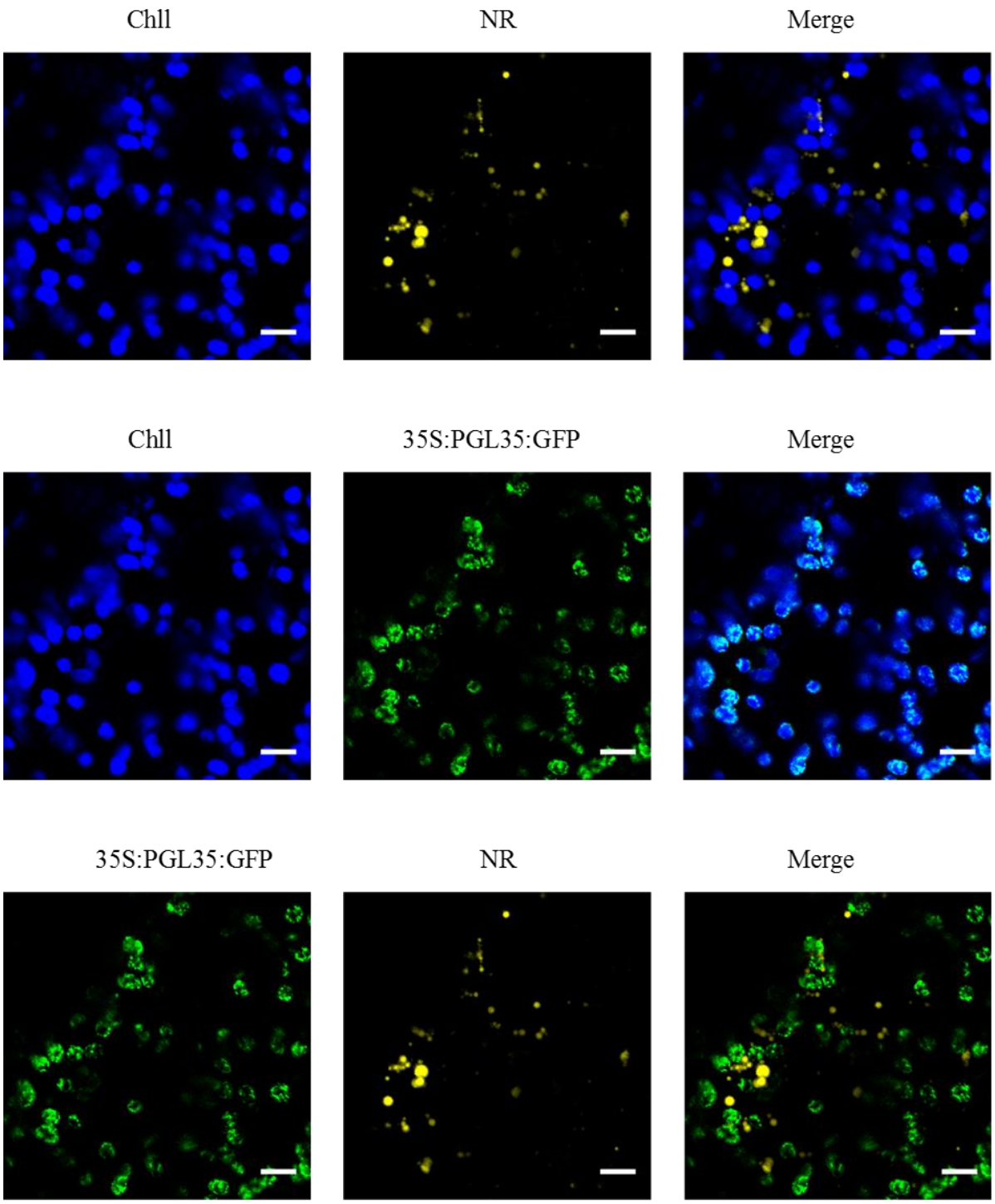

Figure S2.7: Nile red stains lipid droplets (LDs) but not plastoglobuli (PGs).
Fourteen-day-old seedlings constitutively expressing a PG protein GFP fusion (PGL35:GFP) were stained with Nile red and examined by laser scanning confocal microscopy. The fluorescence of Nile red is false coloured in yellow, GFP in green and chloroplast autofluorescence in blue. White scale bar, 10 µm.

Table S2.1: Estimation of Kok effect in seven-day-old seedlings and mature leaves.
Measurements were performed by oxygraphy and slopes were determined as shown in Figure 2.4 (n=4). Means were significantly different according to Student's t-test ($p<0.05$).

Seedlings

Slope A	Slope B	**Ratio**	**1-(A/B)**	**100*(1-(A/B))**
0.1789	0.2029	**0.882**	**0.118**	**11.8**
0.1363	0.1780	**0.766**	**0.234**	**23.4**
0.1662	0.2050	**0.811**	**0.189**	**18.9**
0.1695	0.2252	**0.753**	**0.247**	**24.7**

Mean (%)	**19.7**
SD (%)	**5.8**

Leaves

Slope A	Slope B	**Ratio**	**1-(A/B)**	**100*(1-(A/B))**
0.0662	0.1359	**0.487**	**0.513**	**51.3**
0.0972	0.1443	**0.674**	**0.326**	**32.6**
0.0672	0.1471	**0.457**	**0.543**	**54.3**
0.0640	0.1145	**0.559**	**0.441**	**44.1**

Mean (%)	**45.6**
SD (%)	**9.6**

Table S2.2: Amino acids, organic acids and sugars contents in mature leaves, dry seeds or liquid-grown seedlings.

Amino and organic acids were quantified by GC-MS analysis and sugars by HPLC (n=3). Letters and colours correspond to statistically different groups according to ANOVA and Tukey's test ($p<0.05$).

Mean / SD

grouping	nmol mg-1 DW	Leaves	DS	d4	d7	d14	d21	d28
a	alanine	9.61 / 1.66	0.52 / 0.1	1.24 / 0.14	0.97 / 0.15	1.11 / 0.15	1.23 / 0.34	0.87 / 0.14
ab	glycine	1.57 / 0.77	0.16 / 0.02	0.76 / 0.33	0.76 / 0.13	0.82 / 0.33	3.91 / 0.77	4.55 / 0.57
b	valine	1.07 / 0.03	0.41 / 0.06	1.84 / 0.03	1.16 / 0.13	1 / 0.28	0.96 / 0.52	0.77 / 0.06
bc	leucine	0.68 / 0.12	0.15 / 0.01	1.68 / 0.12	0.62 / 0.14	0.45 / 0.08	0.45 / 0.13	0.46 / 0.07
c	isoleucine	0.43 / 0.05	0.17 / 0.02	1.26 / 0.04	0.82 / 0.1	0.72 / 0.12	0.66 / 0.37	0.53 / 0.05
cd	gABA	11.07 / 1.32	0.04 / 0.07	5.56 / 0.15	5.57 / 1.27	4.37 / 1.89	4.08 / 1.86	3.76 / 1.11
d	methionine	0.44 / 0.03	0.13 / 0.01	0.38 / 0.02	0.33 / 0.06	0.32 / 0.07	0.33 / 0.03	0.37 / 0.02
de	serine	8.87 / 2.2	0.52 / 0.12	1.29 / 0.17	1.26 / 0.39	1.47 / 0.14	1.61 / 0.28	1.46 / 0.1
e	threonine	13.35 / 2.7	0.33 / 0.05	1.68 / 0.23	1.6 / 0.32	1.42 / 0.48	1.44 / 0.09	1.21 / 0.27
abc	phenylalanine	0.55 / 0.04	0.38 / 0.09	0.7 / 0.04	0.71 / 0.1	0.72 / 0.22	0.85 / 0.17	0.74 / 0.15
	aspartate	6.77 / 4.16	1.33 / 0.4	0.45 / 0.02	0.34 / 0.05	0.45 / 0.1	0.35 / 0.09	0.25 / 0.03
	cysteine	0.24 / 0.03	0.08 / 0.07	0.16 / 0.01	0.16 / 0.01	0.17 / 0.01	0.18 / 0.01	0.18 / 0.01
	glutamate	6.89 / 3.7	4.07 / 2.26	5.08 / 0.52	4.9 / 0.78	3.87 / 1.27	3.64 / 1.04	3.11 / 0.64
	asparagine	1.34 / 0.84	2.09 / 2.01	0.81 / 0.14	0.89 / 0.31	0.54 / 0.45	0.69 / 0.74	0.21 / 0.02
	glutamine	23.28 / 9.52	0.19 / 0.33	11.03 / 0.8	13.53 / 2.41	12.74 / 4.54	14.63 / 5.3	10.44 / 1.17
	arginine	0.24 / 0.09	0.05 / 0.08	0.62 / 0.02	0.69 / 0.17	0.58 / 0.15	0.76 / 0.13	0.57 / 0.04
	lysine	2.74 / 0.51	NA	NA	NA	NA	NA	NA
	tyrosine	0.35 / 0.03	0.16 / 0.02	0.31 / 0.01	0.28 / 0.04	0.26 / 0.06	0.26 / 0.08	0.23 / 0.01
	tryptophan	1.1 / 0.24	0.23 / 0.27	0.3 / 0.02	0.4 / 0.04	0.43 / 0.09	0.48 / 0.11	0.42 / 0.12
	proline	1.97 / 0.46	0.24 / 0.07	0.6 / 0.01	0.36 / 0.02	0.22 / 0.05	0.25 / 0.06	0.22 / 0.01
	succinate	1.34 / 0.37	0.34 / 0.06	4.01 / 0.15	3.23 / 0.31	2.99 / 0.32	3.43 / 0.94	2.33 / 0.16
	fumarate	62.12 / 14.37	1.3 / 0.07	11.72 / 2.22	13.17 / 0.28	16.75 / 0.91	27.94 / 5.08	30.03 / 2.6
	2-oxoglutarate	1.42 / 0.06	0.14 / 0.01	20.75 / 1.39	52.39 / 6.38	36.05 / 21.85	64.74 / 42.31	42.19 / 8.29
	malate	45.31 / 10.45	3.53 / 0.35	188.74 / 9.09	166.6 / 14.61	315.04 / 25.78	350.53 / 37.99	352.78 / 15.9
	isocitrate	0.32 / 0.03	0.15 / 0.01	0.71 / 0.07	1.14 / 0.28	1.06 / 0.26	0.8 / 0.17	0.64 / 0.21
	citrate	13.19 / 4.85	3.55 / 0.38	85.44 / 12.74	89.47 / 11.42	70.67 / 16.68	44.67 / 16.6	37.13 / 2.01
	pyruvate	6.01 / 0.42	0.58 / 0.02	5 / 0.29	4.6 / 0.82	5.48 / 0.69	4.98 / 0.42	5.2 / 0.19
	glucose	22.92 / 2.49	NA	41.91 / 0.48	39.45 / 1.16	40.42 / 5.09	36.12 / 2.4	40.95 / 3.01
	fructose	3.99 / 0.37	NA	6.59 / 0.41	4.98 / 0.47	4.79 / 1.11	4.24 / 0.67	6.4 / 0.9
	sucrose	0.2 / 0.08	7.25 / 0.75	0.34 / 0.06	0.4 / 0.2	0.55 / 0.26	0.25 / 0.2	0.32 / 0.07
	raffinose	NA	0.3 / 0.06	NA	NA	NA	NA	NA
	stachyose	NA	1.81 / 0.19	1.22 / 0.19	0.83 / 0.11	0.66 / 0.26	0.31 / 0.08	0.71 / 0.17

Total amino acids	92.58 / 25.21	11.25 / 5.77	36.77 / 1.6	36.39 / 5.62	32.33 / 9.96	37.78 / 9.79	31.21 / 1.39
Total organic acids	129.72 / 28.76	9.58 / 0.74	316.38 / 21.97	377.58 / 31.44	448.04 / 13.64	497.09 / 38.07	470.29 / 14.43
Total sugars	27.12 / 2.18	9.37 / 0.97	50.06 / 1.05	45.65 / 1.45	46.43 / 6.63	40.93 / 2.75	48.37 / 3.96

Table S2.3: Amino acids, organic acids and sugars contents in liquid-grown seedlings during daytime. Amino and organic acids were quantified by GC-MS analysis and sugars by HPLC (n=3). Letters and colours correspond to statistically different groups according to ANOVA and Tukey's test ($p<0.05$).
NE, night end; MD, midday; DE, day end

		Mean/SD					
	nmol mg-1 DW	d7 NE	d7 MD	d7 DE	d14 NE	d14 MD	d14 DE
grouping	alanine	0.52 / 0.04	0.97 / 0.15	0.68 / 0.04	0.9 / 0.23	1.11 / 0.15	0.62 / 0.06
a	glycine	0.38 / 0.05	0.76 / 0.13	0.86 / 0.07	0.52 / 0.14	0.82 / 0.33	2.23 / 0.12
ab	valine	0.81 / 0.06	1.16 / 0.13	1.01 / 0.01	0.54 / 0.26	1 / 0.28	0.61 / 0.01
b	leucine	0.5 / 0.02	0.62 / 0.14	0.6 / 0.02	0.32 / 0.11	0.45 / 0.08	0.4 / 0.02
	isoleucine	0.61 / 0.02	0.82 / 0.1	0.82 / 0.01	0.32 / 0.16	0.72 / 0.12	0.54 / 0.02
	gABA	4.06 / 0.73	5.57 / 1.27	4.16 / 0.18	4.41 / 2.3	4.37 / 1.89	1.87 / 0.06
	méthionine	0.32 / 0.04	0.33 / 0.06	0.39 / 0.01	0.32 / 0.05	0.32 / 0.07	0.38 / 0.01
	serine	0.86 / 0.17	1.26 / 0.39	2.85 / 0.1	1.23 / 0.1	1.47 / 0.14	3.89 / 0.24
	threonine	1.44 / 0.1	1.6 / 0.32	1.99 / 0.18	1.22 / 0.05	1.42 / 0.48	1.65 / 0.17
	phenylalanine	0.66 / 0.05	0.71 / 0.1	0.86 / 0.03	0.51 / 0.16	0.72 / 0.22	0.83 / 0.02
	aspartate	0.43 / 0.06	0.34 / 0.05	0.34 / 0.05	0.79 / 0.08	0.45 / 0.1	0.36 / 0.02
	cystéine	0.18 / 0.01	0.16 / 0.01	0.18 / 0	0.17 / 0.02	0.17 / 0.01	0.18 / 0.01
	glutamate	5.17 / 0.38	4.9 / 0.78	4.69 / 0.23	3.7 / 0.13	3.87 / 1.27	2.62 / 0.14
	asparagine	0.7 / 0.2	0.89 / 0.31	0.59 / 0.04	0.64 / 0.35	0.54 / 0.45	0.25 / 0.04
	glutamine	7.78 / 1.71	13.53 / 2.41	10.34 / 0.53	10.6 / 1.07	12.74 / 4.54	10.44 / 1.14
	arginine	0.47 / 0.19	0.69 / 0.17	0.66 / 0.09	0.61 / 0.05	0.58 / 0.15	0.63 / 0.07
	tyrosine	0.25 / 0.02	0.28 / 0.04	0.29 / 0.01	0.22 / 0.06	0.26 / 0.06	0.26 / 0.01
	tryptophan	0.34 / 0.04	0.4 / 0.04	0.5 / 0.01	0.36 / 0.05	0.43 / 0.09	0.45 / 0.02
	proline	0.23 / 0	0.36 / 0.02	0.26 / 0.01	0.17 / 0.02	0.22 / 0.05	0.17 / 0
	succinate	4.39 / 0.37	3.23 / 0.31	3.6 / 0.15	3.65 / 0.82	2.99 / 0.32	3.06 / 0.2
	fumarate	13.22 / 0.13	13.17 / 0.28	11.53 / 0.09	15.72 / 1.82	16.75 / 0.91	17.11 / 0.69
	2-oxoglutarate	67.83 / 1.84	52.39 / 6.38	81.65 / 10.65	46.37 / 24.38	36.05 / 21.85	102.83 / 6.29
	malate	175.58 / 13.26	166.6 / 14.61	165.44 / 6.45	322.06 / 13.36	315.04 / 25.78	324.59 / 24.67
	isocitrate	1.78 / 0.18	1.14 / 0.28	1.5 / 0.02	1.18 / 0.2	1.06 / 0.26	1.35 / 0.05
	citrate	141.44 / 10.06	89.47 / 11.42	117.1 / 11.15	92.47 / 10.48	70.67 / 16.68	84.89 / 3.87
	pyruvate	4.16 / 0.46	4.6 / 0.82	4.14 / 0.3	6.14 / 1.2	5.48 / 0.69	4.45 / 0.12
	glucose	43.09 / 2.53	39.45 / 1.16	42.29 / 0.33	45.08 / 4.64	40.42 / 5.09	42.08 / 0.95
	fructose	4.92 / 0.24	4.98 / 0.47	5.35 / 0.55	5.24 / 1.17	4.79 / 1.11	4.63 / 0.21
	sucrose	0.36 / 0.03	0.4 / 0.2	0.33 / 0.04	0.4 / 0.13	0.55 / 0.26	0.55 / 0.2
	stachyose	0.76 / 0.15	0.83 / 0.11	0.72 / 0.07	0.75 / 0.13	0.66 / 0.26	0.53 / 0.06

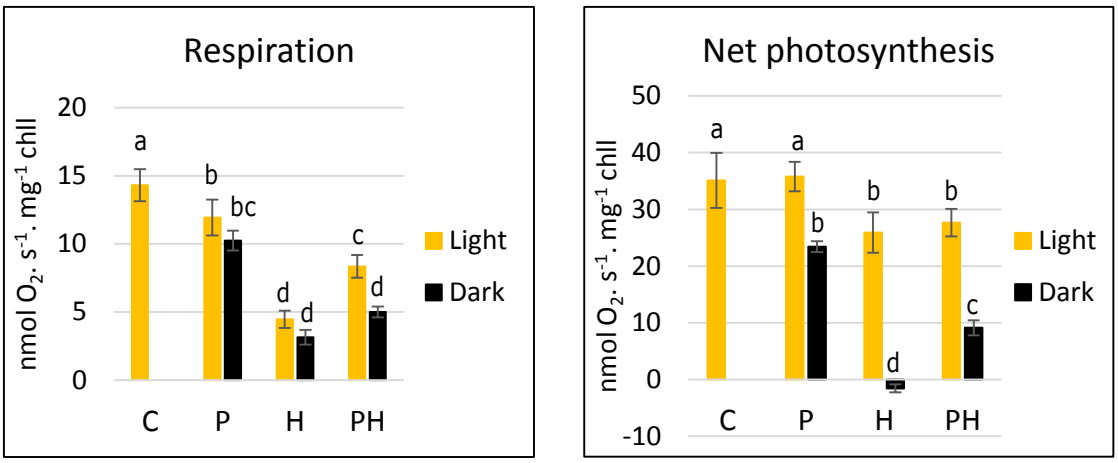

Figure 3.1: Respiration and net photosynthesis after heat treatment in the light or in the dark.
Oxygraphic measurements were performed at 25°C in the dark (respiration) or with saturating light (800 µmol photons.m^{-2}.s^{-1}; net photosynthesis) after 2 h of recovery post-treatment (C: control in the light, P: 38°C 2 h, H: 43°C 2 h; PH: 38°C 2 h, 21°C 2 h, 43°C 2 h); control in the dark was not performed in this assay but was shown to be not significantly different from control in the light in another experiment; 3<n<9; letters correspond to statistically different groups according to ANOVA and Tukey's test ($p<0.05$).

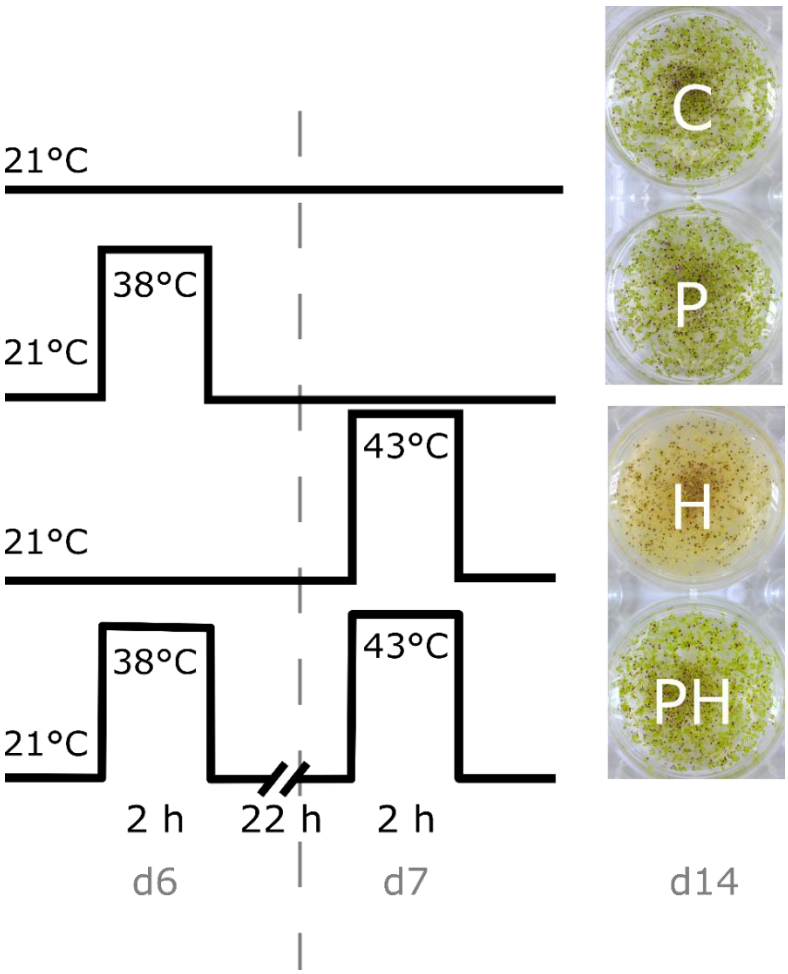

Figure 3.2: Heat stress regimes and representative pictures of wells at day 14 (one week after 43°C treatment), illustrating the survival or death of seedlings.
After the transfer of seedlings and medium in 25 mL glass containers, treatments were performed in a water bath in the presence of low light (150 µmol photons.m^{-2}.s^{-1}). After treatment, seedlings are transferred back into the six-well plates.

Chapter III- Physiological and cellular acclimation to heat stress in Arabidopsis seedlings

1. Introduction

As presented in Chapter I, heat stress (HS) has a major effect on plant physiology, especially on photosynthesis and respiration. However, most studies have focused on the impact of HS on these processes over a relatively short term. Moreover, the impact of a pre-treatment on photosynthesis and respiration during and after heat shock has not been evaluated, to our knowledge. Therefore, the role and adaptations of energy metabolism in the context of acquired thermotolerance are still unclear. Taking advantage of our experimental system which provides homogenous developmentally arrested seedlings, we aimed to characterize physiological and cellular adaptive responses to heat shock with, or without acclimation. This chapter will focus on the respiratory and photosynthetic response, but also on the impact of heat on organelle dynamics by using *in vivo* fluorescence microscopy.

2. Results and discussion

2.1. Heat stress regimes

In order to discriminate between acclimated and non-acclimated seedlings, we first needed to set up stress conditions in which seedlings grown in liquid culture would be protected by a previous priming against an otherwise lethal heat shock. This kind of experiment was previously done for Arabidopsis seedlings grown on MS medium (Queitsch *et al.*, 2000; Echevarría-Zomeño *et al.*, 2016), but it was necessary to optimize it for our conditions. We initially designed an acclimation regime of 2 h at 38°C (priming), 2 h at 21°C (recovery) and 2 h at 43°C (heat shock) by transferring seedlings with their medium in glass containers (25 mL Schott) immersed into a water bath set at the proper temperature and in the dark. These conditions allowed seedlings to survive against the otherwise lethal heat shock at 43°C. These results are concordant with those of previous HS treatments found in the literature, meaning that seedlings grown in our system develop a thermotolerance close to that observed with seedlings grown on plates (Queitsch *et al.*, 2000; Kang *et al.*, 2016; Halter *et al.*, 2017). However, we decided to change the HS conditions in order to get closer to natural conditions, in which severe HS occurs during the light period. Therefore, during the heat treatments (priming and heat shock) we applied a low-light intensity close to that applied in the growth room (around 150 µmol photons.m^{-2}.s^{-1}). This appeared to be more "physiological", avoiding the necessity to combine HS with transfer to darkness, as was done in almost all other published work. Indeed, even if HS is applied under darkness in most published studies, it was previously shown that the HSR is very different in the light or in the dark (Caldana *et al.*, 2011). Moreover, in our system in which seedlings are placed in a closed system during the 2 h of treatment, respiration at 38°C or 43°C led to hypoxia under darkness (around 10 µM dissolved O_2 after 2 h at 38°C). When the heat treatments were performed in the light, the medium remained hyperoxic (270 µM dissolved O_2 after 2 h at 38°C), thanks to photosynthetic

A

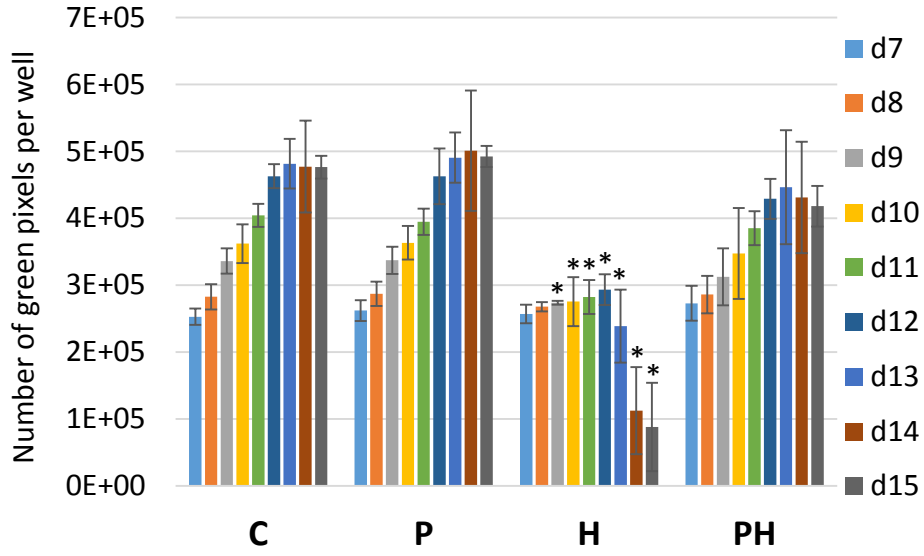

B

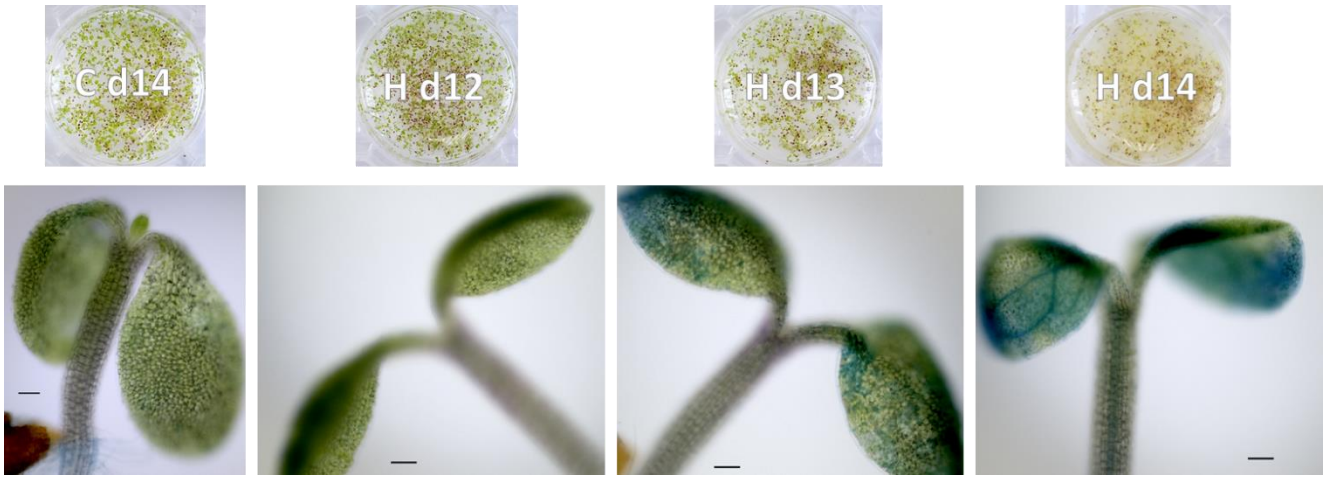

Figure 3.3: Impact of heat treatments on seedling growth and viability.

A- Green pixel analysis in liquid-grown seedlings. The evolution of green pixel number per well reflects the expansion of cotyledons (in C, P and PH) or growth arrest and progressive death (in H) occurring during seedling liquid culture from day 7 to 15 (0 to 8 days post 43°C treatment); * significantly different from C according to ANOVA and Dunnett's test ($p<0.05$); $4<n<11$.

B- Evans blue viability assay after heat-shock. Representative images of wells illustrating the slow death of seedlings after heat shock at 43°C (top); H d12, 13, 14: H seedlings after 5, 6 or 7 days of recovery post treatment; C d14: control on day 14; detection of dead cells coloured in blue by Evans blue staining in the same samples (bottom); scale bar, 100 µm.

oxygen evolution. Clearly, the impact of heat treatments on both net photosynthesis and respiration was more severe in the dark than in the light, as shown by the oxygraphic measurements performed after 2 h of recovery (Figure 3.1). When heat treatment was performed in the dark, respiration was around 1.4x lower than in the light for non-acclimated seedlings (H, heat shock), and 1.7x for primed seedlings (PH, priming+heat shock), while net photosynthesis was below the compensation point in H and decreased by 2.5x in PH compared to the control. This was correlated with a quicker death of the heat shocked seedlings and a lower survival rate of seedlings, which were pre-acclimated before heat shock. In contrast to our results, Larkindale & Knight (2002) found that recovery in the dark after a heat treatment of 1 h at 40°C allowed a higher survival than recovery in the light. They hypothesized that the higher membrane peroxidation observed during recovery in the light was due to photo-oxidative stress. However, there was no information about the light intensity used in these experiments, and, moreover, their experimental conditions for HS treatment (0.5 g seedlings transferred to 1 mL MS medium in a 1.5 mL microtube placed in a heat block) should lead to a rapid hypoxia. The combination of hypoxia with HS was likely to be noxious in their experiments since the heat shocked seedlings were totally bleached after three days, while, in our system they remained green for several days before yellowing progressively. The beneficial effect of low light during and after HS is likely to be related to the maintenance of energy metabolism (Figure 3.1), which could be essential for the high energy demand required for stress tolerance. It was also shown that the expression of *HSPs* follows a diurnal pattern controlled by light-induced chloroplast retrograde signalling (Dickinson *et al.*, 2018), which could also contribute to the higher thermotolerance observed in the light.

Although this acclimation system (2 h priming, 2 h recovery, 2 h heat shock) worked well, we decided to increase the recovery period to 22 h, i.e., performing the heat shock one day after the priming treatment. Besides mimicking better what happens during a heat wave, during which the maximum temperature progressively increases for a few days, it allowed us to minimize the effects of the circadian rhythm, with both priming and heat shock applied at the same time of the diurnal cycle. Moreover, it permitted us to better distinguish priming and severe heat shock responses that could have overlapped when recovery lasted only 2 h. Last but not least, it facilitated the acquisition of the lengthy oxygraphic analyses that generally started 2 h after the last treatment, which would mean at 4 pm for the original treatment.

Finally, the optimal conditions for the acquired thermotolerance assay of seedlings were established as follow: at 8 am (after 2 h of photoperiod), six-day-old seedlings were primed for 2 h at 38°C in a water bath, with a light intensity similar to that of the growth room (150 µmol photons.m^{-2}.s^{-1}); they were allowed to recover for 22 h in the growth room conditions (12 h light, 21°C/8 h dark, 19°C), and a heat shock of 2 h at 43°C was then applied (Figure 3.2).

For easier description of the samples, they will be referred hereafter as:

C = control seedlings

P = primed seedlings

H = heat-shocked seedlings

PH = primed + heat-shocked seedlings

The seedling capacity to grow was estimated by the quantification of green pixels in images acquired at different days post-treatment, using an ImageJ macro previously developed in the team (Figure 3.3A; Benamar *et al.*, 2013). In C, P and PH seedlings, the number of green pixels increased progressively, reflecting the expansion of

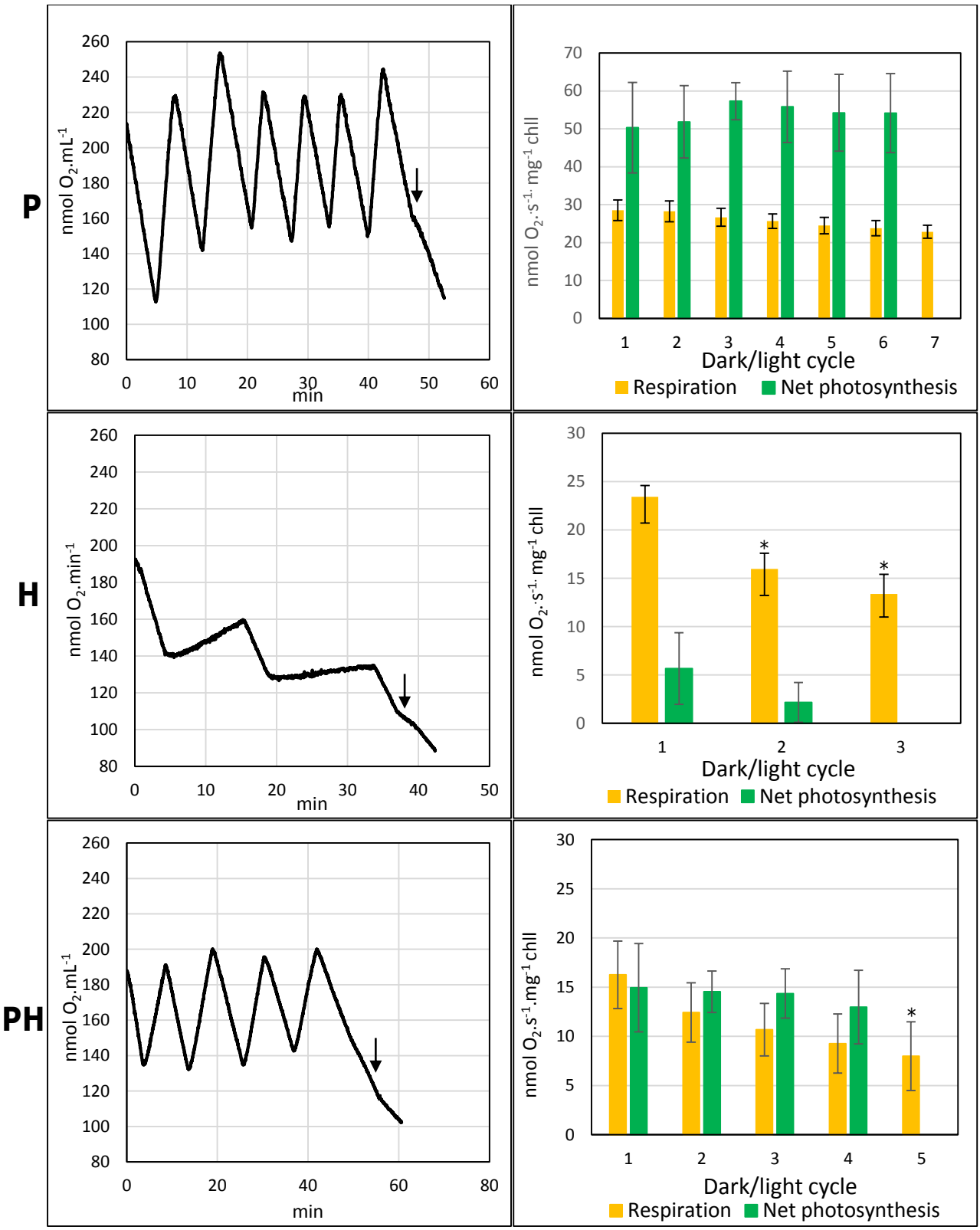

Figure 3.4: Evolution of respiration and net photosynthesis at 38°C and 43°C.
Representative oxygraphs (left) in P, H and PH seedlings; decreasing O_2 concentration corresponds to dark respiration and increasing O_2 concentration to maximal net photosynthesis in the light (measured at 800 µmol photons.m^{-2}.s^{-1}); the arrows indicate addition of KCN (500 µM); Evolution of seedlings respiration and net photosynthesis in the different heat treatments (right); measurements were performed at either 38°C (P) or 43°C (H/PH); values were normalized by chlorophyll content extracted from the same material; the bars indicate SD of the mean (n=3); * indicates a significant difference compared to cycle 1 according to ANOVA and Dunnett's test ($p<0.05$).

cotyledons occurring between day 7 and day 15 of growth (Figure 3.3A; see Chapter II). On the contrary, in H seedlings, the number of green pixels was stable and then dramatically decreased from seven days after the heat shock, revealing growth arrest and subsequent seedling death. To confirm these results, we performed a viability assay on H seedlings using Evans blue, a dye of high molecular weight (961 $g.mol^{-1}$) that can only cross damaged membranes of dead cells (Figure 3.3B). Blue stained cells started to be detected from day 13 (six days after treatment) and cotyledons appeared almost completely blue at day 14, thus confirming a massive cell death around seven days after the heat shock (Figure 3.3B). These results are very different from a previous viability assay performed on tobacco cell culture, in which around 35 % of dead cells were already observed after 24 h recovery following a 5 min treatment at 45°C (Malerba *et al.*, 2010). This may be caused by a slower induction of cell death in developmentally arrested seedlings or simply *in planta*, compared to cell culture, but could also result from the different HS conditions. The relatively long survival of H seedlings, and the fact that they remain green for several days argues in favour of a mechanism of programmed cell death (PCD) induced by heat shock, rather than a necrotic death caused by early rupture of cellular membranes.

2.2. Respiratory and photosynthetic acclimation

2.2.1. Measurements during stress at 38°C or 43°C

Although seedlings, in our experimental system, are arrested in their development, they strongly rely on respiration and photosynthesis to remain alive for long periods in almost pure water, as we have seen in Chapter II. It was thus of primary interest to analyse the impact of the heat treatments on these essential processes. Respiratory and photosynthetic activities were measured by oxygraphy (Clark electrode) during and after the different treatments. The oxygen electrode was calibrated either at the treatment temperature (38°C or 43°C), to measure respiration and photosynthesis during and just after treatment, or at 25°C for measurements after recovery. Figure 3.4 presents the respiratory and photosynthetic activities of seedlings, which were directly incubated in the oxygen electrode chamber at 38°C or 43°C. Cycles of darkness and light were applied to follow the evolution of respiratory and maximal net photosynthetic activity, which was measured with a light intensity of 800 µmol photons.$m^{-2}.s^{-1}$. Activities were normalized by the chlorophyll content. At 38°C, dark respiration (DR) and net photosynthesis (NP) respectively reached 30 and 50 nmol $O_2.s^{-1}.mg^{-1}$ chll (Figure 3.4), which is higher than values usually obtained at 25°C (respectively around 14 and 40 nmol $O_2.s^{-1}.mg^{-1}$ chll). From these data, we estimated the respiratory Q_{10} using the formula: $Q_{10} = \left(\frac{R2}{R1}\right)^{\left(\frac{10}{T2-T1}\right)}$ where R_1 and R_2 are the rates of respiration at T1 (25°C) and T2 (38°C), respectively. We obtained a value of 1.8, which is close to the theoretical respiratory Q_{10} of around 2.0, meaning that R doubles for a 10°C increase (Atkin & Tjoelker, 2003). In the case of photosynthesis, a raw estimation of gross photosynthesis (GP), by using DR as a proximate value for respiration in the light and summing it with NP, led to values of 54 and 80 nmol $O_2.s^{-1}.mg^{-1}$ chll at 25°C and 38°C, respectively. These data and the lower Q_{10} for GP (1.4), estimated using the same formula, confirm that photosynthesis is more sensitive to high temperature than respiration (Yamori *et al.*, 2014). Both NP and DR remained stable over several light-dark cycles during a 38°C treatment, indicating that photosynthesis and respiration were not severely compromised during priming. On the contrary, at 43°C, H seedlings initially

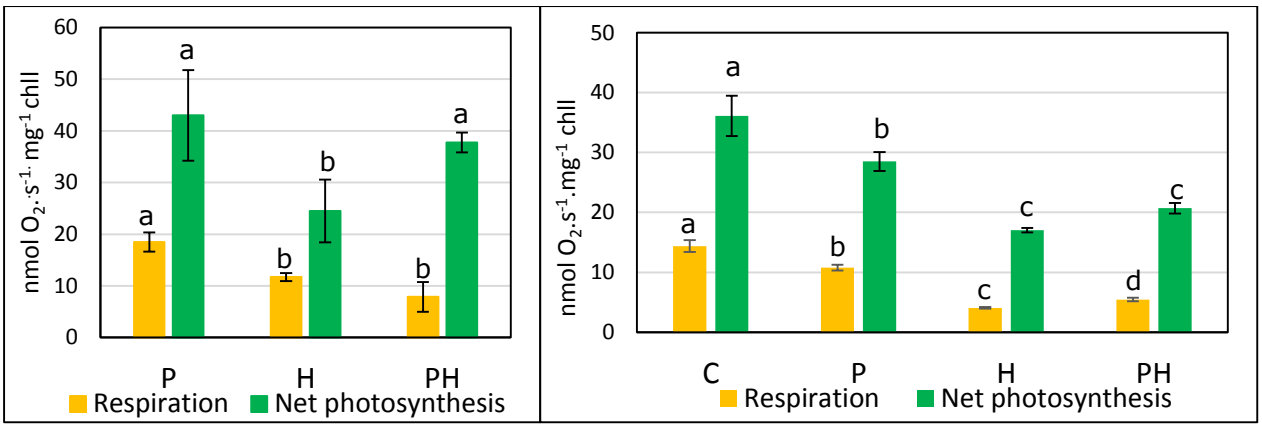

Figure 3.5: Respiratory and net photosynthetic activities measured just after heat treatments.
Dark respiration and net photosynthesis at 800 µmol photons.m^{-2}.s^{-1} were acquired by oxygraphy at either 38°C (P) or 43°C (H/PH) after the 2 h of the corresponding heat treatment (left) or at 25°C after 5 min of the seedlings cooling down after treatment (right); the bars indicate SD of the mean (n=8 (left) or n=4-6 (right)); letters correspond to statistically different groups according to ANOVA and Tukey's test ($p<0.05$).

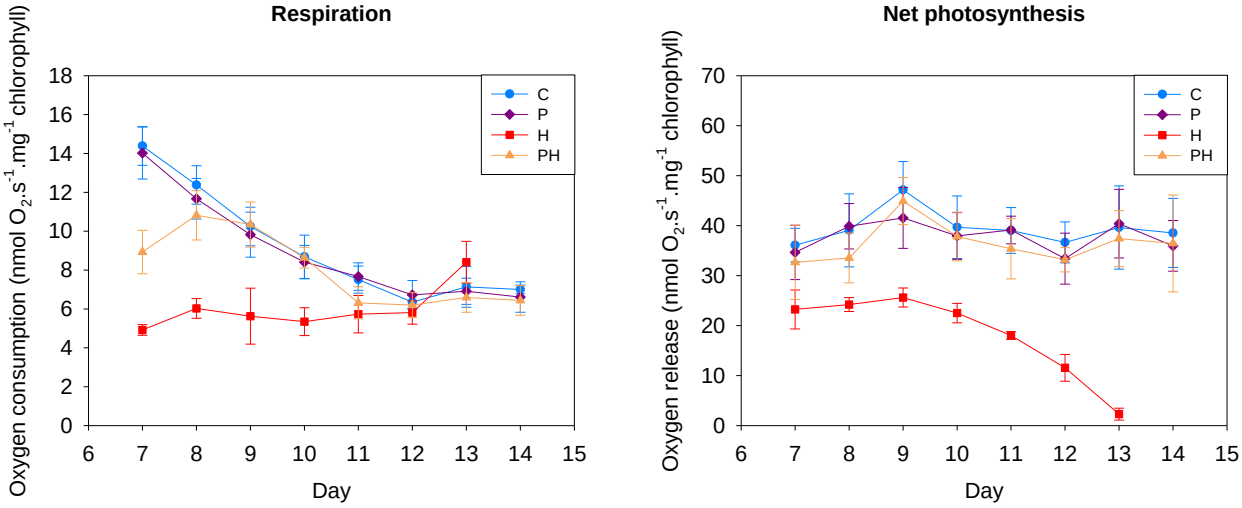

Figure 3.6: Respiratory and net photosynthetic activities measured during recovery.
Dark respiration and net photosynthesis at 800 µmol photons.m^{-2}.s^{-1} were acquired by oxygraphy at 25°C after 2 h of recovery post 43°C treatment on day 7 (H and PH) and compared to their respective controls C and P, and on the following days of recovery; the bars indicate SD of the mean (n=6).

displayed a high DR rate (around 23 nmol $O_2.s^{-1}.mg^{-1}$ chll), which decreased by around 40 % after two more cycles. NP appeared to be strongly affected by this high temperature, as it hardly reached 5 nmol $O_2.s^{-1}.mg^{-1}$ chll in the first cycle and rapidly declined over the first 30 minutes of treatment, photosynthesis dropping below the compensation point at the third cycle. In PH seedlings, the treatment at 43°C also induced a decline in respiratory activity across the different cycles. However, net photosynthesis was maintained at higher levels (around 15 nmol $O_2.s^{-1}.mg^{-1}$ chll) over the first hour of treatment, revealing a protective effect of priming.

2.2.2. Measurements at 38°C or 43°C at the end of stress application

These results were confirmed by measurements acquired at the end of the 2 h HS treatments at 38°C or 43°C, using the oxygen electrode calibrated at the same temperature (Figure 3.5). DR was around 18 nmol $O_2.s^{-1}.mg^{-1}$ chll for P treatment and lower for both H and PH treatments (around 12 and 8 nmol $O_2.s^{-1}.mg^{-1}$ chll, respectively). NP was similar for P and PH (around 40 nmol $O_2.s^{-1}.mg^{-1}$ chll), whereas it was lower for H treatment (around 25 nmol $O_2.s^{-1}.mg^{-1}$ chll). The higher values of NP for H and PH in this experiment (compared to Figure 3.4) are likely to be related to the differences in light intensity applied during HS in the water bath and in the electrode (150 vs 800 µmol photons.$m^{-2}.s^{-1}$), the alternation of dark and light cycles occurring in the oxygen electrode, compared to constant light in the bath, and the high agitation required in the oxygen electrode. Thus, photosynthesis could be more severely affected by the experimental conditions encountered by the seedlings in the oxygen electrode conditions.

2.2.3. Measurements at 25°C after heat stress and during recovery

After heat treatments and a short recovery (5 minutes) to cool down the seedlings, measurements were performed at 25°C to compare respiration and photosynthetic capacity with respect to the control conditions (Figure 3.5). For P seedlings, DR and NP were lower (25 % and 22 %, respectively) than the control (day seven) and they were much lower for both H (72 % and 53 %) and PH (62 % and 43 %) seedlings. However, an enhancement of DR (34 %) was observed for PH seedlings (compared to H), suggesting a beneficial effect of priming on respiration visible at the end of the HS treatment.

Altogether, these data indicate that photosynthetic and respiratory activities were increased during priming, but upon return to 25°C, they reverted close to the control values. On the contrary, heat shock had a significant impact on both respiration and photosynthesis, which was not reversible after transfer back to 25°C in H seedlings. However, in the PH treatment, the previous priming clearly had a protective effect on the respiratory response after HS. To get further insight into the long-term effect of the treatments on energy metabolism after heat shock, we further measured respiratory and photosynthetic activities after 2 h of recovery, and during the following days (Figure 3.6).

For the control seedlings, DR decreased around two times from day 7 to day 11 and then stabilized, while NP was stable from 7 to 14 days (around 40 nmol $O_2.s^{-1}.mg^{-1}$ chll), which corresponds to the results obtained in Chapter II. In the case of P seedlings, after 24 h, both DR and NP values were similar to those of the control, indicating that this treatment is apparently innocuous for the seedlings, with no long term effect on energy metabolism, and viability. However, for H seedlings, DR and NP values were markedly and irreversibly affected from 2 h of recovery (Figure 3.6). NP was 36 % lower than the control after 2 h of recovery and decreased after day 9 when the seedlings were progressively dying, while DR remained stable during the days following treatment.

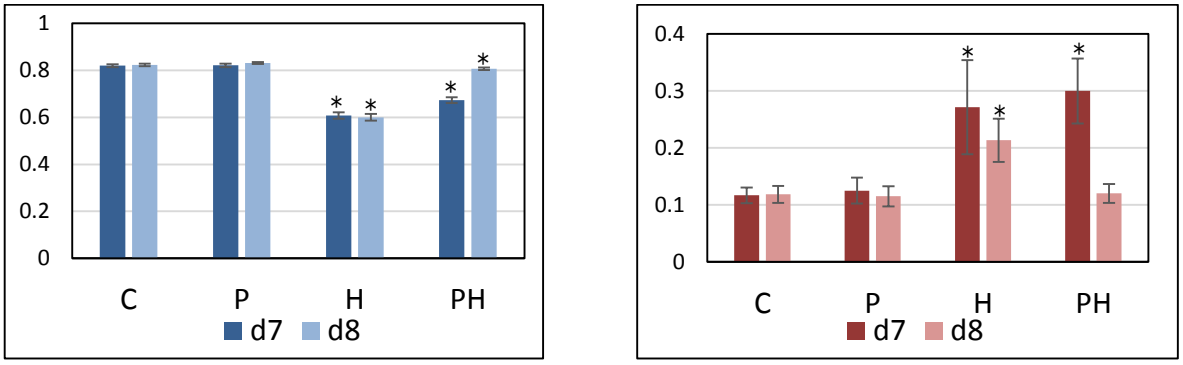

Figure 3.7: Heat response of photosystem II quantum yield and non-photochemical quenching. Maximum photosystem II quantum yield (left) and steady-state non-photochemical quenching in light (right) 2 h (d7) and 24 h (d8) after heat shock; the bars indicate SD of the mean for three biological repeats x2 technical repeats; * indicates a significant difference compared to cycle 1 according to ANOVA and Dunnett's test or Kruskall-Wallis on ranks (p-value<0.05).

The increase in DR observed after day 12 could be due to the spreading of cell death and uncontrolled oxidase activities. Interestingly, after 2 h of recovery, PH seedlings displayed DR and NP rates (9 and 32 nmol O_2.s^{-1}.mg^{-1} chll, respectively) which were lower than C, but higher than H, and which became similar to those of the control after 24 h of recovery. Thus, priming has a major beneficial effect on seedling energy metabolism during recovery from heat shock.

2.2.4. Chlorophyll fluorescence after heat-shock

The impact of the heat treatments on photosynthesis was also measured by analysing chlorophyll fluorescence, which is a non-destructive approach useful to estimate the effect of stress on photosynthetic efficiency (Baker, 2008). Fluorescence quenching analyses were performed by fluorescence imaging after 2 h recovery and during the days following heat shock. The maximum photosystem II quantum yield (a parameter related to photochemical quenching) and the steady state non-photochemical quenching (NPQ) in the light are shown in Figure 3.7. Details of their calculation are specified in the Material and Methods section. The maximum photosystem II quantum yield values were around 0.8 for both C and P seedlings, a value which is considered as normal value for healthy plants (Baker, 2008). In H seedlings, after 2 h and 24 h of recovery post-HS, the value was around 0.6, indicating a significant impact of HS on photosynthetic efficiency, which was irreversible on the following days (Figure 3.7). In PH seedlings, there was a transient decrease of the maximum photosystem II quantum yield (0.67) measured after 2 h recovery, with a recovery observed after 24 h. The steady-state NPQ in light was around 0.1 in C and P seedlings, but much higher in H and PH 2 h after HS (around 0.3). Again, the effect was irreversible in H and reversible in PH. These overall data confirmed the previous results obtained by oxygraphy for photosynthetic activity by an independent method.

2.2.5. Overview of energy metabolism responses

In our analysis, DR was shown to be more deeply impacted by heat shock than NP: after 2 h of recovery, DR decreased 3 times and NP 1.5 times in comparison to C. This was surprising since photosynthesis is often considered as more sensitive to heat than respiration (Wahid *et al.*, 2007; Araújo *et al.*, 2014; Yamori *et al.*, 2014). However, most studies have focused on the response of energy metabolism to short and acute HS or on the acclimation to moderate temperature over a long period (Haldimann & Feller, 2005; Bunce, 2008; Hüve *et al.*, 2011). Therefore, it is unclear how energy metabolism reacts to heat shock over a period of several hours. Moreover, in our conditions, the measurement of respiration included both cotyledons and radicles, and we cannot exclude a differential response from the organs that could affect the response. Indeed, it was shown that under moderate temperature, the respiratory Q_{10} of roots was generally lower than that of leaves, even if the response was species-dependent (Loveys *et al.*, 2003). However, to our knowledge, whether it is also the case at temperature above 40°C remains unknown. Besides this, measurements of DR can also be influenced by the previous light period (Araújo *et al.*, 2014). Respiration in the light could also respond differently than DR, as the latter was shown to be more sensitive to temperature (Atkin *et al.*, 2000). However, we have not investigated the temperature response of the Kok effect previously studied with seedlings at 25°C (cf Chapter II).

Table 3.1: Percentages of KCN-insensitive respiration reflecting the capacity of the alternative oxidase.
Rates of KCN-resistant respiration were acquired during the last cycle of dark respiration (as shown in Figure 3.4 and Figure 7.1) following the injection of 500 µM KCN. Mean and SD for 3<n<6 are presented for measurements acquired at the treatment temperature (38°C for P and 43°C for P and PH) or at 25°C after 2 h, or one day of recovery.

Treatment	At treatment temperature (38°C or 43°C)	At 25°C after 2 h recovery	At 25°C after 1 d recovery
C		72.6 ± 2.5 %	78.8 ± 3.3 %
P	54.3 ± 1.5 %	75.7 ± 3.8 %	76.8 ± 5.1 %
H	60.0 ± 1.5 %	88.3 ± 1.7 %	66.6 ± 5.9 %
PH	74.2 ± 3.7 %	93.1 ± 3.5 %	90.4 ± 2.2 %

Since a major player in plant stress tolerance is the mitochondrial alternative oxidase (AOX), whose activity influences energy and ROS homeostasis (Vanlerberghe, 2013), we measured the proportion of KCN-resistant respiration as a proxy for AOX capacity. As we have seen in Chapter II, seedlings grown in our conditions have a high AOX capacity, which contributes to energy dissipation in the context of the developmental arrest of seedlings. At 43°C, KCN-insensitive respiration was higher in PH than in H (Table 3.1), which suggests that AOX plays a role in the acclimation process. After 2 h of recovery, and even one day later, KCN-resistant respiration was higher in PH seedlings compared to C and P, which supports a potential involvement of the AOX in the acclimation process. These data show that, even if the AOX capacity is already high in liquid grown seedlings, it is still increasing after the application of HS, which would further help to prevent oxidative damage in the mitochondrion and chloroplast (Noguchi & Yoshida, 2008). Although photorespiration was shown to be another important actor of energy dissipation in seedlings and could thus potentially play a role in heat acclimation (Chapter II), we were not able to measure its activity. While photorespiration of C3 plants is generally associated with drought because of stomatal closure and leaf CO_2 limitation (Atkin & Macherel, 2009), whether it would play a role in HS tolerance in seedlings is not known. We can hypothesize that photorespiration would be enhanced by HS, as it was shown that CO_2 solubility, together with the affinity of Rubisco for CO_2 decreased at high temperature, which would favour the fixation of O_2 (Mathur *et al.*, 2014).

Priming resulted in a partial protection of photosynthesis but not of respiration during the exposure of seedlings to 43°C, but after 2 h of recovery, the beneficial effect of priming was evident for both processes, with NP close to the value of the control, and DR intensity being intermediate between those of the H and C seedlings. Nevertheless, chlorophyll fluorescence analysis revealed a decreased efficiency of photosynthetic machinery in PH seedlings after 2 h of recovery. The full restoration observed for both respiration and photosynthesis of PH seedlings 24 h after the heat shock highlights the primordial role of the recovery period for thermotolerance. Although we have not further investigated the kinetics of recovery between 2 h and 24 h, a progressive improvement of these essential functions is expected. During the recovery period, it is likely that the disaggregation of denatured proteins as well as *de novo* synthesis of proteins is required to repair the damage that occurred in the photosynthetic and respiratory electron transfer chains (Allakhverdiev *et al.*, 2008). The inhibition of translation that occurs when seedlings are exposed to an acute heat shock might be irreversible in H seedlings but reversible in PH seedlings during the recovery period, as previously shown in Arabidopsis seedlings (Echevarría-Zomeño *et al.*, 2016).
Finally, the crucial importance of the protection of energy metabolism for the acquisition of thermotolerance is well illustrated by the fact that, as soon as 2 h after the 43°C heat shock, we can predict from the intensities of respiration and photosynthesis whether the seedlings will survive or die several days later.

2.3. Heat stress response of organelle dynamics

In Chapter I, we presented the impact of heat shock on the cytoskeleton structure and hypothesized that changes in the actin network would affect the dynamics of the organelles, especially those of the mitochondria and ER. It was previously shown that an acute heat shock could block mitochondrial dynamics in Arabidopsis protoplasts (Scott & Logan, 2008), but, to our knowledge, the effect of priming on this response has yet to be studied.

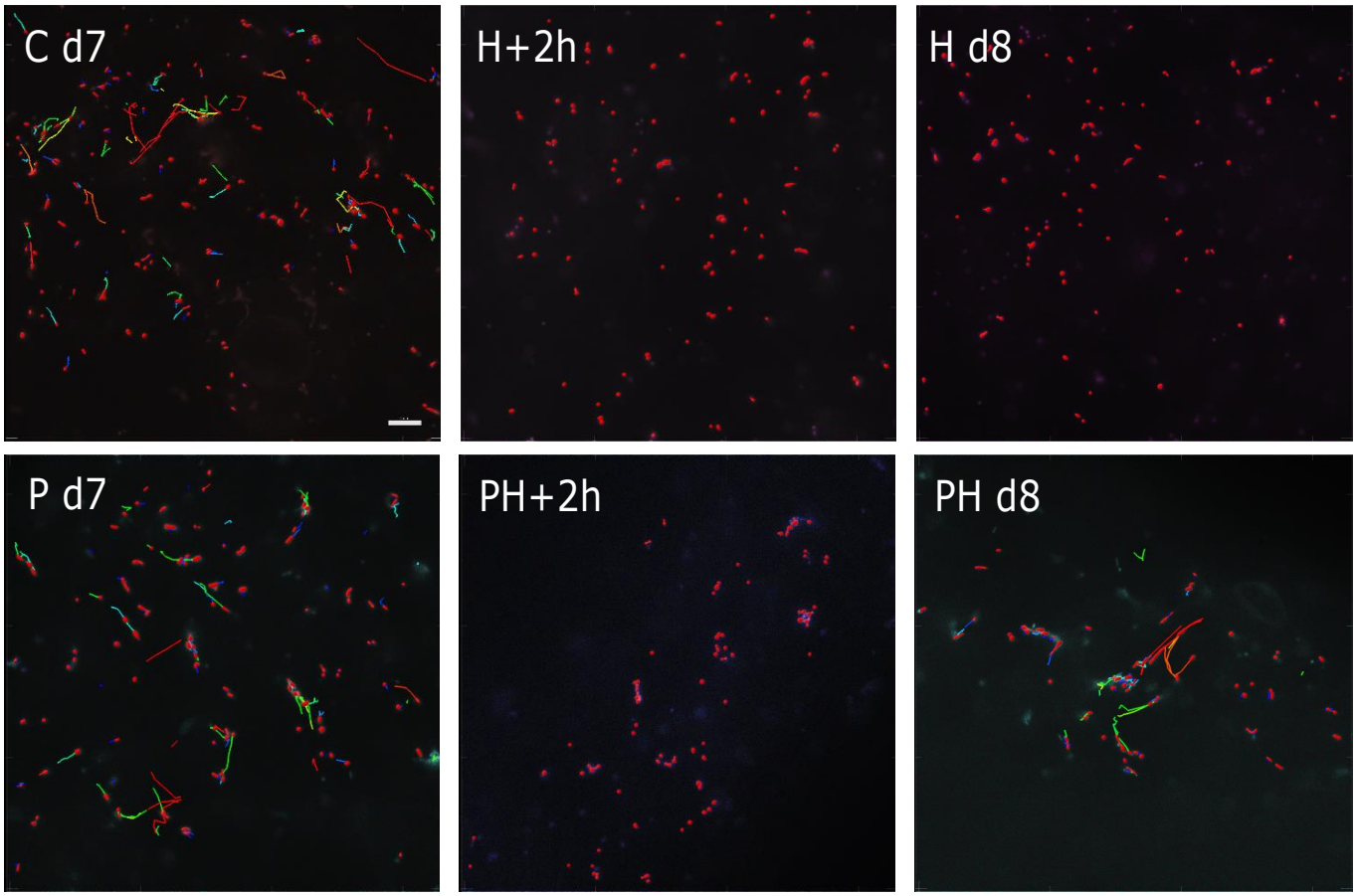

Figure 3.8: Mitochondria tracking in cotyledon cells of Mito-GFP seedlings using Imaris software
The tracks are rainbow-coloured (no movement is purple; and movement above 0.5 µm.s^{-1} is red); C d7: control on day 7; P d7: primed seedlings + 24 h recovery; H+2h/PH+2h: HS seedlings with or without previous priming + 2 h recovery; H d8/PH d8: HS seedlings with or without previous priming + 24 h recovery; scale bar, 5 µm.

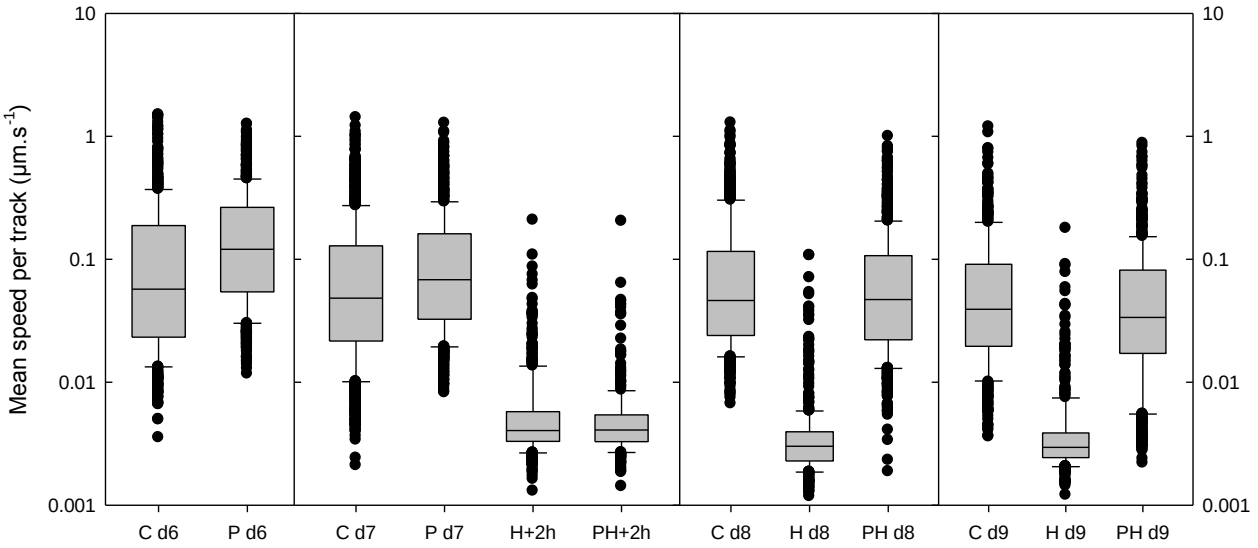

Figure 3.9: Mitochondria mean speed per track in cotyledon cells of Mito-GFP seedlings using Imaris software
Boxplots of the mean speed recorded per track in nm. s^{-1} on images acquired on days 6, 7, 8 and 9; C: control; P: primed seedlings; H: heat-shocked seedlings; PH: primed + heat-shocked seedlings (n=325 to 1062 mitochondria); for P d6, H+2h and PH+2h, data were acquired after 2 h of recovery post-treatment.

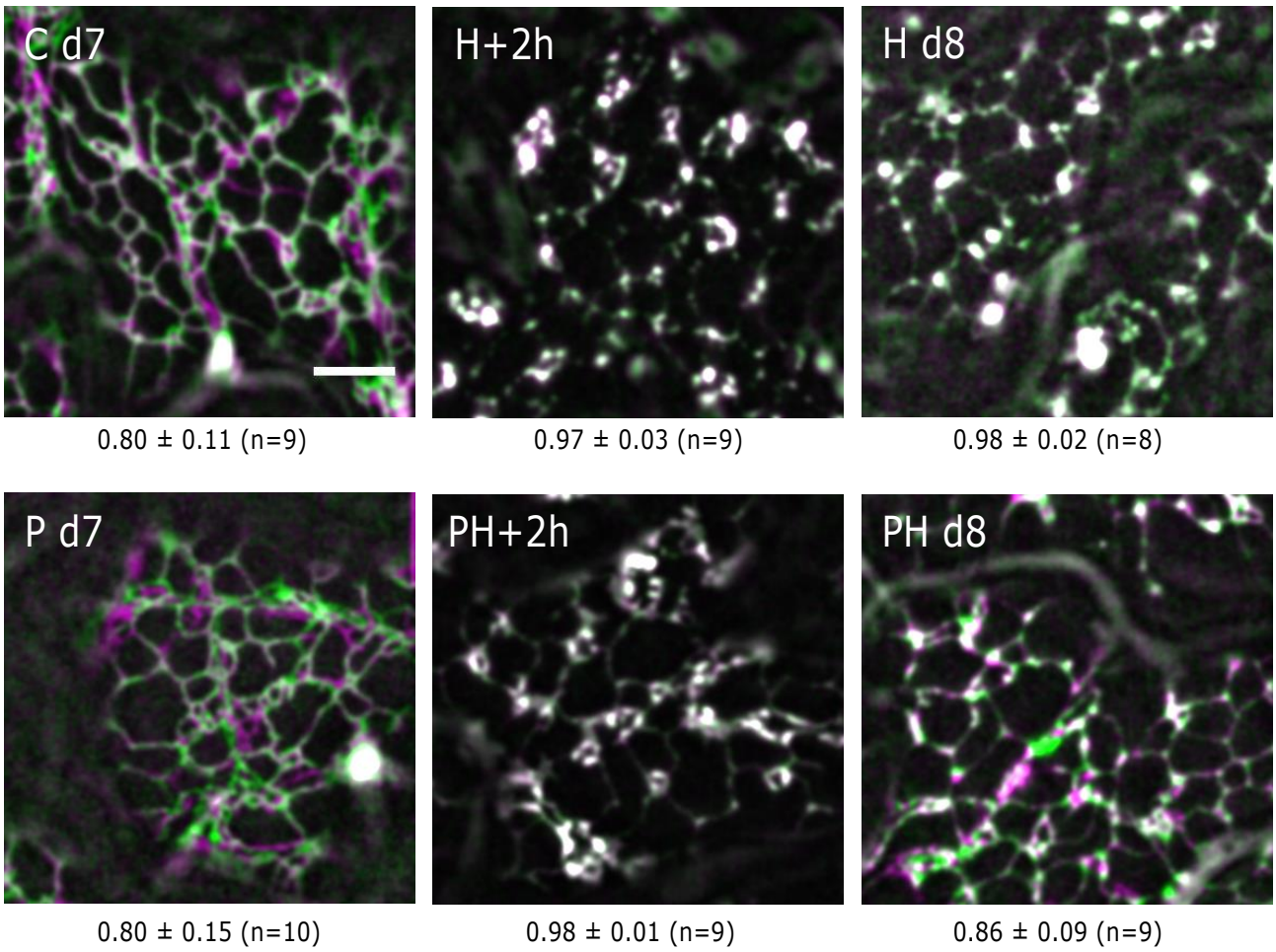

Figure 3.10: Endoplasmic reticulum motility in cotyledon cells depending on the heat treatment
The figure shows merged images of two frames captured 20 s apart in cotyledon cells of ER-GFP seedlings; the first image was false-coloured in green and the second in magenta; co-localization corresponds to white pixels; scale bar, 5 µm; values below the images correspond to mean of Pearson's correlation coefficient ± SD. C d7; P d7; H+2h and PH+2h were acquired on day 7 and H d8 and PH d8 on day 8 (24 h after treatment).

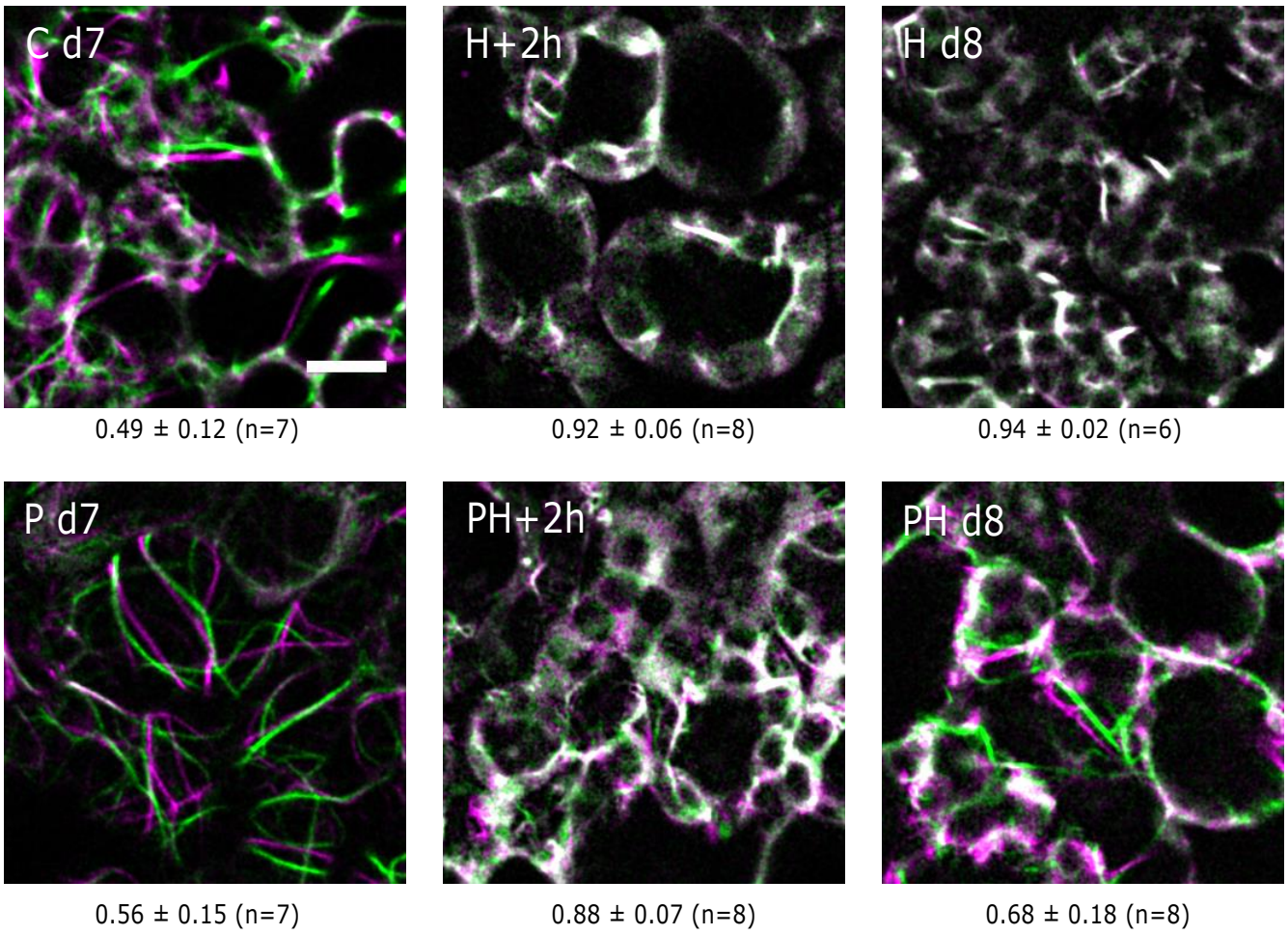

Figure 3.11: Actin motility in cotyledon cells depending on the heat treatment
Merged images of two frames captured 2 min apart in cotyledon cells of Lifeact-GFP seedlings; the first image was false-coloured in green and the second in magenta; co-localization corresponds to white pixels; scale bar, 10 µm; values below the images correspond to mean of Pearson's correlation coefficient ± SD. C d7; P d7; H+2h and PH+2h were acquired on day 7 and H d8 and PH d8 on day 8 (24 h after treatment).

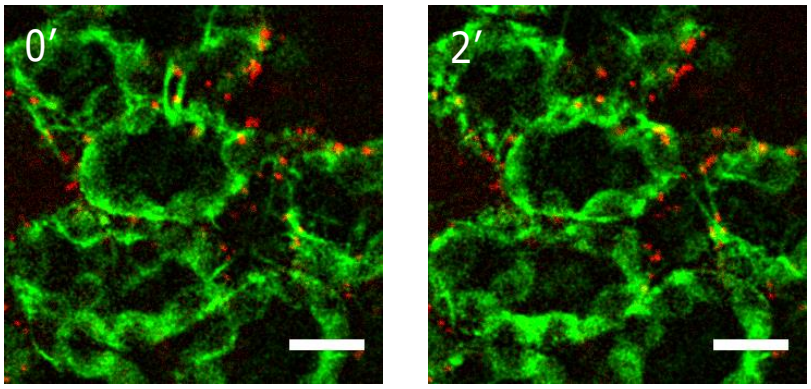

Figure 3.12: Actin and mitochondrial motility in cotyledons of PH seedlings after 4 h recovery
Mitochondria of Lifeact-GFP seedlings were stained using TMRM. Images were acquired by confocal microscopy 2 min apart in cotyledon cells; actin appears in green and mitochondria in red; scale bar, 10 µm.

Therefore, we analysed the heat response of mitochondria, endoplasmic reticulum and actin by using fluorescent lines expressing GFP proteins targeted to these compartments. Image stacks of cotyledon from the Mito-GFP line were acquired every two seconds, during 20 s, using an epifluorescence microscope equipped for high speed acquisition. Mitochondria were tracked using Imaris software to measure their motility (Figure 3.8). In C and P seedlings, the motility of mitochondria was highly variable: some of them reached speeds over 0.5 $nm.s^{-1}$ (red lines). When looking at the mitochondria in H and PH seedlings, 2 h after HS, the organelle movements had almost ceased, while, after 24 h of recovery, mitochondria recovered their motility in PH, but not in H seedlings. The mean speed per track was estimated across biological repeats for each condition (Figure 3.9). It was highly variable in C and P conditions, from 3.5 $nm.s^{-1}$ to 1.5 $\mu m.s^{-1}$ on day 6, reflecting the heterogeneity of mitochondrial dynamics. The mean was around 145 $nm.s^{-1}$ in C and 192 $nm.s^{-1}$ in P on day 6 and respectively around 110 $nm.s^{-1}$ and 125 $nm.s^{-1}$ on day seven. In H and PH seedlings after HS, the speed of mitochondria dropped to 7.2 $nm.s^{-1}$ and 6.5 $nm.s^{-1}$, respectively. Thus, heat shock induced a strong decrease in mitochondrial motility. Interestingly, when measured one day after HS, PH seedlings recovered a motility comparable to that of the control (91 and 110 $nm.s^{-1}$ respectively), while it remained around 5 $nm.s^{-1}$ in H seedlings. Mitochondria in H seedlings did not recover their motility even after two days of recovery (Figure 3.9). In the light of these results, we wondered if movements of other organelles were affected in the same way as mitochondria in response to the heat treatments. The dynamics of ER was investigated using a fluorescent line, expressing an ER-targeted GFP. However, given the complex network structure of ER, we chose to perform a comparative analysis instead of quantification of movement by tracking. Representative merges of two images (ER-GFP signal) acquired 20 s apart are shown in Figure 3.10, the first image being false-coloured in green and the second in magenta. In C and P samples, most of the green and magenta signals were distinct, indicating that there was a major movement of the ER network between the two images. In both H and PH samples, after 2 h of recovery, there was a majority of white signals, reflecting the overlap between green and magenta, and thus the lack of movement of the ER network. These observations were quantified using the Pearson correlation coefficient (+1, perfect correlation; 0, no correlation; -1, perfect anti-correlation), which is indicated in Figure 3.10. Similar to mitochondria, the recovery of ER dynamics was observed in PH seedlings after one day of recovery, but not in H seedlings. As mitochondria and ER move on the actin network in plants (Perico & Sparkes, 2018), we hypothesized that the impact of heat shock and priming on organelle dynamics was due to their effect on the actin microfilament network. We performed a similar analysis using a line expressing a GFP targeted to the actin filaments (Lifeact-GFP). Since it was more difficult to clearly distinguish actin filaments by epifluorescence microscopy, we observed the GFP labelled actin network using laser scanning confocal microscopy (LSCM). Mitochondria were detected in the same samples using TMRM staining, and images were acquired by line scanning (channels for GFP, TMRM and chlorophyll autofluorescence) for 2 min, every 12 s.

Representative merges of images acquired 2 min apart in cotyledons 2 h after treatment are shown in Figure 3.11. The variations of actin microfilament dynamics followed the same pattern as those of mitochondria and ER, as we described above. The network was highly dynamic in the C and P samples, but HS caused an arrest of the movements measured after 2 h of recovery, as shown by the merged images and the Pearson correlation coefficients. The arrest of actin was irreversible in H seedlings, but temporary in PH seedlings since actin filaments recovered a high motility after 24 h of recovery. An experiment performed after 4 h of recovery indicated that

the network already started to move, which is correlated with a slight resumption of mitochondrial motility observed by TMRM staining (Figure 3.12).

The absence of the effect of a 38°C heat shock on organelle dynamics, even when observed after only 2 h of recovery (Figure 3.9), and the arrest of mitochondrial, actin and ER dynamics under lethal heat shock are consistent with previous results (Müller *et al.*, 2007; Scott & Logan, 2008; Zhang *et al.*, 2009a; Malerba *et al.*, 2010; Fan *et al.*, 2016). We did not observe major changes in mitochondrial morphology, such as swelling, as it was reported for protoplasts exposed to a severe heat shock by Scott & Logan (2008) and Zhang *et al.* (2009a), but both the materials and the stress conditions were different.

Our experiments provide strong evidence that, in seedlings, priming does not prevent the blockage of actin network dynamics caused by the 43°C heat shock, and which is likely responsible for the arrest of mitochondrial and ER dynamics. However, in the primed seedlings, a reorganisation and reactivation of the actin cytoskeleton occurs, probably starting between 2 h and 4 h of recovery, allowing the organelles to move with the actin network to resume their normal motility within less than 24 h. It is conceivable that depolymerized actin is reassembled either following *de novo* synthesis or by the recovery of soluble or sequestered actin monomers, with the assistance of the numerous actin-interacting proteins and chaperones. Indeed, in mammals, sHSPs were suggested to interact with actin, by inhibiting actin polymerization and participating in the protection of actin dynamics (Mounier & Arrigo, 2002), but whether such a process is conserved in plants was not investigated, to our knowledge. If similar interactions occur in plants, the cytosolic sHSP isoforms might have had an important role during the recovery period.

We have clearly shown that mitochondrial respiration and dynamics were both affected by heat shock, and that priming conferred a protection of respiratory activity and allowed the resumption of mitochondrial dynamics during recovery, the latter being likely a consequence of cytoskeleton protection. However, it is not clear if the dynamic state of plant mitochondria and their bioenergetics functions are correlated. Indeed, several Arabidopsis mutants, which were strongly affected in the morphology and dynamics of the chondriome did not display severe growth and developmental phenotypes (Logan *et al.*, 2003), and mitochondria in Arabidopsis imbibed seeds were found to be immobile, although respiratory activity was high (Paszkiewicz *et al.*, 2017). In contrast, in yeast and mammals, it seems that mitochondrial dynamics are highly connected to bioenergetics: for example, interconnected mitochondrial networks are mostly characteristic of metabolically and respiratory active cells, while in inactive cells, mitochondria are smaller and more fragmented (Westermann, 2012). Recently, it was also shown in mammals that both respiratory activity and fission/fusion mechanisms are regulated by the circadian clock (Schmitt *et al.*, 2018). The link between mitochondrial dynamics and bioenergetics has scarcely been explored in plants, but the high motility of plant mitochondria, mainly found as discrete units, speaks for a role in energy distribution at the sub-cellular level. A thorough characterization of the Arabidopsis *friendly* (*fmt*) seedlings, in which mitochondria are heavily clustered, revealed a short root phenotype, an increase in AOX capacity and a decrease in photosynthetic efficiency, which could all be related to some dysfunction of mitochondrial energy transduction (and/or distribution) (El Zawily *et al.*, 2014). We challenged the *fmt* mutant in our assay, and found that it was able to acclimate to heat shock as well as the wild type Col-0 (data not shown). This indicates that major perturbations in mitochondrial motility and fusion do not interfere with the HSR and the

acquisition of thermotolerance.

However, in the absence of acclimation like in H seedlings, the incapacity of mitochondria to exchange DNA, proteins and metabolites over a long period could seriously impair mitochondrial function and turnover and finally, participate in the induction of cell death. The link between mitochondrial morphology and cell death has already been well established, as swelling and aggregation of mitochondria and mitochondrial permeability transition were previously identified as markers of plant cell death (Scott & Logan, 2008). Thus, we can postulate that, in H seedlings, the arrest of mitochondrial (and other organelles) dynamics contributes to the signalization towards programmed cell death. Another important process, autophagy, which is involved in the degradation and recycling of cytoplasmic elements, is also known to play a dual role in the regulation of programmed cell death, by either promoting or inhibiting it, especially in response to biotic stresses (Üstün *et al.*, 2017). Therefore, it would be of interest to determine if autophagy mechanisms are induced/repressed in H and/or PH seedlings, and to see if there is a link with the arrest of organelle dynamics, since autophagy is animated by the actin cytoskeleton (Kast & Dominguez, 2017).

In this chapter, we have thus demonstrated that protection and recovery of energy metabolism and organelle dynamics after HS play an important role in the survival of seedlings. On the contrary, disturbance of respiratory and photosynthetic activities together with the arrest of organelle dynamics are likely to signal towards the induction of cell death in non-primed seedlings. In the next chapter, we will investigate the molecular responses that participate in the acquisition of thermotolerance.

Chapter IV- Molecular response to heat treatments

1. Introduction

In Chapter I, we presented the extensive work that has allowed the scientific community to identify the molecular actors of the HS response (HSR) and their interactions, including HSFs, HSPs and other mechanisms of protection and detoxification. However, although the HSR has been investigated for many years at different levels, including transcriptomic, proteomic and metabolic analyses (Kaplan *et al.*, 2004; Larkindale & Vierling, 2007; Echevarría-Zomeño *et al.*, 2016), few studies have attempted to integrate multi-scale data obtained in the same conditions (Caldana *et al.*, 2011; Légeret *et al.*, 2015). In this chapter, we will present and discuss the results of transcriptomic, proteomic and metabolic analyses that were performed in the context of heat shock and acquired thermotolerance in developmentally arrested seedlings. The objective was to gain a wider view of the molecular responses at several levels, and to determine which pathways could be the most important for the acquisition of thermotolerance.

2. Transcriptomics

2.1. Strategy

In order to dissect the transcriptome response to the different heat treatments, we performed a RNA sequencing (RNAseq) analysis. To get access to mRNAs, but also to mitochondrial and plastidial RNAs, which are usually not polyadenylated, we chose to proceed to ribosomal RNA depletion instead of an mRNA enrichment method. Another advantage of RNAseq is the possibility to distinguish sense and antisense reads (strand-specific library) and alternative splicing.

Results were obtained from three biological replicates of four different samples:

C = control (Day 6)

P = 38°C 30 min (Day 6), priming

H = 43°C 30 min (Day 7), heat shock

PH = 43°C 30 min (Day 7), heat shock applied to primed seedlings.

These time points were selected to study the early transcriptomic response to HS. Total RNA was extracted and after quality control, the RNA samples were sent to BGI (Hong-Kong) for library construction and sequencing. Data analysis was performed with the help of the IRHS bioinformatics team. Indexing, counting and alignment of clean reads were performed using Bowtie2 and SAMtools packages. DESeq2 (Bioconductor) was used for differential analysis. In the following part, we will present the results concerning sense transcripts, since antisense transcripts have not been sufficiently analysed so far.

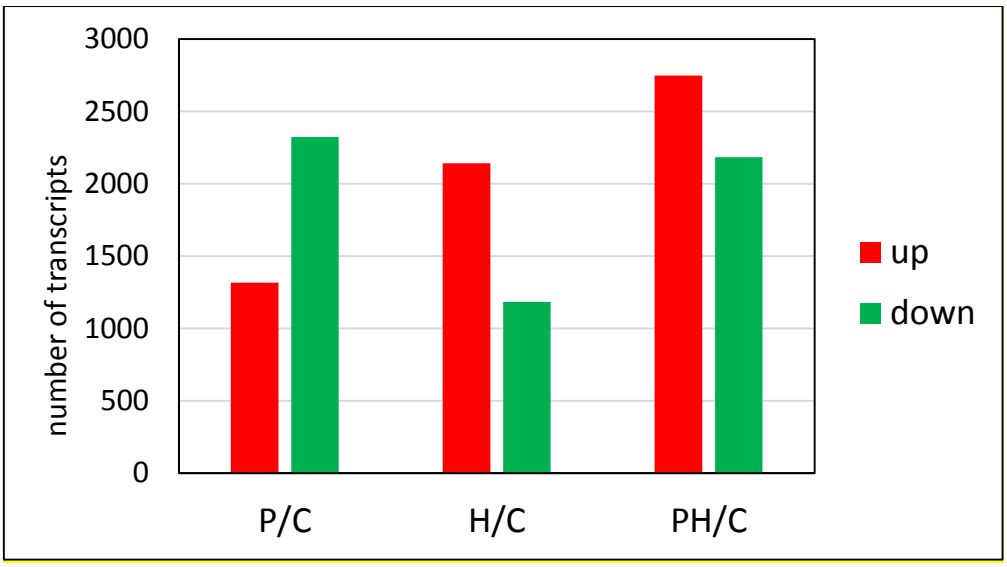

Figure 4.1: Number of significantly differentially expressed transcripts in the different treatments compared to control.
Log2 fold change >1 (up) or <-1 (down) and false discovery rate of 0.05.

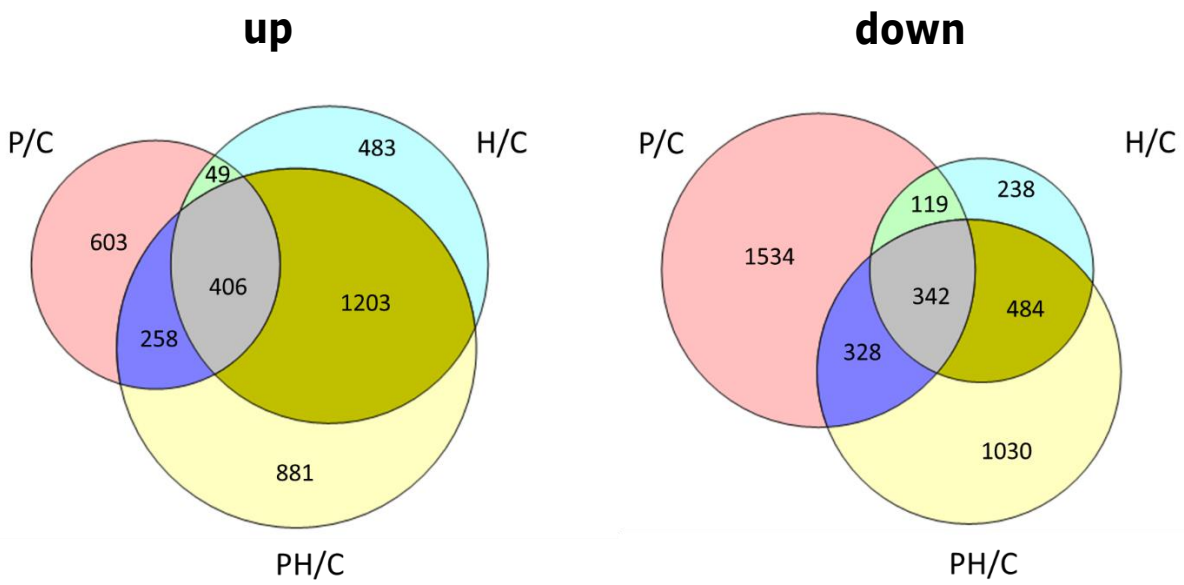

Figure 4.2: Venn diagrams reflecting the overlap in the transcriptomic response to the different heat treatments compared to control.
Numbers correspond to transcripts significantly differentially expressed in the different treatments in comparison with the control (log2 fold change >1 (up) or <-1 (down) and fold discovery rate of 0.05).

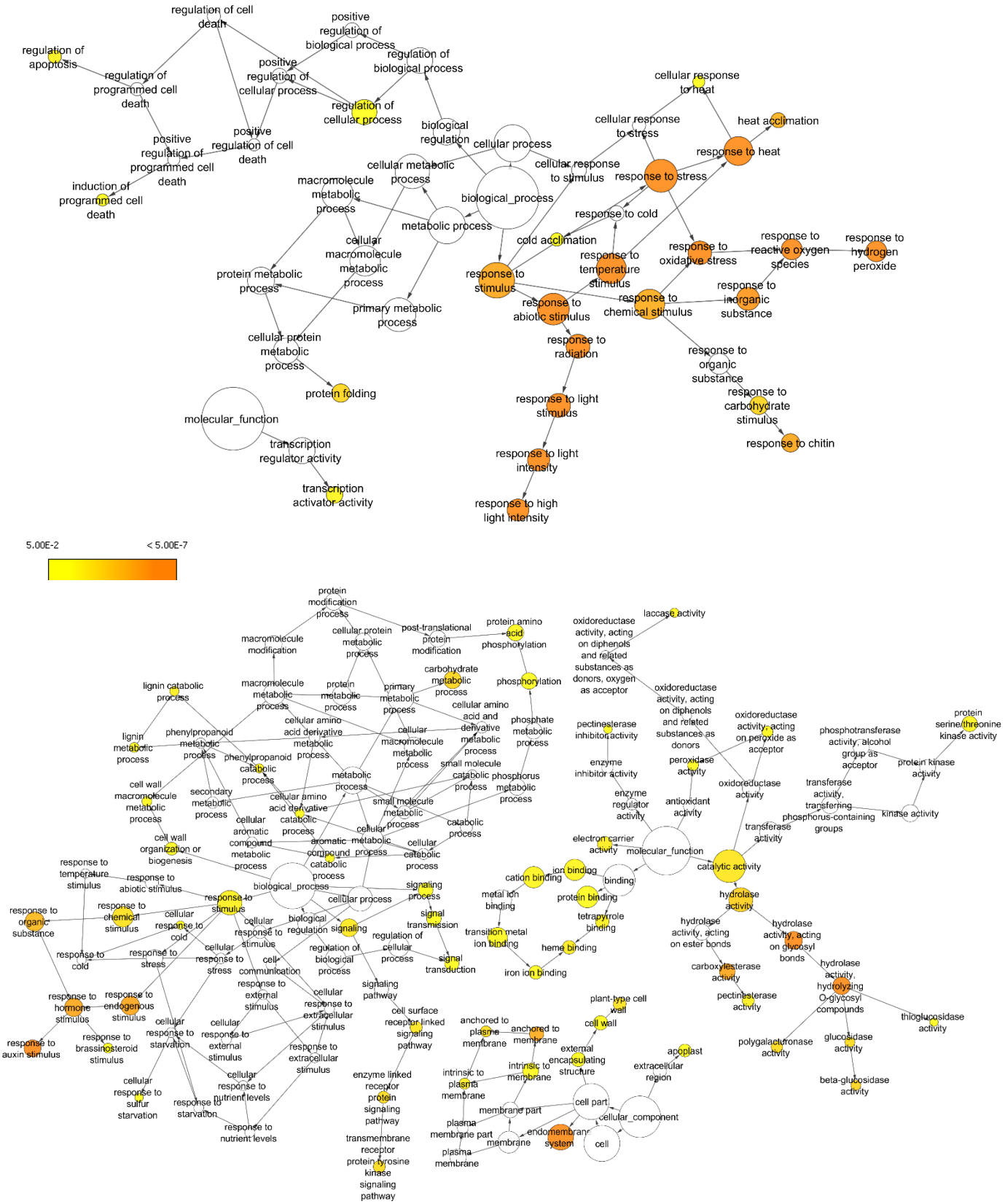

Figure 4.3: Gene ontologies associated with the common significantly upregulated (top) or downregulated (bottom) transcripts in all treatments (P, H, PH).
Overrepresentation gene ontology (GO) network was realized with GO_Full function of the BinGO 3.0.3 package in Cytoscape 3.6.0. Colour corresponds to corrected p-values according to the hypergeometric test and Benjamini and Hochberg False Discovery Rate correction (white, non significant; yellow ($p<0.05$) to orange ($p<0.0000005$)) and node size is representative of the number of genes annotated to each node.

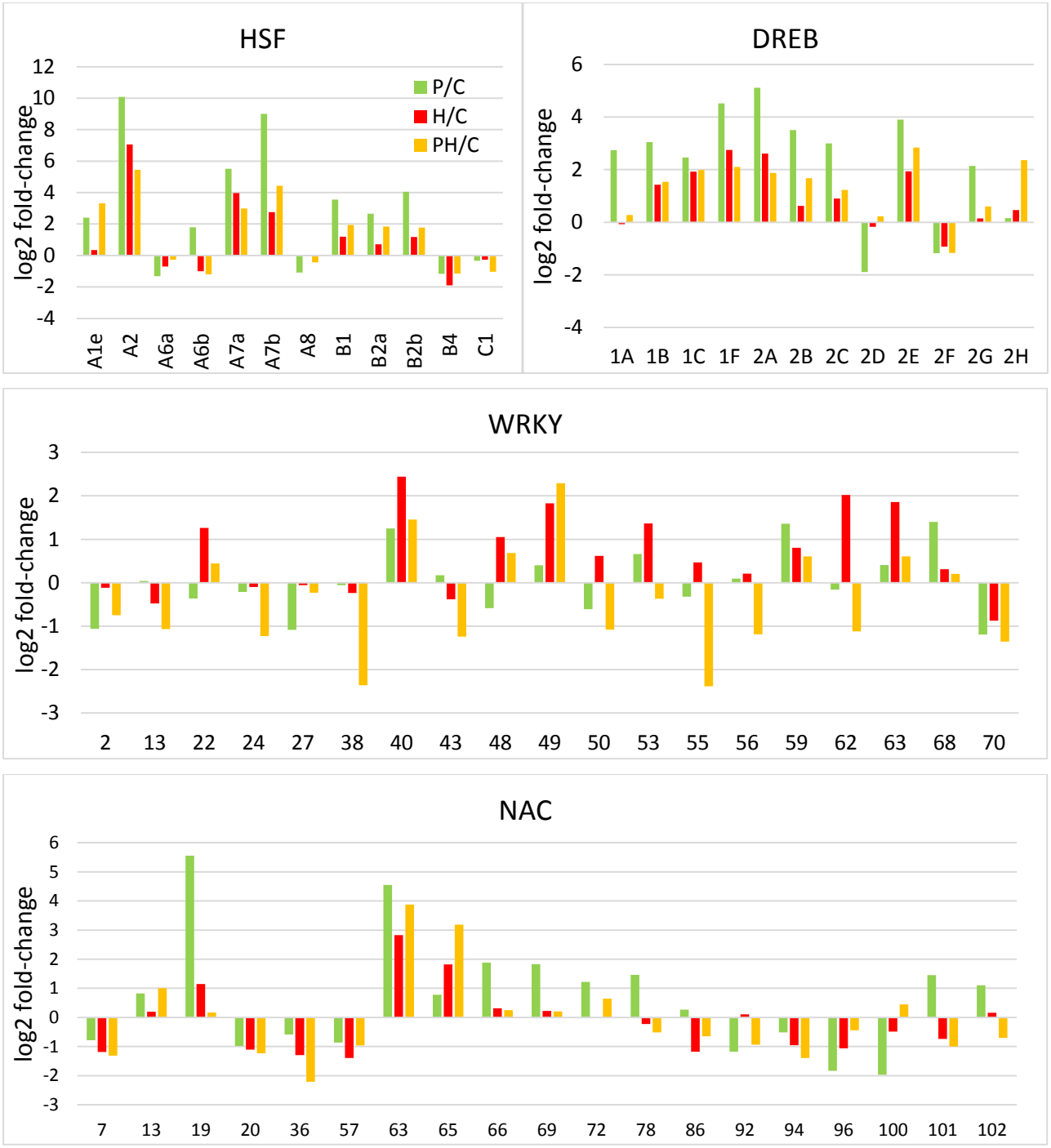

Figure 4.4: Log2 fold-change of differentially expressed transcription factors (heat shock factors, dehydration-responsive element-binding proteins, WRKY, NAC) in response to priming and heat shock.
The abscissa corresponds to the names of the different transcription factors, according to their classification.

Table 4.1: HSP and chaperone family proteins that are differentially expressed upon heat stress.
Id refers to the transcript; colours correspond to differentially expressed transcripts with FDR<0.05 and log2 fold change >1 (pink) or <-1 (green); loc corresponds to location according to SUBA4con: c, cytosol; cp, plastid; ER, endoplasmic reticulum; g, Golgi; m, mitochondrion; n, nucleus and p, peroxisome.

id	Log2 P/C	Log2 H/C	Log2 PH/C	loc	Name
AT3G12050.1	5.20	2.54	1.49	c	Aha1 domain-containing protein
AT1G59980.1	1.55	0.56	2.58	c	ARG1-like 2
AT1G72416.3	3.71	1.08	2.28	c	chaperone DnaJ-domain containing protein
AT1G74310.1	9.03	4.30	4.77	c	chaperone protein ClpB1
AT5G22060.1	1.79	0.19	0.13	c	chaperone protein dnaJ 2
AT2G37390.1	0.17	-1.38	-1.13	c	chloroplast-targeted copper chaperone protein
AT1G54050.1	9.02	5.44	5.99	c	CIII heat shock protein 17.4
AT1G07400.1	10.13	5.84	7.03	c	class I heat shock protein
AT5G12020.1	10.37	4.50	8.06	c	class II heat shock protein 17.6
AT2G20560.1	6.17	2.55	3.15	c	DNAJ heat shock family protein
AT2G21510.1	1.11	0.49	-0.03	c	DNAJ heat shock N-terminal domain-containing protein
AT4G28480.1	1.96	-0.27	-0.17	c	DNAJ heat shock protein
AT3G06778.1	-1.24	-0.63	-0.77	c	DNAJ-domain-containing protein
AT5G02500.1	2.06	0.55	-0.54	c	heat shock cognate protein 70-1
AT5G47600.1	0.33	1.96	5.29	c	heat shock protein 14.7
AT3G46230.1	10.22	5.19	7.98	c	heat shock protein 17.4
AT5G12030.1	9.84	4.70	8.00	c	heat shock protein 17.6A
AT5G02490.1	2.71	0.59	-1.35	c	heat shock protein 70
AT1G11660.1	1.96	-0.09	1.23	c	heat shock protein 70 (Hsp 70) family protein
AT3G09440.1	4.65	1.41	0.32	c	heat shock protein 70-3
AT3G12580.1	5.43	2.20	2.31	c	heat shock protein 70-4
AT1G16030.1	10.11	3.59	6.54	c	heat shock protein 70B
AT5G52640.1	6.77	2.61	3.97	c	heat shock protein 90.1
AT5G56010.1	4.22	0.96	-0.14	c	Heat shock protein 90.3
AT5G56000.1	2.57	0.42	0.06	c	Heat shock protein 90.4
AT2G19310.1	5.23	2.64	2.84	c	heat shock protein 18.5
AT2G32120.1	7.36	1.48	4.64	c	heat-shock protein 70T-2
AT2G29500.1	9.84	4.12	6.57	c	HSP20 family protein
AT1G53540.1	10.08	4.11	8.60	c	HSP20-like chaperone
AT1G59860.1	9.76	6.88	6.49	c	HSP20-like chaperone
AT5G02480.1	-1.34	-0.29	-0.50	c	HSP20-like chaperone
AT2G20550.1	1.61	0.46	1.24	c	HSP40/DnaJ peptide-binding protein
AT4G22670.1	1.30	-0.01	0.45	c	HSP70-interacting protein 1
AT5G53400.1	2.95	0.44	0.54	c	protein BOBBER 1
AT5G04890.1	1.08	0.47	0.65	c	protein RESTRICTED TEV MOVEMENT 2
AT5G25530.1	0.33	1.90	3.04	c	putative DNAJ heat shock protein
AT1G67760.1	-0.94	-1.91	-2.08	c	TCP-1/cpn60 chaperonin family protein
AT1G53300.1	-1.15	-0.71	-0.98	c	TPR repeat-containing thioredoxin TTL1
AT3G13310.1	2.64	0.08	-0.10	cp	chaperone DnaJ-domain containing protein
AT5G15450.1	6.30	0.91	2.96	cp	chaperone protein ClpB3
AT5G20720.1	2.04	0.32	1.10	cp	chaperonin 20
AT2G28000.1	2.94	0.48	1.70	cp	chaperonin 60 alpha
AT4G24280.1	2.60	0.27	2.46	cp	chloroplast heat shock protein 70-1
AT2G04030.1	1.88	-0.20	0.68	cp	chloroplast heat shock protein 90
AT5G23240.1	-0.16	-0.13	-1.03	cp	DNAJ heat shock N-terminal domain-containing protein
AT3G47650.1	0.73	0.44	1.01	cp	DNAJ/Hsp40 cysteine-rich domain-containing protein
AT5G17710.2	0.82	0.24	1.08	cp	embryo defective 1241
AT3G60210.1	0.53	0.17	2.19	cp	GroES-like family protein
AT4G27670.1	10.21	3.31	11.15	cp	heat shock protein 21
AT5G49910.1	2.13	0.32	0.16	cp	heat shock protein 70-2
AT2G22360.1	0.59	0.23	1.52	cp	molecular chaperone DnaJ
AT4G13670.1	1.42	0.67	1.57	cp	protein cp transcriptionally active 5
AT3G13470.1	5.69	0.56	2.13	cp	TCP-1/cpn60 chaperonin family protein
AT4G10250.1	10.71	3.54	9.64	ER	heat shock protein 22
AT4G16660.1	1.17	-0.35	0.58	ER	heat shock protein 70
AT4G24190.1	1.15	-0.82	-0.86	ER	HSP90-like protein GRP94
AT3G08970.1	6.30	1.41	2.14	ER	J domain protein ATERDJ3A
AT5G28540.1	3.08	-0.62	0.51	ER	BIP1
AT5G42020.1	2.56	-0.95	-1.10	ER	BIP2
AT1G79920.1	4.73	1.37	1.40	g	Heat shock protein 70
AT2G25140.1	4.64	0.41	1.76	m	ClpB4

AT1G14980.1	2.30	0.19	0.25	m	chaperonin 10
AT5G51440.1	6.64	2.84	3.27	m	heat shock protein 23.5
AT4G25200.1	10.25	4.58	7.87	m	heat shock protein 23.6
AT1G52560.1	9.61	1.95	8.43	m	heat shock protein 26.5
AT3G23990.1	3.90	0.13	1.39	m	heat shock protein 60
AT3G13860.1	1.47	0.06	1.20	m	heat shock protein 60-3A
AT4G32208.1	6.39	1.37	1.86	m	heat shock protein 70 family protein
AT3G07770.1	2.23	-0.31	-0.17	m	heat shock protein 89.1
AT5G09590.1	6.47	1.96	2.06	m	mitochondrial HSO70 2
AT4G26780.1	4.86	1.12	2.19	m	molecular chaperone GrpE
AT1G78120.1	-0.08	-0.86	-1.31	m	tetratricopeptide repeat-containing protein
AT4G12400.2	6.77	4.25	3.91	n	HOP3
AT1G62740.1	2.57	0.15	0.56	n	HOP2
AT5G58110.1	2.21	0.17	1.07	n	chaperone binding / ATPase activator
AT1G56300.1	2.01	0.23	0.86	n	chaperone DnaJ-domain containing protein
AT1G62970.1	-1.01	-0.81	-1.04	n	chaperone DnaJ-domain containing protein
AT3G14200.1	3.91	0.22	0.05	n	chaperone DnaJ-domain containing protein
AT5G09540.1	-0.31	-0.42	-1.07	n	chaperone DnaJ-domain containing protein
AT1G71000.1	9.65	0.87	2.04	n	chaperone DnaJ-domain containing protein
AT3G44110.1	3.12	0.31	0.49	n	chaperone protein dnaJ 3
AT1G74250.1	-1.06	-0.42	-0.31	n	DNAJ heat shock N-terminal domain-containing protein
AT3G04980.1	-0.90	-0.70	-1.03	n	DNAJ heat shock N-terminal domain-containing protein
AT4G02100.1	-1.56	-0.81	-0.93	n	Heat shock protein DnaJ with tetratricopeptide repeat
AT1G20870.1	0.30	0.12	1.11	n	HSP20-like chaperones superfamily protein
AT4G27890.1	1.11	-0.82	0.53	n	protein BOBBER 2
AT1G02650.1	-1.06	0.64	0.32	n	tetratricopeptide repeat domain-containing protein
AT2G47440.1	-1.18	-0.95	-0.39	n	tetratricopeptide repeat-containing protein
AT3G62570.1	-1.17	-1.43	-1.73	n	tetratricopeptide repeat-containing protein
AT5G56030.2	5.23	2.23	1.96	n,c	heat shock protein 81-2
AT5G37670.1	8.37	3.66	6.72	p	heat shock protein 15.7
AT5G59720.1	10.37	2.99	10.02	p	heat shock protein 18.2

2.2. Results and discussion

2.2.1. General heat stress response

Sequencing data comprised between 8.3 and 17.1 billion clean bases for each sample, allowing a coverage between 30X and 63X (Arabidopsis genome: 135 Mbp). Total mapped reads reached between 82 % and 89 % of total clean reads, among which between 56 and 67 % of pairs were aligned concordantly to only one position and 15 to 20 % of pairs were aligned concordantly to more than one position.

For differential analysis, sense transcripts with a minimum fold change of 2 and a false discovery rate of less than 0.05 were considered as significantly differentially expressed (DE) between two conditions. We found that 3883 transcripts were significantly upregulated and 4075 downregulated in at least one condition. Figure 4.1 shows the number of DE transcripts for each temperature treatment, compared to the control. The number of downregulated transcripts is lower in the **H** condition than in **P** or **PH**, while the number of upregulated transcripts is higher in **PH** than in the other treatments. This is consistent with the results of Larkindale and Vierling (2007), who found that a decrease in gene expression may be of great importance in preventing damage during stress. Conversely, the highest number of overexpressed genes in **PH** seedlings could possibly reflect an efficient protection of the transcriptional machinery or a lower compaction of histones in primed samples, which could allow a better access to genes for the transcriptional machinery.

The overlap in the response to the different conditions is presented in Figure 4.2. A core response of 406 upregulated genes and 342 downregulated genes was found in all heat treatments. Among the gene ontologies (GO) related to these upregulated genes figured: **"response to heat stress"**, **"response to high light intensity"**, **"response to oxidative stress"**, **"transcription activator activity"** and **"protein folding"** (Figure 4.3). Genes that were previously identified as main actors of the HSR were detected among the most upregulated genes in all treatments, even if the fold change was often lower in **H** than in **P** and **PH** for most of them. This is in agreement with previous results that showed that under repetitive treatments at 37°C, the transcription of some stress-responsive genes, such as ascorbate peroxidase 2, was higher in pre-treated seedlings than in non-primed seedlings, whereas *HSP101* was similarly induced in both treatments, like in our conditions (Table 4.1) (Liu *et al.*, 2018). Concerning the transcription factors, *HSFA2*, *HSFA7a*, *HSFA7b*, *HSFB1* and *HSFB2b* were found to be upregulated in all conditions, as well as the *DREB* factors *1B*, *1C*, *1F*, *2A* and *2E* (Figure 4.4). Other actors of the signalling pathway, such as *MBF1C*, *BCL-2-ASSOCIATED ATHANOGENE 5* and *6* (*BAG5* and *BAG6*), *HSA32*, some calmodulin-like proteins (*CLM37* and *CLM39*), calcium-dependent lipid-binding proteins and calcium-dependent protein kinase 34, were also upregulated (data not shown). Other transcription factors, such as *MYB44* and *MYB120* or *WRKY40,* were part of the core response. *MYB44* was previously identified as a component of abiotic stress responses (drought, salt) (Persak & Pitzschke, 2014) and *MYB120* was shown to play a role in the regulation of pollen tube reception, but it was not identified as a component of HS response, to our knowledge (Liang *et al.*, 2013). *WRKY40* was found to be involved in ABA and abiotic stress responses (Chen *et al.*, 2010). *WRKY25*, *26*, *33* and *39*, which were previously identified as major regulators of thermotolerance (Li *et al.*, 2010c, 2011), were not significantly affected by any heat treatment. Since we examined the transcript response after 30 minutes of exposure, these TFs could be upregulated later. Among the NAC factors, *NAC063* was upregulated in all conditions, while the previously identified HSR regulator *NAC019* was only upregulated in **P** and **PH** (Figure 4.3).

Several ethylene responsive transcription factors (*ERF017*, *ERF025*, *ERF109*, *RAP2.4*) were also part of the core response (data not shown). Many *HSPs* were upregulated, among which several *sHSPs* (*HSP17.4B*, *HSP17.6A*, *HSP17.6B*, *HSP17.6C*, *HSP17.8*, *HSP18.5*), but also *HSP70* (*HSP70-4*, *HSP70-8*, *HSP70-10*) and *HSP101* (Table 4.1). We can notice the induction of the three mitochondrial *HSP23.5*, *HSP23.6*, *HSP26.5*, the two peroxisomal *HSP15.7* and *HSP18.2* and the plastidial *HSP21*. ROS detoxifying enzymes, ascorbate peroxidase 2, and several glutathione S-transferases proteins were also among the most upregulated transcripts in response to the three treatments. Concerning the common downregulated genes, the main GO associated were: **"response to auxin"**, **"carbohydrate metabolic process"**, **"cell wall organization"** and **"lignin catabolic process"** (Figure 4.3). The core response (342 transcripts) involved many auxin-responsive genes (*SAUR*), a few ethylene-responsive transcription factors (*ERF*, *CRF* and *LEP*), many cell-wall related enzymes (polygalacturonase, expansins, cellulose synthase, pectin acetylesterases…). All these data could fit with an early response directed towards the arrest of growth and development. Overall, these results are in agreement with previous studies of HS signalling (Lim *et al.*, 2006; Ahuja *et al.*, 2010; Ohama *et al.*, 2017) and validate our experimental system.

When comparing the different conditions, we found that 75 % of significantly upregulated transcripts in **H** condition were also upregulated in **PH** condition compared to the control, while only 21 % of upregulated transcripts in **H** were shared with **P** condition. 50 % of genes upregulated in **P** were also upregulated in **PH** condition. The transcriptome of **PH** seedlings thus comprises a high overlap between **P** and **H** conditions. We will thereafter focus on the DE genes that were found specific to **P** and/or **PH**, and thus are candidates for a role in basal and acquired thermotolerance.

2.2.2. Specific responses of priming

The 258 transcripts that were specifically upregulated in both **P** and **PH** (Figure 4.2) were related to **"protein folding"**, **"response to heat"** and **"cell redox homeostasis"** GO. They comprised *HSFA1e* and *HSFB2a*, *DREB2B*, *DREB2C* (Figure 4.4), *ERF021*, several *HSPs* (*HSP70*, *HSP60*, *HSP20*, Table 4.1) and several glutaredoxins (not shown). Several transcripts encoding peptidyl-prolyl cis-trans isomerases were also part of this acclimation response (AT1G01940, AT2G15790, AT2G43560 and AT4G25340). Some of them are co-chaperones of HSP90/70 complexes, whereas FKBP53 is a histone chaperone involved in the repression of ribosomal RNA expression (Li & Luan, 2010). Transcripts of *LIFEGUARD 3* and *4*, which were identified as anti-apoptotic proteins involved in the unfolded protein response by interacting with IRE1 (Guo *et al.*, 2018), were also overexpressed in these two conditions. Moreover, transcripts of phytocystatin 4 (*AtCYS4*), a cysteine protease inhibitor, and temperature-induced lipocalin (*TIL*), involved in the prevention of lipid peroxidation, were upregulated in **P** and **PH**. Those genes were previously shown to be involved in thermotolerance, since their knock-out mutants exhibited a heat-sensitive phenotype (Chi *et al.*, 2009; Je *et al.*, 2014). Heat-induced TAS1 target 1 and 2 (*HTT1* and *HTT2*), which are components of thermotolerance acting downstream of HSFA1a (Li *et al.*, 2014), were also specifically induced in all primed samples. All these overexpressed genes are expected to have important roles for protection against stress damage and may contribute to prevent cell death of seedlings.

Concerning the downregulated genes, the main GO associated were **"cell wall modification"**, **"defence response to bacterium"**, **"pectin catabolic process"** and **"protein phosphorylation"**. They included transcripts encoding several cysteine-rich RLK (receptor-like protein kinases), aspartyl protease family proteins, ATP-binding cassette

transporter G family proteins and 3-ketoacyl-CoA synthases 1 and 20 involved in wax synthesis (Todd *et al.*, 1999; Lee *et al.*, 2009).

P specifically overexpressed genes included *CNGC7* (cyclic nucleotide gated channel 7), *DREB1A* and *DREB2G*, several *NAC* and *MYB* TF, multiple HSPs (HSP90, HSP70, HSP40 family proteins), several glutathione S-transferases and some late embryogenesis abundant (LEA) proteins. Interestingly, several genes involved in ER stress response (UPR), such as *bZIP28*, *BIP1* and *BIP2*, *BAX inhibitor 1*, *UTR1* (UDP-galactose transporter 1), ribosome associated membrane protein and *RAMP4*, were also overexpressed at 38°C, which confirms the essential role of the ER UPR in the acclimation process. Transcripts encoding proteins of mitochondrial and plastidial electron transport chains together with ATP synthases were also found to accumulate in **P** samples, which could be related to the increase of mitochondrial activity observed at 38°C (Chapter III).

Transcriptional downregulation in **P** samples concerned many leucine-rich repeat (LRR) protein kinase family proteins and other transmembrane receptors of the tyrosine kinase-signaling pathway. The transcripts of many pentatricopeptide repeat proteins (PPR) involved in mRNA modification in mitochondria and chloroplasts including *GUN1*, RNA processing factors *RPF1*, *RPF2* and *RPF3* and mitochondrial editing factors (*MEF3*, *MEF18*, *MEF19*, *MEF20*, *MEF21*, *OTP87* (organelle transcript processing 87)) were also downregulated at 38°C.

881 upregulated transcripts were found to be specific to the **PH** condition (Figure 4.2). GOs for these genes, were related to photosynthetic pigment metabolism or phylloquinone biosynthesis, revealing the importance of chloroplast metabolism in **PH** response. Genes responsive to oxidative stress were also overexpressed, such as *NAC013*, chloroplastic lipocalin, glutathione peroxidases 1 and 4, several thioredoxins and NO associated 1 (*NOA1*). 1030 transcripts were specifically downregulated in **PH**, with GOs related to **"plant-type cell wall biogenesis"**, **"microtubule-based movement"**, and **"lipid metabolic process"**. Their products included many peroxidases, some glutathione S-transferases, many cysteine/histidine-rich C1 domain-containing proteins, some kinesins and microtubule-associated proteins, several arabinogalactan proteins, beta-glucosidases, many UDP-glucosyltransferases, keto-acyl-CoA synthases 4, 8 and 17 and some GDSL esterases/lipases. These results again support the necessity to decrease the expression of defence and cell growth related enzymes for proper acclimation to stress.

2.2.3. Specific responses in heat-shocked samples

Regarding the response to 43°C treatment, there was a high overlap between **H** and **PH** upregulated transcripts (1203 in common) (Figure 4.2). GO for overexpressed genes was related to **"RNA modification"** (pentatricopeptide repeat-containing (PPR) proteins), **"organelle organization"** (ribosomal proteins, *MORC2*, *WEAK CHLOROPLAST MOVEMENT UNDER BLUE LIGHT-like protein*, *NUCLEAR FACTOR Y, SUBUNIT B11*, some mitochondrial transcription termination factors) and **"organonitrogen compound metabolic process"**. Such a response could reflect the disturbance of organelles occurring under severe HS and the necessity to regulate their metabolism under harmful conditions.

The common 484 downregulated genes were related to **"cell wall organization or biogenesis"** and **"polysaccharide metabolic process"** (expansins, xyloglucan endotransglucosylases/hydrolases, pectin lyase-like superfamily proteins, and plant invertase), **"lipid transport"** (bifunctional inhibitor/lipid-transfer protein/seed storage 2S albumin superfamily proteins, OSBP (oxysterol binding protein)-related protein 1D (*ORP1D*), lipid transfer protein 3 (*LTP3*), *SWEET14*) and **"regulation of cell proliferation"** (root meristem growth factor 3 and 4 (*RGF3* and *RGF4*), minichromosome maintenance 2 (*MCM2*), cyclin-dependent kinase B1, ARMADILLO BTB protein 1 (*ABAP1*), repressor of WUSCHEL1 (*ROW1*)).

H-specifically upregulated transcripts (483) were related to **"ethylene-activated signalling pathway"** (*ARF14*, *ERF1B*, *ERF2*, *ERF6*, *ERF11*, *ERF018*, *ERF055*, *ERF105*, *ETR2*, *WRKY48*, *WRKY53*, *WRKY62*, *SAG101*, jasmonate-zim-domain protein 1 (*JAZ1*), salicylic acid induction deficient 2 (*SID2*), *CYP81F2*), **"protein phosphorylation"** (protein kinases, leucine-rich repeat protein kinases, cysteine-rich receptor-like protein kinases, SNF1-related protein kinase 2.9 (*SNRK2.9*)), **"response to chitin"** (*MYB15*, *MYB27*, *MYB31*, *WRKY22*, salt-inducible zinc finger 1 (*SZF1*), response regulator 7 (*ARR7*), Cys, Met, Pro, and Gly protein 1 (*CMPG1*), *RDUF2*), **"response to absence of light"** (SAG21, dark inducible 4 (*DIN4*), glutamine-dependent asparagine synthase 1 (*ASN1*), thiamin diphosphate-binding fold (THDP-binding) superfamily protein), **"cellular response to decreased oxygen levels"** (phospholipase A 2A, ARIADNE 12 (*ARI12*), hypoxia responsive ERF (ethylene response factor) 1 (*HRE1*), plastidial protein *CP12-3*).
H-downregulated transcripts (238) were related to **"response to gibberellin"** (GAST1 protein homolog 3 (*GASA3*), BANQUO 3 (*BNQ3*), cysteine proteinase 1 (*CP1*), asymmetric leaves 1 (*AS1*), late elongated hypocotyl (*LHY*), gamma tonoplast intrinsic protein (*GAMMA-TIP*)), **"response to auxin"** (SAUR-like auxin-responsive proteins, indole-3-acetic acid inducible 8 and 20 (*IAA8* and *IAA20*), auxin-induced in root cultures 1 (*AIR1*), TORNADO 2 (*TRN2*), like AUXIN RESISTANT 2 (*LAX2*), big grain like 1), **"lipid localization"** (lipid transfer protein 2 (*LTP2*), *OLEOSIN 1*, *ATSWEET13*, seed storage albumin 5 (*SESA5*), defective in induced resistance 1 (*DIR1*), several bifunctional inhibitor/lipid-transfer protein/seed storage 2S albumin superfamily proteins). Several LEA proteins were also downregulated in **H**.

Altogether, these transcriptomic data reveal a common downregulation of cell wall enzymes and growth related genes in the different heat treatments, even though a higher number of these genes were downregulated in primed samples. Thus, this process seems to be important for acclimation, as previously suggested by Larkindale & Vierling (2007). Concerning the overexpressed genes, even though many *HSFs*, *HSPs* and ROS detoxifying enzymes were upregulated in all conditions, some of them were specifically induced in primed samples, which could favour the acclimation process. In **PH** samples, chloroplast metabolism regulation seems to be an important process, which is in agreement with the high sensitivity of chloroplast to HS and the necessity to induce protective mechanisms to enhance its function (Wang *et al.*, 2018). On the contrary, the upregulation of ethylene responsive genes in **H** samples might promote senescence or programmed cell death (Trobacher, 2009). However, we did not observe a general induction of the expression of senescence-associated genes (except mitochondrial *SAG21*/*LEA38*) or PCD-related genes in **H** samples, but since our data were acquired after 30 minutes of stress, this is likely to be too early to uncover their upregulation, especially in the case of a late induction of death, as

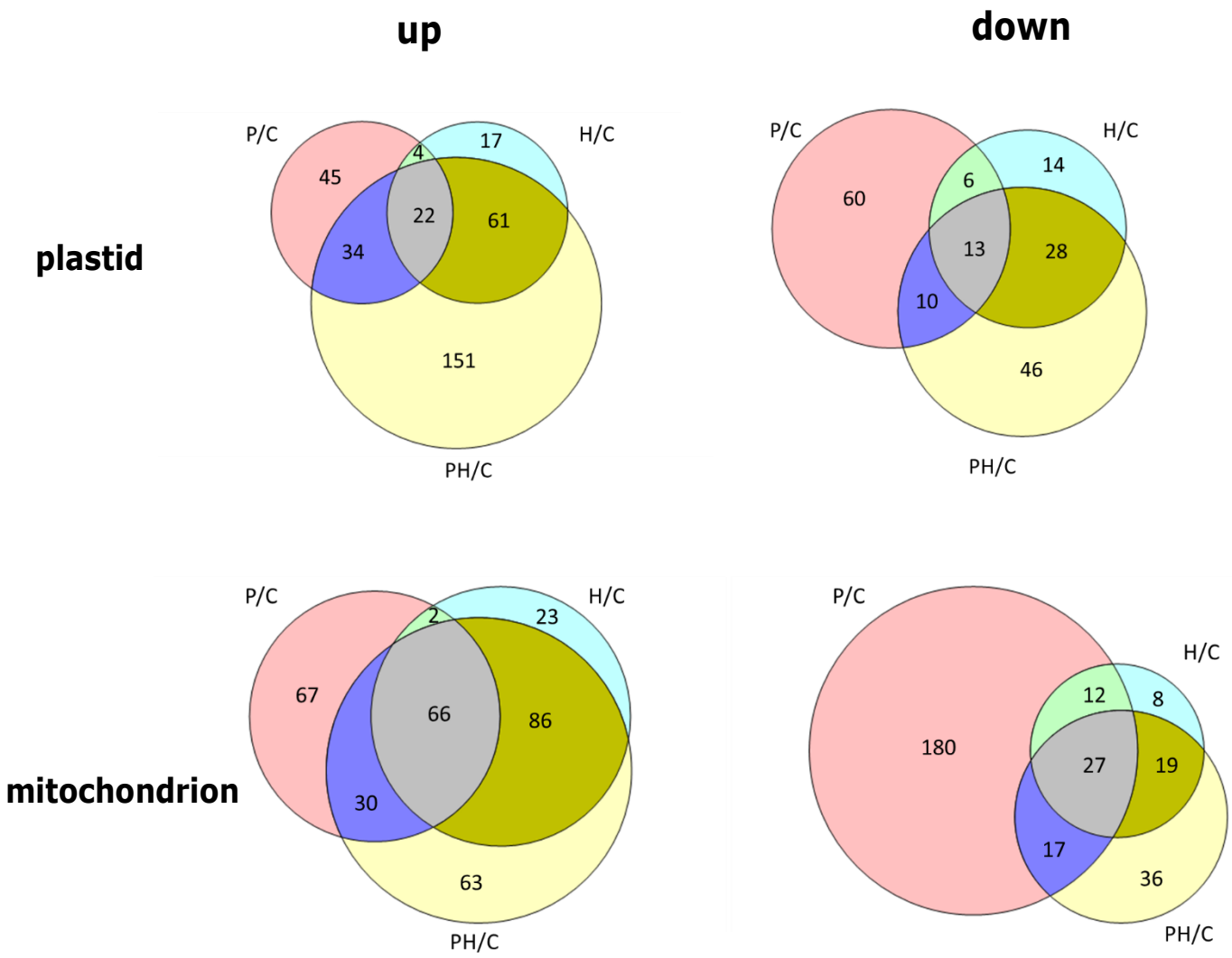

Figure 4.5: Venn diagrams reflecting the overlap between the responses to the different heat treatments of the plastidial and mitochondrial proteins encoding genes.
Genes were selected according to SUBAcon predictor (SUBA4); shown are the number of differentially expressed transcripts in the different treatments compared to the control with a log2 fold change >1 (up) or <-1 (down) and a fold discovery rate of 0.05.

Table 4.2: Transcriptional responses of the plastidial genome.
Id refers to the transcript; coloured cells correspond to significant differential expression of transcripts with false discovery rate <0.05 and log2 fold change >1 (pink) or <-1 (green).

id	log2 P/C	log2 H/C	log2 PH/C	Gene description
ATCG00130.1	0.70	-1.31	-1.34	ATPF
ATCG00140.1	1.00	0.03	-0.34	ATPH
ATCG00150.1	0.74	-0.67	-1.02	ATPI
ATCG01010.1	-0.33	-1.11	-1.37	NDHF
ATCG00600.1	1.23	0.75	0.36	PETG
ATCG00020.1	1.03	1.28	0.98	PHOTOSYSTEM II REACTION CENTER PROTEIN A, PSBA
ATCG00680.1	1.05	0.44	0.30	PHOTOSYSTEM II REACTION CENTER PROTEIN B, PSBB
ATCG00280.1	1.24	0.76	0.42	PHOTOSYSTEM II REACTION CENTER PROTEIN C, PSBC
ATCG00270.1	1.12	0.63	0.35	PHOTOSYSTEM II REACTION CENTER PROTEIN D, PSBD
ATCG00580.1	1.03	0.44	0.45	PHOTOSYSTEM II REACTION CENTER PROTEIN E, PSBE
ATCG00080.1	-0.14	1.54	1.33	PHOTOSYSTEM II REACTION CENTER PROTEIN I, PSBI
ATCG00700.1	0.99	1.42	0.42	PHOTOSYSTEM II REACTION CENTER PROTEIN N, PSBN
ATCG00510.1	0.99	0.66	1.09	PHOTOSYSTEM I SUBUNIT I, PSAI
ATCG00780.1	0.34	-1.08	-0.58	RIBOSOMAL PROTEIN L14, RPL14
ATCG00790.1	0.59	-1.04	-0.56	RIBOSOMAL PROTEIN L16, RPL16
ATCG00650.1	-0.30	-2.33	-2.44	RIBOSOMAL PROTEIN S18, RPS18
ATCG01210.1	1.45	1.68	1.32	RIBOSOMAL RNA16S, RRN16S.2
ATCG00920.1	1.32	1.60	1.28	RIBOSOMAL RNA16S, RRN16S.1
ATCG00950.1	1.43	1.66	1.24	RIBOSOMAL RNA23S, RRN23S.1
ATCG01180.1	1.32	1.59	1.17	RIBOSOMAL RNA23S, RRN23S.2
ATCG01000.1	0.53	-1.01	-0.05	YCF1.1
ATCG00210.1	1.35	-0.18	-0.03	YCF6

Table 4.3: Transcriptional responses of the mitochondrial genome.
Id refers to the transcript; coloured cells correspond to significantly upregulated transcripts with false discovery rate <0.05 and log fold change >1.

id	log2 P/C	log2 H/C	log2 PH/C	Gene description
ATMG00480.1	1.01	0.70	0.59	ATP SYNTHASE 8, ATP8, ORFB
ATMG01190.1	1.06	0.68	0.55	ATP SYNTHASE SUBUNIT 1, ATP1
ATMG01080.1	1.08	0.77	0.50	ATP9, MITOCHONDRIAL F0-ATPASE SUBUNIT 9
ATMG00960.1	1.11	0.72	0.48	CCB203
ATMG00180.1	1.08	0.93	0.78	CCB452, CYTOCHROME C BIOGENESIS 452
ATMG01360.1	1.01	0.92	0.89	COX1, CYTOCHROME OXIDASE
ATMG00730.1	1.06	0.80	0.76	COX3, CYTOCHROME C OXIDASE SUBUNIT 3
ATMG00010.1	1.47	1.24	1.43	
ATMG00040.1	1.76	1.19	1.28	ATP synthase subunit C family protein
ATMG00050.1	1.32	-0.04	0.45	
ATMG00120.1	2.65	1.75	1.91	
ATMG00140.1	1.61	1.21	1.69	
ATMG00150.1	1.27	1.59	1.44	
ATMG00170.1	2.82	1.44	1.83	
ATMG00200.1	1.30	0.91	1.52	
ATMG00280.1	1.19	0.69	0.94	
ATMG00320.1	1.77	1.22	1.84	
ATMG00400.1	0.83	0.59	1.22	
ATMG00430.1	2.94	2.00	2.83	
ATMG00440.1	3.44	2.57	3.09	
ATMG00470.1	1.19	1.20	1.36	
ATMG00500.1	1.03	0.55	0.72	
ATMG00590.1	1.25	1.11	1.40	Cytochrome b/b6 protein
ATMG00600.1	3.53	2.40	3.76	
ATMG00620.1	2.90	1.60	1.87	
ATMG00630.1	3.06	1.57	1.95	
ATMG00640.1	1.09	0.75	0.51	encodes a plant b subunit of mitochondrial ATP synthase
ATMG00660.1	1.26	0.81	0.94	
ATMG00710.1	1.43	1.41	2.15	Polynucleotidyl transferase, ribonuclease H-like superfamily protein
ATMG00750.1	1.47	1.66	1.87	
ATMG00760.1	1.80	0.42	1.28	
ATMG00820.1	0.44	0.90	1.56	Reverse transcriptase (RNA-dependent DNA polymerase)
ATMG00860.1	0.58	0.35	1.84	DNA/RNA polymerases superfamily protein.
ATMG00870.1	1.29	1.04	1.46	
ATMG00880.1	0.92	0.75	1.25	
ATMG00890.1	1.80	1.31	1.96	
ATMG00910.1	1.64	1.24	1.82	
ATMG00920.1	1.07	1.45	1.60	
ATMG00940.1	2.34	1.96	2.24	DNA binding

ATMG01000.1	1.06	0.55	0.36	
ATMG01010.1	1.24	0.67	0.77	
ATMG01020.1	1.05	0.55	0.89	
ATMG01060.1	1.56	1.11	1.45	
ATMG01090.1	1.23	1.15	1.35	ATP synthase 9 mitochondrial
ATMG01110.1	1.64	1.41	1.94	Mitovirus RNA-dependent RNA polymerase
ATMG01140.1	3.41	2.67	3.15	
ATMG01150.1	3.28	2.49	2.97	
ATMG01180.1	1.97	1.27	1.76	
ATMG01220.1	1.03	0.60	0.52	
ATMG01230.1	2.51	1.86	2.87	
ATMG01250.1	1.47	1.44	2.04	RNA-directed DNA polymerase (reverse transcriptase)
ATMG01280.1	1.04	0.60	0.78	encodes a cytochrome c oxidase subunit II
ATMG01290.1	1.37	0.96	1.26	
ATMG01300.1	0.69	0.86	1.45	
ATMG01410.1	1.35	1.47	1.70	
ATMG00520.1	1.06	0.88	0.96	MATR
ATMG00650.1	1.07	0.68	0.43	NAD4L, NADH DEHYDROGENASE SUBUNIT 4L
ATMG00510.1	1.05	0.79	0.63	NAD7, NADH DEHYDROGENASE SUBUNIT 7
ATMG00080.1	1.07	0.63	0.83	RIBOSOMAL PROTEIN L16, RPL16
ATMG00210.1	1.04	0.57	0.57	RIBOSOMAL PROTEIN L5, RPL5
ATMG00980.1	1.24	0.80	0.53	RPSL2, ribosomal protein L2
ATMG01390.1	1.33	0.94	0.59	RRN18, 18S ribosomal RNA

observed in our model of developmentally arrested seedlings.

2.2.4. Mitochondria and chloroplast heat stress response

Since we previously observed a protection of energy metabolism in **PH** seedlings compared to **H** seedlings (Chapter III), we wondered if this was correlated with an early transcriptional regulation of plastidial and mitochondrial protein encoding genes. For this purpose, we selected genes encoding mitochondrial and chloroplastic proteins, according to the subcellular location database for Arabidopsis proteins (SUBA4), using SUBAcon, a subcellular location Arabidopsis consensus predictor that integrates 22 computational prediction algorithms, experimental GFP and MS localizations, protein-protein interaction and co-expression data (Hooper *et al.*, 2014). Among the differentially expressed genes affected by HS in at least one treatment, 506 encoded plastidial proteins and 625 mitochondrial proteins. Venn diagrams representing the number of genes up- or downregulated for each organelle are presented in Figure 4.5.

For plastid, the highest number of upregulated genes was found in **PH**, with 151 genes (representing 17 % of PH-specifically upregulated transcripts) related to **"photosynthesis"** (Photosystem II proteins, chlororespiration reduction 1 (*CRR1*), phosphoglycerate kinase 1, early light induced protein 1), **"protein folding"** (*CpHSC70-1*, chaperonin 60-alpha, putative *HSP10*), chlorophyll metabolic process (biosynthesis), **"cellular amino acid biosynthetic process"** (Phe, Leu, Tyr, Lys, and Cys biosynthesis) or **"ribosome biogenesis and translation"** GO (50S, 30S and S21 ribosomal proteins, an elongation factor P (EF-P) family protein, chloroplast ribosome release factor 1 (*CPRF1*) and *CSP41A* involved in rRNA maturation). Also, 46 were found to be specifically downregulated in **PH** and were mainly linked to the **"lipid biosynthetic process"** GO (*CYP86B1*, putative acyl-(acyl-carrier-protein) desaturases, putative geranylgeranyl pyrophosphate synthase, gibberellin biosynthesis (*GA2*)).

Concerning mitochondrial proteins, among the 63 genes specifically overexpressed in **PH** (representing 7 % of PH-specifically upregulated transcripts), nine encoded PPR proteins and one *MORF3* (multiple organellar RNA editing factor 3). On the contrary, the expression of more than 80 mitochondrial PPR proteins was downregulated in the **P** condition. Regulation of organellar RNA processing and translation thus appears to be an important component of heat tolerance at 38°C but also at 43°C, probably to fit with organellar metabolic activity at these different temperatures. Other **PH**-overexpressed genes were related to **cellular amino acid metabolic process** (proline catabolism, glycine decarboxylase H-protein, GTPase/nitric-oxide synthase) and **oxidoreductase activity** (cytochrome-c oxidase, NADPH-dependent thioredoxin reductase b, proline dehydrogenase, protein disulfide oxidoreductase).

Regarding the transcription of organellar genomes, we could detect overexpression of 82 out of 122 mitochondrial-encoded genes in at least one treatment and no decreased mitochondrial transcript, whereas 22 out of 88 plastidial transcripts were differentially expressed in at least one treatment. Interestingly, in the **P** condition, no organellar transcript was significantly downregulated, while many were upregulated (encoding ribosomal proteins, photosystem II reaction centre proteins, ATP synthase subunits, cytochrome c oxidase subunits *COX1* and *COX3*, subunits of NADH-ubiquinone oxidoreductase *NAD4L* and *NAD7*), which would be in agreement to cope with the increased activity of the organelles observed at 38°C (Tables 4.2 and 4.3). The higher respiratory and photosynthetic activities observed during priming (cf Chapter II) could indeed require an

increased turnover of components of the electron transport chains.

In Chapter I, we previously presented the importance of retrograde and anterograde signalling in the regulation and coordination of organelle activity. Thus, we had a closer look at the expression of several genes that were previously identified as components of these pathways. Among the *GUN* family, the only affected gene was *GUN1*, which was only found to be downregulated in **P**. Concerning genes encoding nuclear transcriptional factors that were found to be involved in the regulation of nuclear-encoded organellar proteins, *WRKY40* was found to be upregulated in all treatments, whereas *WRKY63* was only upregulated in **H** (Figure 4.4). Finally, *NAC013* was only upregulated in **PH** condition. Whether these transcriptional factors respond to signals originating from mitochondrion and/or chloroplast or to other signals is not clear, but it is likely that they integrate multiple signals.

We also analysed the expression of genes related to dynamics because HS affected organelle dynamics (Chapter III). The only transcripts involved in mitochondrial dynamics and displaying changes in expression were *DRP1E* (upregulated in **P**) and *DRP5A* (downregulated in **PH**), both encoding dynamin-related proteins. As mentioned above, several transcripts for kinesin motor were downregulated in **PH**. The actin-related protein C2B transcript was downregulated in both **H** and **PH**. Concerning plastid dynamics, the plastid movement impaired 2 (*PMI2*) transcript was downregulated in **P** and **H**. However, transcript levels of genes involved in mitochondrial dynamics *DRP3A* and *DRP3B*, cardiolipin synthase, *BIGYIN*, *NETWORK*, *FRIENDLY* were not significantly affected by any heat treatment. These results suggest that the early signalling response to HS does not dramatically affect the regulation of actin and organelle dynamics that would be rather impacted at the translational or post-translational level.

We also investigated the expression of genes related to autophagy, but none of them was significantly affected after 30 minutes of heat stress. It would be interesting to examine their expression after a longer period of stress or during the recovery phase, since autophagy could be activated during later phases of stress response.

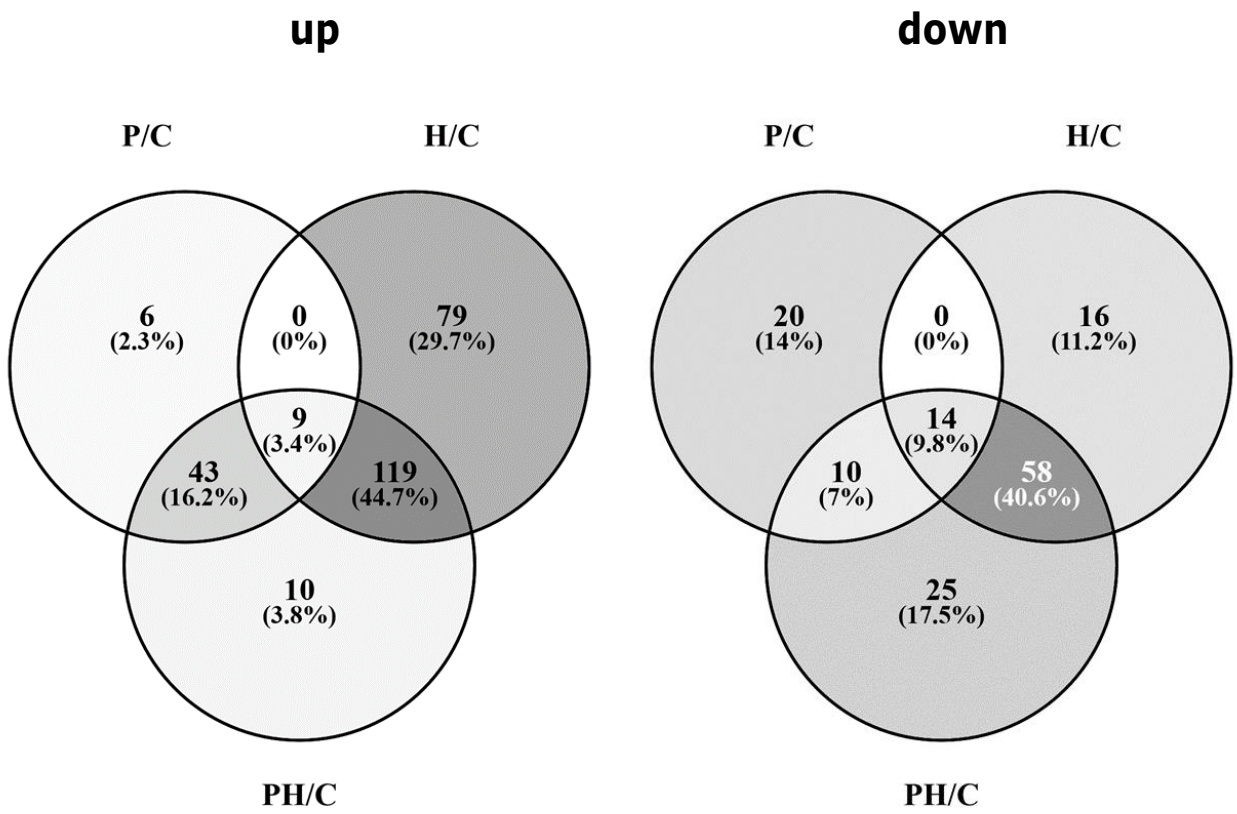

Figure 4.6: Venn diagrams reflecting the overlap in the proteomic response to the different heat treatments compared to the control.

The numbers indicate the number of proteins in each section with the corresponding percentage of total differentially expressed proteins (ANOVA and Tukey $p<0.05$). Greyscale is dependent on the number of proteins in each section.

Table 4.4: Fold change of common significantly upregulated and downregulated proteins in response to the three treatments determined by Extracted Ion Chromatogram analysis (XIC) and correlation with their corresponding gene expression changes.

Pink: upregulated; green: downregulated proteins; loc corresponds to location according to SUBA4con: c, cytosol; ER, endoplasmic reticulum; ex, extracellular; n, nucleus; p, peroxisome; pm, plasma membrane and v, vacuole. In bold are indicated the significantly upregulated (red) or downregulated (blue) transcripts after 30 min of treatment (false discovery rate<0.05 and log2 fold change >1 or <-1).

id	description	P/C	H/C	PH/C	loc
AT1G01940.1	Cyclophilin-like peptidyl-prolyl cis-trans isomerase family protein	**2.00**	1.59	**2.27**	c
AT1G12780.1	UGE1, ATUGE1 | UDP-D-glucose/UDP-D-galactose 4-epimerase 1	1.41	2.27	1.92	c
AT1G60740.1	Thioredoxin superfamily protein	2.49	1.54	2.21	c
AT3G09350.1	Fes1A	**10.95**	**2.98**	**14.69**	c
AT3G09440.1	Heat shock protein 70 (HSP 70) family protein	**1.84**	**1.18**	1.89	c
AT3G12580.1	HSP70	**4.83**	**1.12**	**5.08**	c
AT3G55120.1	TT5, A11, CFI | Chalcone-flavanone isomerase family protein	1.38	1.26	1.51	ER
AT4G28910.1	NINJA | novel interactor of JAZ	1.72	1.99	1.90	n
AT5G27030.1	TPR3 | TOPLESS-related 3	2.01	1.41	1.65	pm,g
AT2G05920.1	Subtilase family protein	**0.76**	0.58	0.51	ex
AT2G33830.1	Dormancy/auxin associated family protein	0.81	0.80	0.54	p
AT2G35780.1	scpl26 | serine carboxypeptidase-like 26	0.81	0.48	0.41	v
AT3G08030.1	Protein of unknown function, DUF642	0.66	0.30	0.20	ex
AT3G45970.1	ATEXLA1, EXPL1, ATEXPL1, ATHEXP BETA 2.1, EXLA1 | expansin-like A1	0.74	0.43	**0.37**	ex
AT4G11210.1	Disease resistance-responsive (dirigent-like protein) family protein	0.47	**0.37**	**0.31**	ex
AT4G12290.1	Copper amine oxidase family protein	**0.87**	0.45	**0.44**	pm
AT4G23690.1	Disease resistance-responsive (dirigent-like protein) family protein	0.58	**0.24**	**0.19**	ex
AT4G34260.1	FUC95A | 1,2-alpha-L-fucosidases	0.69	0.29	**0.29**	ex
AT5G19240.1	Glycoprotein membrane precursor GPI-anchored	**0.59**	0.45	**0.34**	pm
AT5G26280.1	TRAF-like family protein	0.74	0.50	0.41	ex
AT5G43060.1	RD21B, granulin repeat cysteine protease family protein	0.84	0.47	0.42	ex
AT5G49360.1	BXL1, ATBXL1 | beta-xylosidase 1	0.71	0.36	0.35	ex
AT5G66920.1	sks17 | SKU5 similar 17	**0.62**	0.21	**0.20**	ex

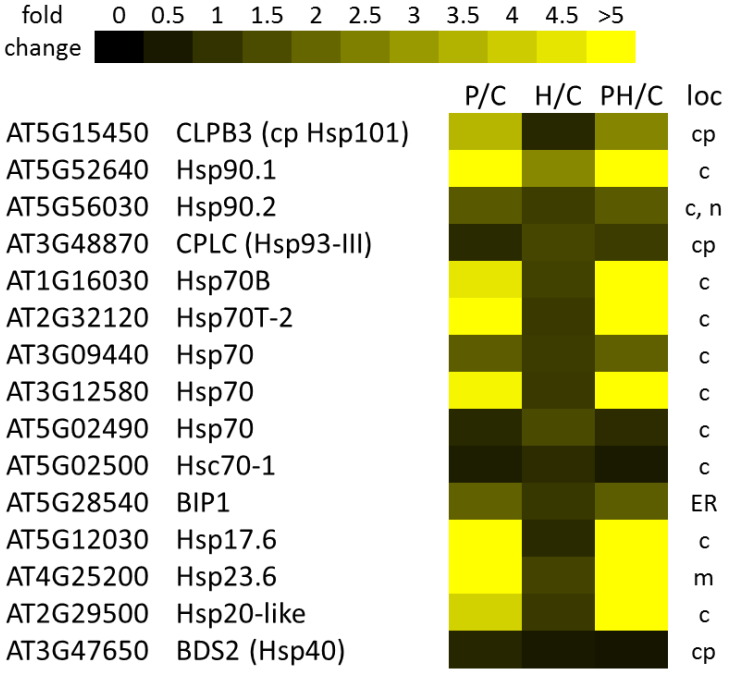

Figure 4.7: HSP protein differential accumulation in response to the different heat treatments based on XIC data.

loc corresponds to location according to SUBA4con: c, cytosol; cp, plastid; ER, endoplasmic reticulum; m, mitochondrion; n, nucleus.

Table 4.5: Fold change of common significantly upregulated and downregulated proteins in response to P and PH treatments determined by Extracted Ion Chromatogram analysis (XIC) and correlation with their corresponding gene expression changes.

Pink: upregulated; green: downregulated proteins; loc corresponds to location according to SUBA4con: c, cytosol; cp, plastid; ER, endoplasmic reticulum; ex, extracellular; m, mitochondrion; n, nucleus and pm, plasma membrane. In bold are indicated the significantly upregulated (red) or downregulated (blue) transcripts after 30 min of treatment (false discovery rate<0.05 and log2 fold change >1 or <-1).

id	Description	P/C	H/C	PH/C	Loc
AT5G12030.1	HSP17.6, HSP17.6A | heat shock protein 17.6A	**18.91**	**0.82**	**18.76**	c
AT3G10020.1	unknown protein	**14.96**	**1.18**	**16.86**	n
AT1G18270.1	ketose-bisphosphate aldolase class-II family protein	8.90	0.92	10.71	c
AT2G32120.1	HSP70T-2, heat-shock protein 70T-2	**10.03**	**1.13**	**10.16**	c
AT2G29500.1	HSP20-like chaperones superfamily protein	**4.13**	**1.14**	**8.66**	c
AT4G25200.1	HSP23.6-MITO, mitochondrion-localized small heat shock protein 23.6	**8.43**	**1.34**	**8.18**	m
AT5G52640.1	HSP90.1, heat shock protein 90.1	**8.08**	**2.66**	**8.10**	c
AT3G16050.1	A37, ATPDX1.2, PDX1.2, pyridoxine biosynthesis 1.2	**7.80**	**1.11**	**6.61**	c
AT1G16030.1	HSP70b, heat shock protein 70B	**4.52**	**1.29**	**5.65**	c
AT1G30070.1	SGS domain-containing protein	**4.52**	1.02	**5.01**	c
AT5G12110.1	Translation elongation factor EF1B/ribosomal protein S6	**4.30**	1.64	**4.70**	c
AT1G66080.1	unknown protein	**4.16**	**1.73**	**4.26**	c
AT5G15960.1	KIN1, stress-responsive protein	3.58	1.33	2.79	c
AT5G18230.1	transcription regulator NOT2/NOT3/NOT5 family protein	2.51	1.42	2.73	n
AT5G15450.1	APG6, CLPB3, CLPB-P, casein lytic proteinase B3	**3.58**	0.77	**2.61**	cp
AT4G27450.1	Aluminium induced protein with YGL and LRDR motifs	2.28	1.06	2.15	c
AT4G02980.1	ABP1, ABP, endoplasmic reticulum auxin binding protein 1	**2.04**	1.44	**2.12**	ER
AT1G68300.1	Adenine nucleotide alpha hydrolases-like superfamily protein	**2.40**	1.35	**2.11**	pm
AT5G09590.1	MTHSC70-2, HSC70-5, mitochondrial HSO70 2	**1.96**	**1.18**	**2.08**	m
AT3G07090.1	PPPDE putative thiol peptidase family protein	**2.37**	**0.98**	**2.02**	c
AT5G13200.1	GRAM domain family protein	**2.08**	1.04	**1.95**	n,pm
AT5G58070.1	ATTIL, TIL, temperature-induced lipocalin	**2.01**	1.07	**1.95**	ER
AT5G19110.1	Eukaryotic aspartyl protease family protein	**1.93**	1.56	**1.94**	ex
AT1G67360.1	LDAP1; Lipid droplet-associated protein 1	**1.82**	0.97	**1.91**	c
AT1G18500.1	MAML-4, IPMS1, methylthioalkylmalate synthase-like 4	1.85	0.98	1.91	cp
AT5G11680.1	unknown protein	**2.05**	0.92	**1.86**	pm
AT5G28540.1	BIP1, heat shock protein 70 (HSP 70) family protein	**1.92**	1.09	1.81	ER
AT1G20440.1	COR47, RD17, AtCOR47, cold-regulated 47	**1.76**	1.07	1.81	n
AT1G44820.1	Peptidase M20/M25/M40 family protein	1.70	1.18	1.80	ER
AT5G56030.1	HSP90.2, heat shock protein 81-2	**1.76**	1.20	**1.77**	c,n
AT5G17310.2	UGP2, UDP-glucose pyrophosphorylase 2	**1.63**	1.13	**1.73**	c
AT1G26110.1	DCP5, decapping 5	1.88	1.18	1.73	n
AT4G30480.2	TPR1, Tetratricopeptide repeat (TPR)-like superfamily protein	1.64	1.09	1.72	n
AT4G05150.1	Octicosapeptide/Phox/Bem1p family protein	1.71	1.19	1.68	n
AT5G64430.1	Octicosapeptide/Phox/Bem1p family protein	1.53	1.40	1.62	n
AT4G28300.1	Protein of unknown function (DUF1421)	1.56	1.28	1.62	n
AT4G21580.1	oxidoreductase, zinc-binding dehydrogenase family protein	**1.54**	1.15	**1.58**	c
AT4G20020.2	MORF1, multiple organellar RNA editing factor	**1.70**	1.11	**1.58**	m
AT3G09220.1	LAC7, laccase 7	1.68	0.75	**1.53**	ex
AT5G48180.1	NSP5, nitrile specifier protein 5	1.36	1.25	1.53	c
AT1G77120.1	ADH1, alcohol dehydrogenase 1	1.44	0.95	1.51	c
AT5G54960.1	PDC2, pyruvate decarboxylase-2	1.55	1.09	1.51	c
AT1G09740.1	Adenine nucleotide alpha hydrolases-like superfamily protein	1.65	1.03	**1.47**	c
AT1G69830.1	ATAMY3, AMY3, alpha-amylase-like 3	0.49	0.91	0.42	cp
AT4G19170.1	NCED4, CCD4, nine-cis-epoxycarotenoid dioxygenase 4	0.46	0.73	0.42	cp
AT1G30510.1	ATRFNR2, RFNR2, root FNR 2	0.50	0.73	0.50	cp
AT5G35940.1	Mannose-binding lectin superfamily protein	0.60	**1.06**	**0.56**	c
AT1G78880.1	Ubiquitin-specific protease family C19-related protein	0.58	0.82	0.57	pm
AT2G37040.1	PAL1, ATPAL1, PHE ammonia lyase 1	0.55	0.88	0.60	c
AT4G26900.1	AT-HF, HISN4, HIS HF	0.64	1.25	0.64	cp
AT5G07460.1	PMSR2, ATMSRA2, peptidemethionine sulfoxide reductase 2	0.70	1.24	0.71	n
AT4G18480.1	CHLI1, magnesium chelatase subunit	0.72	1.22	**0.80**	cp
AT1G08520.1	ALB1, ALB-1V, V157, PDE166, CHLD, ALBINA 1	0.65	1.08	0.82	cp

3. Proteomics

3.1. Methods

Even though transcriptomic analysis provides clues about the pathways involved in heat response, it does not necessarily correlate with changes at the protein level since the correlation between the transcript level and protein abundance is generally poor (Maier *et al.*, 2009). Thus, we performed a non-targeted proteomic study by nanoLC/MS/MS analysis to detect major changes in protein profiles after HS. This work was performed at the platform PAPPSO (Gif sur Yvette) in collaboration with Thierry Balliau and Michel Zivy. Results were obtained from four biological replicates of four different samples:

C = control (Day 7)
P = 38°C (Day 6) + 24 h recovery
H = 43°C 2 h (Day 7) + 2 h recovery, using control seedlings
PH = 43°C 2 h (Day 7) + 2 h recovery, using primed seedlings.

We chose to perform the proteomic analysis after 2 h of recovery, as we could already detect physiological differences at this time. In a recent study, proteome analysis was performed after 5 h of recovery, a time that was selected because it corresponded to the resumption of *de novo* protein synthesis in primed (but not in heat shocked) seedlings (Echevarría-Zomeño *et al.*, 2016).
The approach of Extracted Ion Chromatogram (XIC) analysis allowed the relative quantification of proteins when peptides were detected in all the treatments. It consists in the integration of the peak area at the same m/z and RT (using a deviation cut-off of 20 s). When a peptide was undetectable in at least one treatment, individual peptide quantification by spectral counting (SC) was performed. SC is based on the spectra number per peptide and peptide number per protein. ANOVA and Tukey's post hoc tests were used to determine significantly differently accumulated proteins in the different conditions.

3.2. Results and discussion

3.2.1. Core response

Among the 4544 identified proteins, 740 were retained after data filtration and removal of proteins with little abundance variation. Of these, 266 proteins were found to be significantly upregulated and 143 proteins downregulated in at least one treatment, based on peak-area integration on XIC. Interestingly, there was a high overlap between **H** and **PH** differentially abundant proteins (Figure 4.6). Concerning the core HSR, nine proteins were significantly increased and fourteen decreased in all treatments (Table 4.4). Two HSP70 and the protein Fes1A, which was previously shown to play an important role in thermotolerance by stabilizing HSP70 proteins (Zhang *et al.*, 2010a) and a cyclophilin family protein (also involved in protein folding) were found to accumulate, although to a lower extent in **H** than in **P** and **PH**. Other proteins were: UGE1, an enzyme involved in galactose synthesis, which is a precursor for galactinol and raffinose biosynthesis; NINJA protein, which is a methyl jasmonate (MeJA)-responsive protein involved in the repression of the jasmonate signalling pathway;

TOPLESS-RELATED3, which seems to interact with NINJA protein (Pauwels *et al.*, 2010); a chalcone flavanone isomerase called TT5 of the anthocyanin biosynthetic pathway and a thioredoxin. Only one of these proteins (HSP70, AT3G12580.1) was also highlighted in the study of Echevarría-Zomeño *et al.* (2016) as "common to the general heat stress response", which may reflect differences in experimental conditions, but also the difficulty to quantify variations in protein abundance by proteomics.

Concerning the 14 proteins with decreased abundance in the three treatments, they were involved in proteolysis (subtilase, SCPL26, RD21B), defence (disease resistance-responsive proteins) or cell wall metabolism (ATEXLA1, FUC95A, beta-xylosidase 1, sks17). SC also allowed us to identify a eukaryotic aspartyl protease and a GDSL-like lipase (Supporting Information Table S4.1). Interestingly, even though all proteins were not correlated with a transcriptional downregulation, they were related to GO similar to those of downregulated transcripts, showing that the global response is conserved.

3.2.2. Specific responses of primed samples

Concerning the primed samples (**P** and **PH**), most of the upregulated proteins were common to both treatments, whereas downregulated proteins were less conserved, based on XIC results (Figure 4.6). The conserved response between **P** and **PH** for accumulated proteins included many HSPs, such as HSP17.6, mitochondrial HSP23.6, CLPB3 (plastidial HSP101) and many HSP70s (including BIP1), HSP90.1 and HSP90.2 (Figure 4.7 and Table 4.5). Many HSPs could be identified and quantified by XIC (Figure 4.7) and others by SC: HSP90.3, HSP90.4, HSP17.4, HSP17.6 II, HSP18.2, HSP21, HSP23.5, HSP26.5, HSA32, five HSP20-like proteins, a DNAJ HSP and HSP101 (Supporting Information Table S4.1). Interestingly, in contrast to the study of Echevarría-Zomeño *et al.* (2016) who found that the core response to HS (**P**, **H**, **PH**) involved many HSPs, we did not find any significant upregulation of HSP101, HSP90.1 or some sHSPs in **H** seedlings (Figure 4.7). This is likely to be due to the fact that they applied HS in an oven instead of a water bath as in our study, so the temperature rise was likely to have been slower in their conditions, allowing translation of HSPs when the tissue temperature was below 40°C. In our conditions, the temperature of 43°C was reached within around 10 minutes, therefore, translation was probably inhibited within a few minutes, preventing any accumulation of HSPs during the temperature increase. In the study of Echevarría-Zomeño *et al.* (2016), BAG6 (a calmodulin binding protein) was identified as an acclimation specific protein, and JASMONATE RESPONSIVE 1 (JR1) as a **H** specifically induced protein. In our conditions, we could also detect the upregulation of BAG6 by SC in **P** and **PH**, even if it was transcriptionally upregulated in all treatments. However, JR1 was not significantly affected at the protein level or at the transcriptional level.

Two major components of heat tolerance that were transcriptionally overexpressed in all treatments, ascorbate peroxidase 2 (APX2) and HSFA2, were only accumulated in **P** and **PH**, as determined by SC (Supporting Information Table S4.1). TETRATRICOPEPTIDE REPEAT 1 (TPR1), a protein that interacts with HSP90/HSP70 (Prasad *et al.*, 2010), was upregulated in all primed samples, as well as a temperature-induced lipocalin (TIL), which was previously identified as an important component of basal and acquired thermotolerance (Chi *et al.*, 2009) (Table 4.5). TIL would participate in the prevention of lipid peroxidation (Boca *et al.*, 2014). Among the most over-accumulated proteins figured pyridoxine biosynthesis 1.2 (PDX1.2), which was recently shown to play an important role in the maintenance of vitamin B6 biosynthesis under HS (Dell'Aglio, Boycheva & Fitzpatrick,

2017), an elongation factor EF1B involved in translational elongation, the cold and ABA-responsive protein KIN1, an auxin-binding protein ABP1, and COLD-REGULATED 47 (COR47), which is a dehydrin (target of DREB2A) (Schramm *et al.*, 2008). Interestingly, an enzyme involved in mRNA decapping and translational repression called DECAPPING 5 (DCP5) was also upregulated in the primed samples. This enzyme was proposed to participate in the recruitment of mRNA decapping enzymes prior to mRNA degradation by XRN4, which was shown to be important for the regulation of ABA signalling and survival under long-term heat treatment (Merret *et al.*, 2013; Chantarachot & Bailey-Serres, 2018; Wawer *et al.*, 2018). In our study, we did not observe any upregulation of XRN4, or its cofactor LARP1, at the transcriptional or protein level, but the upregulation of DCP5 may be an indicator of mRNA decay under HS as observed by Merret *et al.* (2013).

Interestingly, alcohol dehydrogenase (ADH) and pyruvate decarboxylase 2 (PDC2), which are involved in fermentation, were also specifically induced in **P** and **PH** treatment, even though there was no apparent hypoxia during treatments. In tall fescue, fermentation-related genes were found to be overexpressed upon short HS but not under long-term HS (Alam *et al.*, 2018). ADH and PDC were found to be upregulated in response to cold treatment and it was proposed that ethanol would be beneficial for protecting the membrane by fluidizing it (Kaplan *et al.*, 2009). In the context of HS, additional fluidization of the membrane would be noxious, but ethanol could contribute to the upregulation of ROS scavenging enzymes, as observed by the effect of the exogenous application of ethanol on the response to salt stress in rice and Arabidopsis (Nguyen *et al.*, 2017). A simple explanation for the induction of ADH and PDC would be to favour glycolytic ATP production under stress conditions where mitochondrial oxidative phosphorylation could be compromised.

Concerning plastidial proteins, CLPB3 (plastidial HSP101) and isopropylmalate synthase 1 (involved in Leu synthesis) were upregulated in **P** and **PH**, according to XIC (Table 4.5; Figure 4.7). HSP21 was also upregulated according to SC (Supplemental Information Table S4.1), and could participate in the protection of PS II subunits and to the maintenance of plastidial transcription through interaction with the plastid-encoded RNA polymerase (Zhong *et al.*, 2013; Chen *et al.*, 2017). In mitochondria, HSP23.6, HSC70-5 and MORF1 (multiple organellar RNA editing factor 1) were the only mitochondrial proteins upregulated in both conditions, according to XIC (Table 4.5), whereas HSP23.5 and HSP26.5 were upregulated in these two treatments according to SC (Supplemental Information Table S4.1). MORF1 could play a role in RNA editing, since it was shown to interact with PPR proteins and potentially with RNA (Haag *et al.*, 2017; Bayer-Császár *et al.*, 2017).

Overall, the accumulated proteins in the primed samples displayed a rather good correlation with the transcriptome response since 63 % of the proteins had their respective transcripts upregulated after 30 minutes of heat treatment. On the contrary, twelve of these genes were upregulated in **H** at the transcriptional but not at the protein level, suggesting that their translation was affected in this condition. Since we pointed out earlier that translation was likely fully inhibited in **H** conditions, this is not surprising.

Among the ten common downregulated proteins in **P** and **PH** treatments, six were found to be plastidial according to XIC (Table 4.5). They included ALBINA1 and CHLI1, which are involved in chlorophyll biosynthesis, and NCED4 in carotenoid and ABA metabolism. The three others were an alpha-amylase-like 3 involved in starch catabolism, HISN4 in histidine synthesis and a root-type ferredoxin called FNR2 identified as a component of nitrite

detoxification (Hachiya *et al.*, 2016). An important enzyme of the phenylpropanoid pathway PAL1 (phenylalanine ammonia-lyase 1), PMSR2 (peptidemethionine sulfoxide reductase 2) and a ubiquitin-specific protease family C19-related protein were also decreased in **P** and **PH**. PMSR proteins are involved in the repair of oxidatively damaged proteins by transforming methionine sulfoxide back into Met (Romero *et al.*, 2006) and it is thus surprising that this enzyme is downregulated in primed samples. By SC, we could also identify two JA-responsive proteins OPR1 and a LRR transmembrane protein kinase. The downregulated proteins were poorly correlated with their transcript level, which suggests a major role for protein degradation in the response.

Six proteins were specifically accumulated in the **P** condition: HRU1 (a hypoxia-responsive protein), a peroxidase, LTP2 (a lipid-transfer protein involved in cuticle integrity), the thioredoxin TRX-H5, BCB (an enzyme involved in lignin biosynthesis for cold tolerance) and a cysteine-proteinase protein.
Among the twenty proteins specifically decreased in **P** samples, we could detect eleven plastidial proteins including GUN4, a rhodanese-like domain-containing protein, IPP2 involved in isoprenoid metabolism via the mevalonate pathway (Okada *et al.*, 2008), 1-deoxy-D-xylulose 5-phosphate reductoisomerase (DXR) from the MEP (2-C-methyl-d-erythritol 4-phosphate) pathway, HSP93-III of CLP protease complex, PAB (protein in chloroplast ATPase biogenesis) involved in the assembly of plastidial ATP synthase. Only one mitochondrial protein, lipoyltransferase 2 (LIP2), which is involved in the lipoylation of components of glycine decarboxylase and α-ketogluratate dehydrogenase (Ewald *et al.*, 2014), was specifically downregulated in **P**.

In **PH**, only ten proteins were specifically over-accumulated, among which were: UBP1B (oligouridylate binding protein 1B), which is a RNA–binding protein involved in stress granule formation and plays an essential role in HS tolerance, since its overexpression led to increased thermotolerance (Nguyen *et al.*, 2016); a chaperone binding/ATPase activator; SAY1 (involved in growth regulation); gamma-adaptin 1 (a protein of AP-1 complex mediating intracellular transport through trans-Golgi network); two thioredoxins; CGS1 (cystathionine gamma-synthase 1 involved in Met synthesis); a short-chain dehydrogenase/reductase 1 involved in ABA and glucose signalling. Although many transcripts were specifically induced during **PH** during treatment, such as those related to pigment and phylloquinone biosynthesis, they could not be detected at the protein level.

Among the 25 specifically downregulated proteins in **PH**, five were linked to the **"hydrogen peroxide catabolic process"** GO: purple acid phosphatase 26 (PAP26) and four peroxidases (including PER57, PRX71, PRX72). Other decreased proteins included GGT3 (GAMMA-GLUTAMYL TRANSPEPTIDASE 3, involved in glutathione catabolism), GDPDL1 (glycerophosphodiester phosphodiesterase (GDPD) like 1, involved in Pi release under phosphate starvation), BGLC3 (betaglucosidase involved in xyloglucan metabolism), UDP-GLUCOSYL TRANSFERASE 72B3, NRT3.1 (nitrate transporter, involved in wounding response), MLP34 (plant defence), ROP2 (rho-related protein from plants 2, involved in the regulation of microtubule organization (Li *et al.*, 2017)). PMSR3 (peptidemethionine sulfoxide reductase 3) was also downregulated in **PH**, confirming the downregulation of this class of detoxifying enzymes observed in the primed samples. The only downregulated plastidial protein in the **PH** condition was a GPI-anchored adhesion-like protein.

3.2.3. Specific responses of heat-shocked samples

Regarding proteins that were upregulated in response to 43°C treatment (common to **H** and **PH** treatments), we could find 119 proteins identified by XIC (Figure 4.6, Supporting Information Table S4.2). Several proteins were related to translational initiation: EIF3E, EIF4A1 and EIF4A-2, EIF6A (emb1624), NagB/RpiA/CoA transferase-like superfamily protein. Several others were related to protein import into nucleus: importin alpha isoform 1 and 4 (IMPA1 and IMPA4), nuclear transport factor 2B (NTF2B), RAN GTPase activating protein 1 (RANGAP1) and KETCH1. By SC, three ARM repeat superfamily proteins (including importin beta 4 IMB4) and exportin 1 (XPO1A), which is a receptor for nuclear export, were also found to be specifically accumulated in **H** and **PH** (Supporting Information Table S4.1). Another protein involved in thylakoid organization, FZL, could also play an important role in plastidial response to heat shock.

The common response to 43°C treatment included downregulation of many proteinases (Supporting Information Table S4.3): SAG2, which encodes a senescence-associated thiol protease, two cysteine proteases AEP3 (asparaginyl endopeptidase 3) and RD19A (responsive to dehydration 19), SCPL35 (serine carboxypeptidase-like 35), three aspartic proteases (including ASPG1 and APA1) and two caspases involved in stress-induced cell death ATCATHB2, ATCATHB3. Decreased proteins also included many proteins of the PSII (PSB27, PPD5, PPD6, PSBQ), or involved in PSII repair (degradation of periplasmic proteins 8, FTSH protease 1). Our results are in agreement with those of Echevarría-Zomeño *et al.* (2016), who also showed repression of photosynthesis-related proteins and proteases as a common response to heat shock. One protein involved in chlororespiration, PIFI (post-illumination chlorophyll fluorescence increase), was also downregulated. Finally, enzymes involved in cell wall modifications were also in lower amounts in **H** and **PH** conditions: two xyloglucan endotransglucosylases/hydrolases 4 and 7, glycosyl hydrolase 9B7, a O-glycosyl hydrolase family 17 protein, a plant invertase/pectin methylesterase inhibitor superfamily protein and a glucuronidase 3.

A set of 79 proteins were specifically accumulated in **H**, and included components of **"ubiquitin-dependent protein catabolic process"** (ubiquitin C-terminal hydrolase 3 (UCH3), S phase kinase-associated protein 1 (SKP1), regulatory particle non-ATPase 13 (RPN13), RAN binding protein 1 (RANBP1), ubiquitin-conjugating enzyme 35 (UBC35), constitutive photomorphogenic 13 (COP13), UBC36 (ubiquitin-conjugating enzyme 36)) and of **"protein transport"** (Arabidopsis RAB GTPase homolog A2C (ATRAB-A2C), homolog of human KPNB1, translocase of the inner mitochondrial membrane 13 (TIM13), alpha-soluble NSF attachment protein 2 (ALPHA-SNAP2), ATSLY1, Adaptin family protein, RAN binding protein 1 (RANBP1), importin alpha isoform 2 (IMPA2)) (Supporting Information Table S4.4). Several enzymes involved in the **"brassinosteroid signalling pathway"** were also accumulated in **H**: general regulatory factors GRF4, GRF8, GRF10, ATMP1, ATMP2. It is noticeable that FIS1A, a protein involved in mitochondrial fission was also only overexpressed in **H** samples. This protein might play a role in the induction of an aberrant morphology of mitochondria under HS, as previously observed in protoplasts (Scott & Logan, 2008), even though this phenotype was not obvious in our conditions (Chapter III). CHLI1 and CHLI2, two enzymes of the chlorophyll biosynthetic pathway, were also upregulated, together with PDS3 (phytoene desaturase 3 involved in carotenoid biosynthesis). Concerning sugar metabolism and signalling, hexokinase 2, fructokinases 6 and 7, fructose-bisphosphate aldolase 8, UGE5 (involved in galactose metabolism) and KING1

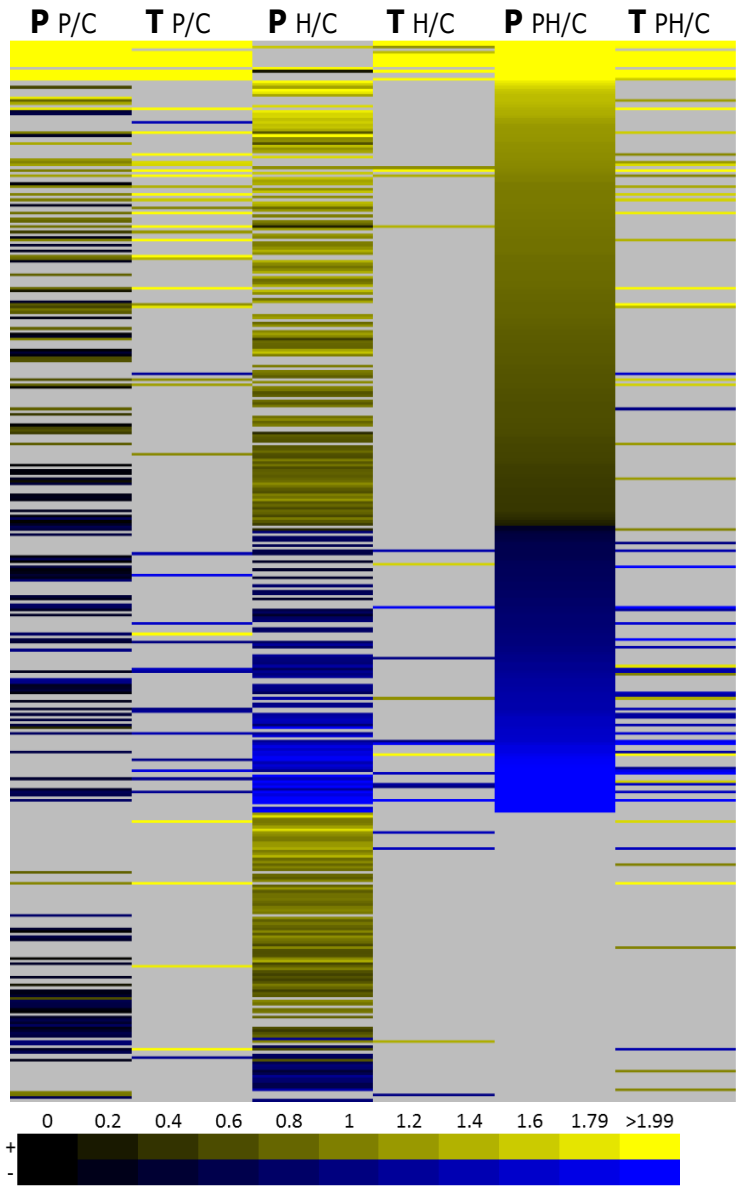

Figure 4.8: Overlap between transcriptomic and proteomic responses.
The columns **P** present the log2 fold-change for each protein in each treatment. These data correspond to the 396 proteins significantly affected in at least one treatment according to XIC. The columns **T** show the log2 fold-change at the transcriptomic level of the corresponding genes during the respective treatment. For P/C columns, protein data were acquired after 22 h of recovery post 38°C treatment and transcriptomic data after 30 min of 38°C treatment. In H/C and PH/C columns, protein data were acquired after 2 h recovery post 43°C treatment and transcriptomic data after 30 min of 43°C treatment. Log2 fold-change are coloured from yellow (>2) to blue (<-2) and grey areas correspond to non-significantly affected proteins (p-value>0.05 according to ANOVA and Tukey) and transcripts (-1<log2 fold change<1 and/or false discovery rate>0.05).

(SNF1-related protein kinase regulatory subunit gamma 1) were increased. An enzyme involved in DNA repair called DRT102 (DNA-damage-repair/toleration 2) was also accumulated in the **H** condition.

A set of 16 proteins were found to be specifically downregulated in **H** (Supporting Information Table S4.5). Among them, six were ribosomal proteins (RPL7B, RPL16A, RPL14 family protein, RPL14p, RNA binding plectin/S10 domain-containing protein and chloroplast ribosomal protein S3). Interestingly, two proteins involved in poly(A) mRNA export and splicing (MOS11 (modifier of SNC1) and SCL30 (SC35-like splicing factor 30) also decreased in **H**. In yeast, poly(A) mRNAs are accumulated in the nucleus under severe HS, as a consequence of downregulation of mRNA export (Saavedra *et al.*, 1996). However, some heat-stress responsive RNAs are selectively exported and can bypass mRNA quality control, probably because of the interaction of HSF1 with a protein export component called Mex67 (Zander *et al.*, 2016). Whether such a phenomenon occurs in plants is not known, to our knowledge. We can also notice a decrease in the abundance of several cell wall modifying enzymes, of chalcone synthase which is involved in flavonoid biosynthesis including anthocyanins, of PSAF (photosystem I subunit F) and of TIC55 which is implicated in plastidial protein import. In pea, the downregulation of plastidial protein import (TIC and TOC proteins) was previously shown to occur under HS and was hypothesized to participate in the downregulation of photosynthetic activity in addition to decreased gene and protein expression (Dutta *et al.*, 2009). All these data confirm the perturbation of protein metabolism occurring at 43°C. In the next section, we will focus on the link between transcriptomic and proteomic data.

3.2.4. Data integration between transcriptomic and proteomic analyses

In order to examine to what extent modifications detected in the proteome after a heat treatment could be correlated with an early transcriptomic response (after 30 minutes of stress exposure), we compared the variations of the 396 proteins analysed by XIC and those of their respective transcripts. Figure 4.8 shows a heat map of the log2 fold change of proteins that were differentially accumulated in at least one treatment compared to the control and the log2 fold change of their corresponding transcripts.

Among the 58 proteins significantly accumulated in **P** (after 24 h of recovery), 32 (55 %) of their transcripts were also significantly overexpressed after 30 min of heat treatment, whereas only 4 out of 44 (9 %) proteins with decreased abundance were also downregulated at the transcriptional level. In **H** seedlings, 207 proteins were accumulated, among which only five (2.4 %) had their transcripts upregulated, while two proteins (unknown protein DUF538 and a UDP-Glycosyltransferase superfamily protein) had their transcripts downregulated. Only seven out of 88 (8 %) proteins with decreased amounts in **H** had their transcripts downregulated, while two proteins were upregulated at the transcript level (FLOR1 and a cyclophilin-like peptidyl-prolyl cis-trans isomerase family protein). In **PH**, 181 proteins were accumulated, among which 33 (18 %) were also upregulated and two downregulated (enzymes involved in wax biosynthesis and lignin catabolism) at the transcript level. There were 107 proteins with decreased amounts, among which 26 corresponding transcripts (24 %) were downregulated and six upregulated (FLOR1 and 5 plastidial proteins: PSBP domain protein 5, CH42, HSP40 family protein, a cyclophilin-like peptidyl-prolyl cis-trans isomerase family protein and a FKBP-like peptidyl-prolyl cis-trans isomerase family protein).

Interestingly, the protein/transcript correlation was the highest for the increased proteins in **P** samples, even though the transcriptomic and proteomic data were acquired with a one day difference, compared to less than 4 h for **H** and **PH** samples. However, the proteins with decreasing abundance were poorly correlated with their transcript level changes. Of course, these results are based on a relatively small number of proteins and a detailed kinetics of transcriptomic and proteomic changes occurring during, and after, heat treatment would be necessary to conclude about any wide co-regulation of transcription and translation. Nevertheless, our data are in agreement with a severe impact of heat shock on translation, as observed by the low correlation between the transcripts and protein levels in **H**, whereas **PH** is in-between the **P** and **H** conditions. The lower correlation in **H** samples may be also linked to the decrease in proteins involved in mRNA export and the decrease in ribosomal protein abundance. Clearly, although we did not actually measure its activity, translation appeared severely impaired under heat shock, which is in agreement with previous studies (Yángüez *et al.*, 2013). Therefore, the rather large set of 207 proteins (207), for which we detected a higher abundance than in the control after 2 h of recovery, were necessarily synthesized after the heat shock. Since the correlation with their transcript levels during early stress exposure is very low, how can we explain their accumulation? If we consider a transcriptional regulation, these proteins were likely to be translated using transcripts having accumulated during later heat shock exposure, or/and early stress recovery. However, this view remains naive, not only because of the complexity of translational control (Shoemaker & Green, 2012), but also because the impairment of translation occurring under heat shock has a strong impact on RNA quality control by triggering a massive decay of translating mRNAs (Merret *et al.*, 2015). A more detailed kinetic analysis of the transcriptome during, and after, HS would be of interest to dissect the mechanisms actually governing the accumulation (or decrease) of proteins highlighted in our study.

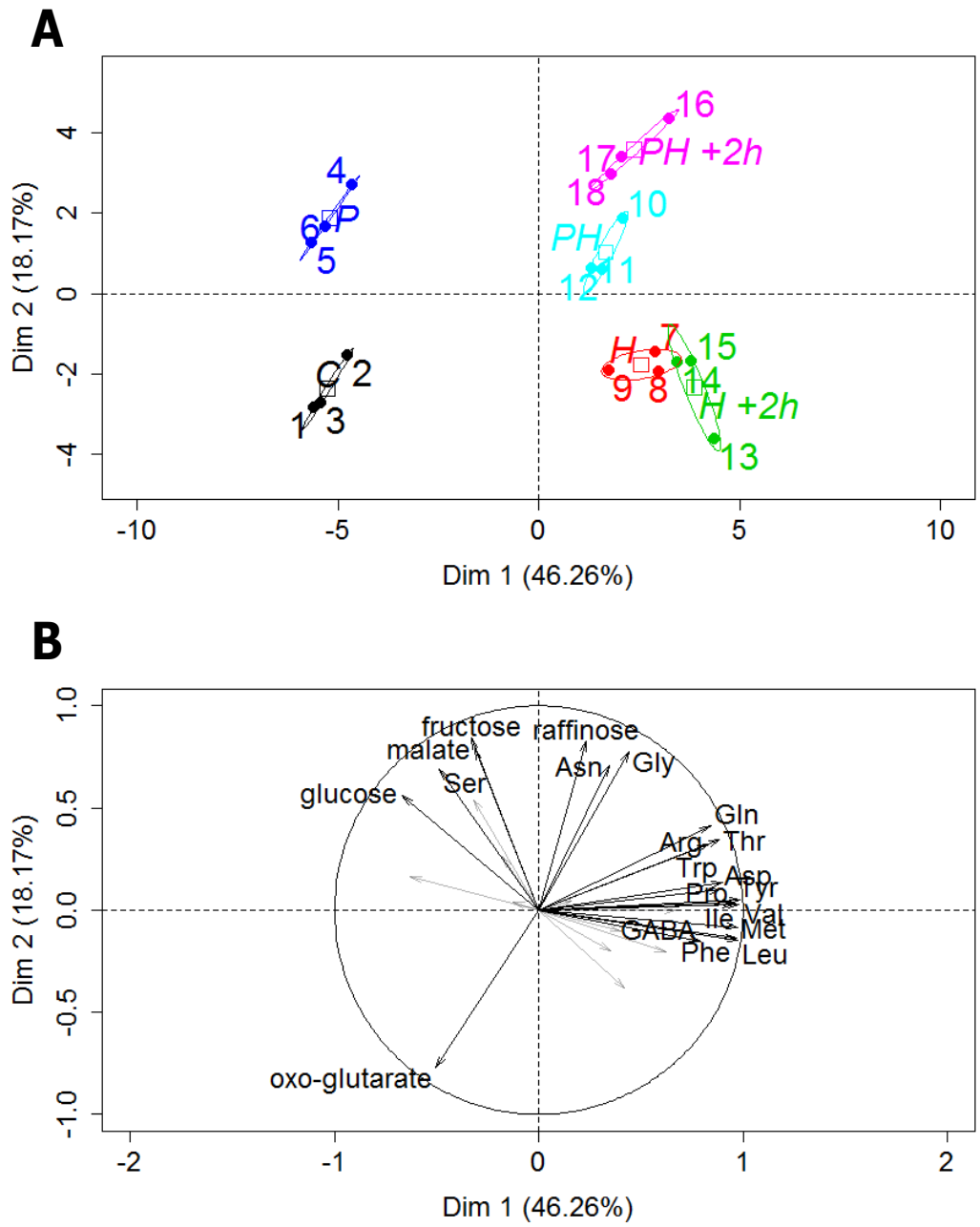

Figure 4.9: Principal component analysis of amino acids, organic acids and sugars data (dimensions 1 and 2)

A: Individual graph with confidence ellipse at 95 %; numbers correspond to each sample; C: collected before HS; P: collected before HS; H and PH: collected just after HS; H+2h and PH+2h: collected after 2 h of recovery

B: Graph of the variables (correlation circle) with cos^2>0.5.

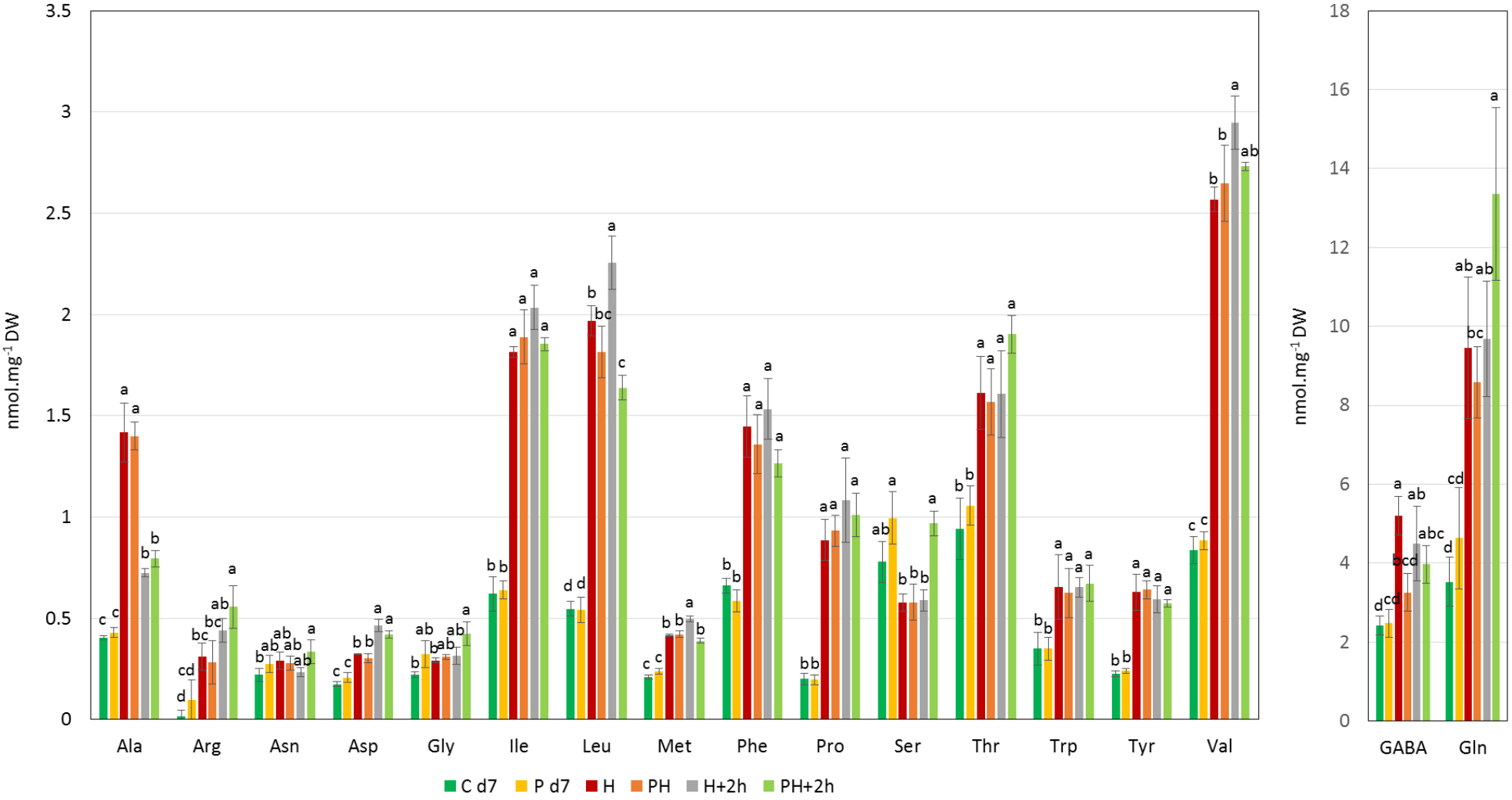

Figure 4.10: Main heat-responsive amino acids quantified by GC/MS
C d7: control; P d7: priming D+1; H: heat-shock; PH: priming + heat-shock; H+2h: heat-shock + 2 h recovery; PH+2h: priming + heat-shock + 2 h recovery; a, b, c, d correspond to statistically different groups according to ANOVA followed by Tukey's test ($p < 0.05$).

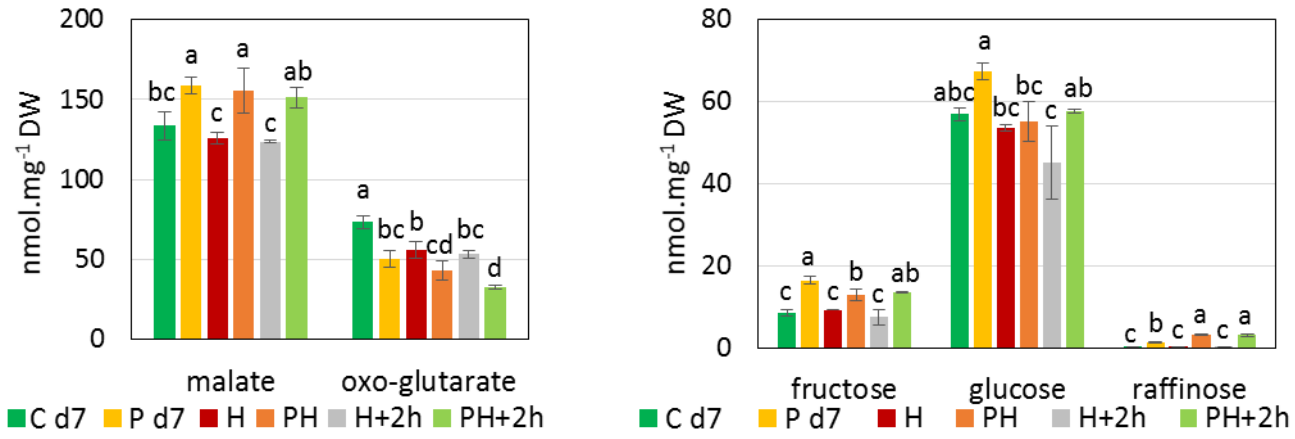

Figure 4.11: Main heat-responsive organic acids and sugars.
Organic acids were quantified by GC/MS (left) and sugars by HPLC (right). C d7: control; P d7: priming D+1; H: heat-shock; PH: priming + heat-shock; H+2h: heat-shock + 2 h recovery; PH+2h: priming + heat-shock + 2 h recovery; a, b, c, d correspond to statistically different groups according to ANOVA followed by Tukey's test ($p < 0.05$).

4. Metabolic profiling

4.1. Methods

In order to explore further the molecular response of the seedlings to HS, we performed a targeted metabolic profiling to evaluate the impact of high temperature on major components of primary metabolism. This study focused on amino acids, organic acids (both measured by GC/MS), and sugars (measured by HPLC). Sampling was performed in triplicates just before HS (**C**, **P**), just after HS (**H**, **PH**), and after 2 h of recovery (**H+2h**, **PH+2h**). Raw data were normalized by dry weight and data analysis was performed using principal component analysis (PCA) to determine how the samples were separated and which major metabolites could explain the variability observed. A fatty acid profiling was also performed using GC-FID analysis.

4.2. Results and discussion

4.2.1. Profiling of polar primary metabolites

Figure 4.9 shows the PCA analysis of polar metabolites for the first two dimensions, which accounted for 64.43 % of the observed variability. The different treatment groups are clearly separated on the individual graph: the first dimension (46.26 % of the observed variability) allows us to distinguish heat shocked and non-heat shocked samples, while the second dimension (18.17 % of the observed variability) is linked to the priming effect (Figure 4.9A). **H** samples just after, and 2 h after HS, are not separated as well as the corresponding primed samples. The inspection of the variables, which could explain the variability (Figure 4.9B), indicates that the most correlated metabolites with dimension 1 are the amino acids, Val, Ile, Leu, Met, Phe, Tyr, Pro, Trp, Asp, Thr, Gln, Arg and GABA, for which an increased pool (between two and fifteen-fold change compared to control) was observed in **H** and **PH** condition compared to **C** and **P** (Figure 4.10). The most impressive increase was observed for Arg, for which content was very low in the control condition. The rise in the pool of branched-chain, aromatic acids, and also of oxoglutarate-derived amino acids (Pro and Arg) is in agreement with previous work (Kaplan *et al.*, 2004; Caldana *et al.*, 2011), although the temperature applied was higher in our study (43°C) than in the others (40°C and 32°C, respectively). However, the increase in Pro observed in both **H** and **PH** seedlings is in contradiction with another work, which showed that acclimation led to a lower increase in Pro level, in agreement with the toxicity of Pro under high temperature (Larkindale & Vierling, 2007). Another study showed that Pro over-accumulation led to an increased generation of ROS, together with a decreased synthesis of ethylene and ABA (Lv *et al.*, 2011). In our conditions, the Pro level was not correlated with survival or later death of seedlings, since it accumulated to a similar extent in **H** and **PH**. Surprisingly, for most amino acids, there was no significant difference in their accumulation between **H** and **PH**, even after 2 h of recovery post HS, which suggests that amino acid metabolism is not a major component of the protective effect of priming.

In the second dimension of the PCA, which discriminates between primed and non-primed samples, several sugars, organic acids and a few amino acids were correlated with the priming effect (Figure 4.9A). Fructose, raffinose, malate, Gly, Asn, Ser, glucose and oxo-glutarate appear as the most correlated with dimension 2, with increased levels of sugars, malate, Gly, Asn and Ser and a decreased level of oxo-glutarate in primed samples (Figure 4.9B and Figure 4.11). Accumulation of sugars was also previously reported at temperatures comparable

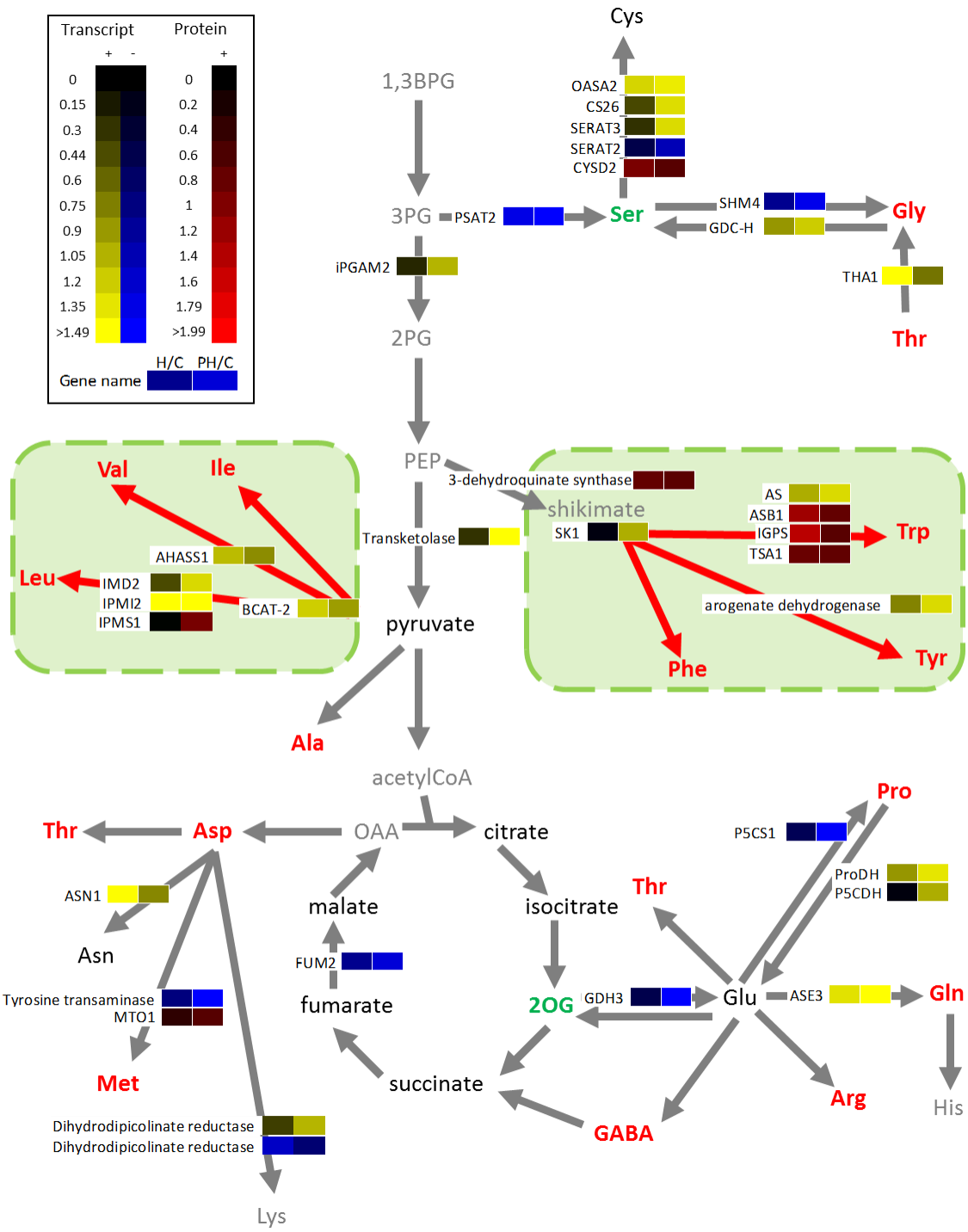

Figure 4.12: Transcriptomic and proteomic responses to heat shock related to metabolism of amino and organic acids.

Metabolites written in red are upregulated in both H and PH; green downregulated; black not significantly affected and grey not measured; the colours correspond to log2 fold change of expression (blue to yellow) or abundance (red) compared to control in H and PH after 2 h of heat shock, respectively; green boxes indicate the major plastidial upregulated metabolic pathways; 1,3BPG, 1,3-bisphosphoglycerate; 3PG, 3-phosphoglycerate; 2PG, 2-phosphoglycerate; 2OG: 2-oxoglutarate; AHASS1, acetolactate synthase small subunit 1; AS, anthranilate synthase; ASB1, anthranilate synthase beta subunit 1; ASE3, Gln phosphoribosyl pyrophosphate amidotransferase 3; ASN1, glutamine-dependent asparagine synthase 1; BCAT-2, branched-chain amino acid transaminase 2; CS26, cysteine synthase 26; CYSD2, cysteine synthase D2; FUM2, fumarase 2; GDC-H, glycine decarboxylase complex H; GDH3, glutamate dehydrogenase 3; IGPS, indole-3-glycerol phosphate synthase; IMD2, isopropylmalate dehydrogenase 2; iPGAM2, 2,3-bisphosphoglycerate-independent phosphoglycerate mutase 2; IPMI2, isopropylmalate isomerase 2; IPMS1, isopropylmalate synthase 1; MTO1, methionine over-accumulation 1; OASA2, O-acetylserine (thiol) lyase (OAS-TL) isoform A2; P5CDH, Δ-1-pyrroline-5-carboxylate dehydrogenase; P5CS1, Δ-1-pyrroline-5-carboxylate synthetase 1; ProDH, proline dehydrogenase; PSAT2, phosphoserine aminotransferase 2; SERAT 2/3, serine acetyltransferase 2/3; SHM4, serine hydroxymethyltransferase 4; SK1, shikimate kinase 1; THA1, threonine aldolase 1; TSA1, tryptophan synthase alpha chain.

to priming, 38°C or 40°C (Kaplan *et al.*, 2004; Rizhsky *et al.*, 2004), but it may possibly not occur at temperature above 43°C (**H** treatment). Indeed, a recent study showed that the highest accumulation of raffinose under HS was observed at 36°C in Arabidopsis seedlings and that it decreased above this temperature (Mueller *et al.*, 2015). The accumulation of raffinose in primed samples could participate in a better protection against oxidative stress, by scavenging hydroxyl radicals (Nishizawa *et al.*, 2008). The increase in Ser and Gly in **P** and **PH+2h** is possibly linked to a higher photorespiratory activity in these samples compared to **C** and **H+2h**, while the decrease in oxo-glutarate in heat-stressed samples is likely to be due to a higher demand for carbon skeletons towards Arg, GABA or Gln synthesis compared to the control.

To evaluate whether changes in metabolites could be correlated with changes in transcript and protein levels, we scrutinised the response of the major metabolic pathways involved in the TCA cycle and amino acid biosynthesis. In Figure 4.12 we have compiled, on a metabolic map background, the significant fold-changes we could measure of transcripts (after 30 min at 43°C) or proteins (after 2 h recovery post HS) for different enzymes, and colour-coded the variations of metabolite contents in response to heat shock. The upregulation of the expression of several plastidial enzymes (green boxes), at either transcriptional or protein level, was well correlated with the increase of aromatic amino acids and branched chain amino acids, suggesting that accumulation of these amino acids was an active process and did not only result from a decreased catabolism, protein synthesis and/or increase in protein degradation. However, we cannot exclude the fact that amino acid degradation in mitochondria and cytosol is lower under HS. Branched-chain amino acids may act as compatible solutes, or could provide an alternate electron donor to the mitochondrial electron transport chain (Obata & Fernie, 2012), while accumulation of aromatic amino acids could be related to auxin or glucosinolate metabolism, as precursors (Tzin & Galili, 2010). Concerning glucosinolates, their level is upregulated in response to elevated temperatures in *Brassica oleracea* and *Brassica rapa*, while in Arabidopsis, a mutant deficient in glucosinolate synthesis exhibited a lower thermotolerance and lower amounts of HSP90, indicating an important role of these metabolites in the stress response (Ludwig-Müller *et al.*, 2000; Martínez-Ballesta *et al.*, 2013). In our conditions, nitrile specifier protein 5 (NSP5), an enzyme involved in glucosinolate catabolism was accumulated in **P** and **PH**, while the level of phenylalanine ammonia-lyase 1 (PAL1), an enzyme involved in phenylpropanoid metabolism (a concurrent pathway), was decreased (Table 4.5). Another protein involved in glucosinolate biosynthesis, IGMT4 (indole glucosinolate O-methyltransferase 4), was accumulated in **H** samples. However, a deeper metabolic analysis (metabolites, enzyme activities) would be necessary to validate a connexion between these changes in amino-acid contents and secondary metabolism.

Regarding Pro accumulation, which was similar in **H** and **PH**, it was not correlated with the observed transcriptional down-regulation of Δ-1-pyrroline-5-carboxylate synthetase 1 gene (*P5CS1*) and the up-regulation of proline dehydrogenase and Δ-1-pyrroline-5-carboxylate dehydrogenase (*P5CDH*), a mitochondrial enzyme involved in Pro catabolism, observed in **PH** samples. Although the increase of Arg in both **H** and **PH** was impressive, it was not correlated to any significant change in enzyme transcript levels of the biosynthetic pathway. Therefore, the increase could be due to the later induction of biosynthetic genes, metabolic regulation, or a decrease in its catabolism. Indeed, Arg is a precursor of polyamines (Bitrián *et al.*, 2012), which were shown to accumulate during heat stress in wheat (Goyal & Asthir, 2009). In Arabidopsis, Kaplan *et al.* (2004) found that putrescine

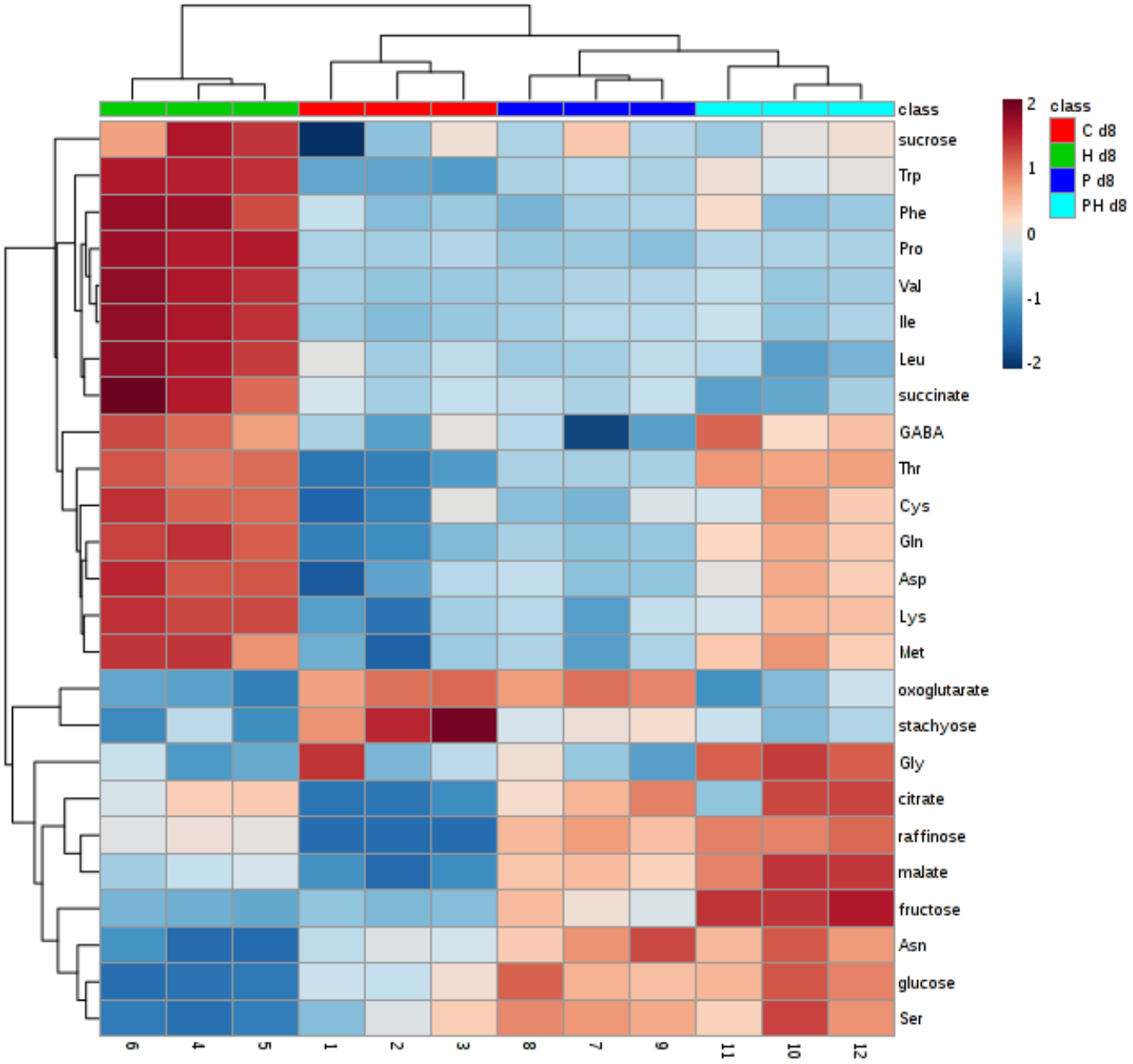

Figure 4.13: Heatmap of significantly differentially accumulated metabolites in at least one treatment on day 8.

Heatmap was performed on log-transformed and mean-centred data using the average linkage method based on Euclidean distance (MetaboAnalyst4.0); significantly differentially accumulated metabolites were selected according to ANOVA and Tukey's test ($p<0.05$); each column corresponds to a sample (n=3) and each line to a metabolite.

accumulated under HS (40°C) in three-week-old plants. It would be of interest to examine if such a response occurs in Arabidopsis seedlings. Regarding sugar metabolism, galactinol synthase, an enzyme involved in raffinose and galactinol synthesis which was previously identified as a HSF-target (Panikulangara *et al.*, 2004), was significantly upregulated at the transcriptional level in **P**, **H** and **PH**. Moreover, UGE1, an enzyme involved in galactose synthesis, which is a precursor for galactinol and raffinose biosynthesis, was also upregulated in the three treatments at the protein level (Table 4.4). However, we cannot exclude the fact that these enzymes were active at 38°C, but not at 43°C, or that others pathways were favoured in **H** and led to substrate limitations. Untargeted metabolic analysis and further transcriptomic analysis would help to elucidate such dynamics of metabolism under temperature stress.

After the analysis of these data, we also decided to investigate the metabolic response one day after the 43°C treatment (**C d8**, **P d8**, **H d8** and **PH d8**), to determine if stronger variations would discriminate **H** and **PH** seedlings at this stage. As shown by the heat map presented in Figure 4.13, several metabolites (Ile, Leu, Phe, Pro, Val, succinate and sucrose) reverted to the level of the control (**C**) in **PH**, but not in **H** seedlings. The amounts of Asp, Cys, Met, Lys, Thr, Trp, and Gln were in-between **C** and **H** levels, revealing the decrease in the concentration of these metabolites compared to **H**. Interestingly, all the branched chain and the aromatic amino acids were lowered in **PH** compared to **H**, which is likely to be related to a different recovery of plastidial metabolism. We can also notice the downregulation of Pro in **PH**, which could confirm the importance of decreasing its level for seedling survival during the recovery period.
On the contrary, some metabolites were accumulated in **PH** but not in **H**, such as Asn, Gly and Ser, glucose, fructose and raffinose. Lower levels of Gly and Ser are likely to be due to a lower photorespiration in **H** than in **PH**, whereas lower levels of glucose and fructose could be due to the lower photosynthetic activity observed in **H** seedlings. Of course, it would be necessary to study the transcriptional and proteomic responses of the enzymes involved in primary metabolism on day 8 to confirm these hypotheses.

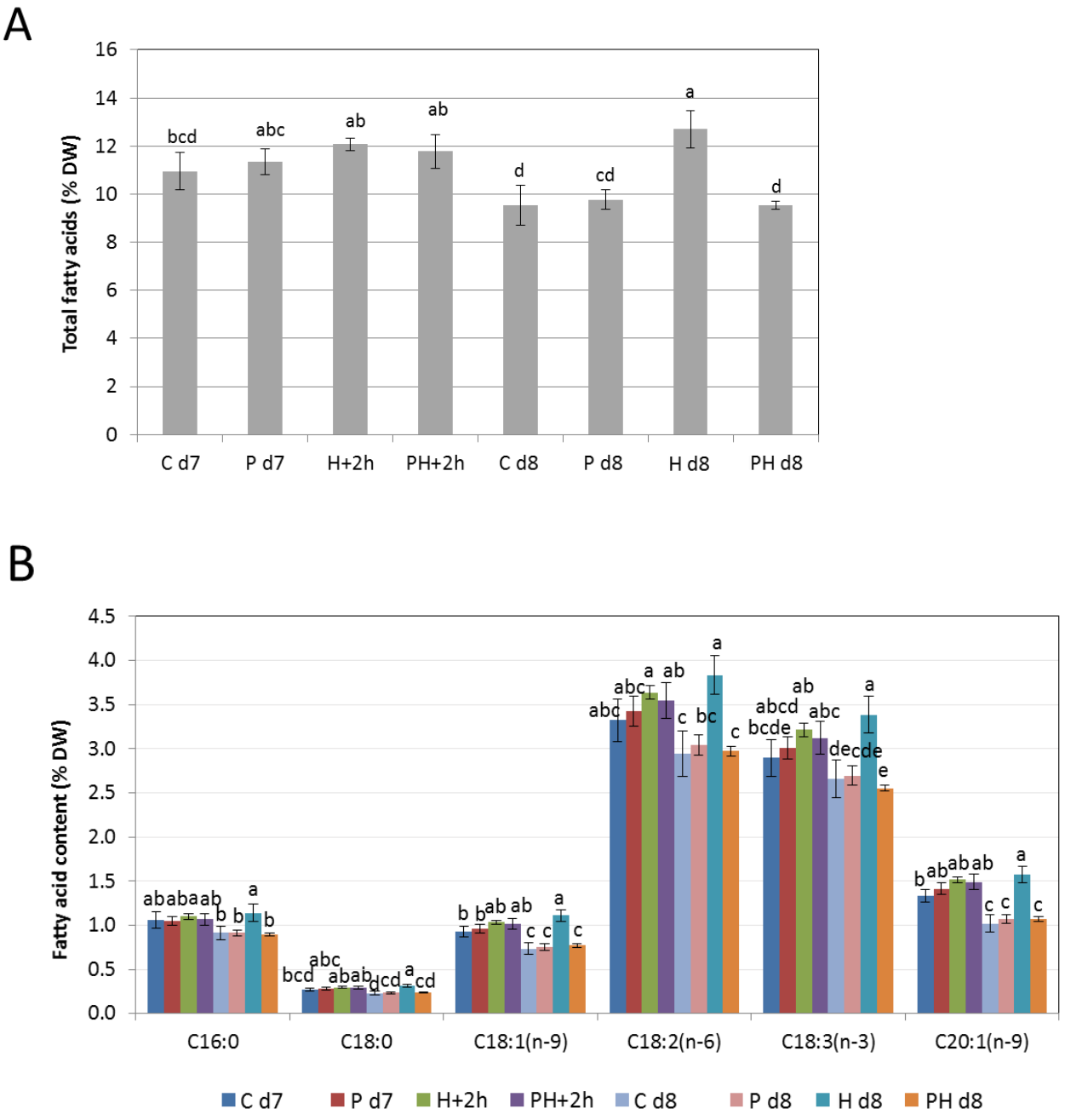

Figure 4.14: Evolution of fatty acid content and composition in response to heat treatments.
A: Total fatty acid content on days 7 and 8; B: Seedling content of major fatty acids on days 7 and 8; bars indicate SD of the mean (n=3); letters correspond to statistically different groups according to ANOVA and Tukey's test ($p<0.05$).

4.2.2. Fatty acid profiling

In Chapter II, we revealed the importance of fatty acids (FA) in young seedling development and adaptation to nutrient limitation. We therefore decided to characterize their evolution in response to HS by performing GC-FID analysis. This work was realized in collaboration with Sabine d'Andrea (Institut Jean-Pierre Bourgin, Versailles). Figure 4.14 presents the FA profiles in the different heat conditions. Total FA content was similar in all treatments on day 7, whereas, on day 8, it was significantly higher in **H** than in the other conditions, in which the content had decreased compared to day 7 (Figure 4.14A). Interestingly, this response was similar for all major FAs, suggesting there was a global inhibition of FA breakdown in **H**, while in **PH** the degradation of FA was comparable to that observed in **C** and **P** (Figure 4.14B). Recently, several studies have shown that unsaturated triacylglycerols (TAGs) accumulated in cytosolic lipid droplets during HS in both Arabidopsis seedlings and 14-day-old plants, even though the levels of total FA were not significantly affected (Mueller *et al.*, 2015, 2017; Higashi *et al.*, 2015). It was suggested that remodelling of membrane lipids (especially plastidial) served as a source for transient storage of fatty acids into cytosolic TAGs, avoiding the accumulation of toxic lipid intermediates and providing a temporary source of energy during recovery. Interestingly, this mechanism seems to be conserved, since it was also observed in the model green algae *Chlamydomonas reinhardtii* (Légeret *et al.*, 2015). The role of this stress-induced cytosolic TAG accumulation in basal thermotolerance was supported by the use of mutants, either deficient in TAG synthesis, or over accumulating these lipids (Mueller *et al.*, 2017). During the recovery period, the level of TAGs rapidly decreased and returned to the basal level within 2 h (Mueller *et al.*, 2015), which could explain that, in our conditions, we did not observe any significant increase 24 h after priming, or 2 h of recovery after heat-shock. Moreover, in seven-day-old developmentally arrested seedlings, FAs are still abundant in lipid droplets (see Chapter II) and it is likely that, if there was an increase in their level due to HS, it would not be detectable. In our conditions, the capacity of seedlings to degrade lipids during the recovery period may be correlated with their ability to grow, as we previously saw that **H** seedlings arrested their growth, while **PH** seedlings were able to carry on cotyledon expansion, as demonstrated by the green pixel analysis (Figure 3.3A). In order to correlate our results with transcriptomic data, we analysed the expression of genes involved in glycerolipid metabolism, based on genes that had been previously identified (Higashi *et al.*, 2015). Among the 244 genes, only 41 were found to be differentially expressed in at least one condition. There was no clear up- or downregulated pathway but several genes were differentially expressed. Transcripts for *DGD1* and *DGD2*, two digalactosyldiacylglycerol synthases, which are involved in TAGs biosynthesis, were only overexpressed in **P** samples. Except for a decrease of *MGD3* in the **PH** condition, the transcripts coding for monogalactosyldiacylglycerol (MGDG) synthases, which are involved in galactolipid synthesis in the chloroplast, were not affected by HS. Moreover, *HIL1* (heat inducible lipase 1), an enzyme which was recently identified as an important component of MGDG catabolism under HS (Higashi *et al.*, 2018), was only overexpressed in **PH** (after 30 minutes of stress in our conditions). An ER localized FAD5-like desaturase (*ADS2*) involved in MGDG desaturation was downregulated in both **H** and **PH**. Enzymes of the glyoxylic cycle were not significantly differentially expressed, except upregulation of isocitrate lyase in **PH**. Finally, we can notice the upregulation of LDAP1 (lipid-droplet associated protein 1) in **P** and **PH** at the protein level. LDAP1 was previously found to participate in the heat-responsive LD formation in leaves, since *ldap1-1* mutant exhibited a slight decrease in the number of LDs under HS (Table 4.5) (Gidda *et al.*, 2016). Finally, an increase in the number of plastoglobules

(PGs) was also previously observed in response to heat in Arabidopsis leaves (Zhang *et al.*, 2010b). In this context, it would be interesting to perform a TEM analysis and quantify PG size under the different heat treatments, similar to that performed for the seedlings under control conditions (see Chapter II). At the transcriptional level, we could observe in **P** the significant upregulation of *FIB1a* and *FIB1b*, which are part of the fibrillin family proteins expressed in PGs (van Wijk & Kessler, 2017). However, the other fibrillins were not significantly affected. Thus it would be interesting to observe how lipids are partitioned between PGs and LDs under HS in liquid-grown seedlings.

5. Conclusion

Through the analysis of molecular responses at the transcriptional, proteomic and metabolic levels, we could identify the major pathways involved in the response to priming and heat shock. As has been observed in many studies (Payne, 2015; Peng *et al.*, 2015; Liang *et al.*, 2016), the transcriptomic and proteomic data were not highly correlated. This is not surprising, given that proteome differs from transcriptome under HS, as it was previously shown that translation was highly inhibited upon short-term HS (38°C for 45 min) and that mRNA loading on polysomes was partly dependent on RNA length and GC content in the 5' UTR region (Yángüez *et al.*, 2013). Nevertheless, transcripts and proteins of similar pathways (e.g. cell wall enzymes, defence response) were downregulated at the transcript, protein or both levels, revealing the conservation and importance of this process. Although it was not clearly demonstrated at the protein level, probably because of the low levels of these proteins, we could observe a high number of plastidial and mitochondrial genes differentially expressed in primed and non-primed samples, which supports the primordial role of these organelles in the response to HS. Through the transcriptomic analysis, we could see the protective effect of priming on photosynthesis-related genes and on the transcription of plastidial ribosomal proteins and RNA editing in mitochondria, which might play a role in the survival after heat shock. Moreover, transcriptomic and proteomic data seem to be in favour of an active role of chloroplast in the regulation of amino acid metabolism under severe HS, even though further analysis would be necessary to conclude on this point.

At the proteomic level, we could detect the accumulation of most HSPs only in primed samples, which confirms the key role of these proteins in the HSR. In **PH** seedlings, it is expected that the abundant HSPs, and in particular sHSPs, participate in the transient sequestration of proteins, such as translational elongation factors during the HS, and that they favour the rapid release and refolding of these proteins during the recovery period (Cherkasov *et al.*, 2015; McLoughlin *et al.*, 2016). Moreover, mRNA accumulation and processing into processing bodies and stress granules in **PH** samples are likely to participate in the proper recovery after HS (Weber *et al.*, 2008; Chantarachot & Bailey-Serres, 2018). Indeed, we could detect the accumulation of DCP5 and UBP1 proteins in **PH** seedlings, but not in **H** seedlings. Moreover, we could spot a disturbance in mRNA and protein transport in **H** seedlings, together with a decrease in the abundance of ribosomal proteins and an increase in proteins related to ubiquitin-dependent protein degradation. This response is likely to be noxious for the recovery process, as shown by the incapacity of metabolism to fully recover one day after treatment (physiology, lipid degradation and amino acid metabolism). Another important point is that this study validates the use of our liquid culture system to study stress responses, since we observed a global response comparable to that observed on MS plates

(Silva-Correia *et al.*, 2014). Even though the seedlings display metabolic and physiological adaptations in order to survive under mineral starvation (Chapter II), they trigger a similar HSR compared to "normal" seedlings (e.g. grown on MS plates). However, in our study, we analysed the early response to HS and we did not detect huge differences between the response of **H** and **PH** seedlings, especially concerning the induction or prevention of cell death program. Thus, it would be interesting to study the transcriptomic and proteomic response of **H** and **PH** seedlings after one or several days post-treatment to better characterize the timing and events leading to death in non-primed seedlings.

6. Supporting Information

Table S4.1: Proteins that were identified as differentially expressed according to spectral counting (SC).

Pink: significantly upregulated proteins compared to C ($p<0.05$); green: significantly downregulated proteins; numbers correspond to the number of spectra for each replicate in every treatment

descr	C				P				H				PH			
AT1G01960.1 EDA10 | SEC7-like guanine nucleotide exchange family protein	0	0	1	0	0	0	0	0	3	1	5	7	1	0	1	2
AT1G03160.1 FZL | FZO-like	0	0	0	0	0	0	0	0	4	7	3	2	3	6	2	1
AT1G07400.1 HSP20-like chaperones superfamily protein	0	0	0	0	15	13	15	12	0	0	0	0	16	19	18	19
AT1G12250.1 Pentapeptide repeat-containing protein	7	9	8	6	8	8	7	5	0	1	0	0	0	0	1	0
AT1G28570.1 SGNH hydrolase-type esterase superfamily protein	5	2	6	4	4	3	4	3	0	0	0	0	0	0	0	0
AT1G28580.1 GDSL-like Lipase/Acylhydrolase superfamily protein	4	2	8	7	3	3	4	3	0	0	0	0	0	0	0	0
AT1G28600.1 GDSL-like Lipase/Acylhydrolase superfamily protein	4	2	6	4	3	0	4	3	0	0	0	0	0	0	0	0
AT1G33811.1 GDSL-like Lipase/Acylhydrolase superfamily protein	4	4	5	6	4	4	4	2	4	2	1	0	1	0	0	0
AT1G52560.1 HSP26.5	0	0	0	0	6	9	8	8	0	0	0	0	10	11	10	9
AT1G52560.2 HSP26.5	0	0	0	0	6	10	8	10	0	0	0	0	12	11	11	10
AT1G53540.1 HSP20-like chaperones superfamily protein	0	0	0	0	11	16	16	16	0	0	0	0	12	17	19	15
AT1G54050.1 HSP20-like chaperones superfamily protein	0	0	0	0	7	6	5	5	0	0	0	0	4	6	4	6
AT1G59860.1 HSP20-like chaperones superfamily protein	0	0	0	0	15	12	14	11	0	0	0	0	15	17	18	19
AT1G65220.1 ARM repeat superfamily protein	1	1	0	1	1	2	1	0	5	3	6	5	2	3	3	4
AT1G71820.1 SEC6	0	0	1	0	0	1	1	0	2	3	7	4	3	1	2	3
AT1G72910.1 Toll-Interleukin-Resistance (TIR) domain-containing protein	0	0	0	0	0	0	0	0	1	0	5	5	2	1	6	3
AT1G74310.1 ATHSP101, HSP101, HOT1 | heat shock protein 101	0	0	0	0	33	10	50	37	0	0	0	0	38	11	43	40
AT1G76450.1 Photosystem II reaction center PsbP family protein	5	6	5	5	3	5	5	4	0	0	0	0	0	0	0	0
AT1G76680.1 OPR1, ATOPR1 | 12-oxophytodienoate reductase 1	21	18	26	21	11	11	15	11	21	17	15	17	10	6	11	15
AT2G01350.1 QPT | quinolinate phosphoribosyltransferase	1	1	1	1	0	0	0	1	4	3	4	6	3	4	6	4
AT2G20560.1 DNAJ heat shock family protein	0	0	0	0	5	0	10	7	0	0	0	0	7	0	10	7
AT2G26150.1 ATHSFA2, HSFA2 | heat shock transcription factor A2	0	0	0	0	7	7	4	7	0	0	0	0	9	6	5	6
AT2G46240.1 BAG6, ATBAG6 | BCL-2-associated athanogene 6	0	0	0	0	4	0	5	8	0	0	0	0	5	0	9	8
AT2G46520.1 cellular apoptosis susceptibility protein, putative / importin-alpha re-exporter	0	0	0	0	0	0	0	0	2	2	6	7	2	0	1	1
AT2G46930.1 Pectinacetylesterase family protein	5	2	9	6	5	1	5	7	0	0	0	0	0	0	0	0
AT3G08943.1 ARM repeat superfamily protein	1	2	3	1	3	1	1	1	5	6	7	6	6	5	4	3
AT3G09640.1 APX2, APX1B | ascorbate peroxidase 2	0	0	0	0	5	0	6	7	0	0	0	0	6	4	6	5
AT3G14840.2 Leucine-rich repeat transmembrane protein kinase	6	8	5	13	4	4	2	5	7	4	14	9	3	2	2	4
AT3G23920.1 BAM1, BMY7, TR-BAMY | beta-amylase 1	2	2	5	3	10	6	8	9	1	0	0	0	1	0	0	0
AT3G46230.1 ATHSP17.4, HSP17.4 | heat shock protein 17.4	0	0	0	0	10	12	17	15	0	0	0	0	13	16	17	14
AT3G48750.1 CDKA1, CDC2AAT, CDK2, CDC2, CDC2A| cell division control 2	1	1	2	2	0	1	1	0	6	2	4	7	4	6	4	3

AT3G55430.1 O-Glycosyl hydrolases family 17 protein	1	2	7	2	2	2	5	2	0	0	0	0	0	1	0	0
AT3G61820.1 Eukaryotic aspartyl protease family protein	4	3	7	9	0	0	0	2	0	0	0	0	0	0	0	0
AT4G15510.1 Photosystem II reaction center PsbP family protein	4	6	3	4	5	6	3	3	0	0	0	0	0	0	0	0
AT4G16190.1 Papain family cysteine protease	4	4	5	4	5	4	5	7	0	0	1	0	1	0	0	0
AT4G18030.1 S-adenosyl-L-methionine-dependent methyltransferases superfamily protein	4	0	8	10	1	0	3	5	0	0	0	0	0	0	2	0
AT4G21320.1 HSA32 | Aldolase-type TIM barrel family protein	0	0	0	0	2	1	2	1	0	0	0	0	6	2	5	4
AT4G27640.1 ARM repeat superfamily protein	0	0	1	1	0	0	1	1	3	4	4	3	6	2	3	2
AT4G27670.1 HSP21 | heat shock protein 21	0	0	0	0	17	18	14	13	0	0	0	0	23	21	17	18
AT4G30270.1 MERI5B, MERI-5, XTH24, SEN4 | xyloglucan endotransglucosylase/hydrolase 24	4	5	4	3	5	9	6	7	0	0	1	0	0	2	0	3
AT4G39800.1 MI-1-P SYNTHASE, MIPS1, ATMIPS1, ATIPS1 | myo-inositol-1-phosphate synthase 1	3	4	2	2	10	11	7	16	3	6	2	0	14	12	10	12
AT5G01010.1 Unknown protein	1	2	2	1	0	0	1	1	5	6	6	7	7	6	6	5
AT5G06140.1 SNX1, ATSNX1 | sorting nexin 1	1	0	2	2	2	0	3	2	7	1	6	6	5	1	6	6
AT5G10170.1 ATMIPS3, MIPS3 | myo-inositol-1-phosphate synthase 3	1	3	5	2	6	6	4	8	2	1	2	1	9	7	5	8
AT5G12020.1 HSP17.6II | 17.6 kDa class II heat shock protein	0	0	0	0	12	10	13	12	0	0	0	0	11	10	12	10
AT5G14450.1 GDSL-like Lipase/Acylhydrolase superfamily protein	10	11	11	13	7	5	9	7	0	0	0	0	0	0	0	0
AT5G17020.1 XPO1A, ATCRM1, ATXPO1, XPO1, HIT2 | exportin 1A	0	0	0	0	0	0	0	0	2	2	6	5	2	4	2	2
AT5G37670.1 HSP20-like chaperones superfamily protein	0	0	0	0	9	12	12	9	0	0	0	1	9	10	8	11
AT5G42970.1 COP8, FUS4, EMB134, COP14, FUS8, ATS4 Proteasome component (PCI) domain protein	1	1	0	0	1	3	2	2	7	11	8	9	4	9	2	3
AT5G48570.1 ROF2, ATFKBP65, FKBP65	0	0	1	0	10	1	13	9	1	0	1	1	11	1	12	13
AT5G51440.1 HSP23.5	0	0	0	0	6	0	7	4	0	0	0	0	6	2	6	7
AT5G52310.1 COR78, LTI78, RD29A, LTI140 | low-temperature-responsive protein 78 (LTI78)	12	16	18	13	26	20	33	21	17	17	17	10	23	27	21	21
AT5G56000.1 HSP81.4, AtHSP90.4 | HEAT SHOCK PROTEIN 81.4	39	39	57	50	57	49	76	67	52	38	64	52	57	55	70	73
AT5G56010.1 HSP81-3, HSP81.3, AtHSP90-3, AtHSP90.3 | heat shock protein 81-3	49	52	71	66	72	61	91	84	64	50	78	69	75	70	90	91
AT5G59720.1 HSP18.2 | heat shock protein 18.2	0	0	0	0	12	12	15	12	0	0	0	0	12	15	14	14
AT5G61820.1 Unknown protein	3	4	5	7	4	4	5	8	0	2	1	1	2	1	3	3
AT5G65760.1 Serine carboxypeptidase S28 family protein	3	7	2	6	2	3	4	5	0	0	0	0	0	0	0	0

Table S4.2: Fold changes of proteins that were upregulated in both H and PH treatments.
Pink: significantly upregulated proteins compared to C ($p<0.05$); loc corresponds to location according to SUBA4con: c, cytosol; cp, plastid; ER, endoplasmic reticulum; ex, extracellular; g, Golgi; m, mitochondrion; n, nucleus; p, peroxisome; pm, plasma membrane and v, vacuole.

id	description	P/C	H/C	PH/C	Loc
AT2G21385.1	unknown protein	1.29	5.19	5.26	cp
AT5G47770.1	FPS1, farnesyl diphosphate synthase 1	0.98	4.21	3.64	c
AT5G04900.1	NOL, NYC1-like, chlorophyll b reductase involved in the degradation of chlorophyll b and LHCII	1.18	3.11	3.41	cp
AT3G03990.1	alpha/beta-Hydrolases superfamily protein, DWARF 14 involved in strigolactone signalling	1.46	2.42	3.18	c
AT1G61150.1	LisH and RanBPM domains containing protein	1.28	5.10	2.97	n
AT5G19940.1	Plastid-lipid associated protein PAP / fibrillin family protein	0.89	3.56	2.89	cp
AT3G56940.1	CRD1, CHL27, ACSF, dicarboxylate diiron protein, putative (Crd1)	0.99	2.47	2.80	cp
AT4G02570.1	ATCUL1, CUL1, AXR6, cullin 1, involved in response to auxin and jasmonate	1.38	3.29	2.68	n
AT2G45990.1	ribosomal RNA small subunit methyltransferase G	0.73	3.66	2.58	cp
AT3G02780.1	IPP2, isopentenyl pyrophosphate:dimethylallyl pyrophosphate isomerase 2	0.68	3.19	2.56	cp
AT3G61140.1	FUS6, 26S proteasome, regulatory subunit Rpn7	1.16	3.24	2.52	c,n
AT4G34920.1	PLC-like phosphodiesterases superfamily protein	0.95	2.86	2.41	c
AT4G31500.1	CYP83B1, cytochrome P450, family 83, subfamily B, polypeptide 1	0.83	3.11	2.39	ER
AT5G65020.1	ANNAT2, annexin 2	1.04	2.84	2.31	c,pm
AT1G55450.1	S-adenosyl-L-methionine-dependent methyltransferases superfamily protein	0.83	2.92	2.29	g
AT5G58490.1	NAD(P)-binding Rossmann-fold superfamily protein	1.00	2.52	2.28	c
AT1G13320.1	PP2AA3 | protein phosphatase 2A subunit A3	0.83	3.97	2.27	c
AT4G34350.1	CLB6, ISPH, HDR, 4-hydroxy-3-methylbut-2-enyl diphosphate reductase	1.16	2.09	2.26	cp
AT1G71697.1	ATCK1, CK, CK1, choline kinase 1	0.87	2.19	2.25	c
AT1G02930.1	ATGSTF6, GST1, ERD11, ATGSTF3, glutathione S-transferase 6	0.98	2.85	2.19	c
AT5G42080.1	ADL1, ADL1A, AG68, DRP1A, RSW9, DL1, dynamin-like protein	1.19	2.20	2.19	pm
AT3G42050.1	vacuolar ATP synthase subunit H family protein	0.87	2.46	2.18	v,g
AT5G20400.1	2-oxoglutarate (2OG) and Fe(II)-dependent oxygenase superfamily protein	1.07	3.28	2.16	c
AT5G43450.1	2-oxoglutarate (2OG) and Fe(II)-dependent oxygenase superfamily protein	1.05	2.18	2.10	c
AT5G19820.1	KETCH1, emb2734, karyopherin enabling the transport of the cytoplasmic HYL1	0.97	2.97	2.05	g
AT3G46000.1	ADF2, actin depolymerizing factor 2	0.70	2.86	2.01	c
AT3G29350.1	AHP2, histidine-containing phosphotransmitter 2	0.88	2.42	2.01	c
AT3G45640.1	ATMPK3, MPK3, ATMAPK3, mitogen-activated protein kinase 3	0.96	2.57	1.96	c
AT3G13920.1	EIF4A1, RH4, TIF4A1, eukaryotic translation initiation factor 4A1	1.05	2.19	1.95	c
AT2G17340.1	Uncharacterised conserved protein (UCP030210)	0.98	2.92	1.95	c
AT5G58250.1	unknown protein	1.00	2.16	1.94	cp
AT5G10450.1	GRF6, AFT1, 14-3-3lambda, G-box regulating factor 6	1.09	2.77	1.94	c
AT1G24050.1	RNA-processing, Lsm domain	0.87	2.52	1.94	c
AT3G60190.1	ADL4, ADLP2, EDR3, DRP1E, ADL1E, DL1E, DYNAMIN-like 1E	1.38	1.76	1.93	c
AT3G62530.1	ARM repeat superfamily protein	0.95	1.98	1.91	m
AT3G59400.1	GUN4, enzyme binding;tetrapyrrole binding	0.62	1.78	1.89	cp
AT5G48020.1	2-oxoglutarate (2OG) and Fe(II)-dependent oxygenase superfamily protein	1.02	2.40	1.88	c
AT1G06650.2	2-oxoglutarate (2OG) and Fe(II)-dependent oxygenase superfamily protein	0.99	2.24	1.87	c
AT1G54270.1	EIF4A-2	0.89	2.07	1.87	c
AT3G26070.1	Plastid-lipid associated protein PAP / fibrillin family protein	1.00	1.99	1.85	cp
AT5G35170.1	adenylate kinase family protein	0.79	1.96	1.85	cp
AT4G38460.1	GGR | geranylgeranyl reductase	1.02	2.21	1.85	cp
AT1G05010.1	EFE, ACO4, EAT1, ethylene-forming enzyme	0.87	2.62	1.85	g
AT1G76790.1	O-methyltransferase family protein	1.08	2.14	1.85	c
AT5G47840.1	AMK2, adenosine monophosphate kinase	0.88	2.66	1.81	cp
AT1G12230.1	Aldolase superfamily protein	0.96	2.10	1.80	cp
AT3G20810.1	JMJD5, 2-oxoglutarate (2OG) and Fe(II)-dependent oxygenase superfamily	0.82	1.87	1.80	c,n
AT4G16060.1	unknown protein	0.84	2.11	1.80	cp
AT2G42590.1	GRF9, GF14 MU, general regulatory factor 9	0.99	2.55	1.80	c
AT1G50670.1	OTU-like cysteine protease family protein	1.03	2.49	1.79	c
AT1G27020.1	unknown protein	1.00	1.80	1.79	c
AT5G51110.1	Transcriptional coactivator/pterin dehydratase	0.96	1.95	1.78	cp
AT5G39340.1	AHP3, ATHP2, histidine-containing phosphotransmitter 3	1.17	2.58	1.78	c
AT1G63460.1	GPX8, ATGPX8, glutathione peroxidase 8	1.12	2.79	1.76	c
AT4G02620.1	vacuolar ATPase subunit F family protein	1.07	2.15	1.75	v
AT1G75270.1	DHAR2 | dehydroascorbate reductase 2	1.40	1.83	1.74	c
AT4G15550.1	IAGLU, indole-3-acetate beta-D-glucosyltransferase	0.80	2.48	1.74	cp
AT5G02790.1	GSTL3 | Glutathione S-transferase family protein	1.17	2.15	1.71	c
AT3G19010.1	2-oxoglutarate (2OG) and Fe(II)-dependent oxygenase superfamily protein	0.91	2.38	1.71	c
AT3G54640.1	TSA1, TRP3, tryptophan synthase alpha chain	1.10	1.77	1.70	cp
AT1G30230.1	Translation elongation factor EF1B/ribosomal protein S6	1.07	2.18	1.69	c
AT1G03030.1	P-loop containing nucleoside triphosphate hydrolases superfamily protein	1.13	2.07	1.67	cp
AT1G04530.1	TPR4, Tetratricopeptide repeat (TPR)-like superfamily protein	0.96	2.40	1.66	c
AT5G45170.1	Haloacid dehalogenase-like hydrolase (HAD) superfamily protein	0.84	2.06	1.65	cp
AT3G55620.1	emb1624, Translation initiation factor IF6	1.08	1.78	1.64	c

AT1G72640.1	NAD(P)-binding Rossmann-fold superfamily protein	0.96	1.73	1.63	cp
AT5G66120.2	3-dehydroquinate synthase, putative	1.01	1.72	1.63	cp
AT2G31570.1	ATGPX2, GPX2, glutathione peroxidase 2	1.01	2.43	1.63	c
AT4G00490.1	BAM2, BMY9, beta-amylase 2	0.75	2.90	1.63	cp
AT2G05830.1	NagB/RpiA/CoA transferase-like superfamily protein	0.94	1.98	1.63	c
AT3G50210.1	2-oxoglutarate (2OG) and Fe(II)-dependent oxygenase superfamily protein	1.05	1.97	1.60	c
AT1G27390.1	TOM20-2, translocase outer membrane 20-2	0.85	1.97	1.59	m
AT4G24510.1	CER2, VC2, VC-2, HXXXD-type acyl-transferase family protein	1.14	1.85	1.59	g
AT4G02520.1	ATGSTF2, ATPM24.1, ATPM24, GST2, glutathione S-transferase PHI 2	1.31	1.67	1.59	c
AT1G09270.1	IMPA-4, importin alpha isoform 4	1.05	2.11	1.58	n
AT1G04420.1	NAD(P)-linked oxidoreductase superfamily protein	1.03	2.01	1.58	cp
AT3G57290.1	EIF3E, INT-6, eukaryotic translation initiation factor 3E	1.03	1.91	1.56	c
ATCG01110.1	NDHH, NAD(P)H dehydrogenase subunit H	0.81	1.58	1.56	cp
AT2G46750.1	D-arabinono-1,4-lactone oxidase family protein	1.05	1.66	1.55	ex
AT2G31750.1	UGT74D1, UDP-glucosyl transferase 74D1	0.93	1.82	1.55	cp
AT2G25830.1	YebC-related	0.89	1.61	1.53	cp
AT1G10590.1	Nucleic acid-binding, OB-fold-like protein	1.10	1.92	1.53	c
AT1G71860.1	PTP1, ATPTP1, protein tyrosine phosphatase 1	1.24	1.84	1.53	pm
AT3G06720.1	AT-IMP, ATKAP ALPHA, AIMP ALPHA, IMPA1, importin alpha isoform 1	1.06	2.12	1.52	n
AT3G16640.1	TCTP, translationally controlled tumor protein	1.10	1.73	1.52	c
AT4G30530.1	Class I glutamine amidotransferase-like superfamily protein	0.99	1.94	1.52	c
AT1G09640.1	Translation elongation factor EF1B, gamma chain	1.00	1.67	1.50	c
AT4G04910.1	NSF, AAA-type ATPase family protein	0.98	1.59	1.48	g
AT5G45390.1	CLPP4, NCLPP4, CLP protease P4	1.03	1.56	1.48	cp
AT5G64270.1	splicing factor, putative	1.02	1.59	1.46	n
AT2G32260.1	ATCCT1, CCT1, phosphorylcholine cytidylyltransferase	1.23	1.61	1.46	c
AT2G37660.1	NAD(P)-binding Rossmann-fold superfamily protein	0.99	1.80	1.46	cp
AT1G76080.1	CDSP32, chloroplastic drought-induced stress protein of 32 kD	0.93	1.55	1.45	cp
AT3G19760.1	EIF4A-III, eukaryotic initiation factor 4A-III	1.03	1.52	1.45	n
AT2G24020.1	Uncharacterised BCR, YbaB family COG0718	1.02	1.96	1.45	cp
AT1G06000.1	UDP-Glycosyltransferase superfamily protein	0.91	1.61	1.43	c
AT2G31670.1	Stress responsive alpha-beta barrel domain protein	0.98	1.87	1.41	p
AT5G38660.1	APE1, acclimation of photosynthesis to environment	0.89	1.52	1.41	cp
AT1G15140.1	FAD/NAD(P)-binding oxidoreductase	0.94	1.67	1.40	cp
AT1G49660.1	AtCXE5, CXE5, carboxyesterase 5	0.96	1.70	1.40	c
AT4G04950.1	thioredoxin family protein	1.22	1.64	1.39	c
AT3G08740.1	elongation factor P (EF-P) family protein	0.83	1.71	1.39	cp
AT1G01800.1	NAD(P)-binding Rossmann-fold superfamily protein	1.09	1.80	1.39	c
AT1G73110.1	P-loop containing nucleoside triphosphate hydrolases superfamily protein	0.74	2.15	1.38	cp
AT5G54160.1	ATOMT1, OMT1, O-methyltransferase 1	1.03	1.87	1.38	c
AT4G17870.1	PYR1, Polyketide cyclase/dehydrase and lipid transport superfamily protein	1.06	1.63	1.37	n
AT1G14830.1	ADL1C, ADL5, DRP1C, DL1C, DYNAMIN-like 1C	0.91	1.55	1.37	c
AT1G62380.1	ACO2, ATACO2, ACC oxidase 2	0.90	2.00	1.37	g
AT4G13660.1	ATPRR2, PRR2, pinoresinol reductase 2	0.86	1.86	1.36	c
AT3G63130.1	RANGAP1, ATRANGAP1, RAN GTPase activating protein 1	0.90	2.25	1.36	c,n
AT5G48960.1	HAD-superfamily hydrolase, subfamily IG, 5-nucleotidase	0.97	1.60	1.36	cp
AT1G27970.1	NTF2B, nuclear transport factor 2B	1.11	1.76	1.35	n
AT1G51110.1	Plastid-lipid associated protein PAP / fibrillin family protein	0.97	1.50	1.35	cp
AT1G28130.1	GH3.17, Auxin-responsive GH3 family protein	0.84	1.77	1.35	c
AT1G60420.1	DC1 domain-containing protein	1.11	1.69	1.31	c
AT1G57720.1	Translation elongation factor EF1B, gamma chain	0.92	1.48	1.30	c
AT4G34090.1	unknown protein	0.61	1.96	1.27	cp
AT1G27130.1	ATGSTU13, GST12, GSTU13	1.01	1.62	1.21	pm
AT3G48870.1	ATCLPC, ATHSP93-III, HSP93-III, Clp ATPase	0.83	1.38	1.19	cp

Table S4.3: Fold changes of proteins that were downregulated in both H and PH treatments.
green: significantly downregulated proteins compared to C ($p<0.05$); loc corresponds to location according to SUBA4con: c, cytosol; cp, plastid; ex, extracellular; m, mitochondrion; n, nucleus; pm, plasma membrane and v, vacuole.

id	description	P/C	H/C	PH/C	Loc
AT5G60360.1	SAG2, AALP, ALP, aleurain-like protease	0.87	0.12	0.07	v
AT2G37130.1	Peroxidase superfamily protein	1.02	0.33	0.16	ex
AT4G32940.1	GAMMA-VPE, GAMMAVPE, gamma vacuolar processing enzyme	0.82	0.16	0.19	v
AT1G02305.1	Cysteine proteinases superfamily protein	0.66	0.19	0.20	ex
AT2G41430.1	ERD15, LSR1, CID1, dehydration-induced protein	0.79	0.44	0.21	c
AT5G62200.1	Embryo-specific protein 3, (ATS3)	0.70	0.20	0.22	v
AT2G06850.1	EXGT-A1, EXT, XTH4, xyloglucan endotransglucosylase/hydrolase 4	0.59	0.30	0.22	ex
AT5G13410.1	FKBP-like peptidyl-prolyl cis-trans isomerase family protein	1.19	0.11	0.22	cp
AT1G28660.1	GDSL-like Lipase/Acylhydrolase superfamily protein	0.77	0.37	0.23	ex
AT4G39090.1	RD19, RD19A, Papain family cysteine protease	1.16	0.18	0.23	v,n
AT3G07320.1	O-Glycosyl hydrolases family 17 protein	0.78	0.47	0.24	ex
AT1G75680.1	AtGH9B7, GH9B7, glycosyl hydrolase 9B7	0.75	0.36	0.25	pm
AT5G23830.1	MD-2-related lipid recognition domain-containing protein	0.85	0.32	0.25	ex
AT5G10770.1	Eukaryotic aspartyl protease family protein	0.82	0.38	0.26	ex
AT3G18490.1	Eukaryotic aspartyl protease family protein	0.83	0.26	0.26	ex
AT4G37800.1	XTH7, xyloglucan endotransglucosylase/hydrolase 7	0.80	0.26	0.26	ex
AT3G12145.1	FLR1, FLOR1, Leucine-rich repeat (LRR) family protein	0.91	0.30	0.28	ex
AT5G64350.1	FKBP12, ATFKBP12, FK506-binding protein 12	0.97	0.34	0.29	c
AT1G21680.1	DPP6 N-terminal domain-like protein	0.74	0.29	0.29	ex
AT4G18760.1	AtRLP51, RLP51, receptor like protein 51	0.78	0.45	0.33	pm
AT5G08260.1	scpl35, serine carboxypeptidase-like 35	0.94	0.32	0.33	ex
AT4G01610.1	Cysteine proteinases superfamily protein	1.23	0.26	0.34	ex
AT4G30170.1	Peroxidase family protein	0.72	0.54	0.35	ex
AT5G13690.1	CYL1, NAGLU, alpha-N-acetylglucosaminidase family / NAGLU family	0.85	0.37	0.35	v
AT5G19230.1	Glycoprotein membrane precursor GPI-anchored	0.84	0.40	0.35	ex
AT3G10720.2	Plant invertase/pectin methylesterase inhibitor superfamily	0.94	0.46	0.39	ex
AT1G07080.1	Thioredoxin superfamily protein	0.72	0.49	0.39	ex
AT3G15520.1	Cyclophilin-like peptidyl-prolyl cis-trans isomerase family protein	0.90	0.41	0.40	cp
AT2G21660.1	ATGRP7, CCR2, GR-RBP7, GRP7, cold, circadian rhythm, and rna binding 2	0.94	0.61	0.40	n
AT5G39830.1	DEGP8, DEG8, Trypsin family protein with PDZ domain	1.05	0.44	0.43	cp
AT3G47650.1	DnaJ/Hsp40 cysteine-rich domain superfamily protein	0.75	0.51	0.44	cp
AT1G30600.1	Subtilase family protein	0.73	0.60	0.45	ex
AT5G11450.1	Mog1/PsbP/DUF1795-like photosystem II reaction center PsbP family protein	1.00	0.42	0.45	cp
AT4G05180.1	PSBQ, PSBQ-2, PSII-Q, photosystem II subunit Q-2	0.85	0.53	0.46	cp
AT4G13850.1	ATGRP2, GR-RBP2, GRP2, glycine-rich RNA-binding protein 2	0.99	0.51	0.47	m
AT1G49740.1	PLC-like phosphodiesterases superfamily protein	0.69	0.51	0.47	ex
AT3G02110.1	scpl25, serine carboxypeptidase-like 25	0.86	0.44	0.48	ex
AT5G18470.1	Curculin-like (mannose-binding) lectin family protein	0.82	0.59	0.50	ex
AT1G07790.1	HTB1, Histone superfamily protein	0.65	0.44	0.51	n
AT1G11910.1	APA1, ATAPA1, aspartic proteinase A1	1.03	0.58	0.53	v
AT1G12240.1	ATBETAFRUCT4, VAC-INV, Glycosyl hydrolases family 32 protein	0.97	0.59	0.53	v
AT1G76160.1	sks5, SKU5 similar 5	0.85	0.54	0.54	ex
AT2G04690.1	Pyridoxamine 5-phosphate oxidase family protein	0.95	0.59	0.54	ex
AT5G12950.1	Putative glycosyl hydrolase of unknown function (DUF1680)	0.90	0.60	0.55	ex
AT3G20370.1	TRAF-like family protein	0.82	0.69	0.55	ex
AT2G37220.1	RNA-binding (RRM/RBD/RNP motifs) family protein	0.86	0.79	0.57	cp
AT3G56650.1	Mog1/PsbP/DUF1795-like photosystem II reaction center PsbP family protein	1.06	0.62	0.58	cp
AT3G60340.1	alpha/beta-Hydrolases superfamily protein	1.08	0.63	0.58	v
AT1G78680.1	ATGGH2, GGH2, gamma-glutamyl hydrolase 2	1.02	0.56	0.59	v
AT2G35120.1	Single hybrid motif superfamily protein	0.87	0.79	0.61	m
AT3G15840.1	PIFI, post-illumination chlorophyll fluorescence increase	0.93	0.79	0.61	cp
AT3G06050.1	PRXIIF, ATPRXIIF, peroxiredoxin IIF	1.01	0.82	0.62	m
AT3G14920.1	Peptide-N4-(N-acetyl-beta-glucosaminyl)asparagine amidase A protein	0.90	0.68	0.65	ex
AT4G31840.1	ENODL15, AtENODL15, early nodulin-like protein 15	0.96	0.67	0.65	ex
AT1G50250.1	FTSH1, FTSH protease 1	0.80	0.65	0.65	cp
AT5G34940.2	AtGUS3, GUS3, glucuronidase 3	0.97	0.62	0.68	ex
AT1G03600.1	PSB27, photosystem II family protein	0.95	0.61	0.70	cp
AT2G24280.1	alpha/beta-Hydrolases superfamily protein	0.88	0.53	0.73	ex

Table S4.4: Fold changes of proteins that were specifically upregulated in H treatment.
Pink: significantly upregulated proteins compared to C ($p<0.05$); loc corresponds to location according to SUBA4con: c, cytosol; cp, plastid; ER, endoplasmic reticulum; ex, extracellular; g, Golgi; m, mitochondrion; n, nucleus; p, peroxisome; pm, plasma membrane and v, vacuole.

id	description	P/C	H/C	PH/C	loc
AT2G33255.1	Haloacid dehalogenase-like hydrolase (HAD) superfamily protein	0.92	3.45	1.85	m
AT2G33470.1	GLTP1, ATGLTP1, glycolipid transfer protein 1	1.17	3.33	1.70	g
AT4G17510.1	UCH3, ubiquitin C-terminal hydrolase 3	1.53	2.73	1.50	c
AT3G24200.1	FAD/NAD(P)-binding oxidoreductase family protein	1.36	2.60	1.25	m
AT1G09310.1	Protein of unknown function, DUF538	1.16	2.55	1.57	c
AT1G25220.1	ASB1, TRP4, WEI7, anthranilate synthase beta subunit 1	1.73	2.38	1.71	cp
AT5G14250.1	COP13, CSN3, FUS11, Proteasome component (PCI) domain protein	1.44	2.34	2.18	n
AT3G57090.1	BIGYIN, FIS1A, Tetratricopeptide repeat (TPR)-like superfamily protein	1.23	2.32	1.58	cp,p,m
AT1G78870.2	UBC35, UBC13A, ubiquitin-conjugating enzyme 35	1.27	2.30	1.58	c
AT1G01390.1	UDP-Glycosyltransferase superfamily protein	1.57	2.28	1.68	pm
AT4G24130.1	Protein of unknown function, DUF538	1.21	2.25	1.43	c
AT4G39970.1	Haloacid dehalogenase-like hydrolase (HAD) superfamily protein	0.68	2.19	1.30	cp
AT3G46830.1	ATRAB11A, ATRABA2C, RAB GTPase homolog A2C	1.03	2.15	1.51	c
AT4G18930.1	RNA ligase/cyclic nucleotide phosphodiesterase family protein	1.07	2.14	1.62	c
AT1G79500.1	AtkdsA1, Aldolase-type TIM barrel family protein	1.40	2.13	1.48	c
AT2G26590.1	RPN13, regulatory particle non-ATPase 13	1.28	2.11	1.28	c
AT1G54290.1	Translation initiation factor SUI1 family protein	1.03	2.09	1.25	c
AT5G66170.3	STR18, sulfurtransferase 18	1.27	2.09	1.34	c
AT4G15940.1	Fumarylacetoacetate (FAA) hydrolase family	1.01	2.09	1.31	m
AT5G45930.1	CHLI2, CHL I2, CHLI-2, magnesium chelatase i2	0.65	2.06	1.11	cp
AT1G35160.1	GRF4, 14-3-3PHI, GF14 PHI, GF14 protein phi chain	0.99	2.05	1.35	c
AT3G29250.1	NAD(P)-binding Rossmann-fold superfamily protein	1.10	2.05	1.43	ex
AT2G19860.1	ATHXK2, HXK2, hexokinase 2	0.74	2.04	1.46	m
AT1G21130.1	O-methyltransferase family protein	0.54	2.02	0.90	c
AT4G27700.1	Rhodanese/Cell cycle control phosphatase superfamily protein	0.88	2.00	1.73	cp
AT1G15950.1	CCR1, IRX4, ATCCR1, cinnamoyl coa reductase 1	1.13	2.00	1.24	c
AT1G61570.1	TIM13, translocase of the inner mitochondrial membrane 13	1.11	1.96	1.19	m
AT4G14210.1	PDS3, PDS, PDE226, phytoene desaturase 3	0.81	1.96	1.54	cp
AT5G28020.1	CYSD2, ATCYSD2, cysteine synthase D2	1.07	1.95	1.61	c
AT1G30470.1	SIT4 phosphatase-associated family protein	1.58	1.93	1.61	g
AT4G11380.1	Adaptin family protein	1.00	1.93	1.82	pm
AT5G52240.1	MSBP1, ATMP1, AtMAPR5, membrane steroid binding protein 1	0.94	1.93	1.35	ER
AT3G04710.1	TPR10, ankyrin repeat family protein	1.34	1.92	1.77	c
AT3G48890.1	ATMP2, ATMAPR3, MSBP2, membrane-associated progesterone binding protein 3	0.97	1.92	1.35	ER
AT1G66680.1	AR40, S-adenosyl-L-methionine-dependent methyltransferases superfamily protein	1.15	1.90	1.33	c
AT1G22300.1	GRF10, 14-3-3EPSILON, GF14 EPSILON, general regulatory factor 10	1.05	1.90	1.38	c
AT1G75950.1	SKP1, ASK1, ATSKP1, SKP1A, UIP1, S phase kinase-associated protein 1	0.98	1.89	1.09	c
AT4G37470.1	alpha/beta-Hydrolases superfamily protein	0.79	1.88	1.30	c
AT1G16460.1	ATRDH2, ATMST2, MST2, ST2, STR2, RDH2, rhodanese homologue 2	0.69	1.86	1.11	c
AT4G26220.1	S-adenosyl-L-methionine-dependent methyltransferases superfamily protein	0.89	1.86	1.40	c
AT4G16143.1	IMPA-2, importin alpha isoform 2	1.09	1.84	1.38	n
AT2G01530.1	MLP329, MLP-like protein 329	0.93	1.83	1.09	c
AT2G18110.1	Translation elongation factor EF1B/ribosomal protein S6 family protein	0.85	1.78	1.46	c
AT5G65430.1	GRF8, 14-3-3KAPPA, GF14 KAPPA, general regulatory factor 8	0.93	1.78	1.30	n
AT1G30630.1	Coatomer epsilon subunit	0.94	1.78	1.49	g
AT1G06690.1	NAD(P)-linked oxidoreductase superfamily protein	0.81	1.78	1.38	cp
AT3G04880.1	DRT102, DNA-damage-repair/toleration protein (DRT102)	1.36	1.75	1.44	c
AT4G10960.1	UGE5, UDP-D-glucose/UDP-D-galactose 4-epimerase 5	1.05	1.74	1.18	ex
AT1G14030.1	Rubisco methyltransferase family protein	0.89	1.74	1.47	cp
AT5G53480.1	ARM repeat superfamily protein	1.12	1.73	1.32	c,cp,n
AT5G58590.1	RANBP1, RAN binding protein 1	1.15	1.71	1.24	n
AT2G15860.1	unknown protein	0.71	1.71	0.99	c
AT5G13710.1	SMT1, CPH, sterol methyltransferase 1	0.82	1.71	1.08	g
AT5G38480.1	GRF3, RCI1, general regulatory factor 3	0.99	1.69	1.37	c
AT3G48530.1	KING1, SNF1-related protein kinase regulatory subunit gamma 1	1.12	1.69	1.43	c
AT2G17980.1	ATSLY1, Sec1/munc18-like (SM) proteins superfamily	1.10	1.67	1.33	pm
AT1G16890.2	UBC36, UBC13B, ubiquitin-conjugating enzyme 36	0.88	1.66	1.16	c
AT3G58500.1	PP2A-4, protein phosphatase 2A-4	1.17	1.66	1.40	c
AT5G05890.1	UDP-Glycosyltransferase superfamily protein	0.88	1.65	1.44	pm
AT5G10540.1	Zincin-like metalloproteases family protein	0.77	1.64	1.32	c
AT1G25490.1	RCN1, REGA, ATB BETA BETA, EER1, ARM repeat superfamily protein	0.88	1.62	0.84	pm
AT1G08980.1	ATAMI1, AMI1, ATTOC64-I, TOC64-I, amidase 1	1.24	1.62	1.30	c
AT1G56050.1	GTP-binding protein-related	0.77	1.61	1.13	cp

AT5G10860.1	Cystathionine beta-synthase (CBS) family protein	1.04	1.60	1.20	m
AT5G64460.1	Phosphoglycerate mutase family protein	0.84	1.58	1.21	c
AT5G19370.1	rhodanese-like domain-containing protein / PPIC-type PPIASE domain-containing protein	0.66	1.57	1.02	cp
AT5G51830.1	pfkB-like carbohydrate kinase family protein	1.11	1.56	1.26	c
AT3G52930.1	Aldolase superfamily protein	0.99	1.55	1.27	c
AT2G27680.1	NAD(P)-linked oxidoreductase superfamily protein	1.16	1.54	1.24	cp
AT3G56190.1	ALPHA-SNAP2, ASNAP, alpha-soluble NSF attachment protein 2	1.10	1.54	1.26	v
AT2G20630.1	PIA1, PP2C induced by AVRRPM1	0.88	1.54	1.04	c
AT5G47760.1	PGLP2, ATPGLP2, ATPK5, 2-phosphoglycolate phosphatase 2	0.98	1.48	1.30	cp
AT5G02490.1	Heat shock protein 70 (HSP 70) family protein	0.81	1.46	0.87	c
AT1G04870.1	PRMT10, ATPRMT10, protein arginine methyltransferase 10	0.81	1.45	1.24	c
AT2G35270.1	GIK, Predicted AT-hook DNA-binding family protein	0.84	1.44	1.23	n
AT3G04790.1	Ribose 5-phosphate isomerase, type A protein	0.94	1.43	1.20	cp
AT1G66430.1	pfkB-like carbohydrate kinase family protein	0.87	1.42	1.16	cp
AT3G22890.1	APS1, ATP sulfurylase 1	0.78	1.37	1.03	c,cp
AT4G18480.1	CHLI1, CH42, CHL11	0.72	1.22	0.80	cp

Table S4.5: Fold changes of proteins that were specifically downregulated in H treatment.
green: significantly downregulated proteins compared to C ($p<0.05$); loc corresponds to location according to SUBA4con: c, cytosol; cp, plastid; ER, endoplasmic reticulum; ex, extracellular; m, mitochondrion; n, nucleus; pm, plasma membrane and v, vacuole.

id	description	P/C	H/C	PH/C	loc
AT5G13930.1	CHS, TT4, ATCHS, Chalcone and stilbene synthase family protein	0.73	0.41	0.75	ER
AT5G02770.1	unknown protein	0.83	0.46	0.79	n
AT3G55460.1	SCL30, At-SCL30, SC35-like splicing factor 30	1.13	0.46	0.93	n
AT1G04480.1	Ribosomal protein L14p/L23e family protein	0.86	0.53	0.81	c,n
AT3G26380.1	Melibiase family protein	0.84	0.53	0.61	ex
AT3G13790.1	ATCWINV1, ATBFRUCT1, Glycosyl hydrolases family 32 protein	1.01	0.55	0.78	ex
AT2G01250.1	Ribosomal protein L30/L7 family protein	0.90	0.55	0.81	c
AT1G27480.1	alpha/beta-Hydrolases superfamily protein	0.99	0.55	0.78	v,pm
ATCG00800.1	structural constituent of ribosome	0.90	0.59	0.84	cp
AT3G52470.1	Late embryogenesis abundant (LEA) hydroxyproline-rich glycoprotein family	0.99	0.63	0.84	pm
AT2G42740.1	RPL16A, ribosomal protein large subunit 16A	0.84	0.64	0.79	c
AT4G27090.1	Ribosomal protein L14	0.99	0.66	0.82	c
AT5G52650.1	RNA binding Plectin/S10 domain-containing protein	0.96	0.66	0.77	c
AT1G31330.1	PSAF, photosystem I subunit F	0.91	0.66	0.77	cp
AT2G24820.1	TIC55-II, translocon at the inner envelope membrane of chloroplasts 55-II	0.84	0.66	0.87	cp
AT1G62660.1	Glycosyl hydrolases family 32 protein	1.12	0.74	0.80	v

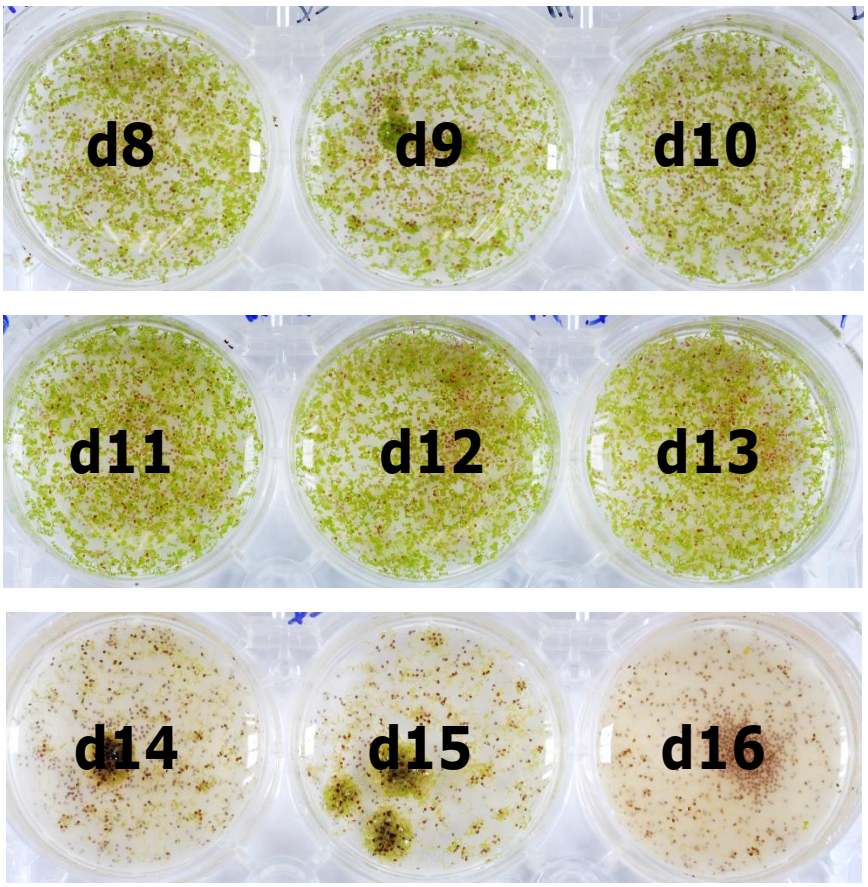

Figure 5.1: Estimation of the priming memory.
Representative images of individual wells containing seedlings that were primed on day 6 and heat-shocked at 43°C on day 8, 9…or 16. Each image was acquired seven days after the 43°C treatment.

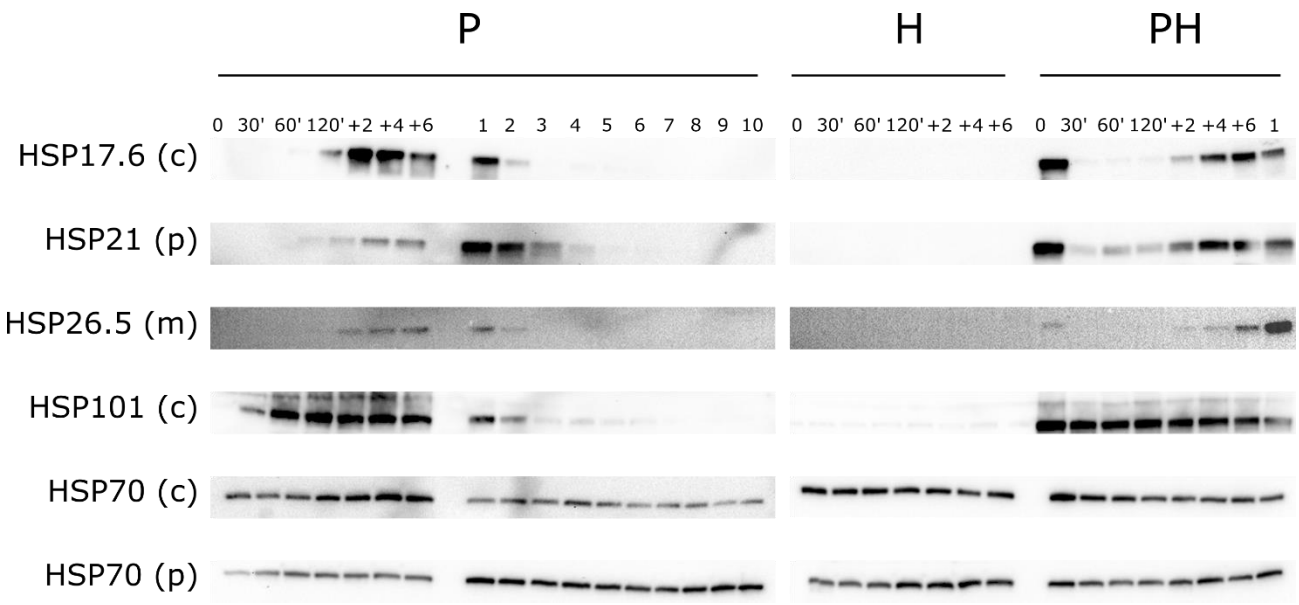

Figure 5.2: Representative immunoblot analysis of HSPs in P, H and PH samples.
Immunodetection was performed with anti-cytosolic HSP70, anti-chloroplastic HSP70, anti-HSP101, anti-HSP17.6, anti-HSP21 and anti-HSP26.5 antibodies (Agrisera); subcellular localizations of these proteins are indicated in brackets (c, cytosol; p, plastid; m, mitochondrion); 0, 30', 60', 120': min of heat treatment; 2 h, 4 h, 6 h: hours of recovery post-treatment; 1, 2, 3…: days post-treatment.

Chapter V- Heat stress memory and HSPs

1. Introduction

In the previous chapter, we described the molecular adaptations that allow primed seedlings to survive heat shock, by using our standard protocol in which priming occurs 24 h before the heat shock. It was also of interest to investigate how long protection can be maintained after the application of priming, which would be of particular relevance in an agronomical context or for crop improvement. In the context of HS, extensive research has recently started to identify heat memory actors. HS memory is defined as the active maintenance of acquired thermotolerance and is regulated by distinct processes other than thermotolerance itself, since several mutants are able to acquire thermotolerance but are unable to maintain it, as quoted in Liu *et al.* (2018) and references herein.

The implication of some transcription factors, especially HSFA2, and epigenetic control such as histone modifications or regulation via small RNAs were found to play an important role in stress memory (Lämke *et al.*, 2016; Ohama *et al.*, 2017). Accumulation of H3K4 methylation induced by HSFA2 was demonstrated to participate in the maintenance of the transcription of HS responsive genes after heat application, such as some sHSPs or ascorbate peroxidase 2 (APX2) (Lämke *et al.*, 2016). Moreover, when a second stress of the same intensity was applied three days after a priming treatment , HSFA2 and HSFA1s were involved in the stronger activation of heat responsive genes (Liu *et al.*, 2018). This priming memory could last up to seven days. In tall fescue (*Festuca arundinacea*), the transcriptional activation of a sHSP and a high molecular weight HSP could be retained for four days of high temperature stress, but not after eight days in pre-acclimated plants and transcriptional induction was much lower in non-primed plants (Hu *et al.*, 2015). Acetylation of H3K56 and ANTI-SILENCING FUNCTION 1 (ASF1) presented in Chapter I could also have a role in the maintenance of HSFA2 and long term memory, but to our knowledge, it is yet to be demonstrated.

Besides histone modifications, several small RNAs were shown to regulate the transcription of HS-responsive genes (Stief *et al.*, 2014b). For example, miR156 was found to be induced during HS and to participate in HS memory by promoting the transcription of HSP genes or APX2 and downregulating SQUAMOSA-PROMOTER BINDING-LIKE (SPL) transcription factors that are involved in developmental transitions and that repress the transcription of HS responsive genes (Stief *et al.*, 2014a). miR398 upregulation by HSFA1b and HSFA7b was also demonstrated to promote basal thermotolerance by downregulating levels of two copper/zinc superoxide dismutases and a copper chaperone which are involved in ROS detoxification (Guan *et al.*, 2013). The lower concentrations of these enzymes led to increased ROS levels which activated HSFs, thus resulting in a positive regulatory loop. Finally, a trans-acting small interfering RNA (ta-siRNA) called TAS1 was found to be downregulated during HS and its target HEAT-INDUCED TAS1 TARGET1 (HTT1) promoted thermotolerance (Li *et al.*, 2014). However, whether these small RNAs are involved in stress memory has not been assessed, to our knowledge.

RNA decay through EXORIBONUCLEASE 4 (XRN4) activity could play a role in the attenuation of HSFA2-mediated heat memory, as *xrn4* exhibited a slower HSFA2 decay than WT (Nguyen *et al.*, 2014). Recently, Ling *et al.* (2018) also suggested a role of alternative splicing in heat memory. They found that under HS, the number of

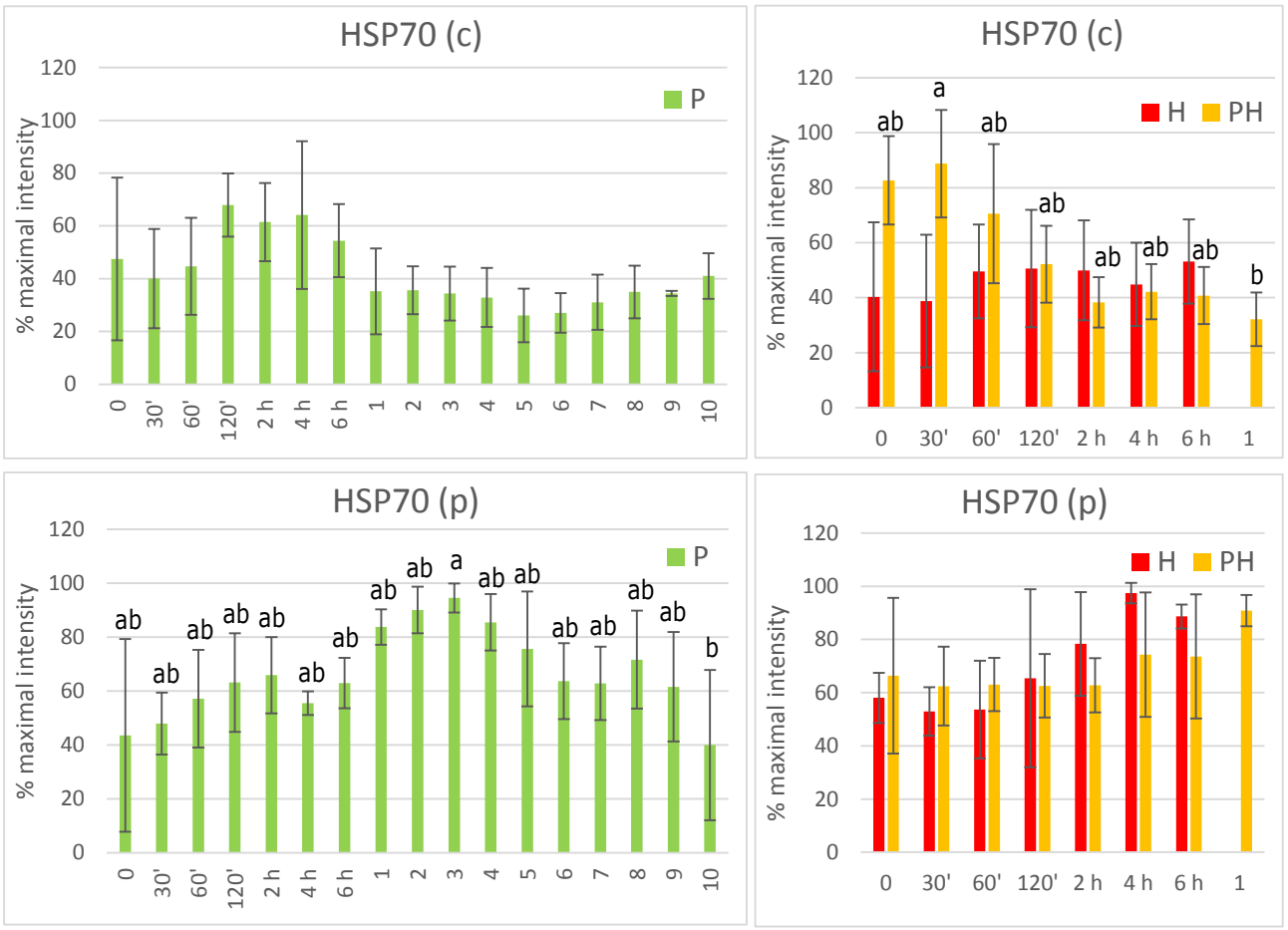

Figure 5.3: Semi-quantitative analysis of cytosolic and chloroplastidial HSP70s protein levels detected in P, H and PH samples during and after treatment.
For each protein, semi-quantification was performed by expressing the intensity of each lane as a percentage of the maximal intensity detected on each membrane; subcellular localization is indicated in brackets (c, cytosol; p, plastid); 0, 30', 60', 120': min of heat treatment; 2 h, 4 h, 6 h: hours of recovery post-treatment; 1, 2, 3…: days post-treatment; letters correspond to statistically different groups according to ANOVA and Tukey's test ($p<0.05$; $n=3$); if no letter is indicated, no significant difference was detected among the samples of one treatment (P, H or PH).

intron retention events increased and that after heat shock recovery, plants that were previously primed were able to resume splicing, while non-primed plants were not. However, how this process is regulated remains elusive. Autophagy was also lately identified as a component of thermomemory (Sedaghatmehr *et al.*, 2018). In this study, the number of autophagosomes was shown to increase following priming and to play a role in the degradation of HSPs after long-term recovery. Autophagy-deficient mutants displayed a lower basal thermotolerance, but their acquired thermotolerance was extended compared to the wild type (Sedaghatmehr *et al.*, 2018). Given all these results and those presented in Chapter I concerning HSP101 and HSA32 crosstalk (Wu *et al.*, 2013), transcript and protein levels of HSPs could play a significant role in the modulation of acquired thermotolerance memory. Thus, we wondered if priming could be remembered in developmentally arrested seedlings for as long as on a Murashige and Skoog medium (Liu *et al.*, 2018), and if memory was strictly correlated with the presence of heat-inducible HSPs.

2. Results and discussion

We first assessed HS memory by determining how long priming could be remembered by seedlings. Priming was performed on day 6 and the heat shock at 43°C was applied either on day 8, 9, etc. Survival was estimated visually on images of the wells acquired seven days after the heat shock treatment, allowing us to establish the duration of priming memory. As shown on Figure 5.1, priming performed on day six could be perfectly memorized up to seven days (at day 13). Interestingly, one day later (on day 14), seedlings were unable to survive the heat shock treatment, and thus, had lost within 24 h their memory of the priming. We therefore investigated whether the memory of the priming was correlated with the presence of HSPs. We performed a western blot analysis of HSP proteins during P, H and PH and after treatment, to follow their kinetics of synthesis and degradation. A set of HSPs from different classes and present in different organelles was selected: HSP101, HSP70, chloroplastic HSP70 and HSP21, cytosolic HSP17.6 and mitochondrial HSP26.5. In Figure 5.2 are presented representative images of the immunoblot signals (chemiluminescence) acquired with specific anti-HSPs antibodies in the different samples. The profiles vary depending on the class of HSPs, with some of them being constitutive (HSP70s) and others only stress inducible (sHSPs and HSP101). To obtain a relative quantification of the protein levels across time after normalization with RbcL band detected by UV, the number of pixels detected by chemiluminescence on each lane was expressed as the percentage of the maximal intensity detected on each membrane. Results of the semi-quantification for constitutive HSP70s are presented in Figure 5.3 and for stress inducible proteins in Figure 5.4. The level of cytosolic HSP70 was stable in P and H, while in PH its level decreased during the recovery period (Figure 5.3). Chloroplast HSP70 did not show a significant variation during the stress treatments nor the recovery periods. These results are not concordant with the data of Chapter IV (Figure 4.7), since an increase in several HSP70 was detected in response to HS according to the proteomic XIC analysis. However, the commercial anti-HSP70 antibody we used was raised against a synthetic peptide found in two HSP70 and three HSC70 (heat shock cognate protein 70), and therefore the immunoblot signal is not specific enough to detect the variations highlighted by XIC.

Interestingly, the profiles of the heat-inducible HSPs are very different (Figure 5.2 and 5.4). HSP101 was detected as soon as 30 min of P treatment, with a peak of accumulation occurring between 2 h of treatment and 2 h of

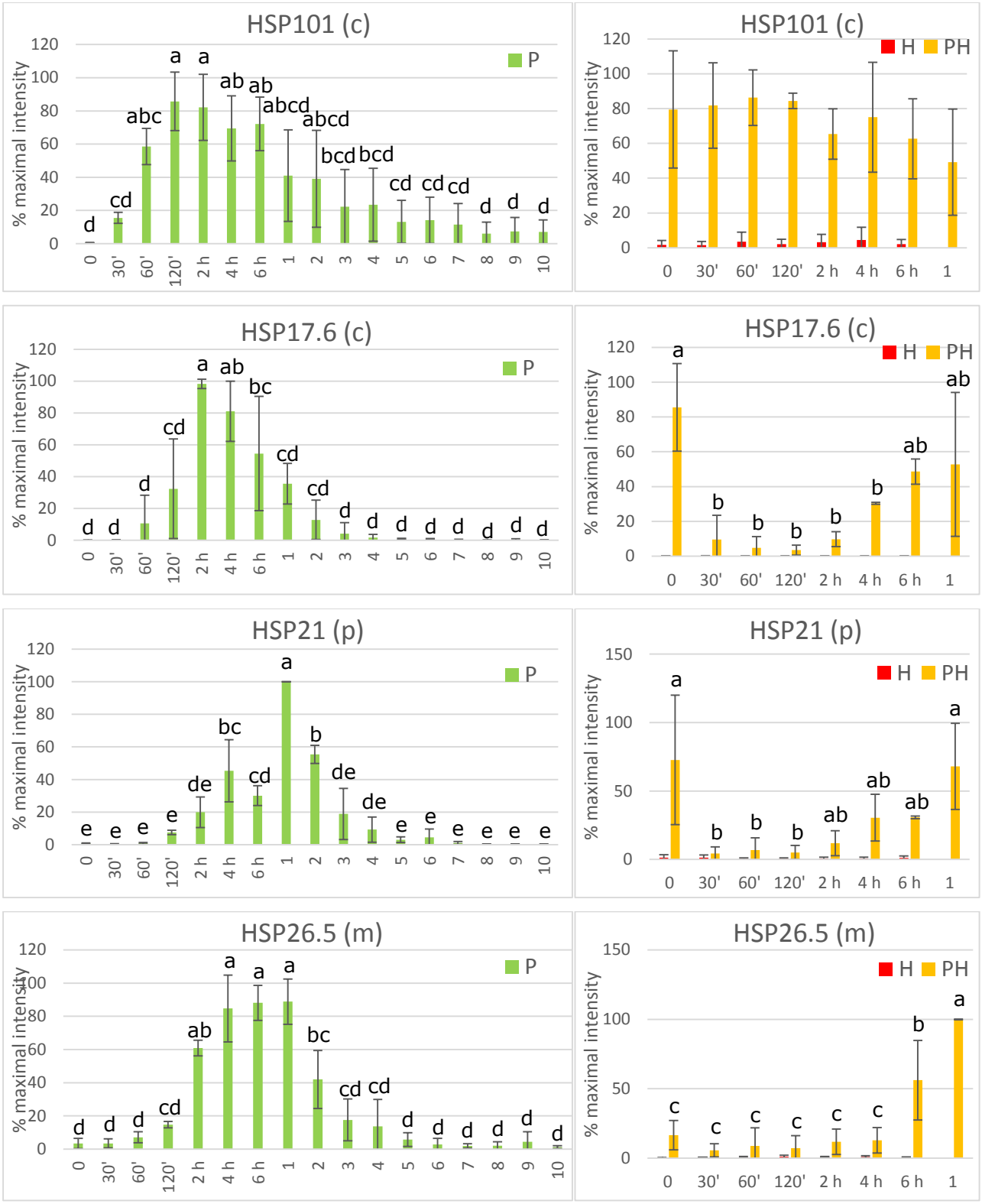

Figure 5.4: Semi-quantitative analysis of stress-inducible sHSPs and HSP101 protein levels detected in P, H and PH samples during and after treatment.

For each protein, semi-quantification was performed by expressing the intensity of the signal in each lane as a percentage of the maximal intensity detected on each membrane; subcellular localization is indicated in brackets (c, cytosol; p, plastid; m, mitochondrion); 0, 30', 60', 120': min of heat treatment; 2 h, 4 h, 6 h: hours of recovery post-treatment; 1, 2, 3…: days post-treatment; letters correspond to statistically different groups according to ANOVA and Tukey's test ($p<0.05$; $n=3$); if no letter is indicated, no significant difference was detected among the samples of one treatment (P, H or PH).

recovery (Figure 5.4). Afterwards, its level decreased and became very low from day five post-treatment. In H samples, HSP101 was detectable but at a very low level, while in PH samples, its level was high and stable across treatment and during early recovery. The lack of synthesis at 43°C concurs with the inhibition of HSP104 synthesis observed above 42°C in *Saccharomyces cerevisiae* (Rikhvanov *et al.*, 2005). Thus, it seems that the response to heat shock reaches a limit at around 43°C. In comparison with HSP101, the sHSPs accumulated later, the detection of HSP17.6, HSP21 and HSP26.5 starting between 2 h of 38°C treatment and after 2 h of recovery. The HSP17.6 protein was the most abundant after 2 h of recovery and its level progressively decreased afterwards. After three days of recovery, this protein was no longer detectable. HSP21 accumulated later than HSP17.6, with a peak detected one day after treatment, and it could no longer be detected five days after priming. Concerning the three mitochondrial sHSPs, we could only detect HSP26.5 (Figure 5.2) and HSP23.6 (not shown) by immunoblotting. HSP26.5 reached its maximum level between 4 h and one day after P treatment and was not detectable after four to five days of recovery. HSP23.6 could be detected on membranes on which 40 µg of total proteins had been loaded, but not with 15 µg (data not shown), likely because of a lower sensitivity to the antibody compared to the others. Mitochondrial HSP23.5 could not be detected in any of the samples, even though peptides of this protein were identified by spectral counting (Table S1). This is likely due to its low abundance and/or to the low sensitivity of the antibody used. Interestingly, no sHSPs were detected in H samples. In PH samples, they were all detected before the heat shock (equivalent to P+1 day samples), but dramatically decreased during the heat shock at 43°C, and "re-accumulated" after treatment. This result was quite surprising, as it was unlikely that these proteins were actively degraded during heat shock. We hypothesized that they would aggregate with unfolded proteins during heat shock and that they might not be properly extracted, even though the extraction buffer contained several detergents and reducing agents. We tested this hypothesis by adding Laemmli buffer to the pellet after protein extraction in order to extract the protein aggregates better. Comparative profiles of HSP17.6 and HSP21 in P, PH and H of the same samples, extracted in 50 mM $NaPO_4$ pH 8, 10 mM EDTA, 0.1 % Triton X-100, 0.1 % sarcosyl, 10 mM DTT, 1 mM PMSF and a cocktail of antiproteases ("up" fraction) and further extracted in Laemmli buffer ("down" fraction), are shown in Figure 5.5. As expected, in PH samples, HSP17.6 and HSP21 were mostly detected in the "down" fraction during the heat shock, while they were detected in both fractions before and after the 43°C treatment. Interestingly, in P samples, HSP17.6 was detected earlier in the "down" fraction than in the "up" fraction (between 30' and 60'). This could explain why sHSPs were detected later than HSP101 in the previous experiment (Figure 5.4). In H samples, no sHSPs were detected in either fraction, confirming the absence of their synthesis in H. This absence of HSP accumulation in H condition concurs with the proteomics shotgun analysis realized after 2 h of recovery post-heat shock (cf Chapter III). Altogether, these data confirm the nanoLC/MS analysis and the primordial role of HSPs in the tolerance to HS. The aggregation of sHSPs during the 43°C treatment in PH seedlings is concordant with the model of stress granule formation under HS, which prevents the irreversible aggregation of proteins and facilitates their refolding upon stress recovery (McLoughlin *et al.*, 2016). Moreover, the presence of HSP101 would favour the translational recovery of mRNAs encoding ribosomal proteins during the recovery period (McLoughlin *et al.*, 2016; Merret *et al.*, 2017).

However, these results of HSP profiling indicate that the priming memory is partially independent of HSPs, as priming could be remembered for seven days, whereas the latest HSPs returned to their basal level between four and five days after P treatment. The duration of HS memory is in agreement with previous studies, in which

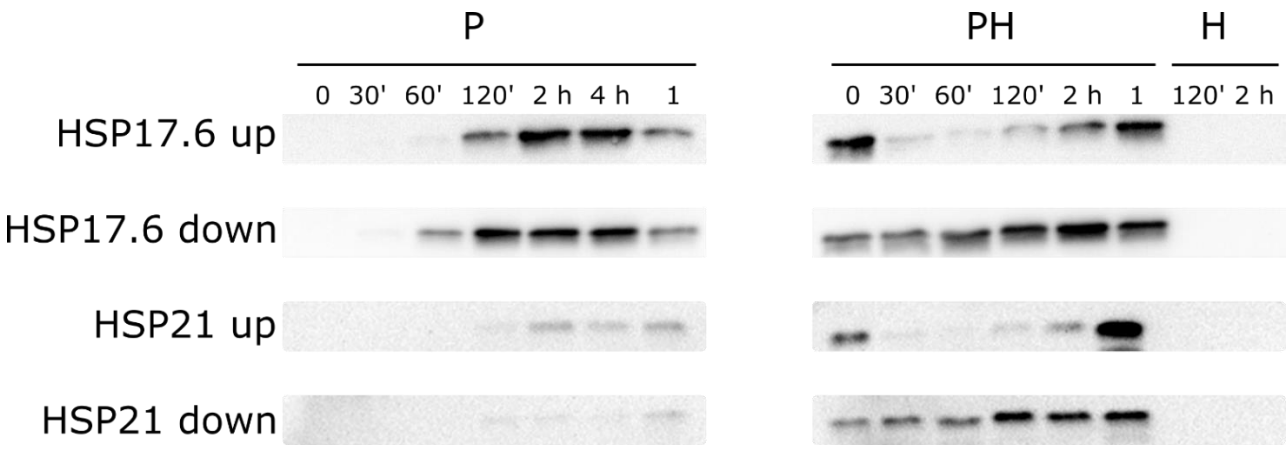

Figure 5.5: Immunoblot analysis of HSP17.6 and HSP21 proteins present in the supernatant or in the pellet.
30 µL of either supernatant (up) or pellet (down) extract were loaded on each lane; anti-HSP17.6 and anti-HSP26.5 antibodies were used for immunoblotting; 0, 30', 60', 120': min of heat treatment; 2 h, 4 h, 6 h: hours of recovery post-treatment; 1: day post-treatment.

memory could be retained between three and ten days depending on the stress (reviewed in Lämke & Bäurle, 2017). Hilker *et al.* (2016) have suggested that the duration of stress memory likely depends on the age of the organism and its nutritional status. They proposed that it would be beneficial for young plants to invest in long term memory, as it would reduce the cost of a future induction of stress tolerance, whereas annual adult plants should invest in short term memory. When considering the nutritional status, it is assumed that a plant with a high availability of nutrients and light would trigger the adaptive response more easily than starved plants (Hilker *et al.*, 2016). However, in *Escherichia coli*, it was found that carbon- or nitrogen-starvation could induce a higher survival rate to a 57°C heat shock (Matin, 1991). Whether such effect also occurs in our system seems unlikely, since the basal thermotolerance of the developmentally arrested seedlings is comparable to that of seedlings grown on MS plates.

The kinetics of HSP expression concurs with the work of Charng *et al.* (2006) who showed that HSP90, HSA32 and sHSPs of class I returned to their basal level within three days after a treatment at 37°C. However, in their study, the abundance of HSA32 was correlated with the maintenance of acquired thermotolerance. A positive regulatory loop between HSA32 and HSP101 was proposed to participate in the maintenance of thermotolerance (Wu *et al.*, 2013). However, this response was not assessed beyond a 48 h recovery. HSP21 was also shown to be a component of thermomemory in Arabidopsis seedlings (Sedaghatmehr *et al.*, 2016). In this study, it was proposed that the degradation of HSP21 following HS was correlated with the expression of a plastid metalloprotease protein called FtsH6. In the knockout *ftsh6* mutant, the abundance of HSP21 was maintained at higher levels during the recovery period and the seedlings exhibited a higher thermomemory than the WT. However, once again, the recovery period between the application of the priming and the heat shock was not prolonged beyond four days.

Even though HSPs are major components of thermotolerance, our results show that their abundance at the protein level before the application of a severe HS apparently does not correlate well with the ability of seedlings to survive this severe HS. Nevertheless, one can notice, although it is not statistically significant, that the signal of HSP101 signal was almost halved between days 7 and 8 after priming, which corresponds to the time at which the memory of priming vanishes. The semi-quantitative western blot analysis is likely accurate but not sensitive enough to discern a threshold below which the amount of one or more inducible HSPs would be too low to provide protection. It would be therefore of high interest to perform an in-depth proteomic analysis of the primed samples after seven and eight days to clarify the requirement of the inducible HSPs for maintenance of thermotolerance.

Other mechanisms such as an epigenetic memory may also play an important role in this process. Several key players of the HS memory have been recently identified. Among them, HSFA2 and HSFA1s were shown to participate in the recruitment of enzymes involved in the hypermethylation of histone H3 lysine 4 in the heat-stress memory genes (Lämke *et al.*, 2016; Liu *et al.*, 2018). Liu *et al.* (2018) showed that the expression of APX2 was significantly higher in primed samples than in non-primed samples, when applying a treatment at 37°C six days after the priming. In this experiment, the transcriptional memory, defined as an enhanced transcriptional activation observed in the onset of HS in primed seedlings compared to naïve seedlings, was maintained for up to one week.

FORGETTER 1 (FGT1) was also found to be an important component of thermomemory by interacting with the chromatin remodelers BRM1 et ISW1 (Brzezinka *et al.*, 2016). According to their model, FGT1 binds to the promoter of heat-inducible genes, such as HSA32 or HSP21, and recruits proteins that permit the repositioning of nucleosomes on this region. The unwrapping of DNA would allow a better transcription of the targets of FGT1. The duration of thermomemory in our conditions suggests such a regulation of transcriptional memory by DNA unwrapping and histone modifications. Epigenetic memory would thus allow a rapid *de novo* synthesis of protective mechanisms under the second application of heat shock, instead of maintaining the costly translation of these proteins under control conditions. BRU1, a component of epigenetic inheritance via DNA replication and cell division, was recently found to be involved in HS memory (Brzezinka *et al.*, 2018). Whether this protein is involved in the maintenance of H3K4 hypermethylation or in the control of nucleosome positioning previously discussed is still unknown. In our liquid culture system, it would be interesting to study the memory after repeated stresses or to check if the memory would be retained seven days after being transferred to soil and after a high number of cell division events due to the resumption of development. Besides mitotic inheritance, evidence was provided that transgenerational memory can also occur (Suter & Widmer, 2013), but it is unlikely that priming at the seedling stage would be remembered by the next generation.

Overall, we provided clear evidence that six-day-old seedlings in our system remember priming during seven days and loose this memory the next day, but we could not ascertain whether HSP abundance was correlated with memory. Further work will be needed to elucidate the actual implication of HSPs, and the epigenetic components of the memory.

General discussion and perspectives

Heat stress is a major abiotic stress affecting plant development and reproduction. In the context of climate change, it is necessary to gain a comprehensive understanding of plant response to temperature, since the frequency and severity of heat waves are expected to increase. The aims of this study were to uncover the molecular responses that allow seedlings to survive a severe heat stress and to determine how energy metabolism is involved in this process. Although the heat stress response has already been widely investigated for the last decades (Guy *et al.*, 2008; Bokszczanin & Fragkostefanakis, 2013; Ohama *et al.*, 2017), we have performed, for the first time to our knowledge, an integrated analysis of the response to acclimation and to heat shock, including physiological, transcriptomic, proteomic and metabolic responses, using an original model system, in which the seedling stage is maintained for weeks. By integrating data at the different scales, we could obtain an overview of the acclimation phenomenon. In this part, we will discuss three major points developed in our results, which are: the high resilience of seedlings observed in the model system, the effect of priming on the heat stress signalling and the critical step of the recovery phase for seedling survival.

1. High resilience of seedlings

In Chapter 1, we explored the physiological and metabolic adaptations that allow seedlings germinated in mineral water to maintain for weeks in a steady-state. In contrast to the common vision of a highly vulnerable seedling stage, we brought to light a remarkable resilience of seedlings under nutrient limitation, which appeared largely due to their metabolic plasticity, such as energy dissipation through AOX pathway and photorespiration. Even under severe mineral starvation, seedlings are able to develop a heat shock response leading to acclimation, and thus, although they are only "germinated embryos" with photosynthetic cotyledons, they have a capacity to adapt to their environment which is comparable to that of mature plants with much more resources. In our experimental system, nitrogen recycling allows the maintenance of a basal metabolism, whereas carbon storage occurs through the accumulation of malate in the vacuole and of lipids inside the plastoglobules, offering the possibility to rapidly fuel growth if nutrients become available. Of course, deeper analyses of molecular responses would be needed to better understand the mechanisms underlying the resilience of seedlings and also to explain why, although apparently in equilibrium, seedlings will finally die (after several months of life). A strong hypothesis is that the accumulation of oxidative damage is the life timer of seedlings in these conditions, and clearly the system is well suited to study the oxidative aging paradigm, but we decided not to explore further this aspect.

Our culture system is very artificial, but well suited to analyse the response of seedlings to stresses. Indeed, in each well, we could grow around thousand seedlings and thus work with a homogenous population. Of course, one could argue that such resilience and developmental arrest would be unlikely to occur in classical culture conditions. However, we could see that the nutrient limitation in our conditions caused a similar phenotype (long root and small cotyledon) as what was previously observed on MS medium, when seeds were germinated under low nitrogen and no sucrose supply (Martin *et al.*, 2002). Moreover, Martin *et al.* (2002) observed a slow degradation of lipids, as observed in our fatty acid profile and Nile red staining. How long seedlings could be maintained under low nitrogen condition was not assessed in their study, but it is likely that senescence would be triggered more rapidly than in our system. In our model, it seems that death occurs slowly, likely because of

the developmental arrest and the rather low metabolic activity. It would be necessary to study the response of senescence-associated genes during the weeks of culture, to better understand how senescence is inhibited in our conditions.

In an ecological context, the success of seedling establishment conditions the life of the future plant and the fitness of the population, even though some species invest in a high number of seeds, compensating for a low rate of successful emergence (Parker *et al.*, 2008). Seedlings face many environmental constraints because of their limited access to nutrients and light. In our conditions, the limitation in mineral nutrients led to the developmental arrest of seedlings and their maintenance in a steady state for weeks without inducing death. In seedlings, senescence might be prevented through miR164 pathway, which would inhibit the expression of ORE1, a master regulator of senescence (Kim *et al.*, 2009). It would be interesting to study the response of this signalling pathway during several weeks of culture. Moreover, it is generally assumed that young tissues are more resilient than mature ones, and that the response of the young tissues will shape the future response of the old tissues. For example, in mammals, it is known that prenatal and early life has a strong influence on the future capacity of the individual to cope with stress (Rogers & Lucchesi, 2014). In plants, it is difficult to compare the seedling stage with the mature plant. However, some studies have compared the stress responses of young and fully expanded leaves. For example, it was shown that Arabidopsis young leaves were less affected by drought than mature leaves (Jung, 2004). This was correlated with a higher efficiency of photosystem II, a lower non-photochemical quenching and lower activities of ROS scavenging enzymes in young leaves than in mature leaves (Jung, 2004). Recently, an analysis of the photosynthetic response to high light revealed that both leaf and plant age influence the response to stress (Bielczynski *et al.*, 2017). In this study, young leaves were found to acclimate better to continuous high light than old leaves, confirming the differential sensitivity of plants during their lifetime. Whether the resilience is higher in seedlings than in mature plants would be difficult to assess, given the different nature of the organs, but it is possible that young tissues better adapt than old ones.

Besides their natural longevity in liquid grown culture, we could see that Arabidopsis seedlings grown in our conditions exhibited a similar thermotolerance than seedlings grown on MS plates. This could confirm the high resilience of these developmentally arrested seedlings, even under stress. Combination of heat stress with mineral deficiency has been scarcely studied. In creeping bentgrass (*Agostis stolonifera*), the effect of N level on the tolerance to heat stress was assessed and it was shown that low or high nitrogen decreased the turfgrass quality, the Fv/Fm value and the amounts of HSPs compared to medium nitrogen supply (Wang *et al.*, 2014b). In a similar way, a combination of heat stress with P deficiency in sheepgrass (*Leymus chinensis*) led to a reduced growth and increased leaf chlorosis, accompanied by a lower PSII and PSI efficiency compared to non P-deficient heat stressed plants (Li *et al.*, 2018). In our conditions, the mineral starvation likely affects the response to heat shock, but it seems that the degree of thermotolerance is not significantly impacted. Of course, a supplementation of our medium with N and P could allow us to study the impact of the deficiency on the stress response, but in these conditions, seedlings would probably recover their development and thus behave differently than under developmental steady state.

Table 6.1: Overall response to heat-shock of the different cell components in H (43°C on day 7) and PH (38°C on day 6, 43°C on day 7) seedlings before, during and after 43°C treatment, according to gas exchanges and omics analyses.
Putative responses are indicated in italic.

	H					**PH**				
Compartment	Mitochondrion	Chloroplast	Cytosol	Nucleus	Actin	Mitochondrion	Chloroplast	Cytosol	Nucleus	Actin
Before stress	Normal respiration No sHSPs	Normal photosynthesis No sHSPs	Ribosomes OK No sHSPs or HSP101 *Low ROS detox*	Export of mRNAs	Normal network	Normal respiration	Normal photosynthesis	*Ribosomes OK* sHSPs and HSP101 High ROS detox	Export of mRNAs	Normal network
During stress	Decreased respiration High AOX capacity No sHSPs	Decreased photosynthesis No sHSPs	Low ribosomal proteins *Inhibition of translation* No sHSPs and low HSP101 *Low ROS detox*	*Blocking of mRNA export*	Aggregation of actin	Decreased respiration Upregulation of PPR expression Very high AOX capacity HSP23.5, HSP23.6, HSP26.5	Decreased photosynthesis but partially protected compared to H Upregulation of photosynthetic genes and chlorophyll biosynthesis HSP21 cpHSP101	*Aggregation of mRNAs and proteins with sHSPs* HSP101 *Inhibition of translation* *High ROS detox*	High number of differentially expressed genes, with a fold-change generally higher than in H *Export of mRNAs*	*Co-aggregation of actin monomers with cytosolic sHSPs*
After (within one day of recovery)	Decreased respiration No sHSPs	Decreased photosynthesis after stress, and further decrease during the following days No sHSPs	Low ribosomal proteins No sHSPs and low HSP101 *Low ROS detox*	*Blocking of mRNA export*	Irreversible aggregation of actin	Full recovery of the activity within one day HSP23.5, HSP23.6, HSP26.5	Full recovery of the activity within one day HSP21 *cpHSP101*	*Ribosomes and polysomes OK* *Protein refolding and de novo synthesis* *High ROS detox*	*Export of mRNAs*	*Disaggregation and/or de novo synthesis of actin monomers*

For developmentally arrested seedlings which are in a metabolic steady state, one can wonder about their homeostasis under heat stress. The synthesis of HSPs and other stress-related proteins obviously requires energy and the use of a large pool of amino acids, certainly at the expense of other proteins. For example, we could see that many enzymes related to cell wall metabolism and regulation of growth were downregulated at the transcriptional and/or the protein level. Moreover, it is likely that stress response involved recycling process such as autophagy. Unfortunately, we were unsuccessful in detecting by immunodetection a clear increase in the protein amount of ATG8 (autophagy-related protein 8) (data not shown), which is a protein involved in the formation of autophagosomes together with ATG12/ATG5 conjugate (Thompson *et al.*, 2005; Chung *et al.*, 2010). It could be interesting to study the formation of autophagosomes by using a fluorescent line, such as mRFP1-ATG8F (Honig *et al.*, 2012), and by following the evolution of autophagy during and after heat shock in H and PH seedlings.

2. Effect of priming on heat shock response

One of the goals of our study was to uncover the effect of a priming treatment on the following response to a severe heat shock. Although the response to heat stress displayed a high overlap between primed and non-primed seedlings, we could detect several features specific of the primed samples (Table 6.1). A major part of this response was similar to that observed by Larkindale & Vierling (2007), which further validated the use of our model to study stress responses. For example, for many transcripts, such as the *HSPs* or the ascorbate peroxidase 2 (*APX2*), the fold change was much greater in PH than in H seedlings, which confirmed the previous observations of Liu *et al.* (2018) that an enhanced transcriptional regulation occurs when applying a second heat treatment. This higher transcriptional response likely involves epigenetic memory, and would deserve further exploration. Moreover, we could detect a large number of specifically overexpressed or downregulated genes in PH condition. Many upregulated genes were related to plastid activity (photosynthesis, pigment biosynthesis) and mitochondrial RNA processing (PPR proteins) (Table 6.1), whereas the downregulated genes were mainly related to cell wall metabolism and lipid metabolism. The activity of mitochondrion and chloroplast was partially protected by the pre-treatment, likely because of the accumulation of HSPs and the operation of the ROS detoxification machinery (APX2, glutaredoxins, glutathione S-transferases…). The increase in AOX capacity in PH compared to H (Table 6.1) may also participate in the dissipation of energy excess, even though it would be necessary to better characterize this response by biochemical analyses. It would also be interesting to study the evolution of photorespiration, since the affinity of Rubisco towards CO_2 decreases with temperature (Mathur *et al.*, 2014). It is likely that a large proportion of the HSPs detected during PH treatment were already present at the beginning of the treatment and were not produced *de novo*, since a large decrease in polysomes and thus in the translational activity during a 45°C treatment occurred in both primed and non-primed seedlings according to Zhang *et al.* (2017). Interestingly, it appeared that a large proportion of the analysed sHSPs precipitated during the 43°C heat shock, supporting their expected role as chaperones co-aggregating with unfolded client proteins, in order to facilitate subsequent refolding by active chaperones (Waters, 2013).

Collectively, our omics data point out to the differential expression of many nuclear encoded plastid and mitochondrial proteins, but also of organellar genes, emphasizing the importance of these two energy-transducing

organelles in the HS response. The best multi-omics correlation was found for the increased synthesis upon heat stress of aromatic and branched chain amino acids occurring in plastids. While such a heat stress-dependent increase in amino acids could contribute to heat tolerance through its effect on auxin or/and glucosinolate metabolism remains to be established, it appears as an important metabolic component of the HS response.
In both H and PH seedlings, we found that heat had major effects on the intra-cellular organization. Indeed, the dynamics of organelles (mitochondria and ER) and of the actin network were blocked during stress in both treatments. However, while disruption of the actin cytoskeleton was irreversible in H seedlings, possibly because of aggregation of actin monomers, the network was found to rapidly recover its structure and dynamics in PH seedlings. This could be possibly due to the protection of actin by stress-induced sHSPs in PH seedlings, which would facilitate the regeneration of the actin cytoskeleton during recovery (Table 6.1). Pull-down experiments with actin and sHSP antibodies would be needed to challenge this hypothesis.

3. Critical step of the recovery phase in thermotolerance

Overall, priming was found to slightly enhance the physiological response of seedlings during an acute heat shock, suggesting its major beneficial impact could intervene during the recovery phase. Indeed, although the response to heat shock in H and PH seedlings was different during the treatment, the main effects of priming were revealed later (Table 6.1). Full recovery of the mitochondrial and photosynthetic activities was observed one day after heat shock and could even occur earlier since the full kinetics of recovery was not studied. The recovery of these two processes is crucial in order to provide the energy necessary for re-establishing homeostasis and lead to the resumption of plant growth. For many stresses, when getting back to control conditions, plants rapidly resume their global transcriptional activity, usually within one to three days, even though some stress memory related genes are still upregulated (Crisp *et al.*, 2016). One of the most important component of recovery is likely to be the resumption of translation. Indeed, it was recently shown that eukaryotic translation initiation factor 5B (eIF5B), which is a component of translational initiation, was essential for heat tolerance, since the mutant could not acquire thermotolerance (Zhang *et al.*, 2017). The authors showed that the translational recovery after heat shock is slower in the mutant than in the wild type, since the polysome fraction in the wild type started to recover 2 h after treatment and fully recovered after 12 h, whereas it required 18 h in the mutant to reach the wild type level (Zhang *et al.*, 2017). Moreover, the translational efficiency of some mRNAs including *MBF1C* and several *HSPs* and *HSFs* was lower in the mutant than in the wild type. Besides translation, the HSP101-mediated refolding of proteins co-aggregated with sHSPs could participate in the faster recovery of metabolism when plants are returned to control conditions (Table 6.1). Recently, a study highlighted a partial correlation between the level of HSP101 and the survival of Arabidopsis seedlings from different natural populations after application of a heat shock (Zhang *et al.*, 2015a).

During recovery in PH seedlings, the preserved translational activity and the refolding of proteins by HSP101 and its co-chaperones could contribute to the better resumption of mitochondrial and photosynthetic activities, by providing components to the electron transfer chains, like the sensitive components of photosystem II, even

though we could not detect differences compared to H condition (chlorophyll fluorescence analysis, abundance of PSII proteins) after 2 h recovery. Higher respiratory and photosynthetic activities could in return provide energy to maintain the costly translation, thus producing a positive regulatory loop. In H seedlings during recovery, the lower amount of HSPs and ribosomal proteins together with a higher amount of proteins related to ubiquitin-dependent protein catabolism would participate in a decreased recovery of translation compared to PH (Table 6.1). This lower translational activity would then decrease the turnover of mitochondrial and plastidial proteins, and could explain the absence of functional recovery of these organelles. In a similar way, we could observe the resumption of organelle dynamics during the recovery period in PH but not in H seedlings, likely thanks to a *de novo* synthesis and/or to the presence of HSPs that could participate in the disaggregation of actin monomers (Table 6.1). The recovery of organelle dynamics could also participate in the better distribution of energy and could favour exchanges (proteins, metabolites, DNA, RNAs) between the organelles, which could not occur in H seedlings. Altogether, these results reveal the importance of a fast recovery and return to homeostasis under control conditions, after the end of the stress period. If metabolism does not recover fast enough, the induction of cell death seems to be unavoidable.

4. Perspectives

During this study, we have highlighted the importance of energy metabolism, HSPs and protection of translation in the acquired thermotolerance. However, several questions remain unanswered, especially concerning the kinetics of recovery after stress and the stress memory. For this purpose, it would be interesting to realize a more detailed transcriptomic and proteomic analysis of the post-stress responses occurring in H and PH seedlings. The degree of implication of HSP proteins in stress memory (such as HSP101) must also be examined in more details, since most recent studies have focused on the transcriptional memory (Hu *et al.*, 2015; Lämke *et al.*, 2016; Brzezinka *et al.*, 2018; Liu *et al.*, 2018), but not on the protein abundance.

From an agronomic point of view, it would also be of interest to study the cross-tolerance with other stresses and to attempt mimicking priming using chemicals (Savvides *et al.*, 2016). Moreover, in our study, we have focused on the response to a short heat stress but it is likely that the response over a longer period (e.g. for several days) would involve other components to achieve a new homeostasis. Our experimental is indeed well suited to study prolonged stress, since seedling development is arrested. Finally, we have studied the response of the Col-0 ecotype, but a larger study involving a genetic diversity would be necessary to determine the common markers. Indeed, it was previously shown that the transcriptomic response of diverse Arabidopsis ecotypes to a 3 h treatment at 38°C was highly variable (Barah *et al.*, 2013). They found that 85 % of the identified transcripts showed an ecotype specific response. Of course, transcriptomic changes do not necessarily correlate with the actual activity of the different pathways. Thus, study of metabolic and proteomic responses would allow to better understand the core response to heat stress, and the specificities of each ecotype. Owing to the importance of the organelles in the acclimation process, an invaluable resource would be the collection of 56 Arabidopsis cytolines, which result from cytoplasmic substitutions among eight natural accessions reflecting within-species genetic diversity (Roux *et al.*, 2016).

Finally, understanding why and when stress memory disappears is a major concern in the context of breeding, and we believe it would be of interest to use our experimental system to explore the mechanisms of heat stress memory. Indeed, we could define that seven days is the limit of thermal memory in our conditions, but we could not strictly correlate it with the presence of HSPs. A deeper analysis, including a quantitative analysis of the HSPs would be necessary to determine if there is a threshold below which the short term "HSP memory" is lost. Alternatively, it would be of high interest to search for priming-induced modifications in the epigenome and mobilome which are certainly major players in the mid- and long-term stress memories (Ito *et al.*, 2011; Lämke & Bäurle, 2017).

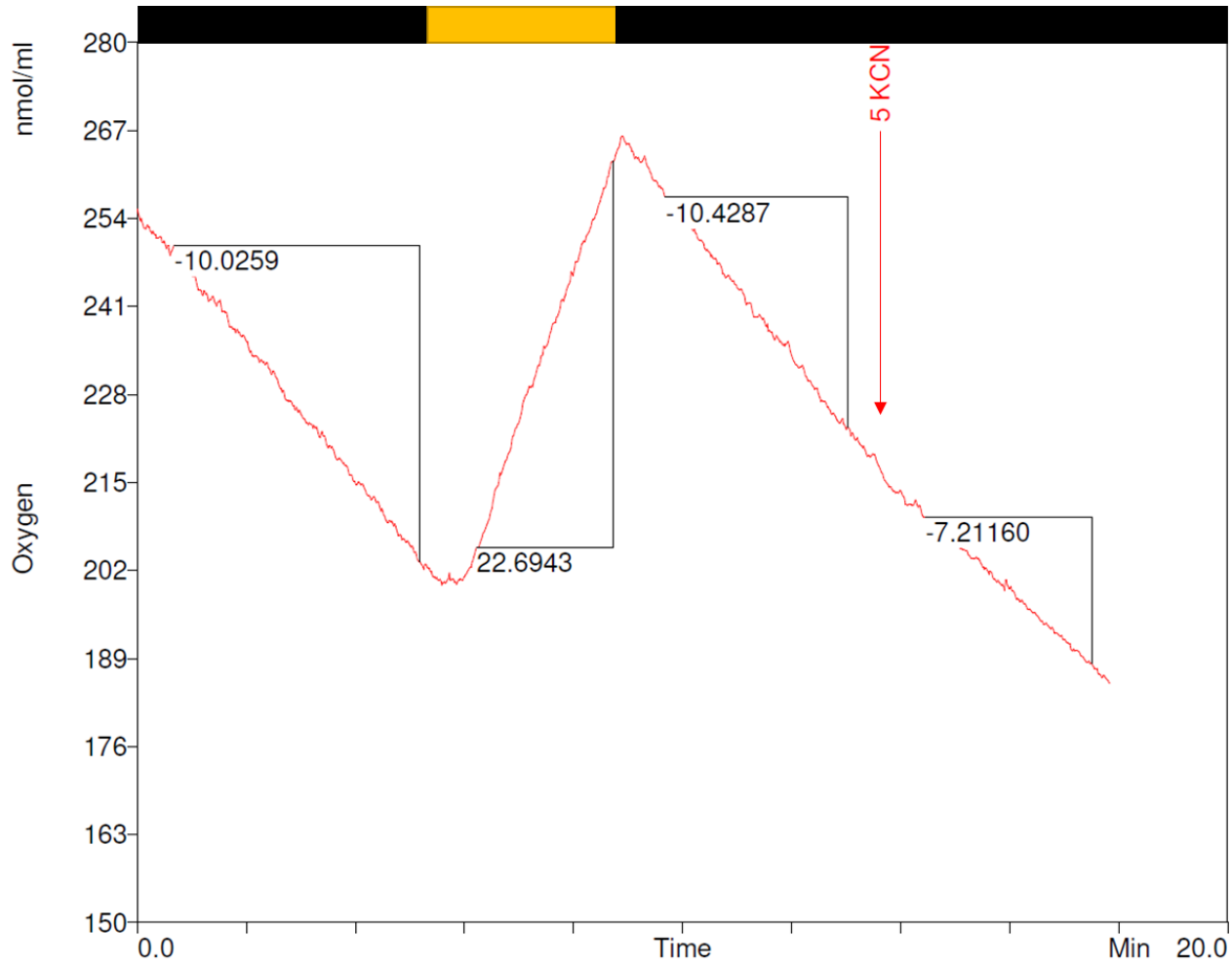

Figure 7.1: Representative oxygraph for measurement of respiratory and net photosynthetic activity. Light period is indicated in orange and dark period in black; red arrow corresponds to the addition of 5 µL of 100 mM KCN (0.5 mM final); numbers correspond to rates of oxygen evolution (nmol.min^{-1}.mL^{-1}).

Material and methods

We present in this section the material and methods concerning chapters III, IV and V. For chapter II, please refer to the material and methods of the publication manuscript.

1. Plant material and growth conditions

All experiments were performed using the *Arabidopsis thaliana* Columbia ecotype (Col-0). Visualisation of mitochondria was performed using a Mito-GFP transgenic line (Logan & Leaver, 2000), of ER with the ER-gk CS16251 line (Nelson *et al.*, 2007) and of actin with the GFP-Lifeact line (Riedl *et al.*, 2008; Garagounis *et al.*, 2017). *Friendly* (*fmt*) mutant which is affected in mitochondrial dynamics (Logan *et al.*, 2003) was also tested for acquired thermotolerance. Seedlings were grown according to Benamar *et al.* (2013): standardized amounts of seeds (around 18 mg) were inoculated in 6 mL of Evian natural mineral water in six-well plates. Plates were stratified at 4°C in the dark for 24 h and then incubated in a growth room (16 h of light/8 h dark, 150 µmol photons.m^{-2}.s^{-1} (PAR), 21°C day/19°C night, 70 % humidity) under rotary shaking (135 rpm).

2. Heat stress regimes

Stresses were always applied at the same time, after 2 h of photoperiod, in order to let seedlings set up their metabolism in the light, but also to have enough time following the stress treatments to perform lengthy experiments, such as oxygraphy for instance. Heat stress treatments were realized by transferring seedlings with their medium (around 5 mL) into 25 mL glass bottles (Schott) and placing them for 2 h in a water bath set up at a define temperature. Priming was performed at 38°C and heat shock at 43°C (Figure 3.1). Two white LED ramps ensured illumination during heat treatments at a PAR intensity similar to that used in the growth room. Control seedlings were kept in the growth room on the rotary shaker. After treatment, seedlings were transferred back into the six-well plates in the growth room for recovery.

3. Green pixel detection and viability assay

Images of the multiwell plates without their lids were acquired with a Nikon D5000 (Nikon France SAS, Champigny sur Marne, France) single lens reflex camera equipped with a 60 mm Nikkor microlens, using a stand equipped with fluorescent lighting on each side. Green pixel detection was performed using Fiji (Schindelin *et al.*, 2012) and the macro described in (Benamar *et al.*, 2013). Statistical analysis was performed using SigmaPlot 11.0 (ANOVA and Dunnett's test).

For detection of cell death, seedlings were incubated for 15 min in 0.5 % (w/v) Evans Blue solution, followed by several rinses with water. Images were acquired using an Axio Imager Z2 microscope driven by ZEN software with an EC Plan-Neofluar 10x objective (NA 0.3) objective (Carl Zeiss Microscopy GmbH, Göttingen, Germany).

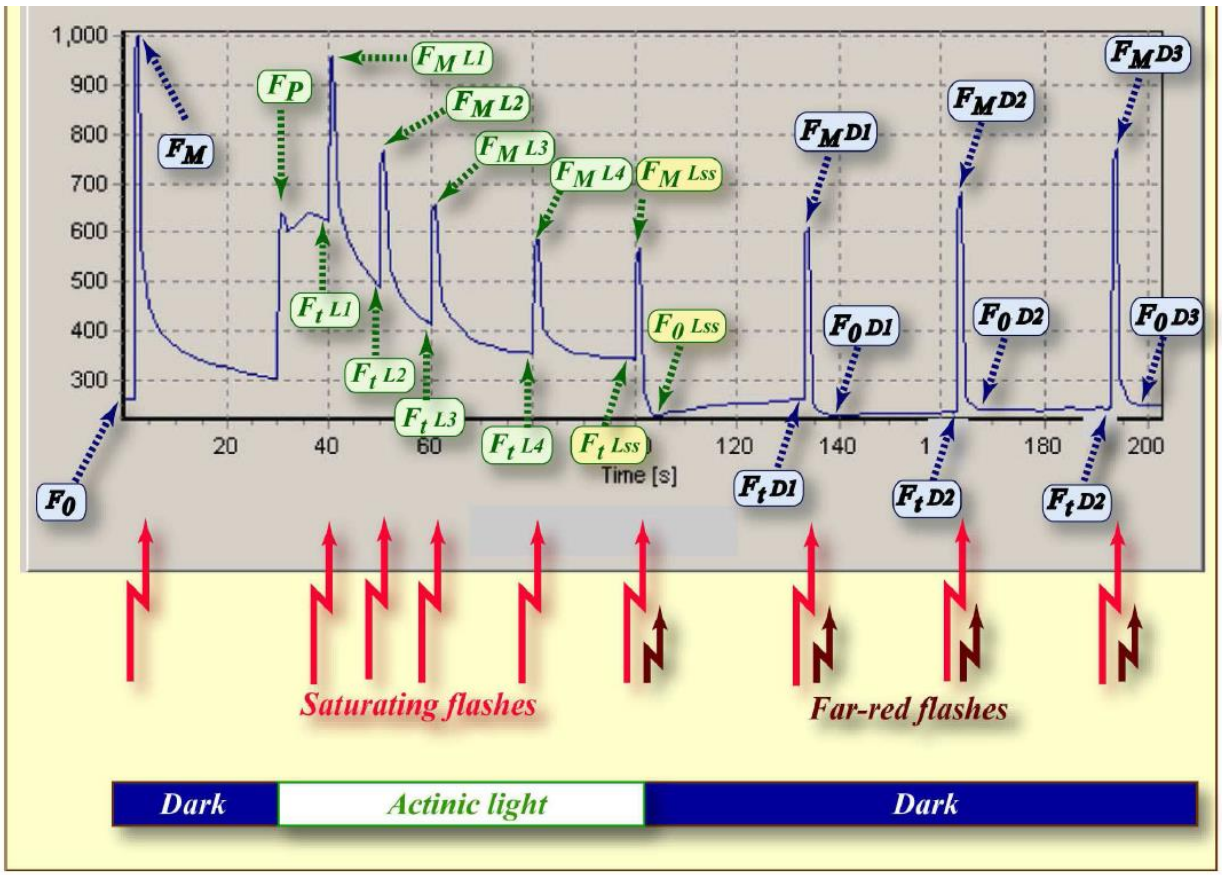

Figure 7.2: Kautsky effect measured in Pulse-Amplitude-Modulated mode (PAM) (FluorCam Software).

Measurements are performed on dark-adapted seedlings; the blue labels mark the fluorescence levels measured either in the dark (F_0, F_M) or during dark relaxation (F_t_Dn, F_M_Dn, F_0_Dn), the green labels mark the fluorescence levels measured during light adaptation (F_t_Ln, F_M_Ln) and the yellow labels show the steady-state fluorescence levels attained in continuous light (F_t_Lss, F_M_Lss, F_0_Lss). The bright-red arrows indicate timing of flashes that transiently saturate the electron transport chain, reducing the plastoquinone pool and Q_A acceptor. The closed reaction centers do not quench fluorescence photochemically, and the fluorescence signal reaches a local maximum that is modulated only by non-photochemical quenching (NPQ): F_M in dark (no NPQ), F_M_Ln during light adaptation, F_M_Lss in light-adapted steady-state, and F_M_Dn during dark adaptation. The dark-red arrows indicate far-red flashes that selectively excite Photosystem I and facilitate effective re-oxidation of the plastoquinone pool and of the Q_A acceptor. The oxidized Q_A acceptor in all PSII reaction centers results in maximum quenching by photochemical charge separation, and a minimum fluorescence signal F_0_Dn that is modulated only by residual non-photochemical quenching (from FluorCam instruction manual).

4. Measurements of respiration and photosynthesis

4.1. Oxygraphy

Measurements of oxygen exchange in 1 mL of Evian natural mineral water containing around 50 mg of seedlings were performed using an Oxygraph electrode system (Hansatech, King's Lynn, UK) calibrated at 25°C, 38°C or 43°C with maximum stirring speed. A halogen cold light source with two fibers, VisiLight CL150 (VWR, Radnor, USA), was used for photosynthesis measurement. It was calibrated at a saturating light of around 800 µmol photons.m^{-2}.s^{-1} (400 for each fiber) using QRT1 Quantitherm (Hansatech) as a light calibration system. A representative oxygraph is presented in Figure 7.1. Respiration was assessed in the second period of dark and maximal net photosynthesis with the saturating light. KCN-resistant respiration was measured after addition of 5 µL KCN at 100 mM (0.5 mM final). Rates were standardized using total chlorophyll amount in each experiment. Seedlings were recovered and pigments were extracted in 1 mL of dimethylformamide at 4°C for at least 24 h. Absorbance at 647 nm and 664 nm were measured from 100 µL of supernatant using a Quartz multi-well plate and a FLUOstar Omega (BMG Labtech, Ortenberg, Germany) spectrophotometer. Total amount of chlorophyll (a+b) was calculated according to Moran (1982) using the formula: total chl = 7.04 A664 + 20.27 A647 (in µg). Statistical analysis was performed using SigmaPlot 11.0 (ANOVA and Dunnett's or Tukey's test).

4.2. Chlorophyll fluorescence

Seedlings were dark-adapted for 30 min before the acquisition of chlorophyll fluorescence. Images of chlorophyll fluorescence from six-well plates were acquired using a PSI Open FluorCam FC 800-O (PSI, Brno, Czech Republic) and a 12-bit dynamic CCD camera with a 512 x 512 pixel resolution. The system included four LED panels divided to two pairs. One pair provided an orange actinic light with a wavelength of 618 nm, with a variable intensity (200-400 µmol.m^{-2}.s^{-1}). The other pair provided a saturating pulse at 455 nm during 0.8 s, with an intensity of up to 3000 µmol.m^{-2}.s^{-1}. The saturating pulse allowed the collection of the maximum fluorescence (F_M) after measurement of F_0 acquisition in the dark-adapted mode. Maximum photosystem II quantum yield was calculated using F_V/F_M in which $F_V=F_M-F_0$. Non-photochemical quenching (NPQ) in the light was estimated by the calculation of $(F_M-F_M^{Lss})/F_M^{Lss}$ after a dark relaxation of 10 s and actinic light exposure of 60 s (5 pulses, last-one: F_M^{Lss}) (Figure 7.2). Statistical analysis was performed using SigmaPlot 11.0 (ANOVA and Dunnett's or Tukey's test).

5. Organelle dynamics

5.1. Live cell imaging

Live cell epifluorescence microscopy was performed using a Zeiss Axio Imager Z2 microscope driven by ZEN software (Zeiss) with 100x Zeiss Plan-Apochromat oil immersion objective (NA 1.4) for the analysis of mitochondrial and ER dynamics. Excitation filters 450-490 m (using LED module 470 nm) and emission filter 500-550 nm were used for GFP fluorescence. The analysis of actin dynamics was performed by confocal laser

scanning microscopy (CLSM) with a Nikon A1 microscope driven by NIS Elements software (Nikon) using Nikon CFI Apo 40x WI objective (NA 1.25). To visualize mitochondria in the tissues of Lifeact-GFP line, seedlings were incubated 20 min in freshly prepared 200 nM tetramethylrhodamine methyl ester (TMRM), which is a fluorescent dye accumulating in energized mitochondria (Brand & Nicholls, 2011). Excitation and emission wavelengths (nm) for the different probes were: mito-GFP, 488/500-550; TMRM, 561/570-620; and chlorophyll autofluorescence, 638/662-737. Live imaging was performed on the same area of cotyledons using sequential acquisition of the three channels. Images were acquired on at least two different areas of the same seedling and at least three different seedlings.

5.2. Quantification of organelle dynamics

For mitochondria and endoplasmic reticulum (ER), stacks of images (66.56 x 66.56 µm) were captured at 2 s intervals for 20 s, with an image size of 1024 x 1024 pixels, giving a pixel size of 0.065 µm. Stacks were processed using IMARIS v8.2 (Bitplane) to enable object identification, tracking and calculation of track speed. Object reconstruction was performed by automatic thresholding using background subtraction (rolling ball of 0.3 µm). Tracking over time was performed using the autoregressive motion algorithm.

ER time stacks were processed using Fiji (Schindelin *et al.*, 2012) to filter noise (Gaussian Blur and background subtraction) and to superimpose two images (25 x 25 µm) of the same field-of-view captured 20 second apart. Colocalisation analysis of these two images was performed using Pearson's correlation coefficient calculated by Coloc 2 plug-in using the Costes method (Costes *et al.*, 2004).

For actin, stacks of images (147.13 x 147.13 µm) were captured at 12 s intervals for 3 min, with an image size of 1024 x 1024 pixels, giving a pixel size of 0.144 µm. Stacks were processed using Fiji (Gaussian blur: 1 and subtract background: 20) and two images (50 x 50 µm) of the same field-of-view captured 2 min apart were superimposed. Colocalisation analysis of these two images was performed using Pearson's correlation coefficient calculated by Coloc 2.

6. Transcriptomic analysis

6.1. RNA extraction and sequencing

Transcriptomic analysis was performed on triplicates samples corresponding to four different conditions:

- C = control (Day 6)
- P = 38°C 30 min (Day 6)
- H = 43°C 30 min (Day 7), using control seedlings
- PH = 43°C 30 min (Day 7), using primed seedlings

Around 100 mg of seedlings were ground in liquid nitrogen using mortar and pestle. RNA extraction was performed using NucleoSpin RNA Plus kit, following manufacturer instructions (Macherey Nagel). A step of on-column DNA digestion was added after the first step of washing with buffer WB1 using 80 µL DNase RNase-free (QIAGEN). RNA quality was checked using Experion automated electrophoresis system (Biorad): all 28S:18S ratios were over 1.5 and RQI>8.5. Samples were sent to BGI (Hong Kong) for RNAseq (Total RNA Resequencing). Ribosomal

RNAs were removed using a RNA depletion kit before cDNA library construction and sequencing using strand-specific long non-coding RNA Illumina HiSeq™ 4000 sequencing with a paired-end read-length of 100 bp (BGI). After removal of low quality reads (data filtering, BGI), mapping was performed with the help of the Bioinfo team at IRHS (Sandra Pelletier & Sylvain Gaillard). Clean reads (>80 M reads of 100 bp per sample) were aligned to the Arabidopsis transcriptome (TAIR10) using Bowtie2 and SAMtools packages. DESeq2 package was used for differential analysis. Transcripts presenting FDR<0.05 and a log2 ratio>1 or <-1 between two conditions were considered as significantly upregulated or downregulated respectively. Gene Ontology Consortium and agriGO v2.0 were used for gene ontology (Mi *et al.*, 2017; Tian *et al.*, 2017), and overrepresentation gene ontology (GO) network was realized with GO_Full function of the BinGO 3.0.3 package in Cytoscape 3.6.0. Subcellular annotation of proteins was performed according to SUBAcon predictor from SUBA 4 database (Hooper *et al.*, 2014, 2017). Venn diagrams were performed using Venn diagram plotter (Department of Energy, PNNL, Richland, WA, USA; https://omics.pnl.gov/software/venn-diagram-plotter).

7. Proteome analysis

Proteomic analysis was performed on four replicates, corresponding to four different conditions:

- C = control before HS (Day 7)
- P = 38°C before HS (Day 7)
- H = 43°C + 2 h recovery 21°C (Day 7), using control seedlings
- PH = 43°C + 2 h recovery 21°C (Day 7), using primed seedlings

Samples of around 200 mg seedlings were ground with two glass beads (3 mm) using a TissueLyser (Qiagen, Hilden) at 30 Hz for 1 min. The powder was suspended using 1.2 mL of 10 % TCA/0.07 % β-mercaptoethanol/cold acetone at -20°C for 1 h. After centrifugation for 20 min at 20 000 g at 4°C, the pellets were rinsed three times with cold acetone/0.07 % β–mercaptoethanol. Pellets were then dried using a miVac QUATTRO concentrator (SP Scientific, Ipswich, UK) and solubilized in a buffer containing 6 M urea, 2 M thiourea, 30 mM Tris pH 8.8, 10 mM dithiothreitol (DTT) and 0.1 % (m/v) ZALS (zwitterionic acid labile surfactant, Proteabio, Morgantown, WV, USA) dissolved in 50 mM ammonium bicarbonate, using 22 µL per mg of pellet. After centrifugation (20 000 g; 20°C) for 20 min, the supernatant was recovered and kept at -80°C until proteomic analysis which was performed at the PAPPSO facility (INRA, Le Moulon, Gif sur Yvette). Protein concentration was determined using Plus One 2D QuantKit (Amersham) and bovine serum albumin (BSA) as a standard. Using 25 µg proteins, reduced cysteine groups were alkylated by incubation in 50 mM iodoacetamide (IAA) in darkness. The protein mixture was diluted to 1:10 in 50 mM ammonium bicarbonate pH 8, to reduce the concentration of urea to less than 1 M. 600 ng sequencing grade modified porcine trypsin (Promega, Charbonnières-les-Bains, France) were added to digest protein at 37°C overnight. Digestion was stopped with trifluoroacetic acid (TFA, final concentration of 1%). Samples were desalted (15 µg) using 96 well Strata™XL 100 µm Polymeric Reversed Phase Plates (Phenomenex, Le Pecq, France). Desalted samples were solubilized in 0.1 % (v/v) formic acid (FA) and 2 % acetonitrile (v/v) (ACN) and were analysed on a HPLC/nanoRSLC Orbitrap tribid Fusion Lumos (Thermo Fisher) spectrometer. Loading buffer contained 2 % ACN and 0.08 % (v/v) TFA. Buffer A was prepared with 2 % ACN and 0.1 % FA

and buffer B with 80 % ACN and 0.1 % FA. 800 ng of proteins were loaded on a 0.3 x 5 mm pre-column with a particle size of 5 µm and a pore size of 100 Å (PepMap 100 C18, Thermo Fisher Scientific, Waltham, MA, USA) and rinsed for 5 min at 20 µL. min^{-1}. Samples were then separated on a 75 µm × 500 mm column with a particle size of 3 µm and a pore size of 100 Å (Acclaim PepMap 100 C18, Thermo Fisher) using a flow of 300 nL. min^{-1}, at 40°C, according to the gradient:

- 1 to 6 % buffer B in buffer A from 0 to 3 min
- 6 to 28 % buffer B in buffer A from 3 to 160 min
- 40 to 98 % buffer B in buffer A from 180 to 185 min
- 98 % buffer B in buffer A from 185 to 195 min
- 98 % to 6 % buffer B in buffer A from 195 to 197 min
- 6 % to 1 % buffer B in buffer A from 197 to 202 min.

Ionization (at 1600 V) and capillary transfer (275°C) were performed using a liquid junction and a capillary probe (SilicaTip™ Emitter, 10 µm, New Objective). Peptide ion analysis was realized with Xcalibur software (Thermo Fisher). The Full MS Orbitrap was set up with a resolution of 120 000, a scan range of 350-1400 m/z, an AGC target of 5e5, a maximum injection time of 54 ms, a profile data type, and a RF lens of 30 %. Parameters for precursor selection were set as follow: TOP speed, 2 s; analysed charge states, 2-4; intensity threshold, 1e4; dynamic exclusion, 60 s; mass precision, ±10 ppm. For MS/MS, the AGC target was 5e4, the maximum injection time 80 ms and the fragmentation mode was HCD with a collision energy of 27 % and a resolution of 30 000.

Raw data were converted to mzXML open format using Proteowizard 3.0.9205 (Kessner *et al.*, 2008). Protein identification and filtering were performed using X!Tandem Alanine (2017.2.1.4) (Craig & Beavis, 2004) and X!Tandem Pipeline 3.4.3 (Langella *et al.*, 2017) by querying MS/MS data against TAIR10 database together with a custom contaminant database (trypsin, keratins). Identified proteins were filtered and grouped using X! Tandem Pipeline according to two criteria: (1) a minimum of two different peptides required with an E-value smaller than 0.01, and (2) a protein E-value (calculated as the product of unique peptide E-values) smaller than 10^{-5}. The false discovery rates (FDRs) at the peptide and protein levels were 0.14 % and 0.2 %, respectively. Relative peptide quantification by peak-area integration on eXtracted ion chromatogram (XIC) was performed using the MassChroQ software (pappso.inra.fr/bioinfo/masschroq/) (Valot *et al.*, 2011). Peptides shared by two or more proteins were removed. Peptides which had more than 10 % of missing data were considered unreproducible and removed. Peptides whose intensity profile deviate from the average profile of the peptides belonging to the same protein (with a coefficient of correlation inferior to 0.5) were also removed. The minimal number of peptides per protein was set to 2. Relative protein abundance was calculated and defined as the sum of peptide intensities considering only (1) reproducible peptides, (2) specific peptides, and (3) correlated peptides belonging to the same protein. Statistical analysis was performed using ANOVA and Tukey's test (glht function of the multcomp R package). When the peptides of a protein were not present or not reproducibly observed in one or more conditions, spectral counting (SC) with a minimum number of spectra set to 5 was used in place of XIC analysis. Statistical analysis of SC was performed using ANOVA on a glm model (Poisson family) and chi-squared test. Venn diagrams were performed using Venny2.0 (Oliveros, 2007). Heatmap of the overlap between transcriptomic and proteomic responses was performed with BAR HeatMapper Plus Tool (http://bbc.botany.utoronto.ca/ntools/cgi-bin/ntools_heatmapper_plus.cgi).

8. Metabolic profiling

Triplicates of around 200 mg seedlings were lyophilized and ground with two glass beads (3 mm) using TissueLyser (Qiagen, Hilden, Germany) at 30 Hz for 1 min. Polar metabolites were extracted with 300 µL methanol/750 µL chloroform/300 µL water. Alpha-aminobutyric acid, adipate and melezitose were used as internal standards for amino acids, organic acids and sugars, respectively. Polar phase was dried using Speedvac evaporator and residue was solubilized in 300 µL water. Standardized volumes of samples were dried and derivatized with 50 µL pyridine/methoxyamine hydrochloride (20 $mg.mL^{-1}$) for 1 h 30 at 30°C in a heating block and then with 50 µL N-tert-butyldimethylsilyl-N-methyltrifluoroacetamide (MTBSTFA) for 30 min at 70°C. Analyses were carried out with a 436-GC coupled to a Simple Quadruple (SQ) SCION MS (Bruker, Billerica, MA, USA). Compounds were separated on a BR5MS column (Bruker; 5 % diphenyl/95 % dimethyl polysiloxane, 30 m × 0.23 mm i.d, 0.25 µm film thickness). The GC was operated in constant pressure mode with helium as carrier gas (1 $mL.min^{-1}$). Injection (0.25 µL) was performed in split mode-4. The elution profile was: 70°C for 5 min, linear gradient of 5°C min^{-1} to 300°C, 300°C for 5 min, resulting in a total run time of 56 min. The injector, MS transfer line and source temperatures were respectively 280°C, 290°C and 220°C. Mass spectra were collected using electron impact (EI) ionization at 70 eV. The GC-MS was operated in the SIM detection mode at mass range m/z 50–650.

For the detection of sugars, samples were diluted to 1:80 and analysed by HPLC at 30°C with 10 % (m/v) NaOH on a Carbopac PA-1 column (Dionex Corp., Sunnyvale, CA, USA) using pulsed amperometric detection, as described by Tetteroo *et al.* (1994). Statistical analysis was performed using R and R Studio (http://www.R-project.org and http://www.rstudio.com/), with ANOVA and HSD.test (Tukey) from agricolae package for posthoc analysis. Principal component analysis (PCA) was performed using FactoMineR package (Lê *et al.*, 2008) on normalized data. Confidence ellipses were drawn using plotellipses function (level=0.95). Heatmap of metabolites on day eight was performed on log-transformed and mean-centred data using the average linkage method based on Euclidean distance of MetaboAnalyst4.0 (Chong *et al.*, 2018). Analysis of metabolic pathways at the transcriptional and proteomic levels was based on KEGG and AraCyc16.0 databases.

Fatty acid profiles in triplicates of around 15 mg lyophilized seedlings were obtained according to Deruyffelaere et al. (2015) with minor modifications. Heptadecanoic acid (C17:0) was used as an internal standard. 2 mL of 2.5 % (v/v) sulphuric acid in methanol were added to the lyophilized samples, which were incubated for 90 min at 80°C during which vortex was carried out every 30 min in the presence of glass beads. After cooling down, addition of 2 mL of 0.9 % (m/v) NaCl and 3 mL hexane and centrifugation at 1500 g for 5 min at room temperature (RT), fatty acid methyl esters were extracted in the organic phase. Aliquots of 0.5 or 1 µL were injected and analysed by GC-FID (flame ionization detector) on a 30 m x 250 µm x 0.25 µm VF-23ms column (Agilent, Les Ulis, France) with splitless injection mode. The oven was programmed for an initial temperature of 40°C for 1 min followed by a 40°C min^{-1} ramp to 120°C, a step at 120°C for 1 min, a secondary ramp of 3°C min^{-1} to 210°C and a final step at 210°C for 10 min. Fatty acid methyl ester peaks were identified from the retention times obtained for standards and quantified from their areas compared with C17:0 methyl ester peak area. Statistical analysis was performed using SigmaPlot 11.0 (ANOVA and Tukey's test).

9. Western blot

For HSP immunoblotting, seedlings were sampled after 0, 30, 60, 120 min of heat treatment (38°C or 43°C with or without previous acclimation) and after 2 h, 4 h, 6 h or one to ten days of recovery. Around 200 mg seedlings were ground with two glass beads (3 mm) using TissueLyser (Qiagen, Hilden, Germany) at 30 Hz for 1 min. Total proteins were extracted with 500 µL of a grinding buffer containing 50 mM $NaPO_4$ pH 8, 10 mM EDTA, 0.1 % (m/v) Triton X-100, 0.1 % (m/v) sarcosyl, 10 mM DTT, 1 mM phenylmethanesulfonyl fluoride (PMSF) and a cocktail of antiproteases (cOmplete EDTA-free, Roche) by performing three cycles of freeze-thaw-vortex. After centrifugation at 20 000 g for 15 min at 4°C, the supernatant was transferred to a new tube. Protein assay was performed using Bradford Protein Assay (Bio-Rad, Marnes-La-Coquette, France) and BSA as a standard. 15 µg of proteins were denatured with Laemmli buffer (12 mM Tris pH 6.8, 10 % (v/v) glycerol, 0.4% (v/v) SDS, 0.02 % (m/v) bromophenol blue, 0.8 mM DTT) at 90°C for 3 min and separated on 12 % Stain Free Gels (Bio-Rad). After separation, gel activation by UV led to the binding of trihalo compounds present in the gel to Trp residues, which allowed visualization of proteins without staining. Proteins were then blotted for 1 h to polyvinylidene fluoride (PVDF) membrane (Immobilon P^{SQ}, 0.2 µM, Merck KGaA, Darmstadt, Germany) using tank transfer (Mini Trans-Blot Cell, Biorad) with 10 mM N-cyclohexyl-3-aminopropanesulfonic acid (CAPS, pH 11), 10 % EtOH buffer. UV detection was used to check protein transfer. Blots were blocked with 3 % (m/v) milk in TBST buffer (10 mM Tris pH 7.5, 150 mM NaCl, 0.1 % (v/v) Tween 20) for 1 h at room temperature (RT) with agitation and incubated with the primary antibody at an appropriate dilution in TBST, for 2 h, at RT. All antibodies were purchased from Agrisera (Vännäs, Sweden). Anti-HSP101, anti-cytosolic HSP70 and anti-HSP17.6 antibodies were diluted to 1:3000 and other antibodies (anti-chloroplastic HSP70, anti-HSP21, anti-HSP26.5) to 1:1000. The antibody solutions were decanted and blots were rinsed briefly twice, then washed three times for 10 min in TBST at RT with agitation. They were incubated with the secondary antibody (goat anti-rabbit IgG horse radish peroxidase conjugated, from Agrisera) diluted to 1:75 000 in TBST for 45 min at RT with agitation, then washed as above. Total proteins were visualized on the membranes using UV detection (Stain Free technology, Biorad), before developing membranes for 5 min with Western Clarity ECL (Bio-Rad), using a ChemiDoc XRS+ imaging system (Bio-Rad).

For immunodetection of HSPs remaining in the tissue pellets after protein extraction, 100 µL of 5X Laemmli buffer and 400 µL grinding buffer were added to the pellet. After vortex for 3x1 min and centrifugation at 20 000 g for 15 min at 4°C, the supernatant was transferred to a new tube and processed as above. 30 µL of each protein extract was loaded on 12 % Stain Free Gels (Bio-Rad) and immunodetection was performed as described above. Semi-quantification of HSPs on western blots was performed using the normalization tool of ImageLab software (Bio-Rad): RbcL protein was used as a reference band on Stain free images for normalization of chemiluminescence signals. For each protein, intensities in each sample were expressed as the percentage of maximal intensity detected on the same membrane. Statistical analysis was performed with SigmaPlot 11.0 (ANOVA and Tukey's test).

References

Adamo A, Pinney JW, Kunova A, Westhead DR, Meyer P. **2008**. Heat stress enhances the accumulation of polyadenylated mitochondrial transcripts in *Arabidopsis thaliana*. *PLoS ONE* **3**: e2889.

Ahammed GJ, Li X, Zhou J, Zhou Y-H, Yu J-Q. **2016**. Role of hormones in plant adaptation to heat stress. In: Ahammed GJ, Yu J-Q, eds. Plant hormones under challenging environmental factors. Dordrecht: Springer Netherlands, 1–21.

Ahuja I, de Vos RCH, Bones AM, Hall RD. **2010**. Plant molecular stress responses face climate change. *Trends in Plant Science* **15**: 664–674.

Van Aken O, Pogson BJ. **2017**. Convergence of mitochondrial and chloroplastic ANAC017/PAP-dependent retrograde signalling pathways and suppression of programmed cell death. *Cell Death and Differentiation* **24**: 955–960.

Akerfelt M, Morimoto RI, Sistonen L. **2010**. Heat shock factors: integrators of cell stress, development and lifespan. *Nature Reviews Molecular Cell Biology* **11**: 545–55.

Alam MN, Zhang L, Yang L, Islam MR, Liu Y, Luo H, Yang P, Wang Q, Chan Z. **2018**. Transcriptomic profiling of tall fescue in response to heat stress and improved thermotolerance by melatonin and 24-epibrassinolide. *BMC Genomics* **19**: 224.

Allakhverdiev SI, Kreslavski VD, Klimov V V., Los DA, Carpentier R, Mohanty P. **2008**. Heat stress: an overview of molecular responses in photosynthesis. *Photosynthesis Research* **98**: 541–550.

Allen JF, de Paula WBM, Puthiyaveetil S, Nield J. **2011**. A structural phylogenetic map for chloroplast photosynthesis. *Trends in Plant Science* **16**: 645–655.

Amuthan G, Biswas G, Zhang S-Y, Klein-Szanto A, Vijayasarathy C, Avadhani NG. **2001**. Mitochondria-to-nucleus stress signaling induces phenotypic changes, tumor progression and cell invasion. *The EMBO Journal* **20**: 1910–1920.

Araújo WL, Nunes-Nesi A, Fernie AR. **2014**. On the role of plant mitochondrial metabolism and its impact on photosynthesis in both optimal and sub-optimal growth conditions. *Photosynthesis Research* **119**: 141–156.

Arimura S. **2018**. Fission and fusion of plant mitochondria, and genome maintenance. *Plant Physiology* **176**: 152–161.

Asseng S, Foster I, Turner NC. **2011**. The impact of temperature variability on wheat yields. *Global Change Biology* **17**: 997–1012.

Atkin OK, Bruhn D, Hurry VM, Tjoelker MG. **2005**. Evans Review No. 2 - The hot and the cold: unravelling the variable response of plant respiration to temperature. *Functional Plant Biology* **32**: 87–105.

Atkin OK, Evans JR, Ball MC, Lambers H, Pons TL. **2000**. Leaf respiration of snow gum in the light and dark. Interactions between temperature and irradiance. *Plant Physiology* **122**: 915–924.

Atkin OK, Macherel D. **2009**. The crucial role of plant mitochondria in orchestrating drought tolerance. *Annals of Botany* **103**: 581–597.

Atkin OK, Tjoelker MG. **2003**. Thermal acclimation and the dynamic response of plant respiration to temperature. *Trends in Plant Science* **8**: 343–351.

Baker NR. **2008**. Chlorophyll fluorescence: a probe of photosynthesis in vivo. *Annual Review of Plant Biology*

59: 89–113.

Baniwal SK, Kwan YC, Scharf KD, Nover L. **2007**. Role of heat stress transcription factor HsfA5 as specific repressor of HsfA4. *Journal of Biological Chemistry* **282**: 3605–3613.

Banti V, Mafessoni F, Loreti E, Alpi A, Perata P. **2010**. The heat-inducible transcription factor HsfA2 enhances anoxia tolerance in Arabidopsis. *Plant Physiology* **152**: 1471–1483.

Banzet N, Richaud C, Deveaux Y, Kazmaier M, Gagnon J, Triantaphylidès C. **1998**. Accumulation of small heat shock proteins, including mitochondrial HSP22, induced by oxidative stress and adaptive response in tomato cells. *The Plant Journal* **13**: 519–527.

Barah P, Jayavelu ND, Mundy J, Bones AM. **2013**. Genome scale transcriptional response diversity among ten ecotypes of *Arabidopsis thaliana* during heat stress. *Frontiers in Plant Science* **4**: 532.

Van Bavel J. **2013**. The world population explosion: causes, backgrounds and projections for the future. *Facts, Views & Vision in ObGyn* **5**: 281–291.

Baxter A, Mittler R, Suzuki N. **2014**. ROS as key players in plant stress signalling. *Journal of Experimental Botany* **65**: 1229–1240.

Bayer-Császár E, Haag S, Jörg A, Glass F, Härtel B, Obata T, Meyer EH, Brennicke A, Takenaka M. **2017**. The conserved domain in MORF proteins has distinct affinities to the PPR and E elements in PPR RNA editing factors. *Biochimica et Biophysica Acta (BBA) - Gene Regulatory Mechanisms* **1860**: 813–828.

Bechtold U, Albihlal WS, Lawson T, Fryer MJ, Sparrow PAC, Richard F, Persad R, Bowden L, Hickman R, Martin C, *et al.* 2013. Arabidopsis HEAT SHOCK TRANSCRIPTION FACTORA1b overexpression enhances water productivity, resistance to drought, and infection. *Journal of Experimental Botany* **64**: 3467–3481.

Begcy K, Mariano ED, Mattiello L, Nunes A V., Mazzafera P, Maia IG, Menossi M. **2011**. An Arabidopsis mitochondrial uncoupling protein confers tolerance to drought and salt stress in transgenic tobacco plants. *PLoS ONE* **6**: e23776.

Belhadj Slimen I, Najar T, Ghram A, Dabbebi H, Ben Mrad M, Abdrabbah M. **2014**. Reactive oxygen species, heat stress and oxidative-induced mitochondrial damage. A review. *International Journal of Hyperthermia* **30**: 513–523.

Benamar A, Pierart A, Baecker V, Avelange-Macherel MH, Rolland A, Gaudichon S, di Gioia L, Macherel D. **2013**. Simple system using natural mineral water for high-throughput phenotyping of *Arabidopsis thaliana* seedlings in liquid culture. *International Journal of High Throughput Screening* **4**: 1–15.

Berry J, Bjorkman O, Björkman O. **1980**. Photosynthetic response and adaptation to temperature in higher plants. *Annual Review of Plant Physiology* **31**: 491–543.

Bhartu K, Von Koskull-Döring P, Bharti S, Pravir K, Tintschl-Körbitzer A, Treuter E, Nover L. **2004**. Tomato heat stress transcription factor HsfB1 represents a novel type of general transcription coactivator with a histone-like motif interacting with the plant CREB binding protein ortholog HAC1. *The Plant Cell* **16**: 1521–1535.

Bheemanahalli R, Sathishraj R, Manoharan M, Sumanth HN, Muthurajan R, Ishimaru T, Krishna JSV. **2017**. Is early morning flowering an effective trait to minimize heat stress damage during flowering in rice? *Field Crops Research* **203**: 238–242.

Bielczynski LW, Łącki MK, Hoefnagels I, Gambin A, Croce R. **2017**. Leaf and plant age affects photosynthetic performance and photoprotective capacity. *Plant Physiology* **175**: 1634–1648.

Bita CE, Gerats T. **2013**. Plant tolerance to high temperature in a changing environment: scientific fundamentals

and production of heat stress-tolerant crops. *Frontiers in Plant Science* **4**: 273.

Bitrián M, Zarza X, Altabella T, Tiburcio AF, Alcázar R. **2012**. Polyamines under abiotic stress: metabolic crossroads and hormonal crosstalks in plants. *Metabolites* **2**: 516–528.

Blanco NE, Guinea-Díaz M, Whelan J, Strand A. **2014**. Interaction between plastid and mitochondrial retrograde signalling pathways during changes to plastid redox status. *Philosophical transactions of the Royal Society of London. Series B, Biological sciences* **369**: 20130231.

Bobik K, Burch-Smith TM. **2015**. Chloroplast signaling within, between and beyond cells. *Frontiers in Plant Science* **6**: 781.

Boca S, Koestler F, Ksas B, Chevalier A, Leymarie J, Fekete A, Mueller MJ, Havaux M. **2014**. Arabidopsis lipocalins AtCHL and AtTIL have distinct but overlapping functions essential for lipid protection and seed longevity. *Plant, Cell and Environment* **37**: 368–381.

De Boeck HJ, Van De Velde H, De Groote T, Nijs I. **2016**. Ideas and perspectives: Heat stress: more than hot air. *Biogeosciences* **13**: 5821–5825.

Bokszczanin KL, Fragkostefanakis S. **2013**. Perspectives on deciphering mechanisms underlying plant heat stress response and thermotolerance. *Frontiers in Plant Science* **4**: 315.

Borghouts C, Benguria A, Wawryn J, Jazwinski SM. **2004**. Rtg2 protein links metabolism and genome stability in yeast longevity. *Genetics* **166**: 765–777.

Brand MD, Nicholls DG. **2011**. Assessing mitochondrial dysfunction in cells. *Biochemical Journal* **437**: 575.1-575.

Brzezinka K, Altmann S, Bäurle I. **2018**. BRUSHY1/TONSOKU/MGOUN3 is required for heat stress memory. *Plant, Cell and Environment*: 1–11.

Brzezinka K, Altmann S, Czesnick H, Nicolas P, Gorka M, Benke E, Kabelitz T, Jähne F, Graf A, Kappel C, *et al.* 2016. Arabidopsis FORGETTER1 mediates stress-induced chromatin memory through nucleosome remodeling. *eLife* **5**: e17061.

Bukhov NG, Wiese C, Neimanis S, Heber U. **1999**. Heat sensitivity of chloroplasts and leaves: Leakage of protons from thylakoids and reversible activation of cyclic electron transport. *Photosynthesis Research* **59**: 81–93.

Bunce JA. **2008**. Acclimation of photosynthesis to temperature in *Arabidopsis thaliana* and *Brassica oleracea*. *Photosynthetica* **46**: 517–524.

Busch W, Wunderlich M, Schöffl F. **2004**. Identification of novel heat shock factor-dependent genes and biochemical pathways in *Arabidopsis thaliana*. *The Plant Journal* **41**: 1–14.

Caldana C, Degenkolbe T, Cuadros-Inostroza A, Klie S, Sulpice R, Leisse A, Steinhauser D, Fernie AR, Willmitzer L, Hannah MA. **2011**. High-density kinetic analysis of the metabolomic and transcriptomic response of Arabidopsis to eight environmental conditions. *The Plant Journal* **67**: 869–884.

Chan KX, Phua SY, Crisp P, McQuinn R, Pogson BJ. **2016**. Learning the languages of the chloroplast: retrograde signaling and beyond. *Annual Review of Plant Biology* **67**: 25–53.

Chang CY, Lin WD, Tu SL. **2014**. Genome-wide analysis of heat-sensitive alternative splicing in *Physcomitrella patens*. *Plant Physiology* **165**: 826–840.

Chantarachot T, Bailey-Serres J. **2018**. Polysomes, stress granules and processing bodies: a dynamic

triumvirate controlling cytoplasmic mRNA fate and function. *Plant Physiology* **176**: 254–269.

Charng Y, Liu H, Liu N, Chi W, Wang C, Chang S, Wang T. **2007**. A heat-inducible transcription factor, HsfA2, is required for extension of acquired thermotolerance in Arabidopsis. *Plant Physiology* **143**: 251–262.

Charng Y -y., Liu H, Liu N, Hsu F, Ko S. **2006**. Arabidopsis Hsa32, a novel heat shock protein, is essential for acquired thermotolerance during long recovery after acclimation. *Plant Physiology* **140**: 1297–1305.

Chen S-T, He N-Y, Chen J-H, Guo F-Q. **2017**. Identification of core subunits of photosystem II as action sites of HSP21, which is activated by the GUN5-mediated retrograde pathway in Arabidopsis. *The Plant Journal* **89**: 1106–1118.

Chen H, Lai Z, Shi J, Xiao Y, Chen Z, Xu X. **2010**. Roles of Arabidopsis WRKY18, WRKY40 and WRKY60 transcription factors in plant responses to abscisic acid and abiotic stress. *BMC Plant Biology* **10**: 281.

Chen L, Song Y, Li S, Zhang L, Zou C, Yu D. **2012**. The role of WRKY transcription factors in plant abiotic stresses. *Biochimica et Biophysica Acta (BBA) - Gene Regulatory Mechanisms* **1819**: 120–128.

Cherkasov V, Grousl T, Theer P, Vainshtein Y, Gläßer C, Mongis C, Kramer G, Stoecklin G, Knop M, Mogk A, *et al.* 2015. Systemic control of protein synthesis through sequestration of translation and ribosome biogenesis factors during severe heat stress. *FEBS Letters* **589**: 3654–3664.

Chi W, Feng P, Ma J, Zhang L. **2015**. Metabolites and chloroplast retrograde signaling. *Current Opinion in Plant Biology* **25**: 32–38.

Chi WT, Fung RWM, Liu HC, Hsu CC, Charng YY. **2009**. Temperature-induced lipocalin is required for basal and acquired thermotolerance in Arabidopsis. *Plant, Cell and Environment* **32**: 917–927.

Chong J, Soufan O, Li C, Caraus I, Li S, Bourque G, Wishart DS, Xia J. **2018**. MetaboAnalyst 4.0: towards more transparent and integrative metabolomics analysis. *Nucleic Acids Research* **46**: W486–W494.

Chung T, Phillips AR, Vierstra RD. **2010**. ATG8 lipidation and ATG8-mediated autophagy in Arabidopsis require ATG12 expressed from the differentially controlled ATG12A and ATG12B loci. *The Plant Journal* **62**: 483–493.

Ciais P, Reichstein M, Viovy N, Granier A, Ogée J, Allard V, Aubinet M, Buchmann N, Bernhofer C, Carrara A, *et al.* 2005. Europe-wide reduction in primary productivity caused by the heat and drought in 2003. *Nature* **437**: 529–533.

Clarke SM, Cristescu SM, Miersch O, Harren FJM, Wasternack C, Mur LAJ. **2009**. Jasmonates act with salicylic acid to confer basal thermotolerance in *Arabidopsis thaliana*. *New Phytologist* **182**: 175–187.

Clarke SM, Mur LAJ, Wood JE, Scott IM. **2004**. Salicylic acid dependent signaling promotes basal thermotolerance but is not essential for acquired thermotolerance in *Arabidopsis thaliana*. *The Plant Journal* **38**: 432–447.

Colombo M, Tadini L, Peracchio C, Ferrari R, Pesaresi P. **2016**. GUN1, a jack-of-all-trades in chloroplast protein homeostasis and signaling. *Frontiers in Plant Science* **7**: 1427.

Coote PJ, Cole MB, Jones M V. 1991. Induction of increased thermotolerance in *Saccharomyces cerevisiae* may be triggered by a mechanism involving intracellular pH. *Journal of General Microbiology* **137**: 1701–1708.

Costes S V., Daelemans D, Cho EH, Dobbin Z, Pavlakis G, Lockett S. **2004**. Automatic and quantitative measurement of protein-protein colocalization in live cells. *Biophysical Journal* **86**: 3993–4003.

Craig R, Beavis RC. **2004**. TANDEM: Matching proteins with tandem mass spectra. *Bioinformatics* **20**: 1466–1467.

Crisp PA, Ganguly D, Eichten SR, Borevitz JO, Pogson BJ. **2016**. Reconsidering plant memory: Intersections

between stress recovery, RNA turnover, and epigenetics. *Science Advances* **2**: e1501340.

Cvikrová M, Gemperlová L, Dobrá J, Martincová O, Prásil IT, Gubis J, Vanková R. **2012**. Effect of heat stress on polyamine metabolism in proline-over-producing tobacco plants. *Plant Science* **182**: 49–58.

Cvjetko P, Balen B, Peharec Štefanić P, Debogović L, Pavlica M, Klobučar GIV. **2014**. Dynamics of heat-shock induced DNA damage and repair in senescent tobacco plants. *Biologia Plantarum* **58**: 71–79.

Czarnecka-Verner E, Pan S, Salem T, Gurley WB. **2004**. Plant class B HSFs inhibit transcription and exhibit affinity for TFIIB and TBP. *Plant Molecular Biology* **56**: 57–75.

Davletova S, Rizhsky L, Liang H, Shengqiang Z, Oliver DJ, Coutu J, Shulaev V, Schlauch K, Mittler R. **2005**. Cytosolic ascorbate peroxidase 1 is a central component of the reactive oxygen gene network of Arabidopsis. *The Plant Cell* **17**: 268–281.

Dell'Aglio E, Boycheva S, Fitzpatrick TB. **2017**. The pseudoenzyme PDX1.2 sustains vitamin B6 biosynthesis as a function of heat stress. *Plant Physiology* **174**: 2098–2112.

Deng Y, Humbert S, Liu J-X, Srivastava R, Rothstein SJ, Howell SH. **2011**. Heat induces the splicing by IRE1 of a mRNA encoding a transcription factor involved in the unfolded protein response in Arabidopsis. *Proceedings of the National Academy of Sciences* **108**: 7247–7252.

Deryng D, Conway D, Ramankutty N, Price J, Warren R. **2014**. Global crop yield response to extreme heat stress under multiple climate change futures. *Environmental Research Letters* **9**: 034011.

Dhaubhadel S, Browning KS, Gallie DR, Krishna P. **2002**. Brassinosteroid functions to protect the translational machinery and heat-shock protein synthesis following thermal stress. *The Plant Journal* **29**: 681–691.

Dhaubhadel S, Chaudhary S, Dobinson KF, Krishna P. **1999**. Treatment with 24-epibrassinololide, a brassinostreroid, increases the basic thermotolerance of Brassica napus and tomato seedling. *Plant Molecular Biology* **40**: 333–342.

Dickinson PJ, Kumar M, Martinho C, Yoo SJ, Lan H, Artavanis G, Charoensawan V, Schöttler MA, Bock R, Jaeger KE, *et al.* 2018. Chloroplast signaling gates thermotolerance in Arabidopsis. *Cell Reports* **22**: 1657–1665.

Dinakar C, Vishwakarma A, Raghavendra AS, Padmasree K. **2016**. Alternative oxidase pathway optimizes photosynthesis during osmotic and temperature stress by regulating cellular ROS, malate valve and antioxidative systems. *Frontiers in Plant Science* **7**: 68.

Divi UK, Rahman T, Krishna P. **2010**. Brassinosteroid-mediated stress tolerance in Arabidopsis shows interactions with abscisic acid, ethylene and salicylic acid pathways. *BMC Plant Biology* **10**: 151.

Downs CA, Heckathorn SA. **1998**. The mitochondrial small heat-shock protein protects NADH:ubiquinone oxidoreductase of the electron transport chain during heat stress in plants. *FEBS letters* **430**: 246–250.

Driedonks N, Xu J, Peters JL, Park S, Rieu I. **2015**. Multi-level interactions between heat shock factors, heat shock proteins, and the redox system regulate acclimation to heat. *Frontiers in Plant Science* **6**: 999.

Dusenge ME, Duarte AG, Way DA. **2019**. Plant carbon metabolism and climate change: elevated CO_2 and temperature impacts on photosynthesis, photorespiration and respiration. *New Phytologist* **221**: 32–49.

Dutta S, Mohanty S, Tripathy BC. **2009**. Role of temperature stress on chloroplast biogenesis and protein import in pea. *Plant Physiology* **150**: 1050–1061.

Dyall SD, Brown MT, Johnson PJ. **2004**. Ancient invasions: from endosymbionts to organelles. *Science* **304**: 253–257.

Easterling, W.E., Aggarwal, P.K., Batima, P., Brander, K.M., Erda, L., Howden, S.M., Kirilenko, A., Morton, J., Soussana, J.-F., Schmidhuber, J. and Tubiello FN. **2007**. Food, fibre and forest products. In: Parry ML, Canziani OF, Palutikof JP, Linden PJ van der, Hanson CE, eds. Climate Change 2007: Impacts, Adaptation and Vulnerability. Contribution of Working Group II to the Fourth Assessment Report of the Intergovernmental Panel on Climate Change. Cambridge, UK: Cambridge University Press, 273–313.

Echevarría-Zomeño S, Fernández-Calvino L, Castro-Sanz AB, López JA, Vázquez J, Castellano MM. **2016**. Dissecting the proteome dynamics of the early heat stress response leading to plant survival or death in Arabidopsis. *Plant, Cell & Environment* **39**: 1264–1278.

Erlejman AG, Lagadari M, Toneatto J, Piwien-Pilipuk G, Galigniana MD. **2014**. Regulatory role of the 90-kDa-heat-shock protein (Hsp90) and associated factors on gene expression. *Biochimica et Biophysica Acta (BBA) - Gene Regulatory Mechanisms* **1839**: 71–87.

Ewald R, Hoffmann C, Florian A, Neuhaus E, Fernie AR, Bauwe H. **2014**. Lipoate-protein ligase and octanoyltransferase are essential for protein lipoylation in mitochondria of Arabidopsis. *Plant Physiology* **165**: 978–990.

Falcone DL, Ogas JP, Somerville CR. **2004**. Regulation of membrane fatty acid composition by temperature in mutants of Arabidopsis with alterations in membrane lipid composition. *BMC Plant Biology* **4**: 17.

Fan T, Wang R, Xiang Y, An L, Cao S. **2016**. Heat stress induces actin cytoskeletal reorganization and transcript profiles of vegetative profilins and actin depolymerizing factors (ADFs) in Arabidopsis. *Acta Physiologiae Plantarum* **38**: 37.

Fernie AR, Carrari F, Sweetlove LJ. **2004**. Respiratory metabolism: glycolysis, the TCA cycle and mitochondrial electron transport. *Current Opinion in Plant Biology* **7**: 254–261.

Finka A, Cuendet AFH, Maathuis FJM, Saidi Y, Goloubinoff P. **2012**. Plasma membrane cyclic nucleotide gated calcium channels control land plant thermal sensing and acquired thermotolerance. *The Plant Cell* **24**: 3333–3348.

Finka A, Mattoo RUH, Goloubinoff P. **2016**. Experimental milestones in the discovery of molecular chaperones as polypeptide unfolding enzymes. *Annual Review of Biochemistry* **85**: 715–742.

Firon N, Pressman E, Meir S, Khoury R, Altahan L. **2012**. Ethylene is involved in maintaining tomato (*Solanum lycopersicum*) pollen quality under heat-stress conditions. *AoB Plants* **2012**: pls024.

Fragkostefanakis S, Mesihovic A, Simm S, Paupière MJ, Hu Y, Paul P, Mishra SK, Tschiersch B, Theres K, Bovy A, *et al.* 2016. Hsfa2 controls the activity of developmentally and stress-regulated heat stress protection mechanisms in tomato male reproductive tissues. *Plant Physiology* **170**: 2461–2477.

Furbank RT, Tester M. **2011**. Phenomics – technologies to relieve the phenotyping bottleneck. *Trends in Plant Science* **16**: 635–644.

Gao H, Brandizzi F, Benning C, Larkin RM. **2008**. A membrane-tethered transcription factor defines a branch of the heat stress response in *Arabidopsis thaliana*. *Proceedings of the National Academy of Sciences* **105**: 16398–16403.

Gao F, Han X, Wu J, Zheng S, Shang Z, Sun D, Zhou R, Li B. **2012**. A heat-activated calcium-permeable channel - Arabidopsis cyclic nucleotide-gated ion channel 6 - is involved in heat shock responses. *The Plant Journal*

70: 1056–1069.

Gao K, Liu YL, Li B, Zhou RG, Sun DY, Zheng SZ. **2014**. Arabidopsis thaliana phosphoinositide-specific phospholipase C isoform 3 (AtPLC3) and AtPLC9 have an additive effect on thermotolerance. *Plant and Cell Physiology* **55**: 1873–1883.

Garagounis C, Kostaki KI, Hawkins TJ, Cummins I, Fricker MD, Hussey PJ, Hetherington AM, Sweetlove LJ. **2017**. Microcompartmentation of cytosolic aldolase by interaction with the actin cytoskeleton in Arabidopsis. *Journal of Experimental Botany* **68**: 885–898.

Gechev TS, Hille J. **2005**. Hydrogen peroxide as a signal controlling plant programmed cell death. *Journal of Cell Biology* **168**: 17–20.

Gidda SK, Park S, Pyc M, Yurchenko O, Cai Y, Wu P, Andrews DW, Chapman KD, Dyer JM, Mullen RT. **2016**. Lipid droplet-associated proteins (LDAPs) are required for the dynamic regulation of neutral lipid compartmentation in plant cells. *Plant Physiology* **170**: 2052–2071.

Gill SS, Tuteja N. **2010**. Reactive oxygen species and antioxidant machinery in abiotic stress tolerance in crop plants. *Plant Physiology and Biochemistry* **48**: 909–930.

Goyal M, Asthir B. **2009**. Polyamine catabolism influences antioxidative defense mechanism in shoots and roots of five wheat genotypes under high temperature stress. *Plant Growth Regulation* **60**: 13–25.

Grams TEE, Lautner S, Felle HH, Matyssek R, Fromm J. **2009**. Heat-induced electrical signals affect cytoplasmic and apoplastic pH as well as photosynthesis during propagation through the maize leaf. *Plant, Cell and Environment* **32**: 319–326.

Gray WM, Ostin A, Sandberg G, Romano CP, Estelle M. **1998**. High temperature promotes auxin-mediated hypocotyl elongation in Arabidopsis. *Proceedings of the National Academy of Sciences* **95**: 7197–7202.

Guan Q, Lu X, Zeng H, Zhang Y, Zhu J. **2013**. Heat stress induction of miR398 triggers a regulatory loop that is critical for thermotolerance in Arabidopsis. *The Plant Journal* **74**: 840–851.

Guan Q, Yue X, Zeng H, Zhu J. **2014**. The protein phosphatase RCF2 and its interacting partner NAC019 are critical for heat stress-responsive gene regulation and thermotolerance in Arabidopsis. *The Plant Cell* **26**: 438–53.

Guillaumot D, Lopez-Obando M, Baudry K, Avon A, Rigaill G, Falcon de Longevialle A, Broche B, Takenaka M, Berthomé R, De Jaeger G, *et al.* 2017. Two interacting PPR proteins are major Arabidopsis editing factors in plastid and mitochondria. *Proceedings of the National Academy of Sciences* **114**: 8877–8882.

Guo M, Liu J-H, Ma X, Luo D-X, Gong Z-H, Lu M-H. **2016**. The plant heat stress transcription factors (HSFs): structure, regulation, and function in response to abiotic stresses. *Frontiers in Plant Science* **7**: 114.

Guo K, Wang W, Fan W, Wang Z, Zhu M, Tang X, Wu W, Yang X, Shao X, Sun Y, *et al.* 2018. Arabidopsis GAAP1 and GAAP3 modulate the unfolded protein response and the onset of cell death in response to ER stress. *Frontiers in Plant Science* **9**: 348.

Guy C, Kaplan F, Kopka J, Selbig J, Hincha DK. **2008**. Metabolomics of temperature stress. *Physiologia Plantarum* **132**: 220–235.

Haag S, Schindler M, Berndt L, Brennicke A, Takenaka M, Weber G. **2017**. Crystal structures of the *Arabidopsis thaliana* organellar RNA editing factors MORF1 and MORF9. *Nucleic Acids Research* **45**: 4915–4928.

Hachiya T, Ueda N, Kitagawa M, Hanke G, Suzuki A, Hase T, Sakakibara H. **2016**. Arabidopsis root-type

ferredoxin: NADP(H) oxidoreductase 2 is involved in detoxification of nitrite in roots. *Plant and Cell Physiology* **57**: 2440–2450.

Haldimann P, Feller U. **2005**. Growth at moderately elevated temperature alters the physiological response of the photosynthetic apparatus to heat stress in pea (*Pisum sativum* L.) leaves. *Plant, Cell and Environment* **28**: 302–317.

Halliwell B. **1978**. The chloroplast at work A review of modern developments in our understanding of chloroplast metabolism. *Progress in Biophysics and Molecular Biology* **33**: 1–54.

Halter G, Simonetti N, Suguitan C, Helm K, Soroksky J, Waters ER. **2017**. Patterns of thermotolerance, chlorophyll fluorescence, and heat shock gene expression vary among four *Boechera* species and *Arabidopsis thaliana*. *Botany* **95**: 9–27.

Hamilton EW, Heckathorn SA. **2001**. Mitochondrial adaptations to NaCl. Complex I is protected by anti-oxidants and small heat shock proteins, whereas complex II is protected by proline and betaine. *Plant Physiology* **126**: 1266–1274.

Haslbeck M, Vierling E. **2015**. A first line of stress defense: small heat shock proteins and their function in protein homeostasis. *Journal of Molecular Biology* **427**: 1537–1548.

Hatfield JL, Prueger JH. **2015**. Temperature extremes: effect on plant growth and development. *Weather and Climate Extremes* **10**: 4–10.

Hickman MJ, Winston F. **2007**. Heme levels switch the function of Hap1 of *Saccharomyces cerevisiae* between transcriptional activator and transcriptional repressor. *Molecular and Cellular Biology* **27**: 7414–7424.

Higashi Y, Okazaki Y, Myouga F, Shinozaki K, Saito K. **2015**. Landscape of the lipidome and transcriptome under heat stress in *Arabidopsis thaliana*. *Scientific Reports* **5**: 10533.

Higashi Y, Okazaki Y, Takano K, Myouga F, Shinozaki K, Knoch E, Fukushima A, Saito K. **2018**. HEAT INDUCIBLE LIPASE1 remodels chloroplastic monogalactosyldiacylglycerol by liberating α-linolenic acid in Arabidopsis leaves under heat stress. *The Plant Cell* **30**: 1887–1905.

Hilker M, Schwachtje J, Baier M, Balazadeh S, Bäurle I, Geiselhardt S, Hincha DK, Kunze R, Mueller-Roeber B, Rillig MC, *et al.* 2016. Priming and memory of stress responses in organisms lacking a nervous system. *Biological Reviews* **91**: 1118–1133.

Hong SW, Vierling E. **2000**. Mutants of *Arabidopsis thaliana* defective in the acquisition of tolerance to high temperature stress. *Proceedings of the National Academy of Sciences* **97**: 4392–4397.

Honig A, Avin-Wittenberg T, Ufaz S, Galili G. **2012**. A new type of compartment, defined by plant-specific Atg8-interacting proteins, is induced upon exposure of Arabidopsis plants to carbon starvation. *The Plant Cell* **24**: 288–303.

Hooper CM, Castleden IR, Tanz SK, Aryamanesh N, Millar AH. **2017**. SUBA4 : the interactive data analysis centre for Arabidopsis subcellular protein locations. *Nucleic Acids Research* **45**: 1064–1074.

Hooper CM, Tanz SK, Castleden IR, Vacher MA, Small ID, Millar AH. **2014**. SUBAcon: A consensus algorithm for unifying the subcellular localization data of the Arabidopsis proteome. *Bioinformatics* **30**: 3356–3364.

Hossain M a, Bhattacharjee S, Armin SM, Qian PP, Xin W, Li HY, Burritt DJ, Fujita M, Tran LSP. **2015**. Hydrogen peroxide priming modulates abiotic oxidative stress tolerance: insights from ROS detoxification and scavenging. *Frontiers in Plant Science* **6**: 420.

Hu T, Liu S-Q, Amombo E, Fu J-M. **2015**. Stress memory induced rearrangements of HSP transcription, photosystem II photochemistry and metabolism of tall fescue (*Festuca arundinacea* Schreb.) in response to high-temperature stress. *Frontiers in Plant Science* **6**: 403.

Huang Y, Niu C, Yang C, Jinn T. **2016**. The heat stress factor HSFA6b connects ABA signaling and ABA-mediated heat responses. *Plant Physiology* **172**: 1182–1199.

Hugly S, Kunst L, Browse J, Somerville C. **1989**. Enhanced thermal tolerance of photosynthesis and altered chloroplast ultrastructure in a mutant of Arabidopsis deficient in lipid desaturation. *Plant Physiology* **90**: 1134–1142.

Hüve K, Bichele I, Rasulov B, Niinemets Ü. **2011**. When it is too hot for photosynthesis: Heat-induced instability of photosynthesis in relation to respiratory burst, cell permeability changes and H_2O_2 formation. *Plant, Cell and Environment* **34**: 113–126.

Ikeda M, Mitsuda N, Ohme-Takagi M. **2011**. Arabidopsis HsfB1 and HsfB2b act as repressors of the expression of heat-inducible Hsfs but positively regulate the acquired thermotolerance. *Plant Physiology* **157**: 1243–1254.

Ikeda M, Ohme-Takagi M. **2009**. A novel group of transcriptional repressors in Arabidopsis. *Plant and Cell Physiology* **50**: 970–975.

Ioannidis NE, Cruz J a., Kotzabasis K, Kramer DM. **2012**. Evidence that putrescine modulates the higher plant photosynthetic proton circuit. *PLoS ONE* **7**: e29864.

Islam MS, Niwa Y, Takagi S. **2009**. Light-dependent intracellular positioning of mitochondria in arabidopsis thaliana mesophyll cells. *Plant and Cell Physiology* **50**: 1032–1040.

Islam MS, Takagi S. **2010**. Co-localization of mitochondria with chloroplasts is a light-dependent reversible response. *Plant Signaling and Behavior* **5**: 146–147.

Ito H, Gaubert H, Bucher E, Mirouze M, Vaillant I, Paszkowski J. **2011**. An siRNA pathway prevents transgenerational retrotransposition in plants subjected to stress. *Nature* **472**: 115–120.

Jacob P, Hirt H, Bendahmane A. **2017**. The heat-shock protein/chaperone network and multiple stress resistance. *Plant Biotechnology Journal* **15**: 405–414.

Jaipargas E-A, Barton KA, Mathur N, Mathur J. **2015**. Mitochondrial pleomorphy in plant cells is driven by contiguous ER dynamics. *Frontiers in Plant Science* **6**: 783.

Jang SJ, Shin SH, Yee ST, Hwang B, Im KH, Park KY. **2005**. Effects of abiotic stresses on cell cycle progression in tobacco BY-2 cells. *Molecules and Cells* **20**: 136–141.

Je J, Song C, Hwang JE, Chung WS, Lim CO. **2014**. DREB2C acts as a transcriptional activator of the thermo tolerance-related phytocystatin 4 (AtCYS4) gene. *Transgenic Research* **23**: 109–123.

Jung S. **2004**. Variation in antioxidant metabolism of young and mature leaves of *Arabidopsis thaliana* subjected to drought. *Plant Science* **166**: 459–466.

Jurivich DA, Sistonen L, Kroes RA, Morimoto RI. **1991**. Effect of sodium salicylate on the human heat shock response. *Science* **255**: 1243–1245.

Kadota Y, Shirasu K. **2012**. The HSP90 complex of plants. *Biochimica et Biophysica Acta (BBA) - Molecular Cell Research* **1823**: 689–697.

Kang CH, Lee YM, Park JH, Nawkar GM, Oh HT, Kim MG, Lee SI, Kim WY, Yun D-J, Lee SY. **2016**. Ribosomal P3 protein AtP3B of Arabidopsis acts as both protein and RNA chaperone to increase tolerance of heat

and cold stresses. *Plant, Cell & Environment* **39**: 1631–1642.

Kannan S, Halter G, Renner T, Waters ER. **2018**. Patterns of alternative splicing vary between species during heat stress. *AoB PLANTS* **10**: ply013.

Kantidze OL, Velichko AK, Luzhin A V., Razin S V. 2016. Heat stress-induced DNA damage. *Acta Naturae* **8**: 75–78.

Kaplan F, Kopka J, Haskell D. **2004**. Exploring the temperature-stress metabolome of Arabidopsis. *Plant Physiology* **136**: 4159–4168.

Kaplan F, Sung DY, Haskell D, Riad GS, Popp M, Amaya M, LaBoon A, Kawamura Y, Tominaga Y, Kopka J, *et al.* 2009. Could ethanolic fermentation during cold shock be a novel plant cold stress coping strategy? In: Gusta L, Wisniewski M, Tanino K, eds. Plant cold hardiness: from the laboratory to the field. Wallingford: CAB International, 80–90.

Kast DJ, Dominguez R. **2017**. The cytoskeleton–autophagy connection. *Current Biology* **27**: R318–R326.

Kataoka R, Takahashi M, Suzuki N. **2017**. Coordination between bZIP28 and HSFA2 in the regulation of heat response signals in Arabidopsis. *Plant Signaling and Behavior* **12**: e1376159.

Kaur N, Reumann S, Hu J. **2009**. Peroxisome biogenesis and function. *The Arabidopsis Book* **7**: e0123.

Kazan K. **2015**. Diverse roles of jasmonates and ethylene in abiotic stress tolerance. *Trends in Plant Science* **20**: 219–229.

Kessner D, Chambers M, Burke R, Agus D, Mallick P. **2008**. ProteoWizard: Open source software for rapid proteomics tools development. *Bioinformatics* **24**: 2534–2536.

Keunen E, Peshev D, Vangronsveld J, Van Den Ende W, Cuypers A. **2013**. Plant sugars are crucial players in the oxidative challenge during abiotic stress: Extending the traditional concept. *Plant, Cell and Environment* **36**: 1242–1255.

Khan MS. **2011**. The role of DREB transcription factors in abiotic stress tolerance of plants. *Biotechnology & Biotechnological Equipment* **25**: 2433–2442.

Kim M, Lee U, Small I, des Francs-Small CC, Vierling E. **2012**. Mutations in an Arabidopsis mitochondrial transcription termination factor-related protein enhance thermotolerance in the absence of the major molecular chaperone HSP101. *The Plant Cell* **24**: 3349–3365.

Kim HJ, Morrow G, Westwood JT, Michaud S, Tanguay RM. **2010**. Gene expression profiling implicates OXPHOS complexes in lifespan extension of flies over-expressing a small mitochondrial chaperone, Hsp22. *Experimental Gerontology* **45**: 611–620.

Kim JH, Woo HR, Kim J, Lim PO, Lee IC, Choi SH, Hwang D, Nam HG. **2009**. Trifurcate feed-forward regulation of age-dependent cell death involving miR164 in Arabidopsis. *Science* **323**: 1053–1058.

Kleine T, Leister D. **2016**. Retrograde signaling: organelles go networking. *Biochimica et Biophysica Acta - Bioenergetics* **1857**: 1313–1325.

Kmiecik P, Leonardelli M, Teige M. **2016**. Novel connections in plant organellar signalling link different stress responses and signalling pathways. *Journal of Experimental Botany* **67**: 3793–3807.

Kong SG, Wada M. **2014**. Recent advances in understanding the molecular mechanism of chloroplast photorelocation movement. *Biochimica et Biophysica Acta - Bioenergetics* **1837**: 522–530.

Königshofer H, Tromballa HW, Löppert HG. **2008**. Early events in signalling high-temperature stress in tobacco BY2 cells involve alterations in membrane fluidity and enhanced hydrogen peroxide production. *Plant,*

Cell and Environment **31**: 1771–1780.

von Koskull-Döring P, Scharf KD, Nover L. **2007**. The diversity of plant heat stress transcription factors. *Trends in Plant Science* **12**: 452–457.

Kotak S, Port M, Ganguli A, Bicker F, Von Koskull-Döring P. **2004**. Characterization of C-terminal domains of Arabidopsis heat stress transcription factors (Hsfs) and identification of a new signature combination of plant class a Hsfs with AHA and NES motifs essential for activator function and intracellular localization. *The Plant Journal* **39**: 98–112.

Kotak S, Vierling E, Baumlein H, Koskull-Doring P von. **2007**. A novel transcriptional cascade regulating expression of heat stress proteins during seed development of Arabidopsis. *The Plant Cell* **19**: 182–195.

Krasensky J, Jonak C. **2012**. Drought, salt, and temperature stress-induced metabolic rearrangements and regulatory networks. *Journal of Experimental Botany* **63**: 1593–1608.

Krishna P, Gloor G. **2001**. The Hsp90 family of proteins in *Arabidopsis thaliana*. *Cell Stress and Chaperones* **6**: 238–246.

Kuhn S, Bussemer J, Chigri F, Vothknecht UC. **2009**. Calcium depletion and calmodulin inhibition affect the import of nuclear-encoded proteins into plant mitochondria. *The Plant Journal* **58**: 694–705.

Kumar M, Busch W, Birke H, Kemmerling B, Nürnberger T, Schöffl F. **2009**. Heat shock factors HsfB1 and HsfB2b are involved in the regulation of Pdf1.2 expression and pathogen resistance in Arabidopsis. *Molecular Plant* **2**: 152–165.

Kumar SV, Wigge PA. **2010**. H2A.Z-containing nucleosomes mediate the thermosensory response in Arabidopsis. *Cell* **140**: 136–147.

Kuzmin E V, Karpova O V, Elthon TE, Newton KJ. **2004**. Mitochondrial respiratory deficiencies signal up-regulation of genes for heat shock proteins. *The Journal of Biological Chemistry* **279**: 20672–20677.

Lai LC, Kosorukoff AL, Burke P V., Kwast KE. **2006**. Metabolic-state-dependent remodeling of the transcriptome in response to anoxia and subsequent reoxygenation in Saccharomyces cerevisiae. *Eukaryotic Cell* **5**: 1468–1489.

Lämke J, Bäurle I. **2017**. Epigenetic and chromatin-based mechanisms in environmental stress adaptation and stress memory in plants. *Genome Biology* **18**: 124.

Lämke J, Brzezinka K, Altmann S, Bäurle I. **2016**. A hit-and-run heat shock factor governs sustained histone methylation and transcriptional stress memory. *The EMBO Journal* **35**: 162–175.

Langella O, Valot B, Balliau T, Blein-Nicolas M, Bonhomme L, Zivy M. **2017**. X!TandemPipeline: a tool to manage sequence redundancy for protein inference and phosphosite identification. *Journal of Proteome Research* **16**: 494–503.

Larkindale J, Hall JD, Knight MR, Vierling E, Larkindale J., Hall J.D., Knight M.R., E. V. **2005**. Heat stress phenotypes of Arabidopsis mutants implicate multiple signaling pathways in the acquisition of thermotolerance. *Plant Physiology* **138**: 882–897.

Larkindale J, Huang B. **2004**. Thermotolerance and antioxidant systems in *Agrostis stolonifera*: Involvement of salicylic acid, abscisic acid, calcium, hydrogen peroxide, and ethylene. *Journal of Plant Physiology* **161**: 405–413.

Larkindale J, Huang B. **2005**. Effects of abscisic acid, salicylic acid, ethylene and hydrogen peroxide in

thermotolerance and recovery for creeping bentgrass. *Plant Growth Regulation* **47**: 17–28.

Larkindale J, Knight M. **2002**. Protection against heat stress-induced oxidative damage in Arabidopsis involves calcium, abscisic acid, ethylene, and salicylic acid. *Plant Physiology* **128**: 682–695.

Larkindale J, Vierling E. **2007**. Core genome responses involved in acclimation to high temperature. *Plant Physiology* **146**: 748–761.

Lê S, Josse J, Husson F. **2008**. FactoMineR : an R package for multivariate analysis. *Journal of Statistical Software* **25**: 1–18.

Lee SB, Jung SJ, Go YS, Kim HU, Kim JK, Cho HJ, Park OK, Suh MC. **2009**. Two Arabidopsis 3-ketoacyl CoA synthase genes, KCS20 and KCS2/DAISY, are functionally redundant in cuticular wax and root suberin biosynthesis, but differentially controlled by osmotic stress. *The Plant Journal* **60**: 462–475.

Légeret B, Schulz-Raffelt M, Nguyen HM, Auroy P, Beisson F, Peltier G, Blanc G, Li-Beisson Y. **2015**. Lipidomic and transcriptomic analyses of *Chlamydomonas reinhardtii* under heat stress unveil a direct route for the conversion of membrane lipids into storage lipids. *Plant, Cell & Environment* **39**: 834–847.

Lewis MR, Lewis WH. **1915**. Mitochondria (and other cytoplasmic structures) in tissue cultures. *American Journal of Anatomy* **17**: 339–401.

Li-Beisson Y, Shorrosh B, Beisson F, Andersson MX, Arondel V, Bates PD, Baud S, Bird D, DeBono A, Durrett TP, *et al.* 2013. Acyl-lipid metabolism. *The Arabidopsis Book* **11**: e0161.

Li M, Berendzen KW, Schöffl F. **2010a**. Promoter specificity and interactions between early and late Arabidopsis heat shock factors. *Plant Molecular Biology* **73**: 559–567.

Li J, Blanchoin L, Staiger CJ. **2015**. Signaling to actin stochastic dynamics. *Annual Review of Plant Biology* **66**: 415–440.

Li M, Doll J, Weckermann K, Oecking C, Berendzen KW, Schöffl F. **2010b**. Detection of in vivo interactions between Arabidopsis class A-HSFs, using a novel BiFC fragment, and identification of novel class B-HSF interacting proteins. *European Journal of Cell Biology* **89**: 126–132.

Li S, Fu Q, Chen L, Huang W, Yu D. **2011**. *Arabidopsis thaliana* WRKY25, WRKY26, and WRKY33 coordinate induction of plant thermotolerance. *Planta* **233**: 1237–1252.

Li S, Fu Q, Huang W, Yu D. **2009**. Functional analysis of an Arabidopsis transcription factor WRKY25 in heat stress. *Plant Cell Reports* **28**: 683–693.

Li S, Liu J, Liu Z, Li X, Wu F, He Y. **2014**. HEAT-INDUCED TAS1 TARGET1 mediates thermotolerance via HEAT STRESS TRANSCRIPTION FACTOR A1a-directed pathways in Arabidopsis. *The Plant Cell* **26**: 1764–1780.

Li C, Lu H, Li W, Yuan M, Fu Y. **2017**. A ROP2-RIC1 pathway fine-tunes microtubule reorganization for salt tolerance in Arabidopsis. *Plant Cell and Environment* **40**: 1127–1142.

Li H, Luan S. **2010**. AtFKBP53 is a histone chaperone required for repression of ribosomal RNA gene expression in Arabidopsis. *Cell Research* **20**: 357–366.

Li L, Yang H, Liu P, Ren W, Wu X, Huang F. **2018**. Combined impact of heat stress and phosphate deficiency on growth and photochemical activity of sheepgrass (*Leymus chinensis*). *Journal of Plant Physiology* **231**: 271–276.

Li S, Zhou X, Chen L, Huang W, Yu D. **2010c**. Functional characterization of *Arabidopsis thaliana* WRKY39 in heat stress. *Molecules and cells* **29**: 475–483.

Liang C, Cheng S, Zhang Y, Sun Y, Fernie AR, Kang K, Panagiotou G, Lo C, Lim BL. **2016**. Transcriptomic,

proteomic and metabolic changes in *Arabidopsis thaliana* leaves after the onset of illumination. *BMC Plant Biology* **16**: 43.

Liang Y, Tan ZM, Zhu L, Niu QK, Zhou JJ, Li M, Chen LQ, Zhang XQ, Ye D. **2013**. MYB97, MYB101 and MYB120 function as male factors that control pollen tube-synergid interaction in *Arabidopsis thaliana* fertilization. *PLoS Genetics* **9**: e1003933.

Liberek K, Lewandowska A, Zietkiewicz S. **2008**. Chaperones in control of protein disaggregation. *The EMBO journal* **27**: 328–335.

Liere K, Weihe A, Börner T. **2011**. The transcription machineries of plant mitochondria and chloroplasts: Composition, function, and regulation. *Journal of Plant Physiology* **168**: 1345–1360.

Lim CJ, Yang KA, Hong JK, Choi JS, Yun D-J, Hong JC, Chung WS, Lee SY, Cho MJ, Lim CO. **2006**. Gene expression profiles during heat acclimation in *Arabidopsis thaliana*. *Journal of Plant Research* **119**: 373–383.

Ling Y, Serrano N, Gao G, Atia M, Mokhtar M, Woo YH, Bazin J, Veluchamy A, Benhamed M, Crespi M, *et al.* 2018. Thermopriming triggers splicing memory in Arabidopsis. *Journal of Experimental Botany* **69**: 2659–2675.

Liu H, Charng Y. **2012**. Acquired thermotolerance independent of heat shock factor A1 (HsfA1), the master regulator of the heat stress response. *Plant Signaling & Behavior* **7**: 547–550.

Liu J, Feng L, Li J, He Z. **2015**. Genetic and epigenetic control of plant heat responses. *Frontiers in Plant Science* **6**: 267.

Liu HT, Gao F, Li GL, Han JL, Liu DL, Sun DY, Zhou RG. **2008**. The calmodulin-binding protein kinase 3 is part of heat-shock signal transduction in *Arabidopsis thaliana*. *The Plant Journal* **55**: 760–773.

Liu H, Lämke J, Lin S, Hung M-J, Liu K-M, Charng Y, Bäurle I. **2018**. Distinct heat shock factors and chromatin modifications mediate the organ-autonomous transcriptional memory of heat stress. *The Plant Journal* **95**: 401–413.

Liu J, Sun N, Liu M, Liu J, Du B, Wang X, Qi X. **2013**. An autoregulatory loop controlling Arabidopsis HsfA2 expression: role of heat shock-induced alternative splicing. *Plant Physiology* **162**: 512–521.

Locato V, Gadaleta C, De Gara L, De Pinto MC. **2008**. Production of reactive species and modulation of antioxidant network in response to heat shock: A critical balance for cell fate. *Plant, Cell and Environment* **31**: 1606–1619.

Logan DC. **2006**. Plant mitochondrial dynamics. *Biochimica et Biophysica Acta (BBA) - Molecular Cell Research* **1763**: 430–441.

Logan DC. **2010**. The dynamic plant chondriome. *Seminars in Cell and Developmental Biology* **21**: 550–557.

Logan DC, Leaver CJ. **2000**. Mitochondria-targeted GFP highlights the heterogeneity of mitochondrial shape, size and movement within living plant cells. *Journal of Experimental Botany* **51**: 865–871.

Logan DC, Scott I, Tobin AK. **2003**. The genetic control of plant mitochondrial morphology and dynamics. *The Plant Journal* **36**: 500–509.

Loveys B, Atkinson L, Sherlock D, Roberts R, Fitter A, Atkin O. **2003**. Thermal acclimation of leaf and root respiration : an investigation comparing inherently fast- and slow- growing plant species. *Global Change Biology* **9**: 895–910.

Ludwig-Müller J, Krishna P, Forreiter C. **2000**. A glucosinolate mutant of Arabidopsis is thermosensitive and

defective in cytosolic Hsp90 expression after heat stress. *Plant Physiology* **123**: 949–958.

Lukoszek R, Feist P, Ignatova Z. **2016**. Insights into the adaptive response of *Arabidopsis thaliana* to prolonged thermal stress by ribosomal profiling and RNA-Seq. *BMC Plant Biology* **16**: 221.

Lv W-T, Lin B, Zhang M, Hua X-J. **2011**. Proline accumulation is inhibitory to Arabidopsis seedlings during heat stress. *Plant Physiology* **156**: 1921–1933.

Ly V, Hatherell A, Kim E, Chan A, Belmonte MF, Schroeder DF. **2013**. Interactions between Arabidopsis DNA repair genes UVH6, DDB1A, and DDB2 during abiotic stress tolerance and floral development. *Plant Science* **213**: 88–97.

Maestri E, Klueva N, Perrotta C, Gulli M, Nguyen HT, Marmiroli N. **2002**. Molecular genetics of heat tolerance and heat shock proteins in cereals. *Plant Molecular Biology* **48**: 667–681.

Maier T, Güell M, Serrano L. **2009**. Correlation of mRNA and protein in complex biological samples. *FEBS Letters* **583**: 3966–3973.

Malerba M, Crosti P, Cerana R. **2010**. Effect of heat stress on actin cytoskeleton and endoplasmic reticulum of tobacco BY-2 cultured cells and its inhibition by Co2+. *Protoplasma* **239**: 23–30.

Manna S. **2015**. An overview of pentatricopeptide repeat proteins and their applications. *Biochimie* **113**: 93–99.

Martin WF, Garg S, Zimorski V. **2015**. Endosymbiotic theories for eukaryote origin. *Philosophical Transactions of the Royal Society B: Biological Sciences* **370**: 20140330.

Martin T, Oswald O, Graham IA. **2002**. Arabidopsis seedling growth, storage lipid mobilization, and photosynthetic gene expression are regulated by carbon:nitrogen availability. *Plant Physiology* **128**: 472–481.

Martínez-Ballesta M del C, Moreno DA, Carvajal M. **2013**. The physiological importance of glucosinolates on plant response to abiotic stress in Brassica. *International Journal of Molecular Sciences* **14**: 11607–11625.

Mathur S, Agrawal D, Jajoo A. **2014**. Photosynthesis: response to high temperature stress. *Journal of Photochemistry and Photobiology B: Biology* **137**: 116–126.

Matin A. **1991**. The molecular basis of carbon- starvation- induced general resistance in *Escherichia coli. Molecular Microbiology* **5**: 3–10.

Mayer RR, Cherry JH, Rhodes D. **1990**. Effects of heat shock on amino acid metabolism of cowpea cells. *Plant physiology* **94**: 796–810.

McLoughlin F, Basha E, Fowler ME, Kim M, Bordowitz J, Katiyar-Agarwal S, Vierling E. **2016**. Class I and II small heat-shock proteins protect protein translation factors during heat stress. *Plant Physiology* **172**: 1221–1236.

Merret R, Carpentier M, Favory J, Picart C, Descombin J, Bousquet-antonelli C, Tillard P, Lejay L, Deragon J, Charng Y, *et al.* 2017. Heat shock protein HSP101 affects the release of ribosomal protein mRNAs for recovery after heat shock. *Plant Physiology* **174**: 1216–1225.

Merret R, Descombin J, Juan Y ting, Favory JJ, Carpentier MC, Chaparro C, Charng Y yung, Deragon JM, Bousquet-Antonelli C. **2013**. XRN4 and LARP1 are required for a heat-triggered mRNA decay pathway involved in plant acclimation and survival during thermal stress. *Cell Reports* **5**: 1279–1293.

Merret R, Nagarajan VK, Carpentier MC, Park S, Favory JJ, Descombin J, Picart C, Charng YY, Green PJ, Deragon JM, *et al.* 2015. Heat-induced ribosome pausing triggers mRNA co-translational decay in *Arabidopsis thaliana*. *Nucleic Acids Research* **43**: 4121–4132.

Mi H, Huang X, Muruganujan A, Tang H, Mills C, Kang D, Thomas PD. **2017**. PANTHER version 11: expanded

annotation data from Gene Ontology and Reactome pathways, and data analysis tool enhancements. *Nucleic Acids Research* **45**: D183–D189.

Millar AH, Whelan J, Soole KL, Day DA. **2011**. Organization and regulation of mitochondrial respiration in plants. *Annual Review of Plant Biology* **62**: 79–104.

Millenaar FF, Lambers H. **2003**. The alternative oxidase: in vivo regulation and function. *Plant Biology* **5**: 2–15.

Mishra RC, Grover A. **2016**. ClpB/Hsp100 proteins and heat stress tolerance in plants. *Critical Reviews in Biotechnology* **36**: 862–874.

Mishra SK, Tripp J, Winkelhaus S, Tschiersch B, Theres K, Nover L, Scharf KD. **2002**. In the complex family of heat stress transcription factors, HsfA1 has a unique role as master regulator of thermotolerance in tomato. *Genes and Development* **16**: 1555–1567.

Mittler R, Finka A, Goloubinoff P. **2012**. How do plants feel the heat? *Trends in Biochemical Sciences* **37**: 118–125.

Mittler R, Vanderauwera S, Gollery M, Van Breusegem F. **2004**. Reactive oxygen gene network of plants. *Trends in Plant Science* **9**: 490–498.

Møller IM. **2001**. Plant mitochondria and oxidative stress: electron transport, NADPH turnover, and metabolism of reactive oxygen species. *Annual Review of Plant Physiology and Plant Molecular Biology* **52**: 561–591.

Møller IM, Sweetlove LJ. **2010**. ROS signalling - specificity is required. *Trends in Plant Science* **15**: 370–374.

Moran R. **1982**. Formulae for determination of chlorophyllous pigments extracted with N,N-dimethylformamide. *Plant Physiology* **69**: 1376–1381.

Moreno AA, Orellana A. **2011**. The physiological role of the unfolded protein response in plants. *Biological Research* **44**: 75–80.

Morrow G, Battistini S, Zhang P, Tanguay RM. **2004a**. Decreased lifespan in the absence of expression of the mitochondrial small heat shock protein Hsp22 in Drosophila. *Journal of Biological Chemistry* **279**: 43382–43385.

Morrow G, Samson M, Michaud S, Tanguay RM. **2004b**. Overexpression of the small mitochondrial Hsp22 extends Drosophila life span and increases resistance to oxidative stress. *The FASEB Journal* **18**: 598–599.

Morrow G, Tanguay RM. **2015**. *Drosophila melanogaster* Hsp22: a mitochondrial small heat shock protein influencing the aging process. *Frontiers in Genetics* **6**: 103.

Mounier N, Arrigo A-P. **2002**. Actin cytoskeleton and small heat shock proteins: how do they interact? *Cell Stress & Chaperones* **7**: 167–176.

Mueller SP, Krause DM, Mueller MJ, Fekete A. **2015**. Accumulation of extra-chloroplastic triacylglycerols in *Arabidopsis* seedlings during heat acclimation. *Journal of Experimental Botany* **66**: 4517–4526.

Mueller SP, Unger M, Guender L, Fekete A, Mueller MJ. **2017**. Diacylglycerol acyltransferase-mediated triacylglyerol synthesis augments basal thermotolerance. *Plant Physiology* **175**: 486–497.

Müller J, Menzel D, Šamaj J. **2007**. Cell-type-specific disruption and recovery of the cytoskeleton in *Arabidopsis thaliana* epidermal root cells upon heat shock stress. *Protoplasma* **230**: 231–242.

Nawkar GM, Lee ES, Shelake RM, Park JH, Ryu SW, Kang CH, Lee SY. **2018**. Activation of the transducers of unfolded protein response in plants. *Frontiers in Plant Science* **9**: 214.

Nelson BK, Cai X, Nebenführ A. **2007**. A multicolored set of in vivo organelle markers for co-localization studies in Arabidopsis and other plants. *The Plant Journal* **51**: 1126–1136.

Ng S, De Clercq I, Van Aken O, Law SR, Ivanova A, Willems P, Giraud E, Van Breusegem F, Whelan J. **2014**. Anterograde and retrograde regulation of nuclear genes encoding mitochondrial proteins during growth, development, and stress. *Molecular Plant* **7**: 1075–1093.

Nguyen AH, Matsui A, Tanaka M, Mizunashi K, Nakaminami K, Hayashi M, Iida K, Toyoda T, Nguyen D Van, Seki M. **2014**. Loss of Arabidopsis 5′-3′ exoribonuclease AtXRN4 function enhances heat stress tolerance of plants subjected to severe heat stress. *Plant and Cell Physiology* **56**: 1762–1772.

Nguyen CC, Nakaminami K, Matsui A, Kobayashi S, Kurihara Y, Toyooka K, Tanaka M, Seki M. **2016**. Oligouridylate binding protein 1b plays an integral role in plant heat stress tolerance. *Frontiers in Plant Science* **7**: 853.

Nguyen HM, Sako K, Matsui A, Suzuki Y, Mostofa MG, Ha C Van, Tanaka M, Tran L-SP, Habu Y, Seki M. **2017**. Ethanol enhances high-salinity stress tolerance by detoxifying reactive oxygen species in *Arabidopsis thaliana* and rice. *Frontiers in Plant Science* **8**: 1001.

Nishizawa A, Yabuta Y, Shigeoka S. **2008**. Galactinol and raffinose constitute a novel function to protect plants from oxidative damage. *Plant Physiology* **147**: 1251–1263.

Nogales E. **2000**. Structural insights into microtubule function. *Annual Review of Biochemistry* **69**: 277–302.

Noguchi K, Yoshida K. **2008**. Interaction between photosynthesis and respiration in illuminated leaves. *Mitochondrion* **8**: 87–99.

Nover L, Bharti K, Döring P, Mishra SK, Ganguli A, Scharf KD. **2001**. Arabidopsis and the heat stress transcription factor world: how many heat stress transcription factors do we need? *Cell Stress & Chaperones* **6**: 177–189.

Nover L, Scharf KD, Neumann D. **1989**. Cytoplasmic heat shock granules are formed from precursor particles and are associated with a specific set of mRNAs. *Molecular and cellular biology* **9**: 1298–1308.

Obata T, Fernie AR. **2012**. The use of metabolomics to dissect plant responses to abiotic stresses. *Cellular and Molecular Life Sciences* **69**: 3225–3243.

Ohama N, Sato H, Shinozaki K, Yamaguchi-Shinozaki K. **2017**. Transcriptional regulatory network of plant heat stress response. *Trends in Plant Science* **22**: 53–65.

Oikawa K, Yamasato A, Kong S-G, Kasahara M, Nakai M, Takahashi F, Ogura Y, Kagawa T, Wada M. **2008**. Chloroplast outer envelope protein CHUP1 is essential for chloroplast anchorage to the plasma membrane and chloroplast movement. *Plant Physiology* **148**: 829–842.

Okada K, Kasahara H, Yamaguchi S, Kawaide H, Kamiya Y, Nojiri H, Yamane H. **2008**. Genetic evidence for the role of isopentenyl diphosphate isomerases in the mevalonate pathway and plant development in Arabidopsis. *Plant and Cell Physiology* **49**: 604–616.

Oliveros J. **2007**. VENNY. An interactive tool for comparing lists with Venn diagrams. : http://bioinfogp.cnb.csic.es/tools/venny/index.htm.

Osteryoung KW, Pyke KA. **2014**. Division and dynamic morphology of plastids. *Annual Review of Plant Biology* **65**: 443–472.

Paila YD, Richardson LGL, Schnell DJ. **2015**. New insights into the mechanism of chloroplast protein import and its integration with protein quality control, organelle biogenesis and development. *Journal of Molecular Biology*

427: 1038–1060.

Pan R, Jones a D, Hu J. **2014**. Cardiolipin-mediated mitochondrial dynamics and stress response in Arabidopsis. *The Plant Cell* **26**: 391–409.

Panikulangara TJ, Eggers-Schumacher G, Wunderlich M, Stransky H, Schöffl F. **2004**. Galactinol synthase1. A novel heat shock factor target gene responsible for heat-induced synthesis of raffinose family oligosaccharides in Arabidopsis. *Plant Physiology* **136**: 3148–3158.

Parankusam S, Adimulam SS, Bhatnagar-Mathur P, Sharma KK. **2017**. Nitric oxide (NO) in plant heat stress tolerance: current knowledge and perspectives. *Frontiers in Plant Science* **8**: 1582.

Parker VT, Simpson RL., Alessio Leck M. 2008. The seedling in an ecological and evolutionary context. In: Parker, V. Thomas; Simpson, Robert L.; Alessio Leck M, ed. Seedling Ecology and Evolution. Cambridge: Cambridge University Press, 393–389.

Paszkiewicz G, Gualberto JM, Benamar A, Macherel D, Logan DC. **2017**. Arabidopsis seed mitochondria are bioenergetically active immediately upon imbibition and specialize via biogenesis in preparation for autotrophic growth. *The Plant Cell* **29**: 109–128.

Pauwels L, Barbero GF, Geerinck J, Tilleman S, Grunewald W, Pérez AC, Chico JM, Bossche R Vanden, Sewell J, Gil E, *et al.* 2010. NINJA connects the co-repressor TOPLESS to jasmonate signalling. *Nature* **464**: 788–791.

Payne SH. **2015**. The utility of protein and mRNA correlation. *Trends in Biochemical Sciences* **40**: 1–3.

Pecinka A, Dinh HQ, Baubec T, Rosa M, Lettner N, Mittelsten Scheid O, Scheid OM. **2010**. Epigenetic regulation of repetitive elements is attenuated by prolonged heat stress in Arabidopsis. *The Plant Cell* **22**: 3118–3129.

Pellegrino MW, Nargund AM, Haynes CM. **2013**. Signaling the mitochondrial unfolded protein response. *Biochimica et Biophysica Acta (BBA) - Molecular Cell Research* **1833**: 410–416.

Peng X, Qin Z, Zhang G, Guo Y, Huang J. **2015**. Integration of the proteome and transcriptome reveals multiple levels of gene regulation in the rice dl2 mutant. *Frontiers in Plant Science* **6**: 351.

Perico C, Sparkes I. **2018**. Plant organelle dynamics: cytoskeletal control and membrane contact sites. *New Phytologist* **220**: 381–394.

Persak H, Pitzschke A. **2014**. Dominant repression by Arabidopsis transcription factor MYB44 causes oxidative damage and hypersensitivity to abiotic stress. *International Journal of Molecular Sciences* **15**: 2517–2537.

Petrov VD, Van Breusegem F. **2012**. Hydrogen peroxide-a central hub for information flow in plant cells. *AoB Plants* **2012**: pls014.

Pfannschmidt T. **2010**. Plastidial retrograde signalling - a true 'plastid factor' or just metabolite signatures? *Trends in Plant Science* **15**: 427–435.

Popova O V., Dinh HQ, Aufsatz W, Jonak C. **2013**. The RdDM pathway is required for basal heat tolerance in Arabidopsis. *Molecular Plant* **6**: 396–410.

Prasad PVV, Boote KJ, Allen LH, Sheehy JE, Thomas JMG. **2006**. Species, ecotype and cultivar differences in spikelet fertility and harvest index of rice in response to high temperature stress. *Field Crops Research* **95**: 398–411.

Prasad BD, Goel S, Krishna P. **2010**. In silico identification of carboxylate clamp type tetratricopeptide repeat

proteins in Arabidopsis and rice as putative co-chaperones of Hsp90/Hsp70. *PLoS ONE* **5**: e12761.

Prasad TK, Hack E, Hallberg RL. **1990**. Function of the maize mitochondrial chaperonin hsp60: specific association between Hsp60 and newly synthesized F1-ATPase alpha subunits. *Molecular and Cellular Biology* **10**: 3979–3986.

Prieto-Dapena P, Almoguera C, Personat JM, Merchan F, Jordano J. **2017**. Seed-specific transcription factor HSFA9 links late embryogenesis and early photomorphogenesis. *Journal of Experimental Botany* **68**: 1097–1108.

Qin D, Wu H, Peng H, Yao Y, Ni Z, Li Z, Zhou C, Sun Q. **2008**. Heat stress-responsive transcriptome analysis in heat susceptible and tolerant wheat (*Triticum aestivum* L.) by using Wheat Genome Array. *BMC Genomics* **9**: 432.

Queitsch C, Hong SW, Vierling E, Lindquist S. **2000**. Heat shock protein 101 plays a crucial role in thermotolerance in Arabidopsis. *The Plant Cell* **12**: 479–492.

Queitsch C, Sangster TA, Lindquist S. **2002**. Hsp90 as a capacitor for genetic variation. *Nature* **417**: 618–624.

Rasmusson AG, Geisler DA, Møller IM. **2008**. The multiplicity of dehydrogenases in the electron transport chain of plant mitochondria. *Mitochondrion* **8**: 47–60.

Ren H, Gao K, Liu Y, Sun D, Zheng S. **2017**. The role of AtPLC3 and AtPLC9 in thermotolerance in Arabidopsis. *Plant Signaling & Behavior* **12**: e1162368.

Rentel MC, Knight MR, Kingdom U. **2004**. Oxidative stress-induced calcium signaling. *Plant Physiology* **135**: 1471–1479.

Rhoads DM, Subbaiah CC. **2007**. Mitochondrial retrograde regulation in plants. *Mitochondrion* **7**: 177–194.

Rhoads DM, White SJ, Zhou Y, Muralidharan M, Elthon TE. **2005**. Altered gene expression in plants with constitutive expression of a mitochondrial small heat shock protein suggests the involvement of retrograde regulation in the heat stress response. *Physiologia Plantarum* **123**: 435–444.

Richter K, Haslbeck M, Buchner J. **2010**. The heat shock response: life on the verge of death. *Molecular Cell* **40**: 253–266.

Riedl J, Crevenna AH, Kessenbrock K, Yu JH, Neukirchen D, Bista M, Bradke F, Jenne D, Holak TA, Werb Z, *et al.* 2008. Lifeact: A versatile marker to visualize F-actin. *Nature Methods* **5**: 605–607.

Rikhvanov EG, Varakina NN, Rusaleva TM, Rachenko EI, Knorre DA, Voinikov VK. **2005**. Do mitochondria regulate the heat-shock response in *Saccharomyces cerevisiae*? *Current Genetics* **48**: 44–59.

Rivero RM, Ruiz JM, Romero LM. **2004**. Importance of N source on heat stress tolerance due to the accumulation of proline and quaternary ammonium compounds in tomato plants. *Plant Biology* **6**: 702–707.

Rizhsky L, Liang H, Mittler R. **2002**. The combined effect of drought stress and heat shock on gene expression in tobacco. *Plant Physiology* **130**: 1143–1151.

Rizhsky L, Liang H, Shuman J. **2004**. When defense pathways collide. The response of Arabidopsis to a combination of drought and heat stress. *Plant Physiology* **134**: 1683–1696.

Rochaix J-D, Ramundo S. **2015**. Conditional repression of essential chloroplast genes: Evidence for new plastid signaling pathways. *Biochimica et Biophysica Acta (BBA) - Bioenergetics* **1847**: 986–992.

Rogers LK, Lucchesi PA. **2014**. Stress adaptation and the resilience of youth: fact or fiction? *Physiology* **29**: 156.

Rolland N, Bouchnak I, Moyet L, Salvi D, Kuntz M. **2018**. The main functions of plastids. In: Maréchal E, ed. Plastids: Methods in molecular biology. New York, NY: Humana Press, 73–85.

Romero HM, Pell EJ, Tien M. **2006**. Expression profile analysis and biochemical properties of the peptide methionine sulfoxide reductase a (PMSRA) gene family in Arabidopsis. *Plant Science* **170**: 705–714.

Roux F, Mary-Huard T, Barillot E, Wenes E, Botran L, Durand S, Villoutreix R, Martin-Magniette M-L, Camilleri C, Budar F. **2016**. Cytonuclear interactions affect adaptive traits of the annual plant *Arabidopsis thaliana* in the field. *Proceedings of the National Academy of Sciences* **113**: 3687–3692.

Ruelland E, Zachowski A. **2010**. How plants sense temperature. *Environmental and Experimental Botany* **69**: 225–232.

Rutherford SL, Lindquist S. **1998**. Hsp90 as a capacitor for morphologival evolution. *Nature* **396**: 336–342.

Saavedra C, Tung KS, Amberg DC, Hopper AK, Cole CN. **1996**. Regulation of mRNA export in response to stress in *Saccharomyces cerevisiae*. *Genes & Development* **10**: 1608–1620.

Sagi M, Fluhr R. **2006**. Production of reactive oxygen species by plant NADPH oxidases. *Plant Physiology* **141**: 336–340.

Saidi Y, Finka A, Goloubinoff P. **2011**. Heat perception and signalling in plants: A tortuous path to thermotolerance. *New Phytologist* **190**: 556–565.

Saidi Y, Finka A, Muriset M, Bromberg Z, Weiss YG, Maathuis FJM, Goloubinoff P. **2009**. The heat shock response in moss plants is regulated by specific calcium-permeable channels in the plasma membrane. *The Plant Cell* **21**: 2829–43.

Saidi Y, Peter M, Finka A, Cicekli C, Vigh L, Goloubinoff P. **2010**. Membrane lipid composition affects plant heat sensing and modulates Ca 2+ -dependent heat shock response. *Plant Signaling & Behavior* **5**: 1530–1533.

Sakata T, Oshino T, Miura S, Tomabechi M, Tsunaga Y, Higashitani N, Miyazawa Y, Takahashi H, Watanabe M, Higashitani A. **2010**. Auxins reverse plant male sterility caused by high temperatures. *Proceedings of the National Academy of Sciences* **107**: 8569–8574.

Sakuma Y, Maruyama K, Qin F, Osakabe Y, Shinozaki K, Yamaguchi-Shinozaki K. **2006**. Dual function of an Arabidopsis transcription factor DREB2A in water-stress-responsive and heat-stress-responsive gene expression. *Proceedings of the National Academy of Sciences* **103**: 18822–18827.

Salvucci ME, Crafts-Brandner SJ. **2004**. Inhibition of photosynthesis by heat stress: the activation state of Rubisco as a limiting factor in photosynthesis. *Physiologia Plantarum* **120**: 179–186.

Sangwan V, Orvar BL, Beyerly J, Hirt H, Dhindsa RS. **2002**. Opposite changes in membrane fluidity mimic cold and heat stress activation of distinct plant MAP kinase pathways. *The Plant Journal* **31**: 629–638.

Sanmiya K, Suzuki K, Egawa Y, Shono M. **2004**. Mitochondrial small heat-shock protein enhances thermotolerance in tobacco plants. *FEBS Letters* **557**: 265–268.

Sano T, Higaki T, Handa K, Kadota Y, Kuchitsu K, Hasezawa S, Hoffmann A, Endter J, Zimmermann U, Hedrich R, *et al.* 2006. Calcium ions are involved in the delay of plant cell cycle progression by abiotic stresses. *FEBS Letters* **580**: 597–602.

Sato H, Mizoi J, Tanaka H, Maruyama K, Qin F, Osakabe Y, Morimoto K, Ohori T, Kusakabe K, Nagata M, *et al.* 2014. Arabidopsis DPB3-1, a DREB2A interactor, specifically enhances heat stress-induced gene expression by forming a heat stress-specific transcriptional complex with NF-Y subunits. *The Plant Cell* **26**: 4954–

4973.

Savada RP, Ozga JA, Jayasinghege CPA, Waduthanthri KD, Reinecke DM. **2017**. Heat stress differentially modifies ethylene biosynthesis and signaling in pea floral and fruit tissues. *Plant Molecular Biology* **95**: 313–331.

Savvides A, Ali S, Tester M, Fotopoulos V. **2016**. Chemical priming of plants against multiple abiotic stresses: mission possible? *Trends in Plant Science* **21**: 329–340.

Scharf K-D, Berberich T, Ebersberger I, Nover L. **2012**. The plant heat stress transcription factor (Hsf) family: Structure, function and evolution. *Biochimica et Biophysica Acta (BBA) - Gene Regulatory Mechanisms* **1819**: 104–119.

Schindelin J, Arganda-Carreras I, Frise E, Kaynig V, Longair M, Pietzsch T, Preibisch S, Rueden C, Saalfeld S, Schmid B, *et al.* 2012. Fiji: an open-source platform for biological-image analysis. *Nature Methods* **9**: 676–682.

Schmitt K, Grimm A, Dallmann R, Oettinghaus B, Restelli LM, Witzig M, Ishihara N, Mihara K, Ripperger JA, Albrecht U, *et al.* 2018. Circadian control of DRP1 activity regulates mitochondrial dynamics and bioenergetics. *Cell Metabolism* **27**: 657–666.

Schramm F, Ganguli A, Kiehlmann E, Englich G, Walch D, Von Koskull-Döring P. **2006**. The heat stress transcription factor HsfA2 serves as a regulatory amplifier of a subset of genes in the heat stress response in Arabidopsis. *Plant Molecular Biology* **60**: 759–772.

Schramm F, Larkindale J, Kiehlmann E, Ganguli A, Englich G, Vierling E, Von Koskull-Döring P. **2008**. A cascade of transcription factor DREB2A and heat stress transcription factor HsfA3 regulates the heat stress response of Arabidopsis. *The Plant Journal* **53**: 264–274.

Scott I, Logan DC. **2008**. Mitochondrial morphology transition is an early indicator of subsequent cell death in Arabidopsis. *New Phytologist* **177**: 90–101.

Sedaghatmehr M, Mueller-Roeber B, Balazadeh S. **2016**. The plastid metalloprotease FtsH6 and small heat shock protein HSP21 jointly regulate thermomemory in Arabidopsis. *Nature Communications* **7**: 12439.

Sedaghatmehr M, Thirumalaikumar VP, Kamranfar I, Marmagne A, Masclaux-Daubresse C, Balazadeh S. **2018**. A regulatory role of autophagy for resetting the memory of heat stress in plants. *Plant, Cell & Environment*.

Sharkey TD. **2005**. Effects of moderate heat stress on photosynthesis: Importance of thylakoid reactions, rubisco deactivation, reactive oxygen species, and thermotolerance provided by isoprene. *Plant, Cell and Environment* **28**: 269–277.

Shoemaker CJ, Green R. **2012**. Translation drives mRNA quality control. *Nature Structural and Molecular Biology* **19**: 594–601.

Siddique M, Gernhard S, Von Koskull-Döring P, Vierling E, Scharf KD. **2008**. The plant sHSP superfamily: Five new members in *Arabidopsis thaliana* with unexpected properties. *Cell Stress and Chaperones* **13**: 183–197.

Silva-Correia J, Freitas S, Tavares RM, Lino-Neto T, Azevedo H. **2014**. Phenotypic analysis of the Arabidopsis heat stress response during germination and early seedling development. *Plant Methods* **10**: 7.

Smertenko A, Dráber P, Viklický V, Opatrný Z. **1997**. Heat stress affects the organization of microtubules and cell division in *Nicotiana tabacum* cells. *Plant, Cell and Environment* **20**: 1534–1542.

Snyman M, Cronjé MJ. **2008**. Modulation of heat shock factors accompanies salicylic acid-mediated potentiation of Hsp70 in tomato seedlings. *Journal of Experimental Botany* **59**: 2125–2132.

Sobol S, Chayut N, Nave N, Kafle D, Hegele M, Kaminetsky R, Wünsche JN, Samach A. **2014**. Genetic variation in yield under hot ambient temperatures spotlights a role for cytokinin in protection of developing floral primordia. *Plant, Cell and Environment* **37**: 643–657.

de Souza A, Wang J-Z, Dehesh K. **2017**. Retrograde signals: integrators of interorganellar communication and orchestrators of plant development. *Annual Review of Plant Biology* **68**: 85–108.

Srivastava R, Deng Y, Howell SH. **2014**. Stress sensing in plants by an ER stress sensor/transducer, bZIP28. *Frontiers in Plant Science* **5**: 59.

Srivastava R, Deng Y, Shah S, Rao AG, Howell SH. **2013**. BINDING PROTEIN is a master regulator of the endoplasmic reticulum stress sensor/transducer bZIP28 in Arabidopsis. *The Plant Cell* **25**: 1416–1429.

Stavang JA, Gallego-Bartolomé J, Gómez MD, Yoshida S, Asami T, Olsen JE, García-Martínez JL, Alabadí D, Blázquez MA. **2009**. Hormonal regulation of temperature-induced growth in Arabidopsis. *The Plant Journal* **60**: 589–601.

Stengel A, Benz PJ, Soll J, Bölter B. **2010**. Redox-regulation of protein import into chloroplasts and mitochondria similarities and differences. *Plant Signaling and Behavior* **5**: 105–109.

Stief A, Altmann S, Hoffmann K, Pant BD, Scheible W-R, Bäurle I. **2014a**. Arabidopsis miR156 regulates tolerance to recurring environmental stress through SPL transcription factors. *The Plant Cell* **26**: 1792–1807.

Stief A, Brzezinka K, Lämke J, Bäurle I. **2014b**. Epigenetic responses to heat stress at different time scales and the involvement of small RNAs. *Plant Signaling & Behavior* **9**: e970430.

Stocker TF. **2013**. The closing door of climate targets. *Science* **339**: 280–282.

Su P-H, Li H-M. **2008**. Arabidopsis stromal 70-kD heat shock proteins are essential for plant development and important for thermotolerance of germinating seeds. *Plant Physiology* **146**: 1231–1241.

Suetsugu N, Higa T, Kong S-G, Wada M. **2015**. PLASTID MOVEMENT IMPAIRED1 and PLASTID MOVEMENT IMPAIRED1-RELATED1 mediate photorelocation movements of both chloroplasts and nuclei. *Plant Physiology* **169**: 1155–1167.

Suetsugu N, Wada M. **2007**. Chloroplast photorelocation movement mediated by phototropin family proteins in green plants. *Biological Chemistry* **388**: 927–935.

Sugio A, Dreos R, Aparicio F, Maule AJ. **2009**. The cytosolic protein response as a subcomponent of the wider heat shock response in Arabidopsis. *The Plant Cell* **21**: 642–654.

Sun A-Z, Guo F-Q. **2016**. Chloroplast retrograde regulation of heat Stress responses in plants. *Frontiers in Plant Science* **7**: 398.

Sung DY, Guy CL. **2003**. Physiological and molecular assessment of altered expression of Hsc70-1 in Arabidopsis. Evidence for pleiotropic consequences. *Plant Physiology* **132**: 979–987.

Sung D-Y, Kaplan F, Guy CL. **2001a**. Plant Hsp70 molecular chaperones: protein structure, gene family, expression and function. *Physiologia Plantarum* **113**: 443–451.

Sung DY, Vierling E, Guy CL. **2001b**. Comprehensive expression profile analysis of the Arabidopsis Hsp70 gene family. *Plant Physiology* **126**: 789–800.

Suter L, Widmer A. **2013**. Environmental heat and salt stress induce transgenerational phenotypic changes in Arabidopsis thaliana. *PLoS ONE* **8**: e60364.

Suzuki N, Bajad S, Shuman J, Shulaev V, Mittler R. **2008**. The transcriptional co-activator MBF1c is a key

regulator of thermotolerance in *Arabidopsis thaliana*. *Journal of Biological Chemistry* **283**: 9269–9275.

Suzuki N, Mittler R. **2006**. Reactive oxygen species and temperature stresses: A delicate balance between signalling and destruction. *Physiologia Plantarum* **126**: 41–51.

Suzuki K, Nakanishi H, Bower J, Yoder DW, Osteryoung KW, Miyagishima SY. **2009**. Plastid chaperonin proteins Cpn60α and Cpn60β are required for plastid division in *Arabidopsis thaliana*. *BMC Plant Biology* **9**: 38.

Suzuki N, Sejima H, Tam R, Schlauch K, Mittler R. **2011**. Identification of the MBF1 heat-response regulon of *Arabidopsis thaliana*. *The Plant Journal* **66**: 844–851.

Sweetlove LJ, Beard KFM, Nunes-Nesi A, Fernie AR, Ratcliffe RG. **2010**. Not just a circle: Flux modes in the plant TCA cycle. *Trends in Plant Science* **15**: 462–470.

Swindell WR, Huebner M, Weber AP. **2007**. Transcriptional profiling of Arabidopsis heat shock proteins and transcription factors reveals extensive overlap between heat and non-heat stress response pathways. *BMC Genomics* **8**: 125.

Tetteroo FAA, Hoekstra FA, Karssen CM. **1994**. Effect of abscisic acid and slow drying on soluble carbohydrate content in developing embryoids of carrot (*Daucus carota* L.) and alfalfa (*Medicago sativa* L.). *Seed Science Research* **4**: 203–210.

Thompson AR, Doelling JH, Suttangkakul A, Vierstra RD. **2005**. Autophagic nutrient recycling in Arabidopsis directed by the ATG8 and ATG12 conjugation pathways. *Plant Physiology* **138**: 2097–2110.

Tian T, Liu Y, Yan H, You Q, Yi X, Du Z, Xu W, Su Z. **2017**. agriGO v2.0: a GO analysis toolkit for the agricultural community, 2017 update. *Nucleic Acids Research* **45**: W122–W129.

Todd J, Post-Beittenmiller D, Jaworski JG. **1999**. KCS1 encodes a fatty acid elongase 3-ketoacyl-CoA synthase affecting wax biosynthesis in *Arabidopsis thaliana*. *The Plant Journal* **17**: 119–130.

Trobacher CP. **2009**. Ethylene and programmed cell death in plants. *Botany* **87**: 757–769.

Tyedmers J, Mogk A, Bukau B. **2010**. Cellular strategies for controlling protein aggregation. *Nature Reviews Molecular Cell Biology* **11**: 777–788.

Tzin V, Galili G. **2010**. New insights into the shikimate and aromatic amino acids biosynthesis pathways in plants. *Molecular Plant* **3**: 956–972.

Urban J, Ingwers MW, McGuire MA, Teskey RO. **2017**. Increase in leaf temperature opens stomata and decouples net photosynthesis from stomatal conductance in *Pinus taeda* and *Populus deltoides x nigra*. *Journal of Experimental Botany* **68**: 1757–1767.

Üstün S, Hafrén A, Hofius D. **2017**. Autophagy as a mediator of life and death in plants. *Current Opinion in Plant Biology* **40**: 122–130.

Vacca RA, de Pinto MC, Valenti D, Passarella S, Marra E, De Gara L. **2004**. Production of reactive oxygen species, alteration of cytosolic ascorbate peroxidase, and impairment of mitochondrial metabolism are early events in heat shock-induced programmed cell death in tobacco bright-yellow 2 cells. *Plant Physiology* **134**: 1100–1112.

Valot B, Langella O, Nano E, Zivy M. **2011**. MassChroQ: A versatile tool for mass spectrometry quantification. *Proteomics* **11**: 3572–3577.

Vanderauwera S, Suzuki N, Miller G, van de Cotte B, Morsa S, Ravanat J-L, Hegie A, Triantaphylides C, Shulaev V, Van Montagu MCE, *et al.* 2011. Extranuclear protection of chromosomal DNA from oxidative stress. *Proceedings of the National Academy of Sciences* **108**: 1711–1716.

Vanlerberghe GC. **2013**. Alternative oxidase: A mitochondrial respiratory pathway to maintain metabolic and signaling homeostasis during abiotic and biotic stress in plants. *International Journal of Molecular Sciences* **14**: 6805–6847.

Vigh L, Maresca B, Harwood JL. **1998**. Does the membrane's physical state control the expression of heat shock and other genes? *Trends in Biochemical Sciences* **23**: 369–374.

Vogel JL, Parsell DA, Lindquist S. **1995**. Heat-shock proteins Hsp104 and Hsp70 reactivate mRNA splicing after heat inactivation. *Current Biology* **5**: 306–317.

Volkov RA, Panchuk II, Mullineaux PM, Schöffl F. **2006**. Heat stress-induced H_2O_2 is required for effective expression of heat shock genes in Arabidopsis. *Plant Molecular Biology* **61**: 733–746.

Wadhwa R, Ryu J, Gao R, Choi IK, Morrow G, Kaur K, Kim I, Kaul SC, Yun CO, Tanguay RM. **2010**. Proproliferative functions of Drosophila small mitochondrial heat shock protein 22 in human cells. *Journal of Biological Chemistry* **285**: 3833–3839.

Wahid A, Gelani S, Ashraf M, Foolad MR. **2007**. Heat tolerance in plants: An overview. *Environmental and Experimental Botany* **61**: 199–223.

Wakim J, Goudenege D, Perrot R, Gueguen N, Desquiret-Dumas V, Chao de la Barca JM, Dalla Rosa I, Manero F, Le Mao M, Chupin S, *et al.* 2017. CLUH couples mitochondrial distribution to the energetic and metabolic status. *Journal of Cell Science* **130**: 1940–1951.

Wallace EWJ, Kear-Scott JL, Pilipenko E V., Schwartz MH, Laskowski PR, Rojek AE, Katanski CD, Riback JA, Dion MF, Franks AM, *et al.* 2015. Reversible, specific, active aggregates of endogenous proteins assemble upon heat stress. *Cell* **162**: 1286–1298.

Wang Q-L, Chen J-H, He N-Y, Guo F-Q. **2018**. Metabolic reprogramming in chloroplasts under heat stress in plants. *International Journal of Molecular Sciences* **19**: 849.

Wang L, Guo Y, Jia L, Chu H, Zhou S, Chen K, Wu D, Zhao L. **2014a**. Hydrogen peroxide acts upstream of nitric oxide in the heat shock pathway in Arabidopsis seedlings. *Plant Physiology* **164**: 2184–2196.

Wang D, Lloyd a. H, Timmis JN. **2012**. Environmental stress increases the entry of cytoplasmic organellar DNA into the nucleus in plants. *Proceedings of the National Academy of Sciences* **109**: 2444–2448.

Wang W, Vinocur B, Shoseyov O, Altman A. **2004**. Role of plant heat-shock proteins and molecular chaperones in the abiotic stress response. *Trends in Plant Science* **9**: 244–252.

Wang K, Zhang X, Goatley M, Ervin E. **2014b**. Heat shock proteins in relation to heat stress tolerance of creeping bentgrass at different N levels. *PLoS ONE* **9**: e102914.

Wang X, Zhuang L, Shi Y, Huang B. **2017**. Up-regulation of HSFA2c and HSPs by ABA contributing to improved heat tolerance in tall fescue and Arabidopsis. *International Journal of Molecular Sciences* **18**: 1981.

Wanniarachchi V, Dametto L, Sweetman C, Shavrukov Y, Day D, Jenkins C, Soole K. **2018**. Alternative respiratory pathway component genes (AOX and ND) in rice and barley and their response to stress. *International Journal of Molecular Sciences* **19**: 915.

Waters ER. **2013**. The evolution, function, structure, and expression of the plant sHSPs. *Journal of Experimental Botany* **64**: 391–403.

Wawer I, Golisz A, Sulkowska A, Kawa D, Kulik A, Kufel J. **2018**. mRNA decapping and 5′-3′ decay contribute to the regulation of ABA signaling in *Arabidopsis thaliana*. *Frontiers in Plant Science* **9**: 312.

Weber C, Nover L, Fauth M. **2008**. Plant stress granules and mRNA processing bodies are distinct from heat stress granules. *The Plant Journal* **56**: 517–530.

Welchen E, García L, Mansilla N, Gonzalez DH. **2014**. Coordination of plant mitochondrial biogenesis: keeping pace with cellular requirements. *Frontiers in Plant Science* **4**: 551.

Weng M, Yang Y, Feng H, Pan Z, Shen W-H, Zhu Y, Dong A. **2014**. Histone chaperone ASF1 is involved in gene transcription activation in response to heat stress in *Arabidopsis thaliana*. *Plant, Cell & Environment* **37**: 2128–2138.

Westermann B. **2012**. Bioenergetic role of mitochondrial fusion and fission. *Biochimica et Biophysica Acta (BBA) - Bioenergetics* **1817**: 1833–1838.

Wiedemann N, Pfanner N. **2017**. Mitochondrial machineries for protein import and assembly. *Annual Review of Biochemistry* **86**: 685–714.

van Wijk KJ, Kessler F. **2017**. Plastoglobuli: plastid microcompartments with integrated functions in metabolism, plastid developmental transitions, and environmental adaptation. *Annual Review of Plant Biology* **68**: 253–289.

Wise RR, Olson AJ, Schrader SM, Sharkey TD. **2004**. Electron transport is the functional limitation of photosynthesis in field-grown *Pima cotton* plants at high temperature. *Plant, Cell and Environment* **27**: 717–724.

Woodson JD, Chory J. **2008**. Coordination of gene expression between organellar and nuclear genomes. *Nature Reviews Genetics* **9**: 383–395.

Wu A, Allu AD, Garapati P, Siddiqui H, Dortay H, Zanor M-I, Asensi-Fabado MA, Munne-Bosch S, Antonio C, Tohge T, *et al.* 2012. JUNGBRUNNEN1, a reactive oxygen species-responsive NAC transcription factor, regulates longevity in Arabidopsis. *The Plant Cell* **24**: 482–506.

Wu T, Juan Y, Hsu Y, Wu S, Liao H, Fung RWM, Charng Y. **2013**. Interplay between heat shock proteins HSP101 and HSA32 prolongs heat acclimation memory. *Plant Physiology* **161**: 2075–2084.

Xu Y, Huang B. **2009**. Effects of foliar-applied ethylene inhibitor and synthetic cytokinin on creeping bentgrass to enhance heat tolerance. *Crop Science* **49**: 1876–1884.

Xu G, Pattamatta A, Hildago R, Pace MC, Brown H, Borchelt DR. **2016**. Vulnerability of newly synthesized proteins to proteostasis stress. *Journal of Cell Science* **129**: 1892–1901.

Xuan Y, Zhou S, Wang L, Cheng Y, Zhao L. **2010**. Nitric oxide functions as a signal and acts upstream of AtCaM3 in thermotolerance in Arabidopsis seedlings. *Plant Physiology* **153**: 1895–1906.

Yamori W, Hikosaka K, Way DA. **2014**. Temperature response of photosynthesis in C3, C4, and CAM plants: Temperature acclimation and temperature adaptation. *Photosynthesis Research* **119**: 101–117.

Yamori W, Shikanai T. **2016**. Physiological functions of cyclic electron transport around photosystem I in sustaining photosynthesis and plant growth. *Annual Review of Plant Biology* **67**: 81–106.

Yángüez E, Castro-Sanz AB, Fernández-Bautista N, Oliveros JC, Castellano MM. **2013**. Analysis of genome-wide changes in the translatome of Arabidopsis seedlings subjected to heat stress. *PLoS ONE* **8**: e71425.

Yoshida K, Noguchi K. **2011**. Interaction between chloroplasts and mitochondria: activity, function, and regulation of the mitochondrial respiratory system during photosynthesis. In: Kempken F, ed. Plant mitochondria. Advances in Plant Biology, vol 1. New York, NY: Springer.

Yoshida T, Ohama N, Nakajima J, Kidokoro S, Mizoi J, Nakashima K, Maruyama K, Kim J-M, Seki M, Todaka D, *et al.* 2011. Arabidopsis HsfA1 transcription factors function as the main positive regulators in heat

shock-responsive gene expression. *Molecular Genetics and Genomics* **286**: 321–332.

Yoshida T, Sakuma Y, Todaka D, Maruyama K, Qin F, Mizoi J, Kidokoro S, Fujita Y, Shinozaki K, Yamaguchi-Shinozaki K. **2008**. Functional analysis of an Arabidopsis heat-shock transcription factor HsfA3 in the transcriptional cascade downstream of the DREB2A stress-regulatory system. *Biochemical and Biophysical Research Communications* **368**: 515–521.

You J, Chan Z. **2015**. ROS regulation during abiotic stress responses in crop plants. *Frontiers in Plant Science* **6**: 1092.

Youle RJ, Bliek AM Van Der, Complementation FP, Mitochondria BD, Fusion M, Proteins F. **2012**. Mitochondrial fission, fusion, and stress. *Science* **337**: 1062–1065.

Zander G, Hackmann A, Bender L, Becker D, Lingner T, Salinas G, Krebber H. **2016**. mRNA quality control is bypassed for immediate export of stress-responsive transcripts. *Nature* **540**: 593–596.

El Zawily AM, Schwarzländer M, Finkemeier I, Johnston IG, Benamar A, Cao Y, Gissot C, Meyer AJ, Wilson K, Datla R, *et al.* 2014. FRIENDLY regulates mitochondrial distribution, fusion, and quality control in Arabidopsis. *Plant Physiology* **166**: 808–828.

Zhang N, Belsterling B, Raszewski J, Tonsor SJ. **2015a**. Natural populations of *Arabidopsis thaliana* differ in seedling responses to high temperature stress. *AoB Plants* **7**: plv101.

Zhang K, Ezemaduka AN, Wang Z, Hu H, Shi X, Liu C, Lu X, Fu X, Chang Z, Yin C-C. **2015b**. A novel mechanism for small heat shock proteins to function as molecular chaperones. *Scientific Reports* **5**: 8811.

Zhang L, Li Y, Xing D, Gao C. **2009a**. Characterization of mitochondrial dynamics and subcellular localization of ROS reveal that HsfA2 alleviates oxidative damage caused by heat stress in Arabidopsis. *Journal of Experimental Botany* **60**: 2073–2091.

Zhang L, Liu X, Gaikwad K, Kou X, Wang F, Tian X, Xin M, Ni Z, Sun Q, Peng H, *et al.* 2017. Mutations in eIF5B confer thermosensitive and pleiotropic phenotypes via translation defects in *Arabidopsis thaliana*. *The Plant Cell* **29**: 1952–1969.

Zhang JX, Wang C, Yang CY, Wang JY, Chen L, Bao XM, Zhao YX, Zhang H, Liu J. **2010a**. The role of Arabidopsis AtFes1A in cytosolic Hsp70 stability and abiotic stress tolerance. *The Plant Journal* **62**: 539–548.

Zhang R, Wise RR, Struck KR, Sharkey TD. **2010b**. Moderate heat stress of *Arabidopsis thaliana* leaves causes chloroplast swelling and plastoglobule formation. *Photosynthesis Research* **105**: 123–134.

Zhang W, Zhou R-G, Gao Y-J, Zheng S-Z, Xu P, Zhang S-Q, Sun D-Y. **2009b**. Molecular and genetic evidence for the key role of AtCaM3 in heat-shock signal transduction in Arabidopsis. *Plant Physiology* **149**: 1773–1784.

Zhao L, Wang P, Hou H, Zhang H, Wang Y, Yan S, Huang Y, Li H, Tan J, Hu A, *et al.* 2014. Transcriptional regulation of cell cycle genes in response to abiotic stresses correlates with dynamic changes in histone modifications in maize. *PLoS ONE* **9**: e106070.

Zheng SZ, Liu YL, Li B, Shang ZL, Zhou RG, Sun DY. **2012**. Phosphoinositide-specific phospholipase C9 is involved in the thermotolerance of Arabidopsis. *The Plant Journal* **69**: 689–700.

Zhong L, Zhou W, Wang H, Ding S, Lu Q, Wen X, Peng L, Zhang L, Lu C. **2013**. Chloroplast small heat shock protein HSP21 interacts with plastid nucleoid protein pTAC5 and is essential for chloroplast development in Arabidopsis under heat stress. *The Plant Cell* **25**: 2925–2943.

UNIVERSITE ECOLOGIE
BRETAGNE GEOSCIENCES
LOIRE AGRONOMIE ALIMENTATION

université angers

Titre : Analyse intégrative de la thermotolérance acquise chez des plantules d'Arabidopsis arrêtées dans leur développement

Mots clés : Arabidopsis, plantules, stress thermique, acclimatation, métabolisme énergétique, HSP

Résumé : Dans le contexte du changement climatique, l'augmentation de la fréquence et de l'intensité des canicules risque d'avoir un impact négatif sur la physiologie des plantes, du fait de la perturbation structurale des protéines et des membranes par les fortes températures. Au cours de cette thèse, nous avons développé et caractérisé un système expérimental original dans lequel des plantules d'*Arabidopsis thaliana* sont arrêtées dans leur développement du fait d'une carence minérale. Ces plantules présentent une grande plasticité métabolique, notamment au niveau énergétique, qui leur permet de survivre pendant des semaines en état stationnaire. Nous avons ensuite réalisé une étude intégrative des processus qui permettent à ces plantules de survivre à un stress thermique normalement létal (43°C, 2 h), grâce à l'application d'un prétraitement à une température non létale (38°C, 2 h). Le pré-traitement à 38°C permet la protection du métabolisme énergétique ainsi que la reprise de la dynamique des organites lors de la phase de récupération. Au niveau transcriptionnel, les plantules pré-acclimatées surexpriment notamment des protéines chaperones et des gènes impliqués dans la photosynthèse et la régulation de l'expression des génomes mitochondriaux et plastidiaux. Au niveau protéique, l'accumulation d'HSPs et d'autres protéines de stress favorise la récupération des plantules, tandis qu'en l'absence d'acclimatation, le choc thermique provoque la diminution des protéines ribosomales et l'accumulation de protéines impliquées dans la dégradation des protéines. Cette étude révèle l'intérêt de l'analyse multi-échelle pour décrypter les mécanismes de réponse des plantes aux stress.

Title: Integrative analysis of acquired thermotolerance in developmentally arrested Arabidopsis seedlings

Keywords: Arabidopsis, seedlings, heat stress, acclimation, energy metabolism, HSP

Abstract: In the context of climate change, the increased frequency and intensity of heat waves will likely have a negative impact on plant physiology, due to the structural destabilization of proteins and of membranes caused by high temperatures. As part of this thesis, we developed and characterized an original experimental setup in which *Arabidopsis thaliana* seedlings are arrested in their development because of mineral starvation. These seedlings exhibit a high metabolic plasticity, especially for energy metabolism, which allows them to survive in a steady state for weeks. Then we performed an integrative analysis of the processes that allow these seedlings to survive to an otherwise lethal heat stress (43°C, 2 h), thanks to a priming at a non-lethal temperature (38°C, 2 h). Priming protects energy metabolism and permits the recovery of organelle dynamics after stress. At the transcriptional level, primed seedlings overexpress many chaperone proteins and genes involved in photosynthesis and in the regulation of the expression of mitochondrial and plastidial genomes. At the protein level, the accumulation of HSPs and other stress proteins favours seedling recovery, whereas in the absence of acclimation, heat shock provokes the decrease of ribosomal proteins and the accumulation of proteins implicated in protein degradation. This study highlights the relevance of multi-scale analysis to decipher mechanisms of stress responses in plants.